NASA Technical Memorandum 105243
ICOMP–91–17; CMOTT–91–07

p. 166

Center for Modeling of Turbulence and Transition (CMOTT)

Research Briefs—1990

October 1991

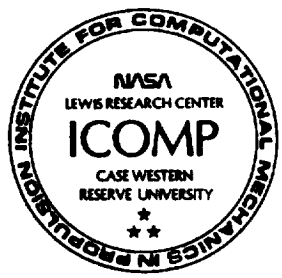

NASA

Table of Contents

Page

Preface vii

The Study of PDF Turbulence Models in Combustion
Andrew T. Hsu 1

Turbulence Modeling
Tsan-Hsing Shih 4

Experiments and Modeling
Aamir Shabbir 9

Modeling of Compressible Turbulent Shear Flows
William W. Liou 13

RNG in Turbulence and Modeling of Bypass Transition
Zhigang Yang 16

Turbulence Modeling in Supersonic Combusting Flows
Tawit Chitsomboon 19

Development of New Flux Splitting Schemes
Meng-Sing Liou and Christopher J. Steffen, Jr. 22

Progress of Simulations for Reacting Shear Layers
Sheng-Tao Yu 24

Appendix A : Organization - 1990 26

Appendix B : Seminars and Meetings 29
B.1 CMOTT Seminar Series 29
B.2 CMOTT Technical Meetings 48

Appendix C : Collection of Publications 52

Preface

The Center for Modeling of Turbulence and Transition (CMOTT), a cooperative turbulence research team, was formally established in May of 1990 as a focal group within the Institute of Computational Mechanics for Propulsion (ICOMP). The location of CMOTT is shown in the organization structure chart in Appendix A. The objectives of the CMOTT are to develop, validate and implement the models for turbulence and boundary-layer transition in practical engineering flows. The flows of interest are three-dimensional, incompressible and compressible flows with chemistry. The schemes being studied include the two-equation (e.g. k-ϵ) and algebraic Reynolds-stress models, the full Reynolds-stress (or second moment closure) models, the probability density function (pdf) models, the Renormalization Group Theory (RNG) and Direct Interaction Approximation (DIA), the Large Eddy Simulation (LES) and Direct Numerical Simulation (DNS).

Currently, CMOTT has eight formal members working on various aspects of turbulence and transition modeling in collaboration with NASA-Lewis scientists and Case Western Reserve University (CWRU) faculty members. The CMOTT members have been actively involved in international and national turbulence research activities through meetings, seminars, workshops and exchange-visitors. Since June of 1990, a CMOTT seminar series has been conducted with speakers invited from within and outside of the NASA Lewis Research Center, including foreign speakers. In 1991, a new series of biweekly CMOTT technical meetings was initiated for informal discussions regarding special issues in turbulence and transition modeling. The CMOTT research activity is advised by a group consisting of Professor J.L. Lumley (Cornell University), Dr. M. Goldstein (NASA/LeRC) and Professor E. Reshotko (CWRU).

This research brief contains the progress reports of the CMOTT Research staff from May 1990 to May 1991. It is intended to be an informational report of the CMOTT activities as well as an annual report to ICOMP and NASA. The current CMOTT roster and its organization are listed in the Appendix A. Listed in Appendix B.1 are the visiting members and their seminar abstracts. Appendix B.2 gives the scientific and technical issues discussed in biweekly CMOTT meetings. Journal and conference publications by CMOTT members are grouped in Appendix C.

Starting in 1991, NASA Technical Memoranda authored by members of the CMOTT staff will be given a specific number to identify them as CMOTT reports. These manuscripts will be made available for early dissemination of completed research results by the CMOTT staff.

Finally, we express our thanks to one of the CMOTT members, Dr. William W. Liou, who carefully assembled the material and provided editorial assistance.

Louis Povinelli
Meng-Sing Liou
Tsan-Hsing Shih

Center for Modeling of Turbulence and Transition
Research Briefs - 1990

The Study of PDF Turbulence Models in Combustion

Andrew T. Hsu

1. Motivation and Objectives

1.1 Motivation

The accurate prediction of turbulent combustion is still beyond reach for today's computation techniques. It is the consensus of the combustion profession that the predictions of chemically reacting flow were poor if conventional turbulence models were used. The main difficulty lies in the fact that the reaction rate is highly non-linear, and the use of averaged temperature, pressure and density produces excessively large errors. The probability density function (pdf) method is the only alternative at present time that uses local instant values of the temperature, density, etc., in predicting chemical reaction rate, and thus is the only viable approach for turbulent combustion calculations.

1.2 Objectives

The present work aims at the development and implementation of the the pdf turbulence models in solving realistic combustion problems. The fact that the pdf equation has a very large dimensionality renders finite difference schemes extremely demanding on computer memories and thus impractical, if not entirely impossible. A logical alternative is the Monte Carlo scheme, which has been used extensively in statistical physics. However, the use of Monte Carlo scheme to solve both the flowfield and the chemical reaction is very time consuming. Further more, since CFD has reached a certain degree of maturity as well as popularity, it seems less beneficial to abandon CFD completely and opt for Monte Carlo schemes. Therefore, we propose the use of a combined CFD and Monte Carlo scheme in the present study. The scheme would use the conventional flow solvers when calculating the flowfield properties such as velocity, pressure, etc., while the chemical reaction part would be solved using Monte Carlo solvers.

2. Works Accomplished

2.1 Code development.

A parabolic code with $k-\epsilon$ turbulence models have been developed in the past months. Three different $k-\epsilon$ models have been tested with satisfactory numerical results.

A grid dependent Monte Carlo scheme is being explored. This scheme discretize the pdf equation on a given grid and write, for parabolic flows:

$$\tilde{P}_{x+dx,j} = \alpha_j \tilde{P}_{x,j+1} + \beta_j \tilde{P}_{x,j} + \gamma_j \tilde{P}_{x,j-1} \tag{1}$$

and we require

$$\alpha_j + \beta_j + \gamma_j = 1 \tag{2}$$

Using a very simple test case of a convection/diffusion process with two scalars, it was found that the previous scheme does not conserve mass fractions due to re-contamination. It is found that in order to conserve the mass fractions absolutely, one needs to add further restriction to the scheme, namely

$$\alpha_j + \gamma_j = \alpha_{j-1} + \gamma_{j+1} \tag{3}$$

A new algorithm was devised and is currently being tested. Again using the simple test case of two scalars with assumed constant coefficients in the pdf equation, the new algorithm is shown to conserve the mass fractions perfectly in cases of uniform flows or pure diffusion problems. Deficiencies such as directional bias and re-contamination that were found in the previous algorithm are completely eliminated.

2.2 Applications.

The code developed has been validated by solving a heated turbulent jet. The temperature is treated as a conserved passive scalar and solved using the pdf Monte Carlo simulation while the flow field is obtained using a conventional CFD solver. The mean temperature profile and RMS of the temperature fluctuation were compared with experimental data.

As a first application to combustion problems, the non-premixed flame of hydrogen and fluorine is being studied. A comparison between primary results from the present study and experimental data show that the present scheme predicts the mean flame temperature accurately.

3. Future Plans

1. Further investigate the case of hydrogen-fluorine reaction.
2. Study finite rate calculation of the same non-premixed flame.
3. Study the interaction between mixing and chemical reaction.
4. Study compressibility effects.

4. Publications

1. Hsu, A.T., "The Study of PDF Turbulence Models in Combustion," 9th National Aero-Space Plane Technology Symposium, November 1-2, 1990.

2. Hsu, A.T., " On Recontamination and Directional Bias Problem in Monte Carlo Simulation of PDF Turbulence Models," NASA CFD Conference, April 12-14, 1991, Moffett Field,California.

3. Hsu, A.T., "Progress in the Development of PDF Turbulence Models for Combustion," 10th National Aero-Space Plane Technology Symposium, April 23-25, 1991, Monterey, California.

4. Hsu, A.T., "The Study of PDF Turbulence Model in Nonequilibrium Hydrogen Diffusion Flames" AIAA Paper 91-1780, Honolulu, Hawaii, June, 1991.

Turbulence Modeling

Tsan-Hsing Shih

1. Motivation and Objectives

(1) Examine the performance of existing two-equation eddy viscosity models and develop better models for the near-wall turbulence using direct numerical simulations of plane channel and boundary layer flows.

(2) Use the asymptotic near-wall behavior of turbulence to examine the problems of current second-order closure models and develop new models with the correct near-wall behavior.

(3) Use Rapid Distortion Theory to analytically study the effects of mean deformation (especially due to pure rotation) on turbulence, obtain analytical solutions for the spectrum tensor, Reynolds stress tensor, anisotropy tensor and its invariants, which can be used in the turbulence model development.

(4) Explore the potential of the renormalization group (RNG) theory in turbulence modeling.

(5) Modeling of compressible turbulent flows.

(6) Modeling of bypass transition.

2. Work Accomplished and Ongoing Work

2.1 k-ϵ model

The k-ϵ model is still the most widely used model for computing engineering flows. We have examined the near-wall behavior of various eddy viscosity models proposed by different researchers, and have studied the near-wall behavior of the terms in the k-equation budget. We found that the modeled eddy viscosity in many existing k-ϵ models does not possess correct near-wall behavior and the pressure transport term in the k-equation is not modeled appropriately. Based on the near-wall asymptotic behavior of the eddy viscosity and the pressure transport term in the k-equation, a new set of improved closure models has been obtained. In addition, a modeled equation for the dissipation rate is derived more rationally. This work is reported in NASA TM 103221 ICOMP-90-16[1].

In addition, all the existing two-equation models (except Jones & Laun-

der model, which unfortunately does not work well even for some simple flows) have an "unacceptable" wall distance parameter (y^+) in their eddy viscosity damping function $f_\mu(y^+)$. This will result in an unphysical zero eddy viscosity near the separation region. In addition, y^+ can not be well defined in many flows with complex geometry. To remove this deficiency, Dr. V. Michelassi, Dr. A. Hsu and I proposed two new eddy viscosity damping functions, and both of them are independent of the wall distance. The new models have been satisfactorily tested in channel and boundary layer flows. This work is reported in two papers: AIAA-91-0611[2] and NASA TM/ICOMP/CMOTT[3].

2.2 Second order modeling of near-wall turbulence

The main emphasis is on developing a near-wall turbulence model for the velocity pressure gradient correlation and the dissipation tensor in the Reynolds-stress equation. A modeled dissipation rate equation is also derived more rationally. Near a wall, a reduction in velocity fluctuations normal to the wall becomes significant. Because of this wall effect, the viscous diffusion term in the Reynolds-stress equations becomes the leading term and it must be properly balanced by the other terms. We have used this as a model constraint for developing a model for the pressure and dissipation terms. To test the models, a fully developed channel flow and boundary layer flows are chosen as the test flows, for which direct numerical simulations and experimental data are available for comparison. The modeled Reynolds stress equations for the channel flow are steady one-dimensional, and for boundary layer flows are steady two-dimensional. Therefore model testing will be very accurate. This part of work[4] is reported in the paper: *Proceedings of the International Symposium on Engineering Turbulence Modeling and Measurements* and NASA TM 103222 ICOMP-90-0017.

2.3 Second order modeling of a three-dimensional boundary layer

A study of three-dimensional effects on turbulent boundary layer was achieved by the direct numerical simulation of a fully developed turbulent channel flow subjected to transverse pressure gradient (see Physics of Fluids, Vol.2 N0.10, 1990, pp. 1846-1853). The time evolution of the flow was studied. The results show that, in agreement with experimental data, the Reynolds stresses are reduced with increasing three-dimensionality and that, near the wall, a lag develops between the stress and the strain rate. In addition, we found that the turbulent kinetic energy also decreased. To model these three-dimensional effects on the turbulence, we have tried different two-equation models and second order closure models. None of the current

closure models can predict the reductions in the shear stress and turbulent kinetic energy observed in direct numerical simulations. Detailed studies of the Reynolds-stresses budgets were carried out. One of the preliminary conclusions from these budget studies is that the velocity pressure-gradient term in the normal stress equation $\langle v^2 \rangle$ plays a dominant role in the reduction of shear stress and kinetic energy. These budgets have been used to guide the development of better models for three dimensional turbulent boundary layer flows. This work[5] was presented in the American Physical Society Forty-Third Annual Meeting, November, 1990.

2.4 The effect of rotation on turbulence

In addition to the above studies of second order closure models, we have carried out some RDT analysis on simple homogeneous turbulent flows. An order of magnitude analysis shows that under the condition of $S\langle q^2 \rangle/\epsilon \gg \sqrt{R_t}$, the equations for turbulent velocity fluctuations can be approximated by a linear set of equations, and if $S\langle q^2 \rangle/\epsilon \gg R_t^{3/4}$, then the turbulent velocity equations can be further approximated by an inviscid linear equation. Therefore, RDT can be used to analytically study some very basic turbulent flows, such as, homogeneous shear flows, irrotational strain flows and pure rotational flows. This work focuses on the effect of rapid rotation on turbulence using RDT. We have obtained analytical expressions for velocity, the spectrum tensor, Reynolds-stress, the anisotropy tensor and its invariants. The solutions show that the turbulence is strongly affected by the rapid rotation. Using RDT, we can calculate the rapid pressure-stain term exactly and we can obtain very useful information for developing corresponding turbulence models. See the report[6] for this work.

2.5 Renormalization Group Theory (RNG) in turbulence modeling

RNG method has been introduced to the turbulence modeling mainly in the Large Eddy Simulation (LES) of turbulence with a subgrid scale model. One also attempted to use it to develop Reynolds-averaged turbulence model equations, for example, k-ϵ model equations. However, we found that there are a few fundamental concepts and important procedures used in the derivation of those model equations which are not clear and well justified. Dr. Z. Yang and I are working on this subject and try to explore the potential of RNG in the turbulence modeling.

2.6 Modeling of compressible turbulent flows

The turbulence models for compressible flows are of great interest in hypersonic flows and turbulent combustion. The modeling scheme greatly de-

pends on the averaging schemes (i.e., conventional average, density weighted average and mixed average) used in the turbulence equations. We start with the analysis of the turbulent equations derived from the different averaging schemes to see what kind of averaging scheme is most convenient for both turbulent modeling and applications in CFD. We concentrate on the second order closure model (i.e. Reynolds stress model) and two-equation model. Dr. W. Liou and I are working on this subject. See Reference[7] for the first report on averaging schemes for compressible flows.

2.7 Modeling of bypass transition

Most common transition phenomena occurred in engineering flows are bypass transition. A few papers on modeling of transition with turbulence models show that the bypass transition can possibly be modeled with the modified turbulence models developed solely for turbulent flows. However, most of the work in this direction was based on the parabolic two-equation models. We expect that the bypass transition phenomena will be more appropriately described by the elliptical equations. Then, the prediction of normal stresses becomes important. Because of the inability of modeling normal stresses with the two-equation models, we are pursuing the elliptical Reynolds stress model equations for the bypass transition studies. Dr. Z. Yang and I are working on the improvement of our previous near-wall Reynolds stress model for the purpose of modeling bypass transition.

2.8 Modeling of scalar turbulence:

Modeling of scalar turbulence is of great importance in turbulent heat transfer. Eddy viscosity models often fail in the prediction of heat transfer in many shear flows. We have developed a set of second order closure models based on the joint realizability (between velocity and scalar) and the experiments. Dr. A. Shabbir and I are working on this subject. A paper[8] was presented in *the Lumley Symposium: Recent developments in turbulence, November, 1990.*

3. Publications:

1. Shih, T.-H., 1990, "An Improved k-ϵ Model for Near-Wall Turbulence and Comparison with Direct Numerical Simulation," NASA TM 103221 ICOMP-90-16.

2. Shih, T.-H. and Hsu, A.T., 1991, "An Improved k-ϵ Model for Near-Wall Turbulence," AIAA-91-0611.

3. Michelassi, V. and Shih, T.-H., 1991, "Low Reynolds Number Two-Equation Modeling of Turbulent Flows," NASA TM 104368, ICOMP-91-06, CMOTT-91-01.

4. Shih, T.-H. and Mansour, N.N., 1990, "Modeling of Near-Wall Turbulence," *Proceeding of the International Symposium on Engineering Turbulence Modeling and Measurements*, September, 1990, Dubrovnic, Yugoslavia, Editors: W. Rodi, E.N. Ganic. or, NASA TM 103222 ICOMP-90-0017.

5. Shih, T.-H., 1990, "Modeling of 3D Turbulent Boundary Layer Flows," American Physical Society Forty-Third Annual Meeting, 1990, Cornell, U. Ithaca, New York.

6. Shih, T.-H., 1991, "Rapid Distortion Theory on Homogenous Turbulence with Rapid Rotation," CMOTT Report.

7. Liou, W.W. and Shih, T.-H., 1991, "On the Basic Equations for the Second-order Modeling of Compressible Turbulence," CMOTT-91-06.

8. Shih, T.-H. and Shabbir, A., 1990, "Advances in Modeling the Pressure Correlation Terms in the Second Order Moment Equations," *the Lumley Symposium: Recent developments in turbulence, November, 1990, ICASE, NASA Langley Research Center, Edited by T.B. Gatski, S.Sarkar and C.G. Speziale*

9. Shih, T.-H., 1990, "Advancements in Engineering Turbulence Modeling," 9th NASP Technology Symposium, Paper-105, November, 1990, Orlando FL.

10. Shih, T.-H., Chen, J.-Y. and Lumley, J.L., 1991, "Second Order Modeling of Boundary Free Turbulent Shear Flows," AIAA 91-1779.

Experiments and Modeling

Aamir Shabbir

1. Motivation and Objectives

The usual approach in establishing the correctness and accuracy of turbulence models is to numerically solve the modeled differential equations and then compare the results with the experiment. However, in the case of a discrepancy, this procedure does not pinpoint where in the model the drawback lies. It is also possible that the model overcompensates one physical phenomenon and undercompensates the other so that the net result is a good agreement between the two. Therefore a more desirable approach is to directly compare the individual terms in the equations with their models. To achieve this objective primarily physical experiments have been used to carry out the second moment budgets. These can then be used to analyze and assess various models and closure assumptions and seek improvements/modifications where models prove deficient.

2. Work Accomplished

2.1 Evaluation and Development of Turbulence Models for Pressure Correlations.

A direct comparison between the pressure strain and pressure temperature-gradient correlations and their closure models is carried out. The flows used include both physical and numerical experiments on homogeneous shear flows and physical experiments on buoyant plumes. Models considered include both the linear and the more elaborate non-linear ones. It is found that the non-linear models provide a much better agreement with these experiments than the linear ones. A new model for the slow part of the pressure temperature-gradient correlation is also derived using joint realizability concept.

2.2 On the Ratio of Mechanical to Thermal Time Scales in Turbulent Flows.

The ratio of these time scales is very often employed in the two equation turbulence models. The study of Béguier et al (1978) recommended this

ratio to be around 2.0. The current analysis using the buoyant plume and homogeneous shear flow experiments shows that this value is about 3.0. It is shown that this departure from the commonly used value is a consequence of the local equilibrium assumption being not satisfied by these experiments.

2.3 Turbulent Buoyant Transport - A Comparative Study between Models and Experiments.

The more popular gradient diffusion type models for the turbulent transport (third moments) were found to underestimate the experiment by an order of magnitude. More complex models (André et al 1976, Lumley et al 1978), based on the simplification of exact transport equations of third moments, do a much better job in reproducing the third moments although the results are still less than satisfactory.

2.4 Experimental Balances of Second Moment Equations for a Buoyant Plume.

Despite large volume of work on second moment closure, there is very little experimental information available about the budgets of the second moments. Part of this reason stems from our inability, at present, to measure the pressure correlations. Experimental budgets for Reynolds stresses and heat fluxes have been carried out for a boundary free shear flow (round plume) and the pressure correlations are obtained as the closing terms in these budgets. These budgets show how different terms in the equations are distributed across the flow and can be used to analyze some of the modeling assumptions. For example they show that the assumption of local equilibrium is not justified for bulk of the flow field - an idea fundamental to the algebraic stress models.

2.5 X-wire Response in Turbulent Flows of High Intensity Turbulence and Low Mean Velocities.

This work is based on an experimental study, which was carried out at SUNY/Buffalo, of angular response of an x-wire, at low velocities (0.25m/s to 1m/s). It is found that the k-factor in the modified Cosine Law is strongly velocity dependent. The implications of this on multi component turbulence measurements are explored. Expressions are also derived for evaluating when the cross-flow errors begin to affect x-wire measurements.

2.6 Modeling of Turbomachinery Flows using the Average Passage Approach.

Turbomachineray flows are turbulent and unsteady and numerical calculation of a flow in a multistage machine, at present, is not possible. However, the effects of periodic unsteadiness can be accounted through the models for deterministic stresses which arise in the average passage equation set (Adamczyk 1985). Exact equations governing the transport of these stresses have been derived and a two equation model is being developed and tested at present. The model uses ideas from turbulence modeling such as the gradient diffusion type hypotheses. This work is being performed in collaboration with J. Adamczyk of the Lewis Research Academy, at the NASA Lewis Research center.

3. Future Plans

3.1 Study the effect of buoyancy on turbulence by computating flows using turbulence models. In addition to environmental flows, such a work also has industrial applications e.g. cooling of nuclear reactors and electronic components, and "geyser" formation in fuel tanks in microgravity.

3.2 Seek improvements in the models for turbulent transport. In general the transport is not too important in most of the turbulent flows but in some applications, e.g. geophysical flows, the modeling of the transport could be critical in the success of a computation.

3.3 Seek improvements in the existing two equation models by incorporating newer models for pressure correlations etc.

3.4 Assess the models for deterministic stresses in a multistage turbomachinery environment.

4. Publications

1. Pressure Correlations in the Reynolds Stress and Heat Flux Equations - A Comparison between Experiment and Models. A. Shabbir. *APS Bulletin*, Vol. 35, No. 10, Nov. 90, Abstract KC4.

2. Evaluation of Turbulence Models for Predicting Buoyant Flows. A. Shabbir and D.B. Taulbee. *J. Heat Transfer*, 1990, Vol 112, No 4, pp 945-951.

3. Experiments on Round Turbulent Buoyant Plumes. A. Shabbir and

W.K. George. Under review for publication in *J. Fluid Mechanics.*

4. Advances in Modeling Pressure Correlation Terms in the Second Moment Equations. T.-H. Shih and A. Shabbir. Presented at the *Symposium honoring J. Lumley's 60th birthday*, November 90, NASA Langley Research Center.

5. X-wire Response in Turbulent Flows of High Intensity Turbulence and Low Mean Velocities. A. Shabbir, P.D. Beuther, and W.K. George. Submitted to *Experimental Thermal and Fluid Science.*

5. References

Adamczyk, J. J. "Model Equation for Simulating Flows in Multistage Turbomachinery", ASME Paper No. 85-GT-226. (1985)

André J.C., G. De Moor, P. Lacarrére and R. du Vachat "Turbulence Approximation for Inhomogeneous Flows: Part I. The Clipping Approximation", *J. Atmos. Sci.*, Vol. **33**, pp. 476-481, (1976)

Béguier, C., I. Dekeyser and B. E. Launder "Ratio of Scalar and Velocity Dissipation Time Scales in Shear Flow Turbulence" ," *Phys. Fluids*, Vol. **21**, pp. 307-310 (1978).

Lumley, J. L., O. Zeman and J. Siess "The influence of Buoyancy on Turbulent Transport", *J. Fluid Mech.*, Vol. **84**, pp. 581-597 (1978).

Center for Modeling of Turbulence and Transition
Research Briefs - 1990

Modeling of Compressible Turbulent Shear Flows

William W. Liou

1. Motivation and Objectives

Despite all the recent development in computer technologies and numerical algorithms, full numerical simulations of turbulent flows are feasible only at moderate Reynolds numbers and for flows with relative simple geometries. Turbulence models provide alternatives in the pressing need for the prediction of turbulent flows and,in fact, have become an important pacing factor for the successful development of computational fluid dynamics (CFD). With the advent of supercomputers, however, it has become more affordable to apply second order closure models in the prediction of flows with complex effects; such as strong curvature, three-dimensionality and compressibility. The main goal of this research is to develop new second order moment closures for compressible turbulence. It has been shown that the models based on the extension of those developed originally for incompressible flows fail to predict adequately turbulent flows at high Mach numbers. In this attempt, the compressibility effects will be explicitly considered. A successful development of these models that take into account directly the compressibility effects may have a range of technological implications in the design of supersonic and hypersonic vehicles.

2. Work Accomplished

During this early stage of the task, the goal is to obtain an objective yet comprehensive understanding of the development and the current status of compressible turbulence modeling. Due to the variable density effects in compressible flows, density correlation terms appear in the governing equations for the mean flow, if the conventional ensemble averaging technique is applied. These terms do not exist in incompressible flows and need to be modeled. On the other hand, the mass-weighted-averaging or Favre procedure generates a set of mean equations that have the similar forms as they are for incompressible flows. One may then incline to use the incompressible analog in compressible flow calculations. A simple test, however, should show that a direct application of the exact incompressible models fails. One of the main effects that is excluded in incompressible models is the finite propagation

speed of disturbances. In compressible flows, modulation of flow properties occurs only within Mach cones of influence, with acoustic time delay. This introduces additional scales for the transport properties. Caution also needs to be exercised in comparing Favre-averaged calculations with experiments, since the differences between Favre-averaged and measured quantities may not be negligible at high Mach numbers.

Compressible turbulence modeling is still in its infancy. This appears to be true both theoretically and computationally. Recently, a new concept called dilatation dissipation was proposed. Dilatation dissipation, as opposed to the solenoidal dissipation in incompressible flows, accounts for the viscous dissipation of turbulent kinetic energy due to volume fluctuations. Models accommodating this effect show the importance of this additional drain of turbulent kinetic energy in order to obtain adequate model predictions. Dilatation dissipation appears to be among the direct consequencies of compressibility effects.

Another school of thought on compressibility effects focuses on the changes of turbulence structures at high Mach numbers. Note that these structures are identified by using conditional sampling techniques in experiments. Due to the communicability problem between interacting elements, structures that are highly efficient in extracting energy from the mean flow at low Mach numbers no longer prevail as the Mach number increases. They are replaced by structures that are less sensitive to the Mach number. This selective amplifying behavior is describable by quasi-linear theory, which view the turbulence energetics as physical manifestations of ongoing nonlinear instability in turbulent shear flows.

The above mentioned matters are described in detail in an ICOMP/ CMOTT report [1] that is in preparation. Equations for the second order moments and the mean flow as a result of the application of different averages will also be given. Modeling methodologies used in compressible flow calculations will be reviewed. The evaluation process performed during the present stage of the research has identified avenues that will be pursued during the next period of this task.

3. Future Plans

(1) Develop second order models for compressible turbulence based on ensemble averages. This may be assisted by first developing $k - \epsilon$ types of models to identify important mechanisms.

(2) Develop unconventional models that incorporate explicitly the characteristics of the structures of compressible turbulence.

The developed models will be applied to certain benchmark flows with and/or without chemical reactions.

4. Publications

1. Liou, W. W. and Shih, T.-H., "On the Basic Equations for the Second-order Modeling of Compressible Turbulence," CMOTT-91-06, 1991.
2. Liou, W. W. and Morris, P. J., "An Comparison of Numerical Methods for the Rayleigh Equation in Unbounded Domains," CMOTT-91-05, 1991.

RNG in Turbulence and Modeling of Bypass Transition

Zhigang Yang

1. Motivation and Objectives

Since I joined CMOTT on July 1990, I have been working on two research projects. The first project concerns the Renormalization Group (RNG) analysis of turbulence and the second project is on the calculation of bypass transition through turbulence modeling. In addition, the preparation of two papers on work performed at was completed.

Application of RNG in turbulence was proposed by Yakhot and Orszag in 1986. RNG is a process which eliminates systematically the small scales, and represents the effect of those eliminated small scales on the uneliminated large scales as the changes in the transport properties. It is because of this property of RNG that Yakhot and Orszag suggested that RNG could be used as a model builder in turbulence modeling. They also presented a $k-\epsilon$ model in their 1986 paper. However, this paper is lengthy, with many unstated assumptions. Our aim is first to understand, and to validate the RNG approach in turbulence through an independent study. We will then study the possibility of constructing RNG based turbulence models, and try to proceed to do the turbulence modeling through RNG in parallel with the classical approach. We will also compare the numerical predictions made by RNG models and by classical models against data from Direct Numerical Simulation and against experimental data from different benchmark cases.

In a quiescent environment, the transition is initiated by the instability of the laminar boundary layer to Tollmien-Schlichting waves. These waves are amplified with streamwise distance and eventually breakdown into turbulent spots, which are precursors of turbulent boundary layer. While in an environment with high freestream turbulence, the transition is found to be a bypass one in which turbulent spots are formed without Tollmien-Schlichting wave amplification. The formation of turbulent spot is a random process, and flow within a turbulent spot is almost fully turbulent. This suggests the possibility of using turbulence modeling to describe and predict the bypass transition. There have been some works in this direction, primarily using different versions of two equation models. Bypass transition is predicted, as the level of the freestream turbulence is increased. However, it is found that the predicted transition is much sharper than that observed in the experi-

ment. In addition, the predicted transition depends on the description of the initial profiles to an certain extent. The works we propose to do are twofold. 1) We will be using a low Reynolds number version of Reynolds stress model rather than the two equation model. This would bring in more physics, and hopefully would fit better the complicated flows such as bypass transition. 2) We will be using an elliptic solver rather than a parabolic solver for this boundary layer transition. This way, we will be able to include the effect of the leading edge. The testing case will be flow passing a flat plate. Both the zero pressure gradient case and the non-zero pressure gradient case will be tested.

2. Work Accomplished

1. Nonlinear dynamics near the stability margin in rotating pipe flow.

The nonlinear evolution of marginally unstable wave packets are studied in rotating pipe flow. These flows depend on two control parameters, which may be taken to be the axial Reynolds number Re and the rotation rate q. Marginal stability is realized on a curve in the (Re, q) plane, and we explore the entire marginal stability boundary. As the flow passes through any point on the marginal stability curve, it undergoes a supercritical Hopf bifurcation and the steady base flow is replaced by a traveling wave. The envelope of the wave system is governed by a complex Ginzburg-Landau equation. The Ginzburg-Landau equation admits Stokes waves, which correspond to standing modulations of the linear traveling wavetrain, as well as traveling wave modulations of the linear wavetrain. Bands of wavenumbers are identified in which the nonlinear modulated waves are subject to a side-band instability.

This work[1] was reported in APS/DFD meeting in November 1990. A paper for this work has been submitted to JFM for consideration of publication. The paper is co-authored with S. Leibovich of Cornell University. This work was supported by AFOSR-89-0346.

2. Unstable viscous wall modes in rotating pipe flow. (AIAA Paper No. 91-1801)

Linear stability of flow in rotating pipe is studied. These flows depends on two parameters, which can be taken as the axial Reynolds number Re and the rotating rate q. In the region of $Re \gg 1$ and $q = O(1)$, the most unstable modes are wall modes. The wall modes are found to satisfy a simpler set of equations containing two parameters rather than four parameters as in the full linear stability problem. The set of equations is solved numerically and asymptotically over a wide range of the parameters. In the limit of $Re \to \infty$,

the eigenvalue reaches the inviscid limit and the eigenfunction shows a two layer structure. The eigenfunction reaches the inviscid limit over the main part of the domain, while near the wall of the pipe, the eigenfunction is represented by a viscous solution of the boundary layer type.

This work[2] is to be presented at the AIAA 22nd Fluid Dynamics, Plasma Physics and Lasers Conferences, June 24-26, 1991. The paper is co-authored with S. Leibovich of Cornell University. This work was supported by AFOSR-89-0346.

3. RNG in turbulence modeling.

This work is done in collaboration with Dr. T.H. Shih of CMOTT. In this work, we carry out an independent study of the work done in the paper by Yakhot and Orszag up to their derivation of $k-\epsilon$ equation. Many of their results are repeated. However, we also found some discrepances, and some unclaimed assumptions in their derivations.

3. Future Plans

1. Currently, we are testing and improving the low Reynolds number version of Reynolds stress model proposed by Shih and Mansour (1990) in the simple shear flows, such as channel flow and boundary layer flow. This model is going to be used in the calculation of bypass transition.

2. We will carry an independent derivation of $k-\epsilon$ equation using RNG, and compare it with the one presented by Yakhot and Orszag. We will also compare the prediction of RNG $k-\epsilon$ model with the other $k-\epsilon$ models, in both the high Reynolds number case and the low Reynolds number case.

4. Publications

[1] Yang, Z. and Leibovich, S. 1990 "Nonlinear dynamics near the stability margin in rotating pipe flow", Submitted to *J. Fluid Mech.*

[2] Yang, Z. and Leibovich, S. 1990 "Unstable viscous wall modes in rotating pipe flow", AIAA Paper 91-1801.

5. References

Yakhot, V. and Orszag, S.A. 1986 Renormalization group analysis of turbulence. *J. Sci. Comput.* Vol. 1, No. 1, 3-51.

Shih, T.H. and Mansour, N.N. 1990 Modeling of near wall turbulence. NASA TM-103222, ICOMP-90-0017.

Turbulence Modeling in Supersonic Combusting Flows

Tawit Chitsomboon

1. Motivation and Objectives

To support the National Aerospace Plane project, the RPLUS3D CFD code has been developed at the NASA Lewis Research Center. The code has the capability to solve three dimensional flowfields with finite rate combustion of hydrogen and air. The combustion processes of the hydrogen-air system are simulated by an 18-reaction path, 8-species chemical kinetic mechanism. The code uses a Lower-Upper (LU) decomposition numerical algorithm as its basis, making it a very efficient and robust code. Except for the Jacobian matrix for the implicit chemistry source terms, there is no inversion of a matrix even though it uses a fully implicit numerical algorithm.

The main purpose of this work is to incorporate a k-ϵ (two equation) turbulence model into the RPLUS3D code.

2. Work Accomplished

Since February 1990, when this work was started, some of the more important accomplishments are categorized as follows:

1) Add a k-ϵ turbulence model: The model selected is in a high Reynolds number form. The low Reynolds number form could not be used economically in the case of a three dimensional flow with chemical reaction since it demands too much in computer resources. The addition was designed to be as modular as possible but some interactions with the main code are needed in order to be more efficient. The first test case tried was a Mach 0.5 flow over a flat plate. The velocity profile compare very well with the log-law profile. The friction coefficient also compares well with the Van Driest correlation. More validations will be performed for other flows such as free shear layer and jet flows.

2) Improved accuracy and convergence rate: According to a stability analysis of a model equation, it is shown that the RPLUS3D code excessively added artificial damping to the right hand side of the algorithm while at the same time it overestimated the spectral radii on the left hand side. These excessive additions would not give an optimum convergent rate. Mod-

ifications were made such that true directional spectral radii were added to the left hand side and the artificial damping terms were reduced to optimum values in accord with the stability analysis.

A test run was made of a Mach 4 flow of air over a 10 degree compression ramp. It was found that the modified code converged to machine zero about five times faster than the original code while at the same time it somewhat improved the shock resolution.

3) Added consistent damping terms at block interfaces: It had been observed that at the block interface of a multi-block grid, wiggles developed. This happened because the damping terms at the interface were not consistent with those at the interior points.

4) Validated RPLUS3D with laminar flows over flat plates: The test cases run were for Mach numbers of 0.1, 0.3 and 0.5. Results of all cases seemed to be good except for the region of high curvature of the velocity profile near the edge of the boundary layer.

5) Add two dimensional capability to the code: It turned out that this is not a trivial task especially for a finite volume code like RPLUS3D. It is nice that now the code can solve a 2D flow without having to carry the 3rd direction along as a redundancy. There is, of course, no need to maintain a separate 2D code.

6) Implemented a local time stepping capability: The original code always ran at a fixed time step of 1 second. For most flows this corresponds to using a very large CFL number which may not be conducive to a fast convergence rate. With the local time stepping, it was found that an optimum CFL number was, in agreement with other investigators, around 5 to 7.

7) Implemented implicit boundary conditions: This addition enhanced the convergence rate by about 30 percent at the expense of a more complex code and an increase of about 20 percent in CPU time per iteration step. There seems to be, then , no net advantage of the implicit boundary condition except maybe in the area of robustness.

8) Changed input file: Instead of having to scan a whole subroutine to set up a problem, a user now can change numbers in a small file of length about one page. To start up a run from a previous run one now needs only to change a parameter in this input file without having to recompile the input subroutine as before.

9) Solved two 3D hypermixing flow fields of W.Hingst and D.Davis: This work was performed in collaboration with Dr. A.C. Taylor of Old Dominion University. My task was to set up the program for these particular problems

and to generate the grid for one of the problems.

3. Future Plans

The work plan for the year 1991 consists of both basic model implementations and practical applications of the code :

- Continue to validate the baseline k-ϵ model.
- Add compressibility effects to the base line model.
- Apply the base line model to re-solve the 3D flowfields mentioned in the previous section.

Development of New Flux Splitting Schemes

Meng-S. Liou and Christopher J. Steffen, Jr.

1. Motivation and Objectives

Maximizing both accuracy and efficiency has been the primary objective in designing a numerical algorithm for computational fluid dynamics (CFD). This is especially important for solution of complex 3D systems of Navier-Stokes equations which often include turbulence modeling and chemistry effects. Recently, upwind schemes have been well received for both their capability of resolving discontinuities and their sound theoretical basis in characteristic theory for hyperbolic systems. With this in mind, we present two new flux splitting techniques for upwind differencing.

2. Work Accomplished

The first method is based upon High-Order Polynomial Expansions (HOPE) of the mass flux vector [1]. The present splitting results in positive and negative mass flux components that vanish at $M=0$. Thus the error in the Van Leer scheme which results in the diffusion of the boundary layer is eliminated. We also introduce several choices for splitting the pressure and examine their effects on the solution.

The second new flux splitting is based on the Advection Upwind Splitting Method (AUSM for short) [2]. In Navier-Stokes calculations, the diffusion error present in Van Leer's flux splitting scheme corrupts the velocity vector near the wall. In the AUSM, a proper splitting of the advective velocity component leads to an accurate resolution of the interface fluxes. The interface velocity is defined using the Mach number polynomial expansion in the mass flux, then the convective fluxes follow directly. Again, several choices of pressure splitting are possible among which a simple Mach number splitting according to characteristics appears to be the best in terms of accuracy. The scheme has yielded results whose accuracy rivals, and in some cases surpasses that of Roe's method, at reduced complexity and computational effort. The calculation of the hypersonic conical flow demonstrates the accuracy of the splittings in resolving the flow in the presence of strong gradients. The second series of tests involving the 2D inviscid flow over a NACA 0012 airfoil demonstrate the ability of the AUSM to resolve the shock

discontinuity at transonic speed and the level of entropy generation at the stagnation point.

In the third case we calculate a series of supersonic flows over a circular cylinder. The Roe splitting in all conditions and grids tested yielded anomalous solutions (sometimes referred to as the carbuncle phenomenon), which could appear as non-symmetric, protuberant, or indented contours. The AUSM gave expected solutions in all calculations.

The fourth test deals with a 2D shock wave/boundary layer interaction. This provides an opportunity to accurately resolve a laminar separation region and to compare the ability to resolve a non grid-aligned shock with other methods.

3. Future Plans

Future plans are primarily concerned with the AUSM. A detailed stability analysis for this new technique will be useful. The idea of splitting the *advective velocity* opens up a whole family of potential schemes. Therefore, a comprehensive study of the interaction between various pressure and advection velocity splitting methods is necessary to optimize both accuracy and efficiency. Additionally, a 2D turbulent calculation would be a good test of the scheme's ability to solve a coupled system of $\kappa - \epsilon$ equations.

4. Publications

1. Liou, M.-S. and Steffen, C.J.Jr., "High-Order Polynomial Expansions (HOPE) for Flux-Vector Splitting," (to be presented at the ICES'91 Conference, August 11-16, 1991)
2. Liou, M.-S. and Steffen, C.J.Jr., "Development of a New Flux Splitting Scheme," (to be presented at the AIAA Tenth CFD Conference, June 24-26, 1991)

Progress of Simulations for Reacting Shear Layers

Sheng-Tao Yu

1. Motivation and Objectives

In the past six months, the effort was devoted to the development of a high speed, chemically reactive shear layer test rig. The purpose of the experiment is to study the mixing of oxidizer and fuel streams in reacting shear layers for various density, velocity, and Mach number. The primary goal is to understand the effects of the compressibility upon mixing and combustion in a fundamental way. Therefore, a two-dimensional shear layer is highly desirable for its simplicity to quantify the compressibility effects.

The facility consists of a two-stream wind tunnel with two independent gas supplies. After passing through flow-management devices located upstream, each gas stream expands to its predetermined Mach number by means of a contoured center body and tunnel walls. Various combinations of flow conditions of high-speed stream and low-speed stream allows for the systematic study of mixing and reactions of compressible shear layers.

2. Work Accomplished

The RPLUS 2D code is used to calculate the flow fields of different sections of the test rig. The emphasis was on the supersonic nozzle design, the vitiation process for the hot air stream and the overall thermodynamic conditions of the test matrix.

The $k-\epsilon$ turbulence model with wall function has been successfully implemented in the RPLUS code. The k and ϵ equations are solved simultaneously and the the LU scheme is used to make it compatible with the flow solver. The coupling between the flow solver and the $k-\epsilon$ solver depends on the turbulence viscosity only, and the $k-\epsilon$ solver is separated from the flow solver to reduce the complexity. The newly developed code has been used for the compressible shear layer calculations. Many cases of the compressible free shear layer with various convective Mach numbers and density ratios have been simulated using the compressible $k-\epsilon$ solver. The results are summarized in two technical papers.[5,6] Currently, the $k-\epsilon$ solver is a standard feature in the RPLUS 2D code and the code has been distributed to the industry and universities through NASP group. Locally, Duncan and Tsai are using the $k-\epsilon$ solver for their research work.

3. Future Plans

Physical phenomena of the reactive free shear layer can not be adequately described by the $k - \epsilon$ model coupled with the Reynolds averaged flow equations. The properties of the vortical flows which dominate the whole flow field of free shear layers can only be illustrated by time marching numerical method with accurate spatial resolution. Traditionally, the spectrum methods were used for this kind of applications. However, very limited success has been reported for compressible flows using spectrum methods. On the other hand, recent development show promising results using high order central differencing and Essentially Non-Oscillatory (ENO) schemes. One developed by Lele of Stanford university using high order compact differencing is especially interesting. Future work includes Direct Numerical Simulation (DNS) of Navier Stokes equations for the chemically reactive flow and application to free shear layers.

In additional to the above mentioned work, I will serve as a consultant for the $k - \epsilon$ solver in the RPLUS code.

4. Publications

1. S. T. Yu, J. S. Shuen, and Y-L P. Tsai, "Three Dimensional Calculations of Supersonic Combustion Using a LU Scheme," to appear in the J. of Comput. Phys.

2. S.T. Yu, C.L. Chang, and C.L. Merkle, "Solar Rocket Plume/Mirror Interactions, " submitted to the J. of Spacecraft and Rockets.

3. S.T. Yu, B.J. McBride, K.C. Hsieh, and J.S. Shuen, "Hypersonic Flows Simulations with Equilibrium or Finite Rate Chemistry," submitted to Computers & Fluids for publication

4. S.T. Yu, "A Convenient Way to Convert 2D CFD Codes to Axisymmetric Ones," submitted to J. of Propulsion and Power as a technical note.

5. S.T. Yu, C.D. Chang, and C.J. Marek, "Modern CFD applications for the Design of a Reacting Shear Layer Facility," presented at the AIAA Science Meeting, 1991.

6. S.T. Yu, C.D. Chang, and C.J. Marek, "Simulation of Free Shear Layers Using a Compressible k-ϵ Model," accepted for presentation at the AIAA Propulsion Conference, 1991.

Appendix A

Organization - 1990

Position Chart

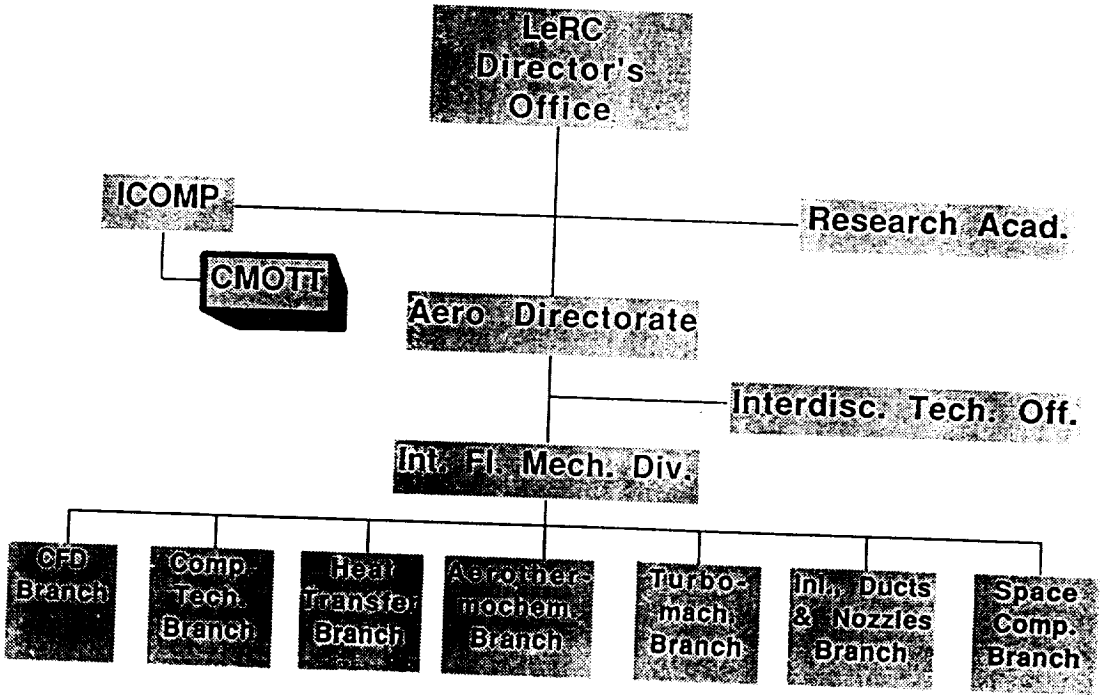

Manager

Dr. Louis A. Povinelli
Deputy Chief
Internal Fluid Mechanics Division
NASA Lewis Research Center

Coordinator

Dr. Meng-Sing Liou
Senior Scientist
Internal Fluid Mechanics Division
NASA Lewis Research Center

Technical Leader

Dr. Tsan-Hsing Shih
Senior Research Associate
ICOMP, NASA Lewis Research Center

Advisors

Dr. Marvin E. Goldstein
Chief Scientist
NASA Lewis Research Center

Professor John L. Lumley
Sibley School of Mechanical and
Aerospace Engineering
Cornell University

Professor Eli Reshotko
Department of Mechanical and
Aerospace Engineering
Case Western Reserve University

Member Listing

Names/Term	Affiliation	Research Areas
Chitsomboon, Tawit 5/90 - present	ICOMP	Algorithms, Code Development
Hsu, Andrew T. 5/90 - present	Sverdrup Tech., Inc.	PDF Turbulence Modeling
Lang, Nancy J. 5/90 - 8/90	NASA Intern Univ. of Michigan	Turbulence Modeling, CFD
Liou, Meng-Sing 5/90 - present	NASA LeRc	CFD Algorithms, High-speed Flow
Liou, William W. 11/90 - present	ICOMP	Compressible Flow Modeling, Weakly Nonlinear Wave Models
Shabbir, Aamir 5/90 - present	NRC	Buoyancy Effects on Turbulence
Shih, Tsan-Hsing 5/90 - present	ICOMP	Turbulence Modeling
Steffen, Christopher J. Jr. 10/90 - present	NASA LeRc	Upwind Algorithms Incompressible Flow
Yang, Zhigang 7/90 - present	ICOMP	RNG in Turbulence Modeling, Modeling of Bypass Transition
Yu, Sheng-Tao 3/90 - present	Sverdrup Tech., Inc.	Modeling of Chemical Reacting Flows, Direct Numerical Simulations

Appendix B

Seminars and Technical Meetings

B.1 CMOTT Seminar Seminars

The purpose of these seminars is to exchange ideas and opinions about the latest developments and current state of turbulence and transition research. The speakers are invited from within and outside of the NASA LeRC, including foreign speakers. This seminar series complements the informal CMOTT technical group meetings.

The abstracts of the seminars are given below.

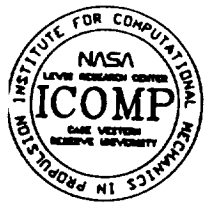

INSTITUTE FOR COMPUTATIONAL MECHANICS IN PROPULSION

ICOMP SEMINAR SERIES

Measurements in a Circular Jet of Helium into Quiescent Air*

by

John L. Lumley
Cornell University

Monday, June 4, 1990
9:00-10:30 a.m.
ERB Building 5, Room 119

The ability to model an inert flow with density fluctuations allows one to model a diffusion flame with fast chemistry, and gives insight into one aspect of the dynamics of compressible flows. With this in view, these measurements were made to calibrate a second order model for such flows. Measurements using shuttle-mounted hotwire and Way-Libby probes are described. For comparison, a jet of air into air was also measured. Moments up to fourth order were computed. The data are used to evaluate various modeling assumptions. Attempts are made to explain the greater spreading rate of the helium jet.

*From the Ph.D. thesis of N. R. Panchapakesan

Contact: Charles Feiler, PABX 3-6681

CENTER FOR MODELING OF TURBULENCE AND TRANSITION

CMOTT SEMINAR SERIES

ENGINEERING TURBULENCE MODELING
Present and Future?

Tsan-Hsing Shih
Center for Modeling of Turbulence and Transition

Wednesday, July 11, 1990
3.00-4:00 PM
ERB Building 5, Room 119

A summary of the present position of eddy-viscosity models (e.g. $k - \epsilon$) and second-order closure models (Reynolds stress models) is presented. Typical examples (comparisons between model predictions and experiments) show their abilities as well as their limitations.

Development of more advanced and complex schemes is discussed. The inclusion of such models into a CFD commercial code is feasible, but need intensive work - **a cooperative effort!**

Contact: T.-H. Shih, PABX 3-6680

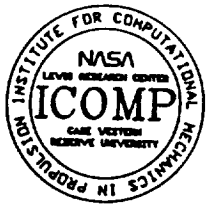

CENTER FOR MODELING OF TURBULENCE AND TRANSITION

CMOTT SEMINAR SERIES

FUNDAMENTAL IN-HOUSE EXPERIMENTS TO SUPPORT THE LEWIS TURBULENCE MODELING PROGRAM

Edward J. Rice
Inlet, Duct and Nozzle Flow Physics Branch

Wednesday, July 25, 1990
3.00 PM
Building 5, Room 119

The fundamental experiments conducted by members of the Inlet, Duct and Nozzle Flow Physics Branch of IFMD have been primarily for support of the shear flow control effort within the Division. Although this support effort is expected to continue, some work could be diverted (and in time expanded) to support the Turbulence Modeling Program currently underway within ICOMP. This new emphasis can be accomplished through an interactive effort between the Numerical Analysts and the Experimentalists. The current and planned experiments will be summarized in this talk and include: unsteady flow around airfoils (stationary and oscillating), 2D rapid diffusers (backward facing ramp), aspirated backward facing step, circular and rectangular jets (subsonic and supersonic), dual stream supersonic shear layer (annular geometry), and boundary layer transition. A swirl generator within the plenum of the CW-17, ERB rig allows the addition of swirling flow to any of the jet or shear layer experiments. The available and planned experimental instrumentation include: single, X-wire and three-wire hot wire anemometry, single and two element corona probe, multiple microphone and pressure transducer channels, Schlieren and laser-sheet flow visualization, and conventional and fiber-optic two-component LDA systems. The new 16 channel anemometry system allows simultaneous measurement with 8 X-wires. Some sample data will be presented to illustrate the current capability.

This is intended to be a group discussion type of workshop. The presentation will take 30 minutes and will be followed by 30 minutes of discussion between the numerical and experimental participants. The presentation will be general in nature intended mainly to acquaint the numerical analyst with the experimental capability which can support the numerical program through a cooperative effort.

For additional information contact: T.-H. Shih, PABX 3-6680

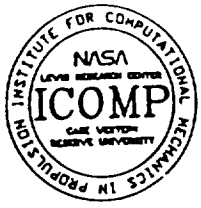

CENTER FOR MODELING OF
TURBULENCE AND TRANSITION

CMOTT SEMINAR SERIES

CFD-RELATED RESEARCH AT THE UNIVERSITY OF BRUSSEL AND TURBULENCE RESEARCH ACTIVITIES IN EUROPE

Prof. Charles Hirsch
Vrije Universiteit Brussel

Wednesday, July 25, 1990
1.00 - 2.00 PM
Building 5, Room 119

For additional information contact: L. Povinelli, PABX 3-5818

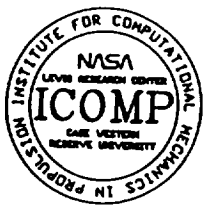

CENTER FOR MODELING OF TURBULENCE AND TRANSITION

CMOTT SEMINAR SERIES

CHAOTIC WANDERINGS THROUGH A LAND OF TURBULENCE MODELS

Russ Claus
Aerothermochemistry Branch

Wednesday, August 8, 1990
3.00 PM
Building 5, Room 119

A turbulence model user details his pursuit of the mythological "correct answer". The talk opens with some failed attempts to calculate seperated flows using a two equation turbulence model. Following this, additional attempts to achieve the "correct answer" through a series of Direct Numerical Simulations and Large Eddy Simulations will be described and the limitations of these approaches are highlighted. Finally, a re-examination of two-equation and a second order closure calculations of a jet in crossflow will be discussed.

A brief discussion of some turbulence modeling efforts being supported under the NASA SBIR program will also be described. This includes RNG modeling with Orszag and Yakhot, and PDF modeling for compressible flows with Kollman and Farshchi.

For additional information contact: T.-H. Shih, PABX 3-6680

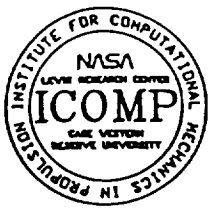

CENTER FOR MODELING OF
TURBULENCE AND TRANSITION

CMOTT SEMINAR SERIES

A COMPARATIVE ANALYSIS OF TWO EQUATION TURBULENCE MODELS

Nancy Lang
CFD Branch

Wednesday, August 22, 1990
3.00 PM
Building 5, Room 119

Several two equation models have been proposed and tested against benchmark flows by various researchers. For each study, different numerical methods or codes were used to obtain the results which were an improvement or success over some other model. However, these comparisons may be overshadowed by the different numerical schemes used to obtain the results. With this in mind, several existing two equation turbulence models, including k-ϵ and k-τ models, are implemented into a common flow solver code for near wall turbulent flows. Calculations are carried out for low Reynolds number, two dimensional, fully developed channel and boundary layer flows. The accuracy of the different models is established by comparing the turbulent kinetic energy, mean velocity, and shear stress profiles with the direct numerical simulations and experimental data.

For additional information contact: T.-H. Shih, PABX 3-6680

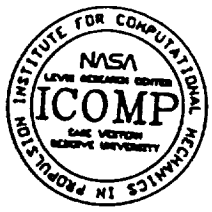

CENTER FOR MODELING OF
TURBULENCE AND TRANSITION

CMOTT SEMINAR SERIES

ON LENGTH SCALE EQUATIONS IN TWO-EQUATION TURBULENCE MODELS

Micha Wolfshtein
Faculty of Aerospace Engineering
Technion, Israel Institute of Technology
Haifa, Israel.

Wednesday, August 29, 1990
3.00 PM
Building 5, Room 119

Two-equation turbulence models show a great survivability between the very successful mixing length models and the Reynolds stress models. Yet the models are often critisized, mainly on the wide scatter of the computed results and on the difficulties encountered in the derivation of a reliable scale equation. The problem has been difficult to resolve due to:
(i) The large resources required for developing solvers and to run test cases on computers;
(ii) The theoretical difficulties to derive turbulence models from the Navier Stokes equations.
The demands from a "good" turbulence model are difficult to satisfy, and are often conflicting with one another. This point will be illustrated in a discussion of some possible approaches to this problem. In particular we shall refer to well established models like the dissipation or length scale models, as well as newer models like the volume of turbulence or time scale models. A generalised two-equation turbulence model will be used to demonstrate a possible approach for the improvement of two-equation models. Finally, a fourth order boundary layer solver for the generalized two equations model will be presented. The solver can handle both compressible and incompressible flows, with any two-equation model, with or without wall functions. Some results will be presented, for a flat plate boundary layer and for unseparated diffuser flows.

For additional information contact: T.-H. Shih, PABX 3-6680

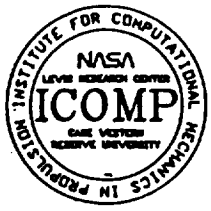

CENTER FOR MODELING OF TURBULENCE AND TRANSITION

CMOTT SEMINAR SERIES

EFFECT OF ACOUSTIC EXCITATION ON STALLED FLOWS OVER AN AIRFOIL

Khairul Zaman
Inlet, Duct and Nozzle Flow Physics Branch

Wednesday, September 5, 1990
3.00 PM
Building 5, Room 119

Experimental results on the subject are to be summarized focussing attention on post-stalled flows, i.e. flows that are fully separated from near the leading edge of the airfoil. The excitation results in a tendency towards reattachement, which is accompanied by an improved airfoil performance, although the flow may still remain fully seperated. It is observed that with increasing excitation amplitude, the effect becomes more pronounced but shifts to a Strouhal number which is much lower than that expected from linear, inviscid instability of the seperated shear layer. In addition, some results from a recent experiment on supersonic jets will be briefly reviewed emphasizing need for collaboration between experiment and computations.

For additional information contact: T.-H. Shih, PABX 3-6680

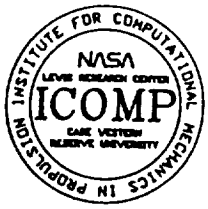

CENTER FOR MODELING OF
TURBULENCE AND TRANSITION

CMOTT SEMINAR SERIES

COMPUTATION OF ELLIPTIC FLOWS USING LOW-REYNOLDS-NUMBER TWO-EQUATION MODELS

Vittorio Michelassi
Energy Engineering Department
University of Florence, Italy

Wednesday, September 19, 1990
3.00 PM
Building 5, Room 119

Two new low-Reynolds number forms of the $k-\epsilon$ model will be presented. These exhibit better stability and stiffness characteristics as compared to the previous formulations. Model generality is improved by formulating the damping functions so that they do not depend on the wall distance. The proposed formulations are compared with eight other low Reynolds number two-equation turbulence models by computing the fully developed channel flow and the incompressible flow past a hill. Results are compared with available direct numerical simulation and experimental data. The flow solver is based on the approximate factorization technique and the artificial compressibility method requiring no (or very little) numerical damping. A simple linearization technique for the turbulence model source terms based on Taylor series expansion ensures implicit algorithm stability for all the models tested. Both numerical accuracy and computational efficiency are discussed.

For additional information contact: T.-H. Shih, PABX 3-6680

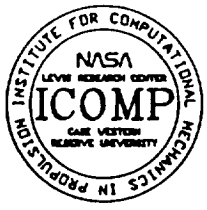

CENTER FOR MODELING OF TURBULENCE AND TRANSITION

CMOTT SEMINAR SERIES

Evaluation of Models for the Pressure Terms in the Second Moment Equations

Aamir Shabbir

Wednesday, October 10, 1990
3.00 PM
Building 5, Room 119

The usual approach in establishing the correctness and accuracy of turbulence models is to numerically solve the modeled differential equations and then compare the results with the experiment. However, in the case of a discrepancy, this procedure does not pinpoint where the drawback of the model lies. It is also possible that the model overcompensates one physical phenomenon and undercompensates another resulting in good agreement between the prediction and experiment. A more desirable approach is to individually compare each term in the equations with its model. This talk will focus on such a comparison for the pressure correlations appearing in the second moment equations. At present these correlations can not be measured but can be obtained by balancing the turbulent flux and Reynolds stress equations. Using this approach, pressure correlations will be directly compared with their models, which range from simple linear to more elaborate nonlinear ones. Also results will be shown for a newly developed model for the return to isotropy part of the pressure temperature-gradient correlation. The data used is from the homogeneous shear flow and the buoyant plume experiments as well as from the direct numerical simulation of homogeneous shear flow.

For additional information contact: T.-H. Shih, PABX 3-6680

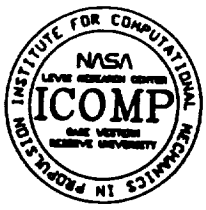

CENTER FOR MODELING OF
TURBULENCE AND TRANSITION

CMOTT SEMINAR SERIES

HEAT TRANSFER WITH INHOMOGENEOUS FREE STREAM TURBULENCE

S.N.B. Murthy
School of Mechanical Engineering
Purdue University, West Lafayette, IN 47907

Thursday, October 25, 1990
2:00 PM
Building 5, Room 119

The presence of free stream turbulence (FST) in a wall-bounded flow with heat transfer presents several interaction complexities. These depend upon (a) the state of the boundary layer, laminar, fully turbulent or transitional, (b) the nature of FST, especially its "peakiness" or inhomogeneity, and (c) other complications such as pressure gradient, geometry and cooling. An investigation is in progress on the possible application of (a) large eddy interaction hypothesis (based on Lumley's rational description of turbulence) and (b) spectral analogy between heat and turbulence kinetic energy to the simplest case of a flat wall, fully developed turbulent boundary layer with zero pressure gradient when there is heat transfer in the presence of homogeneous FST. An extension of the approach to the case of other types of boundary layers with inhomogeneous FST will be discussed.

For additional information contact: T.-H. Shih, PABX 3-6680

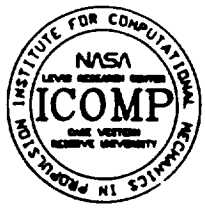

CENTER FOR MODELING OF
TURBULENCE AND TRANSITION

CMOTT SEMINAR SERIES

PRESSURE-STRAIN MODELLING AND THE RETURN TO ISOTROPY

M.M. Gibson
Imperial College of Science Technology,
London, England.

Wednesday, November 14, 1990
1.00 PM
Building 5, Room 119

Calculations of complex shear layers give the best results when the constant in Rotta's return-to-isotropy model is given values greater than those deduced from the measurements in grid turbulence. New data from grid turbulence are presented and assessed in the light of previous experiments. The results show that homogeneous turbulence decay is associated with increasing Reynolds number. It is argued that this finding has important implications for Reynolds-stress Modelling. Recent theoratical and experimental studies of the analogous model for pressure scrambling in the scalar-flux equations reveal even larger discrepancies in them "Monin constant". The implications for the future of second-moment modelling are discussed.

For additional information contact: T.-H. Shih, PABX 3-6680

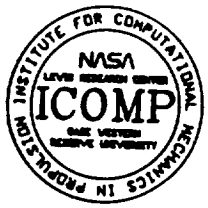

INSTITUTE FOR COMPUTATIONAL MECHANICS IN PROPULSION

ICOMP SEMINAR SERIES

CURRENT TRENDS IN TURBULENCE MODELLING

by

W. Rodi
University of Karlsruhe
Institute for Hydromechanics

Thursday, November 29, 1990
1:00-2:00 p.m.
ERB Building 5, Room 119

A brief review is given of recent work in the area of modelling turbulence in near-wall regions and by Reynolds-stress-equation models. Various low-Reynolds-number versions of the k-ε model and their damping functions are examined with the aid of results from direct numerical simulations and they are compared with respect to their performance in calculating boundary layers under adverse and favorable pressure gradients. A two-layer model is presented in which near-wall regions are resolved with a one-equation model and the core region with the standard k-ε model. Various applications of this model are shown. The ability of the various models to simulate laminar-turbulent transition in boundary layers is discussed. Recent applications of a basic Reynolds-stress-equation model to complex flows of practical interest are presented. Finally, some recent proposals for improved Reynolds-stress-equation models are outlined and an outlook on possible future turbulence model developments is given.

Contact: Charles Feiler, PABX 3-6681

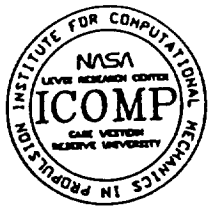

CENTER FOR MODELING OF TURBULENCE AND TRANSITION

COMPUTATION OF TRANSITIONAL AND TURBULENT FLOWS IN COMPLEX GEOMETRIES

George Em Karniadakis

Mechanical and Aerospace Engineering,
Program in Applied and Computational Mathematics,
Princeton University, Princeton, NJ.

Friday, March 22, 1991
2:00 - 3:00 PM
Building 5, Room 119

General, high-order numerical schemes are formulated appropriate for simulation of transitional and turbulent incompressible flows in complex geometries. In particular, the new schemes are based on mixed explicit/implicit stiffly stable time-stepping methods and explicit treatment of the pressure boundary condition that lead to enhanced stability and arbitrarily high-order time-accuracy dictated entirely by the employed integration rule. Hybrid spectral element methods are then used for the spatial discretization of the variable properties governing equations in three-space dimensions. Special Neumann/viscous sponge type boundary conditions are developed for open flows. Large or subgrid scales in the high Reynolds number regime are modeled through renormalization group (RNG) techniques.

Simulations are than performed to study the transitional and fully turbulent stages of spatially developing flows. Here, we consider the flow over a backward- facing step, and the three-dimensional flow past a circular cylinder. For the first flow, the secondary instability is first investigated and the three-dimensional transitional states are computed through direct simulation (DNS). Transport and subgrid RNG models are then employed to simulate the high Reynolds number flow and heat transfer. Comparisons with experimental data in both regimes are presented. For the second, three-dimensional equilibria are accurately resolved via DNS; the series of bifurcations followed is simulated until the cylinder wake becomes turbulent. Our results suggest a successive period doubling in the temporal response of the flow, which eventually leads to a disordered state and renders the wake turbulent.

For additional information contact: T.-H. Shih, PABX 3-6680

CENTER FOR MODELING OF TURBULENCE AND TRANSITION

A DYNAMIC MODEL FOR LARGE EDDY SIMULATION OF TURBULENT FLOWS

Parviz Moin

Stanford University
and NASA Ames Research Center

Tuesday, March 26, 1991
10:00 - 11:00 AM
Room 176, Sverdrup Building

One major drawback of the subgrid scale models currently used in large eddy simulations is their inability to correctly represent with a single universal constant different turbulent flows in rotating or sheared flows, near solid walls or in transitional regimes. A new subgrid scale model will be presented which alleviates many of these drawbacks. The model coefficient is inputted dynamically rather than inputted a priori. The basic idea in the derivation of the model is the utilization of the spectral information which is computed directly. This rather rich spectral information is not available in methods based on Reynolds averaged equations. The subgrid scale stresses obtained using the proposed model vanish in laminar flow and at a solid boundary. The results of large eddy simulation of transitional and turbulent channel flow that use the proposed model are in good agreement with the direct numerical simulation data. The same model was applied to the decay of isotropic turbulence with excellent agreement with the experimental data. The model has been extended to compressible flows. A dynamic subgrid scale turbulent Prandtl number was derived. Its dependence on molecular Prandtl number, direction of scalar gradient, and the distance from the wall are in accordance with direct simulation.

For additional information contact: T.-H. Shih, PABX 3-6680

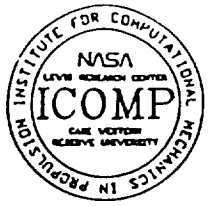

CENTER FOR MODELING OF TURBULENCE AND TRANSITION

CMOTT SEMINAR SERIES

TURBULENCE AND DETERMINISTIC CHAOS

Robert G. Deissler

Lewis Research Academy
NASA Lewis Research Center

Wednesday, April 10, 1991
3:00 - 4:00 PM
Room 119, Building 5

Several turbulent and nonturbulent solutions of the Navier-Stokes equations are obtained. The unaveraged equations are used numerically in conjunction with tools and concepts from nonlinear dynamics, including time series, phase portraits, Poincaré sections, largest Liapunov exponents, power spectra, and strange attractors.

Initially neighboring solutions for a low-Reynolds-number fully developed turbulence are compared. The turbulence, which is fully resolved, is sustained by a nonrandom time-independent external force. The solutions, on the average, separate exponentially with time, having a positive Liapunov exponent. Thus, the turbulence is characterized as chaotic.

In a search for solutions which contrast with the turbulent ones, the Reynolds number (or strength of the forcing) is reduced. Several qualitatively different flows are noted. These are, respectively, fully chaotic, complex periodic, weakly chaotic, simple periodic, and fixed-point. Of these we classify only the fully chaotic flows as turbulent. Those flows have both a positive Liapunov exponent and Poincaré sections without pattern. By contrast, the weakly chaotic flows, although having positive Liapunov exponents, have some pattern in their Poincaré sections. The fixed-point and periodic flows are nonturbulent, since turbulence, as generally understood, is both time-dependent and aperiodic.

For additional information contact: T.-H. Shih, PABX 3-6680

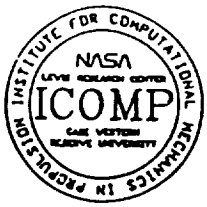

CENTER FOR MODELING OF TURBULENCE AND TRANSITION

CMOTT SEMINAR SERIES

A CRITICAL ASSESSMENT OF TURBULENCE MODELING

Charles G. Speziale

ICASE, NASA Langley Research Center

Monday, April 22, 1991
1:30 - 2:30 PM
Room 175, Sverdrup Building

A variety of turbulence models including zero, one and two-equation models as well as second-order closures will be reviewed. Based on comparisons with results from physical and numerical experiments on homogeneous turbulence, a strong case will be made for the superior predictive capabilities of second-order closure models. It will be shown how some significant improvements in second order closure models have been recently achieved by means of invariance arguments coupled with a dynamical systems approach. Several applications will be discussed including recent extensions to high speed compressible flows that were developed in connection with the National Aerospace Plane Project.

For additional information contact: T.-H. Shih, PABX 3-6680

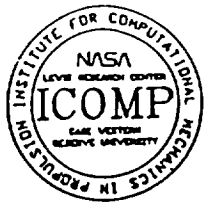

CENTER FOR MODELING OF TURBULENCE AND TRANSITION

CMOTT SEMINAR SERIES

A CRITICAL-LAYER THEORY FOR BOUNDARY-LAYER TRANSITION

Reda R. Mankbadi

Lewis Research Academy
NASA Lewis Research Center

Tuesday, April 30, 1991
10:00 - 11:00 AM
Room 119, Building 5

An asymptotic critical-layer theory is developed to study nonlinear interactions of a triad of instability waves leading to boundary-layer transition. This triad consists of a spatially growing plane fundamental wave and a pair of symmetrical, subharmonic oblique waves. The spatial development of the waves is determined by nonlinear viscous flow in the critical layer. The theory successfully captures not only the linear and parametric resonance stages, but also the later fully interactive regime of the transition process including the saturation and decay stages. The analysis is fully nonlinear, in that all the nonlinearly generated waves that were not originally present, are accounted for in the analysis. The three-dimensional nonlinear modifications of the mean flow are also considered. The theory applies to both ribbon-induced and naturally occurring transition. The analytically obtained amplitude equations are highly accurate but simple enough to be used for practical transition predictions. Results presented explain experimental observations and reveal novel features of the phenomena.

For additional information contact: T.-H. Shih, PABX 3-6680

B.2 CMOTT Technical Meetings

These are CMOTT's biweekly group meetings. In each meeting, one speaker from either CMOTT or other local modeling efforts at the NASA LeRc presents new ideas or work under progress. The informal seminars were intended not noly to keep the members informed of the latest development of local turbulence and transition modeling research but also to increase interactions between group members and other researchers at the NASA LeRc.

The schedule of these biweekly events were widely disseminated before each series began. The following is the meeting schedule during the reporting period.

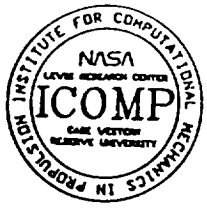

CENTER FOR MODELING OF TURBULENCE AND TRANSITION

Date: December 19, 1990

To: CMOTT Members and SVR and IFMD Staff

From: William W. Liou (6682)

Subject: CMOTT Biweekly Meeting

The following is a tentative schedule for CMOTT biweekly get-together from Dec. 19, 1990 to Feb. 27, 1991. In each meeting, one member of our group will give an informal presentation on the subject she/he is interested in or currently working on. This will not only give us opportunities to interact with each other, but also keep us informed about exciting approaches in modeling turbulence other than our own specialities. However, the format of the meeting after the current period is open to suggestions.

The meeting will start at 4:00 p.m. in Room 228, Sverdrup Building.

Dec. 19, 1990 Zhigang Yang (61-2123)
Understanding RNG in Turbulence: A Preliminary Report

Jan. 2, 1991 Tsan-Hsing Shih (6680)
Realizability Concept and Its Applications in Turbulence Modeling

Jan. 16, 1991 Wai-Ming To (5937)
Spectral Methods

Jan. 30, 1991 Le Tran (61-6701)
Stagnation Point Turbulence and Heat Transfer

Feb. 13, 1991 William W. Liou (6682)
Weakly Nonlinear Models for Turbulent Free Shear Flows

Feb. 27, 1991 Chris Steffen (8508)
Optimizing Laminar Accuracy

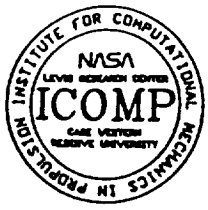

CENTER FOR MODELING OF TURBULENCE AND TRANSITION

Date: March 13, 1991

To: CMOTT Members and SVR and IFMD Staff

From: William W. Liou (6682)

Subject: CMOTT Biweekly Meeting

The following is a tentative schedule for the CMOTT biweekly get–together from March 20, 1991 to May 1, 1991.

This round of biweekly meetings will be more of presentations of progress and hurdles in pursuing the subjects than presentations of results. Therefore, active participation is expected from the attendants. Note that these meetings are different from the CMOTT Seminar Series, whcih are mainly formal presentations.

We would also appreciate some contributions from you. Subjects related to either the theoretical, experimental or computational aspects of turbulence and transition modeling are welcomed. Those who are willing to share their experience in these areas can contact me or Dr. T.-H. Shih at 6680 for further arrangement.

The meeting will start at 4:00 p.m. in Room 228, Sverdrup Building.

Mar. 20, 1991 K. Zaman (5888)
Low Frequency Fluctuations in Separated Flows – Experimental Evidence

Apr. 3, 1991 K. Kirtley (61-6659)
Let's Talk RNG

Apr. 17, 1991 T.-H. Shih (6680)
Lumley's New Formulation of Dissipation Equation

May 1, 1991 K. Kao (5965)
Stability of Compressible Couette Flows

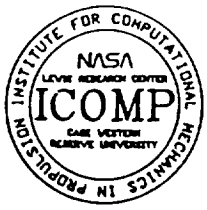

CENTER FOR MODELING OF TURBULENCE AND TRANSITION

Date: April 25, 1991

To: CMOTT Members and SVR and IFMD Staff

From: William W. Liou (6682)

Subject: CMOTT Biweekly Meeting

The following is a tentative schedule for the CMOTT biweekly get-together from May 1, 1991 to June 12, 1991. Please note that Dr. Shih's and Dr. Kao's talks have been rescheduled.

The presentations will be informal and active participation is expected from the attendants. These meetings complement the CMOTT Seminar Series, which are mainly formal presentations.

We would also appreciate some contributions from you. Subjects related to either the theoretical, experimental or computational aspects of turbulence and transition modeling are welcomed. Those who are willing to share their experience in these areas can contact me or Dr. T.-H. Shih at 6680 for further arrangement.

The meeting will start at 4:00 p.m. in Room 228, Sverdrup Building.

May 1, 1991 T.-H. Shih (6680)
Lumley's New Formulation of Dissipation Equation

May 15, 1991 A. Shabbir (5927)
On Some Closure Assumptions Regarding Time Scales, Local Equilibrium and Pressure Diffusion

May 29, 1991 Z. Yang (61-2123)
Near Wall $k-\epsilon$ Modeling: Another Crusade

June 12, 1991 K. Kao (5965)
Stability of Compressible Couette Flows

Appendix C
Collection of Publications

THE STUDY OF PDF TURBULENCE MODELS IN COMBUSTION

Andrew T. Hsu
Sverdrup Technology, Inc.
& Center for Turbulence Modeling
NASA Lewis Research Center
Cleveland, Ohio

9th National Aero-Space Plane
Technology Symposium
November 1-2, 1990

Paper Number 107

I. Introduction

(U) In combustion computations, it is well known that the predictions of chemical reaction rates (the source terms in the species conservation equations) are poor if conventional turbulence models are used. The main difficulty lies in the fact that the reaction rate is highly non-linear, and the use of averaged temperature, pressure and density produces excessively large errors. Moment closure models for the source terms have attained only limited success. The probability density function (pdf) method seems to be the only alternative at the present time that uses local instantaneous values of the temperature, density, etc., in predicting chemical reaction rates, and thus is the only viable approach for more accurate turbulent combustion calculations.

(U) The fact that the pdf equation has a very large dimensionality renders finite difference schemes extremely demanding on computer memories and thus impractical, if not entirely impossible. A logical alternative is the Monte Carlo scheme, which has been used extensively in statistical physics. The evolution equations for the joint pdf of the velocity and species mass fraction have been successfully solved using Monte Carlo schemes, see, e.g., Pope[1]. However, since CFD has reached a certain degree of maturity as well as acceptance, it seems, at least from the stand point of practical applications, that the use of a combined CFD and Monte Carlo scheme is more beneficial. Therefore, in the present study a scheme is chosen that uses a conventional CFD flow solver in calculating the flowfield properties such as velocity, pressure, etc., while the chemical reaction part is solved using a Monte Carlo scheme.

(U) A combined CFD-Monte Carlo computer algorithm has been developed recently. As a first calibration of the Monte Carlo solver recently developed in this work, the discharge of a heated turbulent plane jet into quiescent air is studied. Experimental data for this problem shows that when the temperature difference between the jet and the surrounding air is small, buoyancy effects can be neglected and the temperature can be treated as a passive scalar. The fact that jet flows have a self-similar solution lends convenience in the modeling study. Furthermore, the existence of experimental data for turbulent shear stress and temperature variance (temperature fluctuation) make the case ideal for the testing of pdf models wherein these

values can be directly evaluated.

(U) The following section presents the methodologies used in this study, and a discussion on the numerical results and their comparison with experimental data follows.

II. Method

2.1 Governing equations

(U) The Favre averaged momentum and species transport equations can be written as

$$\bar{\rho}\partial_t\tilde{u}_i + \bar{\rho}\tilde{u}_j\partial_j\tilde{u}_i = -\partial_i\bar{p} + \nu\partial_j\tau_{ij} - \partial_j\widetilde{u_i''u_j''}$$

$$\bar{\rho}\partial_t\tilde{Y}_i + \bar{\rho}\tilde{u}_j\partial_j\tilde{Y}_i = \bar{\rho}\partial_j(D\partial_j\tilde{Y}_i - \widetilde{Y_i''u_j''}) + \partial_j(D\partial_j\bar{\rho}\widetilde{\partial_j Y_i''}) + \rho\bar{w}_i$$

where u_i is the velocity and Y_i is the mass fraction. The major problem encountered in the numerical study of turbulent combustion lies in the modeling of the chemical source term, $\rho\bar{w}_i$, known as the chemistry closure problem. The Source term w_i is an exponential function of temperature, and it is well know that the use of averaged temperature, $\bar{T}$, in evaluating $\rho\bar{w}_i$ can cause egregious errors. Therefore the accurate prediction of turbulent combustion using conventional turbulence models becomes very difficult. This motivated the use of pdf methods. If the pdf, P. is given, then the mean of the source term can be evaluated exactly:

$$\rho\bar{w}_i = \int \cdots \int \rho w_i(Y_1, ..., Y_n, T, \rho)P(Y_1, ..., Y_n, T, \rho)dY_1...dY_n dT d\rho$$

To solve for the pdf, we need the following:

2.2 Evolution equation for the pdf

(U) The evolution equation for the probability density function of the mass fractions, temperature, and density, $P(Y_1, ..., Y_n, T, \rho)$, can be written as[1]

$$\bar{\rho}\partial_t\tilde{P} + \bar{\rho}\tilde{v}_\alpha\partial_\alpha\tilde{P} + \bar{\rho}\sum_{i=1}^{N}\partial_{\psi_i}\{w_i(\psi_1, ..., \psi_N)\tilde{P}\}$$

$$= -\partial_\alpha(\bar{\rho} < v_\alpha''|\psi_i > \tilde{P}) - \bar{\rho}\sum_{i=1}^{N}\sum_{j=1}^{N}\partial^2_{\psi_i\psi_j}(< \epsilon_{ij}|\psi_k > \tilde{P})$$

where the terms represent mean convection, chemical reactions, turbulent convection, and molecular mixing, respectively; $\tilde{P}$ is the density-weighted joint pdf:

$$\tilde{P} = \rho P,$$

ϵ is the scalar dissipation:

$$\epsilon_{ij} = -\rho D_{ij} \partial_j Y_i,$$

ψ_i's are variables such as the mass fractions, density, and temperature, and $<,>$ denotes the mathematical expectation of a function.

(U) The left hand side of the above equation can be evaluated exactly and requires no modeling; the right hand side terms contain the conditional average of the Favre velocity fluctuation and the conditional average of the scalar dissipation and require modeling.

2.3 Finite difference solution for the NS equations

(U) In order to simplify the problem so as to concentrate on the study of the pdf models, we have confined our numerical procedures to parabolic flows. A parabolic NS solver with a $k - \epsilon$ turbulence model has been developed. The $k - \epsilon$ model has been tested by solving standard cases such as flat plate boundary layers and free shear layers with satisfactory numerical results.

2.4 Monte Carlo scheme for the pdf equation

(U) A grid dependent Monte Carlo scheme has been employed, primarily following Chen and Kollmann[5]. The task here is to construct an ensemble of sample points, each sample has its own distinct properties such as temperature, mass fraction, etc.; these properties change with time or location such that the probability function of the ensemble evolves according to the evolution equation. Consequently, the pdf of the ensemble is the desired approximate solution for the pdf equation.

(U) Suppose N samples are assigned to a grid cell in the flow domain, the pdf for the ensemble of N samples can then be written as

$$\tilde{P}^*(\psi) = \frac{1}{N} \sum_{j=1}^{N} \delta(\psi - \phi_j)$$

where ϕ_j is the scalar function value carried by the j^{th} sample, e.g., the mass fractions, etc.

(U) In order to have the pdf $\tilde{P}^*$ evolve according to the pdf evolution equation, we discretize the equation on a given grid and write, for parabolic flows:

$$\tilde{P}^*_{x+dx,j} = \alpha_j \tilde{P}^*_{x,j+1} + \beta_j \tilde{P}^*_{x,j} + \gamma_j \tilde{P}^*_{x,j-1}$$

and require

$$\alpha_j + \beta_j + \gamma_j = 1$$

2.5 Recontamination in a Monte Carlo scheme

(U) Using a very simple test case of a convection/diffusion process with two scalars, it was found that the previous scheme[5] does not conserve mass fractions due to re-contamination. It is found that in order to conserve the mass fractions absolutely, one needs to add further restriction to the scheme, namely

$$\alpha_j + \gamma_j = \alpha_{j-1} + \gamma_{j+1} \qquad (*)$$

A new computer algorithm was devised and tested. This algorithm uses a few extra arrays to store informations form the previous time level and thus eliminates the repetition in the sampling process. With the simple test case of two scalars with assumed constant coefficients in the pdf equation, the new algorithm is shown to conserve the mass fractions perfectly. Deficiencies such as directional bias and re-contamination that were found in the previous algorithm are completely eliminated.

(U) It is not yet known whether one can indeed devise a scheme that satisfies relation (*) in general flows, where the coefficients of the pdf equation are variable and are calculated from the flow velocities, turbulence time scale, etc.

III. Results

(U) The sketch of a heated plane jet is given on this page. The flow domain is divided into 30 cells in the cross direction, and 100 samples are assigned to each cell. The numerical results from the present study are compared with experimental data in the following figures.

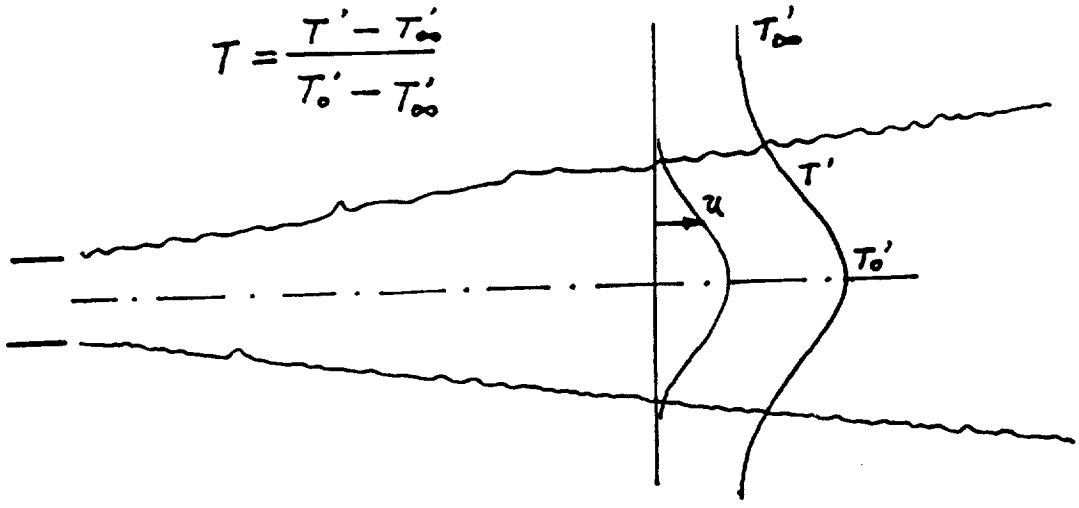

Figure 1. Sketch of a heated turbulent free jet.

(U) The numerical solution for the ensemble averaged pdf's of the temperature: $y/y_{0.5} = 0.$ where $y_{0.5}$ is the location where $T = 0.5T_0$. In order to interpret the data, the ensemble averaged pdfs are integrated to obtain the approximate continuous pdf: $P = P^*(\Delta T)/\Delta T$. The result of this integration is shown as vertical bars. The normal distribution is plotted as a dotted line for comparison.

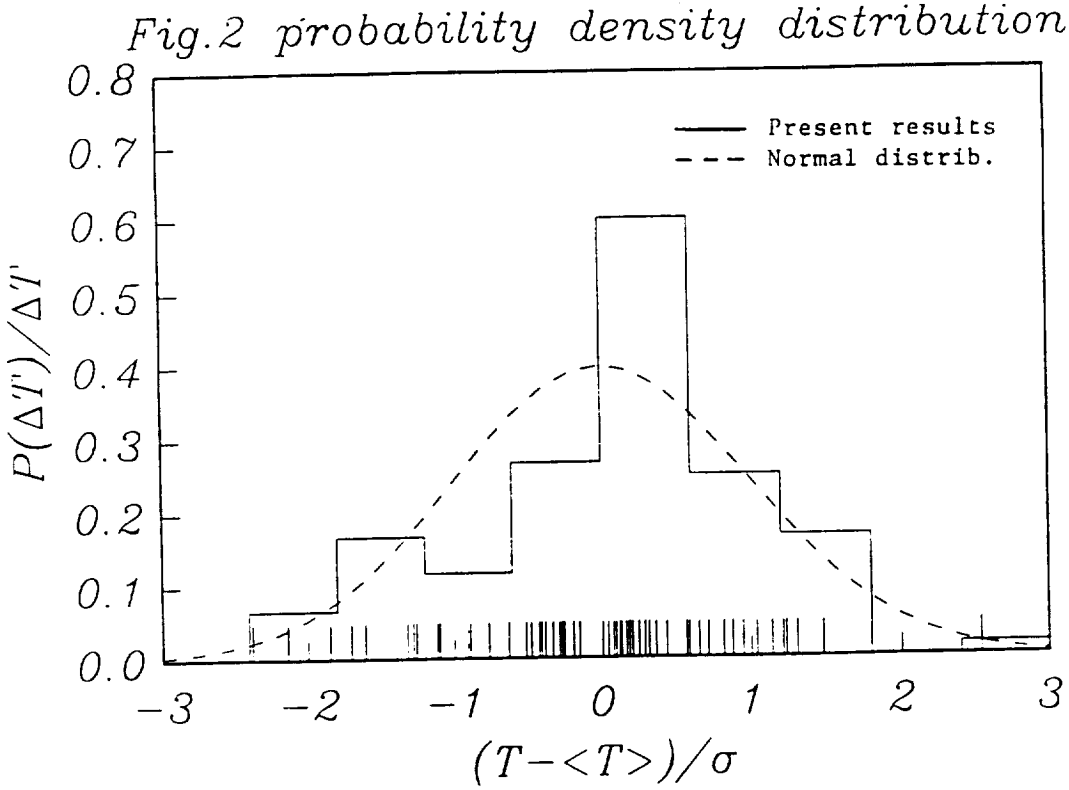

(U) The numerical solution for the ensemble averaged pdf's of the temperature: $y/y_{0.5} = 0.44$, where $y_{0.5}$ is the location where $T = 0.5T_0$. In order to interpret the data, the ensemble averaged pdfs are integrated to obtain the approximate continuous pdf: $P = P^*(\Delta T)/\Delta T$. The result of this integration is shown as vertical bars. The normal distribution is plotted as a dotted line for comparison.

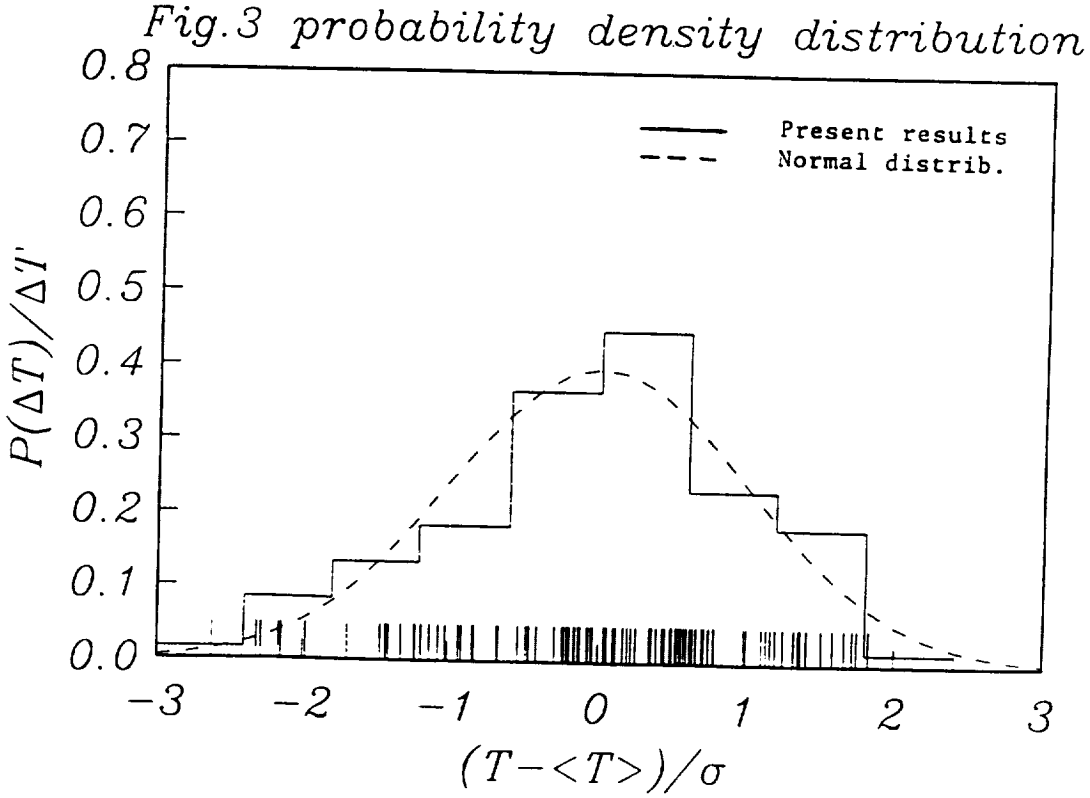

(U) The computed velocity profile is compared with experimental data from Foerthmann[7]. The good agreement between the numerical solution and experiments indicates that the parabolic flow solver employed in the present study is fairly accurate and can serve its purpose.

Fig.4 Velocity distribution

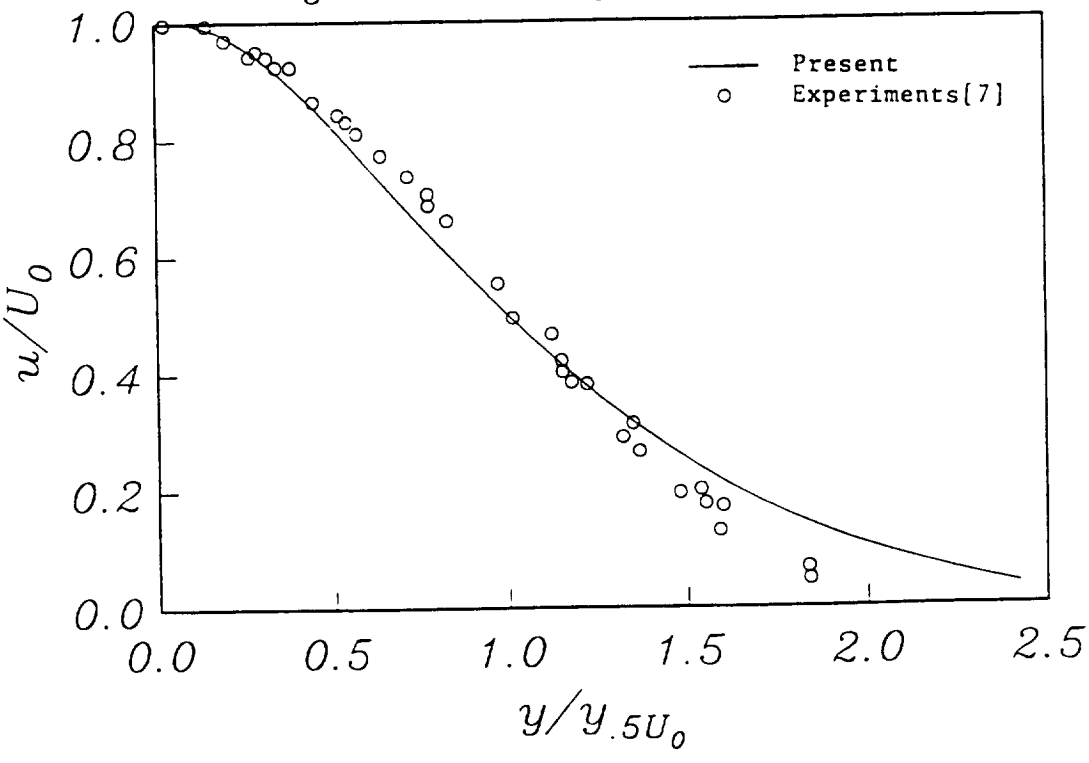

(U) As a calibration for the $k-\epsilon$ turbulence model, the turbulent shear stress from the present study is compared with measurements given by Brandbury[8], and by Gutmark and Wygnanski[9]. Except for a slight over prediction towards the edge of the jet, the numerical solution generally agrees well with the experimental data. This comparison is very crucial for pdf calculations because it is an indicator of the accuracy of the numerically predicted turbulent kinetic energy, k, and dissipation, ϵ, which are used to determine turbulent time scale, t, from $t = k/\epsilon$. An accurate prediction for k and ϵ is essential for the correct modeling of molecular mixing in the pdf calculation.

Fig.5 Turbulent shear stress

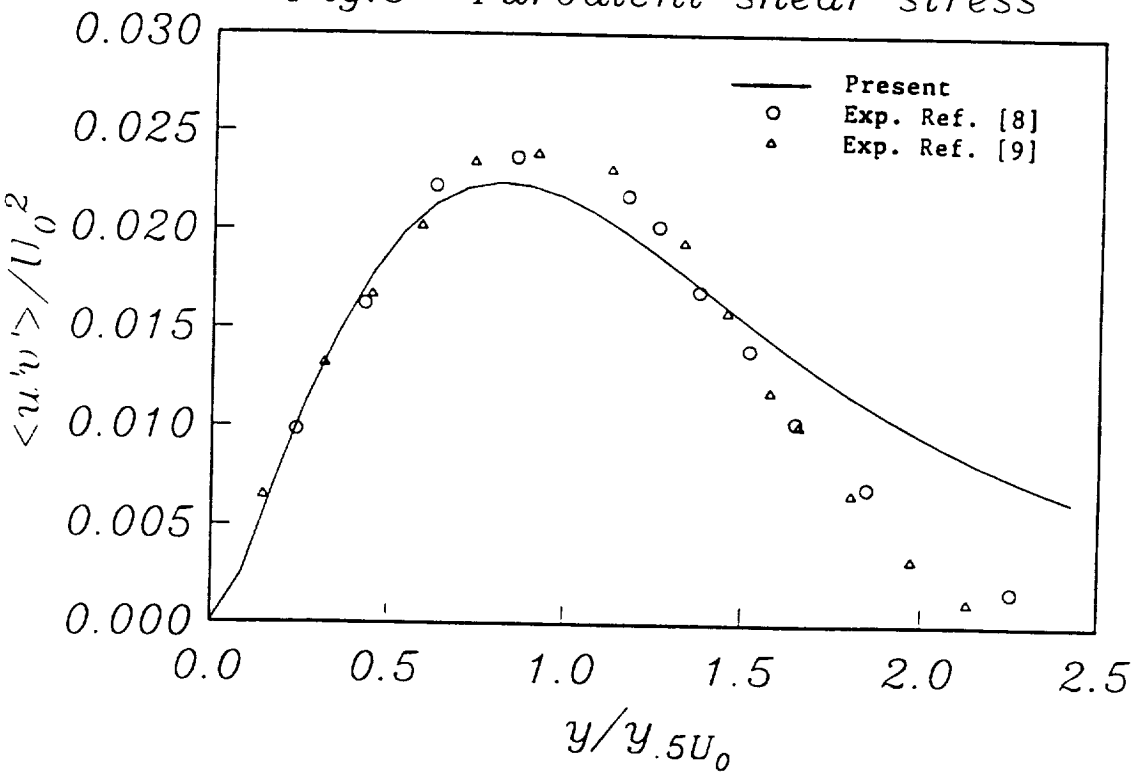

(U) The results for mean temperature from the Monte Carlo solution of the pdf equation for the temperature compared with experimental data from Ref. 10-12.

Fig.6 Mean temperature

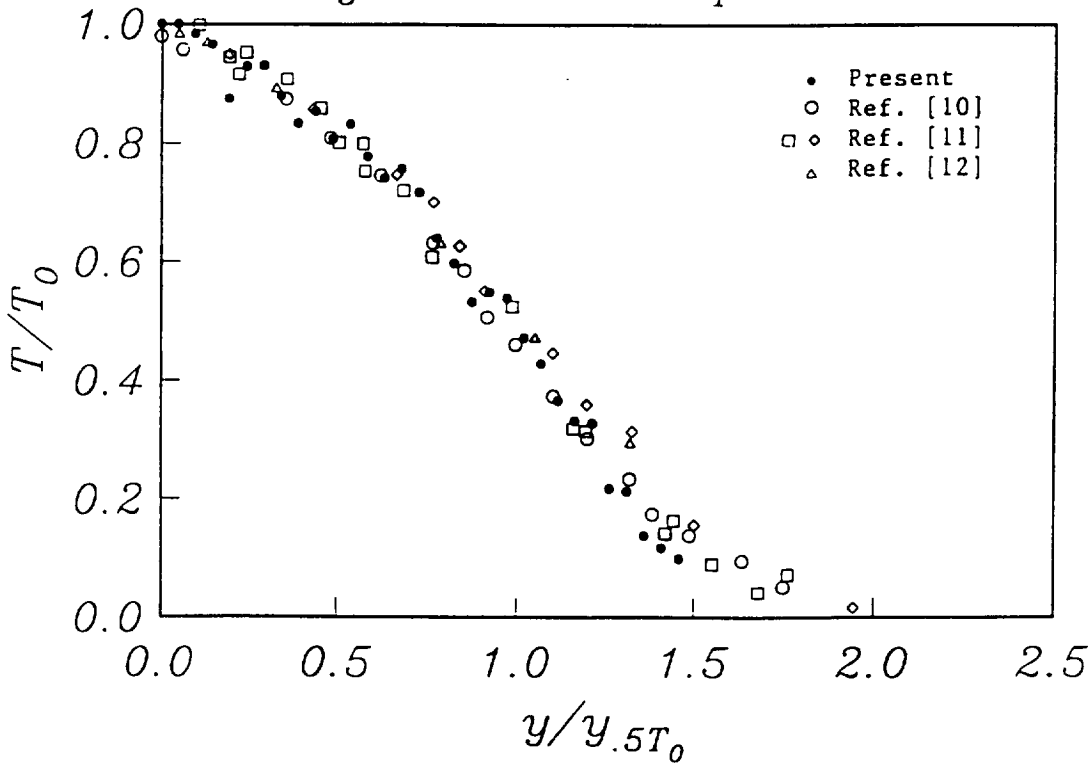

(U) The standard variance of the temperature, or the temperature fluctuation, compared with experimental data from Ref. 12 and 13. Because of the limited number of sample points (N=100) used in the computation, the numerical results are scattered; however, these results agree very well with the experimental observations. Particularly important is the agreement between the predicted and the measured temperature fluctuations, for in case of finite rate chemistry calculations, the instantaneous temperature will be used in determining the reaction rate, and the correct prediction of the temperature distribution will ensure the accuracy in reaction rate calculations.

Fig. 7 Standard variance of temperature

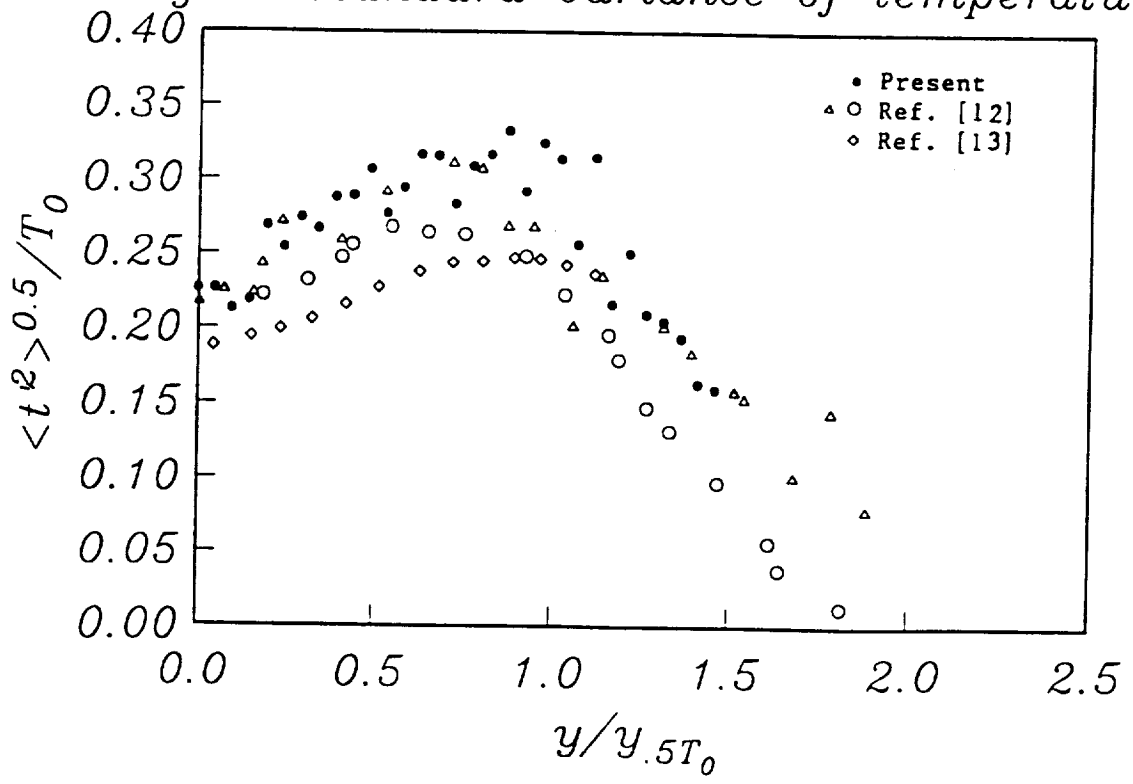

Acknowledgement

The author wish to thank Prof. S.B. Pope of Cornell University and Dr. J.-Y. Chen of Sandia National Labs for their help. This work is supported by the NASA Lewis Research Center under Contract NAS3-25266.

References

1. Pope, S.P., Prog. Energy Combst. Sci. 1985. Vol.11. pp.119-192
2. Kollmann, W., Theoret. Comput. Fluid Dynamics, 90 1. pp. 249-285
3. Chen, J.-Y. and Kollmann, W. Combust. Sci. and Tech. 1989, Vol. 64, pp. 315-346
4. Shuen, J.-S. and Yoon, S. AIAA J. Vol. 27 No. 12, 1989, pp. 1752-1760
5. Chen, J.-Y. and Kollmann, W. Combust. and Flame. 1990, pp.75-99
6. Brabbs, T.A. and Musiak, J.D., Private Communications
7. Schlichting, H., "Boundary Layer Theory." McGraw-Hill, 1989.
8. Brandbury, L.J.S., JFM, Vol. 23, 1965, pp. 31-64.
9. Gutmark, E. and Wygnanski, I., JFM, Vol. 73, 1976, pp. 465-495.
10. Browne, L.J.S., Antonia, R.A., and Chambers, , A.J., JFM, Vol. 149, 1984, pp. 355-373.
11. Uberoi, M.S. and Singh, P.I., Physics of Fluids, Vol. 18, No.17, 1975, pp 764-769.
12. Jenkins, P.E. ASME J. of Eng. for Power., Vol. 98, 1976, pp.501-505.
13. Antonia, R.A., et al., Int. J. of Heat Mass Transfer, Vol. 26, No. 1, 1983, pp. 41-48.

On Recontamination and Directional-Bias Problems in Monte Carlo Simulation of PDF Turbulence Models

Andrew T. Hsu
NASA Lewis Research Center, Cleveland, Ohio 44135
Phone 216/826-6648

Turbulent combustion can not be simulated adequately by conventional moment closure turbulence models. The difficulty lies in the fact that the reaction rate is in general an exponential function of the temperature, and the higher order correlations in the conventional moment closure models of the chemical source term can not be neglected, making the applications of such models impractical. The probability density function (pdf) method offers an attractive alternative: in a pdf model, the chemical source terms are closed and do not require additional models.

The partial differential equation for the probability density function, $\tilde{P}$, can be written as

$$\bar{\rho}\partial_t\tilde{P} + \bar{\rho}\tilde{v}_\alpha\partial_\alpha\tilde{P} + \bar{\rho}\sum_{i=1}^{N}\partial_{\psi_i}\{w_i(\psi_1,...,\psi_N)\tilde{P}\}$$
$$= -\partial_\alpha(\bar{\rho} < v''_\alpha|\psi_i > \tilde{P}) - \bar{\rho}\sum_{i=1}^{N}\sum_{j=1}^{N}\partial^2_{\psi_i\psi_j}(< \epsilon_{ij}|\psi_k > \tilde{P})$$

where the terms represent the time derivative, mean convection, chemical reaction, turbulent convection, and molecular mixing, respectively. The fact that the pdf equation has a very large dimensionality renders finite difference schemes extremely demanding on computer memory and CPU time and thus impractical, if not entirely impossible. A logical alternative is the Monte Carlo scheme, wherein the number of computer operations increases only linearly with the increase of number of independent variables, as compared to the exponential increase in a conventional finite difference scheme.

A grid dependent Monte Carlo scheme following that of J.Y. Chen and W. Kollmann has been studied in the present work. In dealing with the convection and diffusion of the pdf, the pdf equation is discretized on a given grid, e.g.,

$$\tilde{P}_{x+dx,j} = \alpha_j\tilde{P}_{x,j+1} + \beta_j\tilde{P}_{x,j} + \gamma_j\tilde{P}_{x,j-1}$$

where

$$\alpha_j + \beta_j + \gamma_j = 1$$

However, if this is the only restriction satisfied by the numerical algorithm, the mass fractions may not be conserved due to re-contamination, and directional-bias also appears. These phenomena are illustrated in Figure 1: Consider a mixing layer; use white balls to represent contaminants in the upper stream and black balls to represent contaminants in the lower stream. As the two streams move toward right, the location of the white balls and black balls are interchanged randomly to simulate convection and diffusion. From Figure 1, it is clear that directional-bias caused by recontamination caused the center of the mixing layer to drift downward. (Directional-bias can be partially corrected by changing sweeping directions.) One also notices that after the first marching step, the conservation law is violated, reflected in the Figure as missing white or black balls.

It is found that in order to conserve the mass fractions absolutely, one needs to add further restriction to the scheme, namely

$$\alpha_j + \gamma_j = \alpha_{j-1} + \gamma_{j+1}$$

A new algorithm was devised that satisfies this restriction in the case of pure diffusion or uniform flow problems. Using the same example, it is shown that absolute conservation can be achieved. This result is shown in Figure 2. One can see that the diffusion process is symmetric, and the problem of directional-bias is eliminated.

Although for non-uniform flows absolute conservation seems impossible, the present scheme has reduced the error considerably.

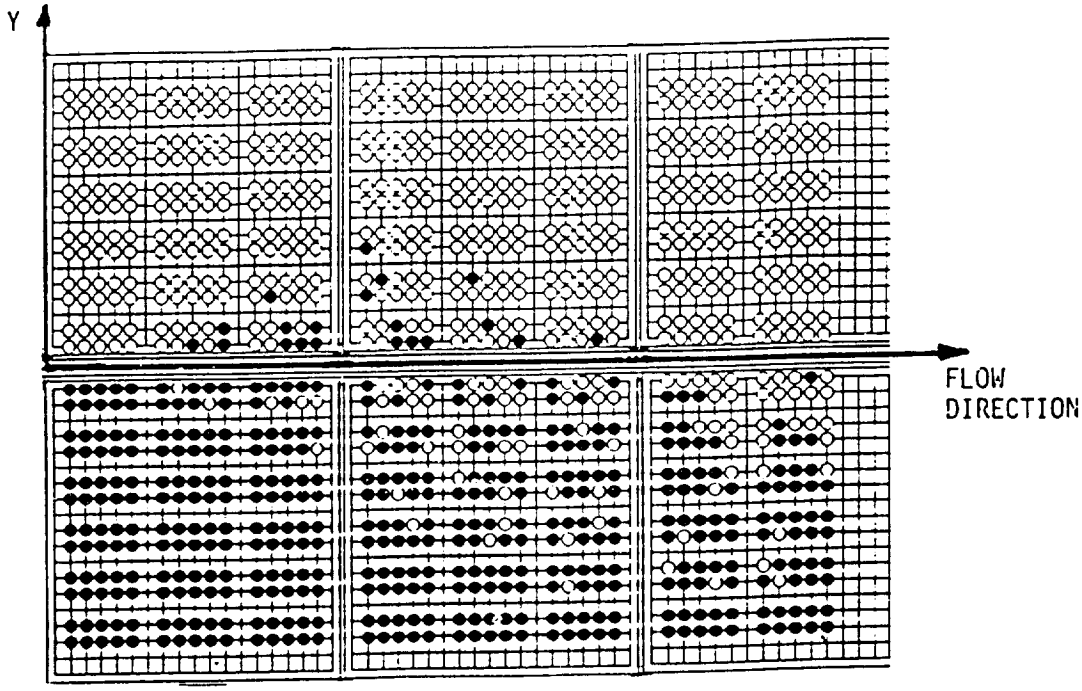

Figure 1. Illustration of directional-bias and recontamination problems in Monte Carlo simulation.

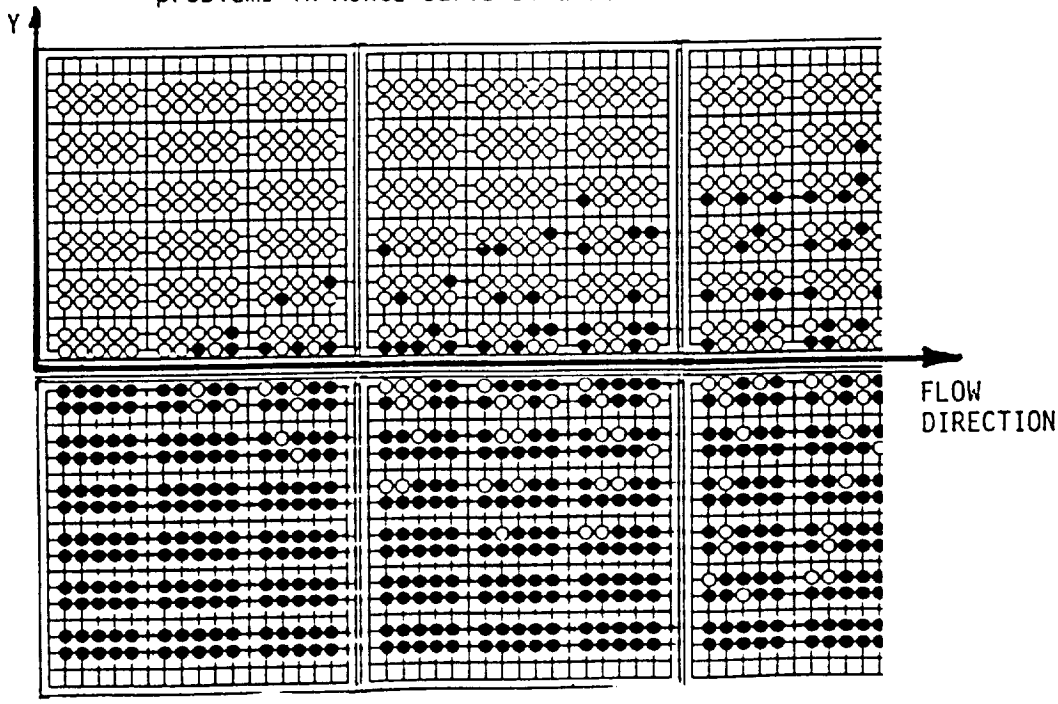

Figure 2. Solution obtained by using additional constraint in the solution procedure.

PROGRESS IN THE DEVELOPMENT OF PDF TURBULENCE MODELS FOR COMBUSTION

Andrew T. Hsu
Sverdrup Technology, Inc.
NASA Lewis Research Center
Cleveland, Ohio

10th National Aero-Space Plane
Technology Symposium
April 23-26, 1991

Paper Number 213

I. Introduction

(U) A combined Monte Carlo—CFD algorithm has been developed recently at NASA lewis Research Center for turbulent reacting flows. In this algorithm, conventional CFD schemes are employed to obtain the velocity field and other velocity related turbulent quantities, and a Monte Carlo scheme is used to solve the evolution equation for the probability density function (pdf) of species mass fraction and temperature.

(U) In combustion computations, the predictions of chemical reaction rates (the source terms in the species conservation equations) are poor if conventional turbulence models are used. The main difficulty lies in the fact that the reaction rate is highly non-linear, and the use of averaged temperature produces excessively large errors. Moment closure models for the source terms have attained only limited success. The probability density function (pdf) method seems to be the only alternative at the present time that uses local instantaneous values of the temperature, density, etc., in predicting chemical reaction rates, and thus may be the only viable approach for more accurate turbulent combustion calculations. The closure problem and the need for pdf has been discussed in detail in a previous paper[1].

(U) Assumed pdf are useful in simple problems; however, for more general combustion problems, the solution of a evolution equation for the pdf is necessary.

II. Method

(U) Conventional CFD flow solvers are quite common and needed no explanation here. We will concentrate on the derivation and solution of the pdf evolution equation in this section.

2.1 PDF evolution equation of mass fraction.

(U) For simplicity, the pdf equation for a single scalar will be derived here. The extension to multi species is trivial. The species transport equations (for a single species) can be written as

$$\rho\partial_t Y = -\rho u_k \partial_k Y + \rho\partial_k(D\partial_k Y) + \rho w \qquad (0.1)$$

where u_k is the velocity, Y is the mass fraction, and w is the chemical source term; summation for repeated indices is understood.

Let $P(Y)$ be the probability density function, and define $\phi = exp(i\lambda c)$, then the characteristic function of the pdf can be written as the ensemble average of ϕ:

$$< \phi >= \int P(Y)\phi dY,$$

and the pdf can be written as the inverse Fourier transform of the characteristic function:

$$P(Y) = \frac{1}{2\pi}\int < \phi > exp(-i\lambda Y)dY.$$

Now differentiate ϕ with respect to time,

$$\partial_t \phi = i\lambda exp(i\lambda Y)(\partial_t Y),$$

and replace $\partial_t Y$ in the above equation with the right hand side of eq. (1), we obtain

$$\rho\partial_t \phi = i\lambda exp(i\lambda Y)[-\rho u_k \partial_k Y + \partial_k(\rho D\partial_k Y) + \rho w],$$

which can be rearranged as

$$\partial_t(\rho\phi) + \partial_k(\rho u_k \phi) = i\lambda\phi\partial_k(\rho D\partial_k Y) + i\lambda\phi\rho w$$

Take ensemble average of the above equation gives

$$\partial_t < \rho\phi > +\partial_k < \rho u_k\phi >= i\lambda < \rho w\phi > +i\lambda < \phi\partial_k(\rho D\partial_k Y) > .$$

The inverse Fourier transform of the above equation gives the evolution equation for the probability density function:

$$\begin{aligned} &\partial_t(\rho P) + \partial_k(\rho < u_k > P) + \partial_Y(\rho w P) \\ &= -\partial_k(\rho < u_k' | Y > P) - \partial_Y(< \partial_k(\rho D\partial_k Y)|Y > P) \end{aligned}$$

where the terms represent mean convection, chemical reactions, turbulent convection, and molecular mixing, respectively.

For multi species and temperature, the pdf is written as $P(\psi_1, ..., \psi_n)$, where $\psi_i, i = 1, ..., n$ represent the scalars including mass fractions and temperature. A similar derivation gives

$$\begin{aligned} &\bar{\rho}\partial_t P + \bar{\rho}\tilde{v}_\alpha \partial_\alpha P + \bar{\rho}\sum_{i=1}^{N}\partial_{\psi_i}\{w_i(\psi_1, ..., \psi_N)P\} \\ &= -\partial_\alpha(\bar{\rho} < v_\alpha'' | \psi_i > P) - \bar{\rho}\sum_{i=1}^{N}\sum_{j=1}^{N}\partial^2_{\psi_i\psi_j}(< \epsilon_{ij}|\psi_k > P). \end{aligned}$$

(U) The left hand side of the above equation can be evaluated exactly and requires no modeling; the right hand side terms contain the conditional average of the Favre velocity fluctuation and the conditional average of the scalar dissipation and require modeling.

2.2 Modeled pdf equation

(U) The first term that needs modeling is the turbulent diffusion term, for which the following gradient model is used:

$$- < u_k' | \psi_i > P \cong D_t \partial_\alpha P,$$

where D_t is the turbulent diffusion coefficient, which is set to be equal to the eddy viscosity, i.e., the turbulent Schmidt number is equal to one.

(U) The next term needs modeling is the molecular mixing term. A coalescence/dispersion model is used for this term, which has the following general form:

$$\begin{aligned} & -\bar{\rho} \sum_{i=1}^{N} \sum_{j=1}^{N} \partial^2_{\psi_i \psi_j} (< \epsilon_{ij} | \psi_k > P) \\ \cong & \frac{C_D}{\tau} \int \int P(\psi') P(\psi'') T(\psi | \phi', \psi'') d\psi' d\psi'' - P \\ & \equiv D_m P \end{aligned}$$

where T is the transition probability. For more detail description of the molecular mixing model, see Ref 2. The modeled the pdf equation is then

$$\begin{aligned} & \bar{\rho} \partial_t P + \bar{\rho} \bar{v}_\alpha \partial_\alpha P + \bar{\rho} \sum_{i=1}^{N} \partial_{\psi_i} \{ w_i(\psi_1, ..., \psi_N) P \} \\ & = \partial_j (D_t \partial_\alpha P) + D_m P \end{aligned}$$

2.3 Solution of the pdf equation

(U) A fractional step method is used to solve the pdf equation in a Monte Carlo simulation. Three processes, namely, (1) convection/diffusion, (2) molecular mixing, and (3) chemical reaction, are simulated consecutively:

$$(\partial_t + \bar{\rho} \sum_{i=1}^{N} \partial_{\psi_i} \{ w_i(\psi_1, ..., \psi_N) \}) (\partial_t - D_m)(\partial_t + \bar{\rho} \bar{v} \partial_\alpha - \partial_\alpha (D_t \partial_\alpha) P = 0.$$

This equation is solved using a Monte Carlo simulation, i.e., the pdf is represented by an ensemble of samples. These sample points move in the hyperspace of $(x_1, x_2, x_3, \psi_1, ..., \psi_n)$ according to the above equation.

III. Results

(U) A heated turbulent plane jet had been calculated and results reported at last NASP symposium. The case has since been recalculated using modified turbulence model, and improved results are shown here.

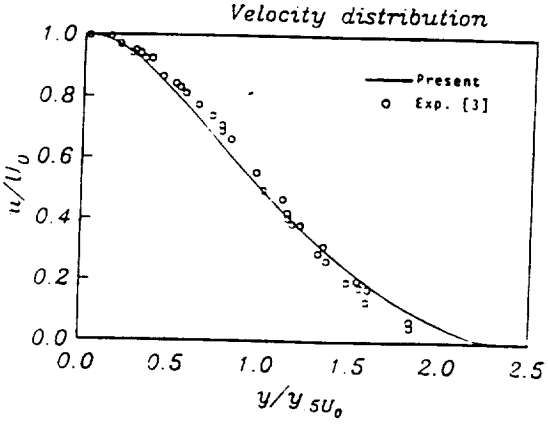

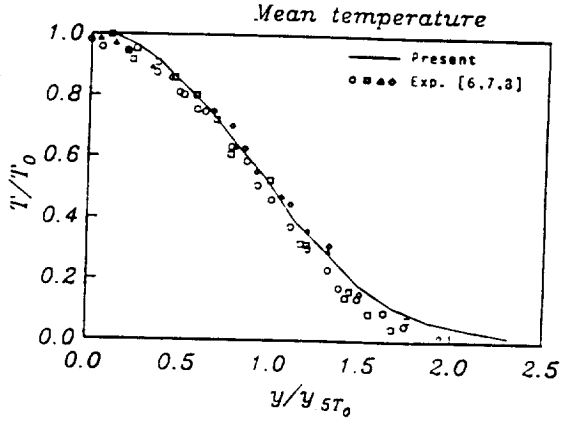

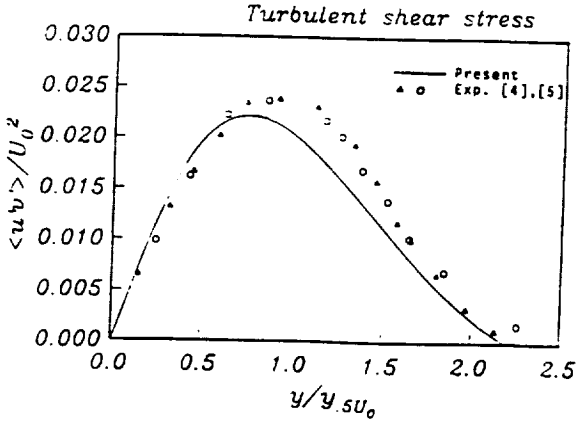

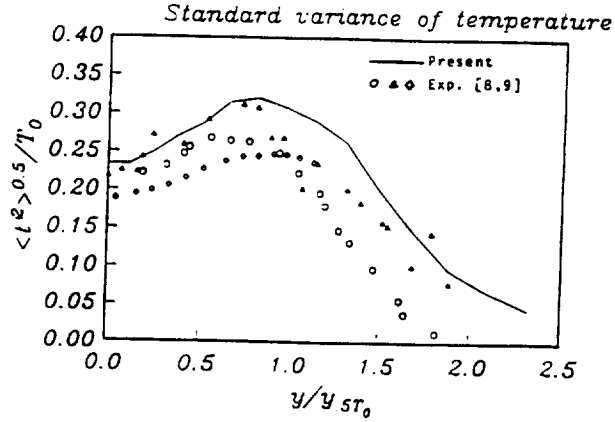

(U) A hydrogen–fluorine diffusion flame was calculated. The flowfield and flow conditions, as well as the calculated velocity and turbulent kinetic energy distribution, are given on this page.

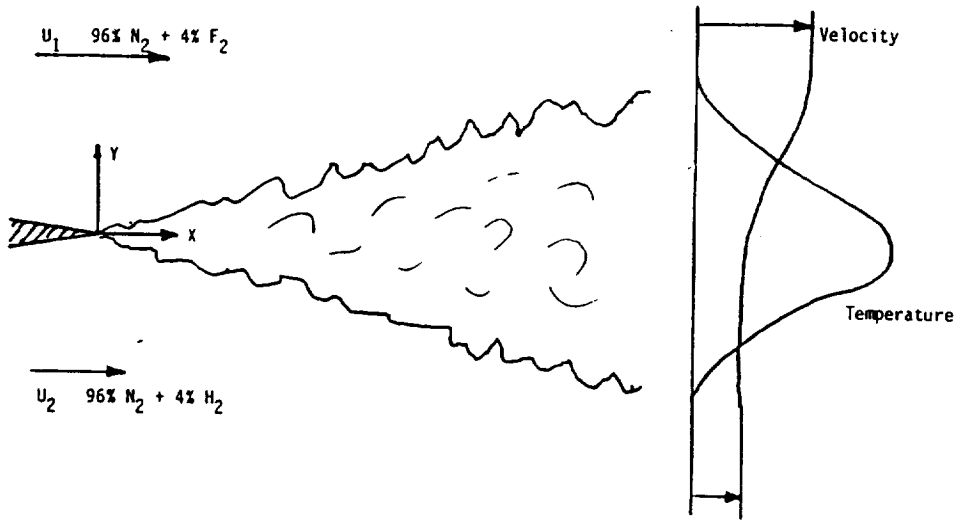

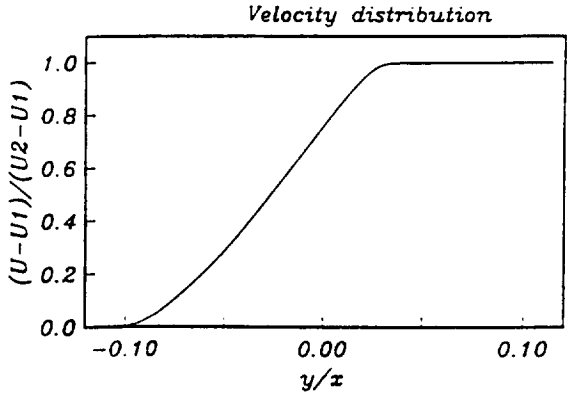

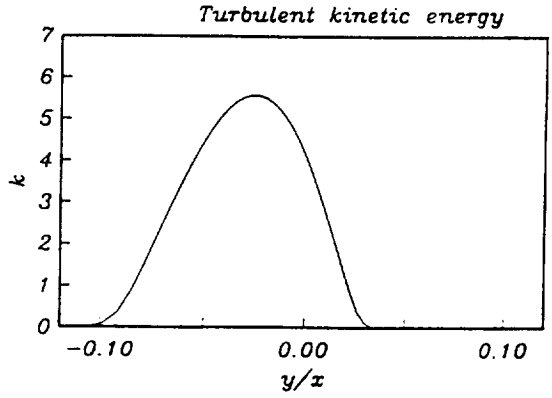

(U) Figures show the calculated heat release of the H2-F2 flame (temperature distribution) compared to experimental data, and the species mass fraction from pdf calculation.

Fig.1 Temperature distribution: H2+F2=2HF

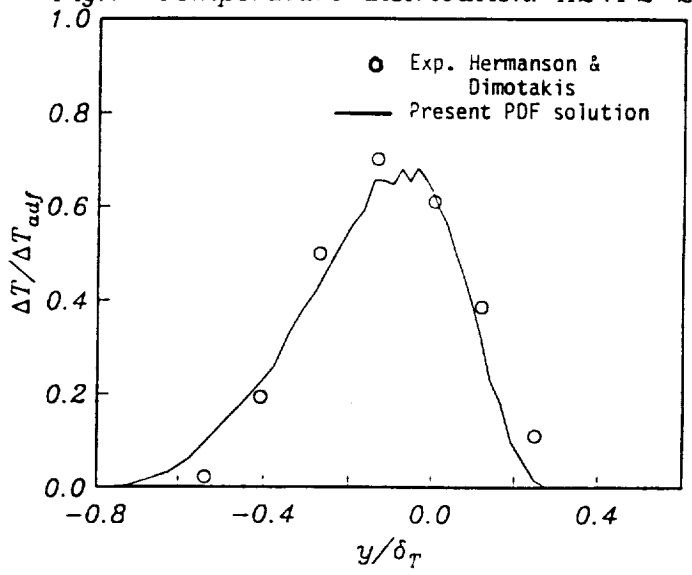

Fig.2 Mass fraction: H2+F2=2HF

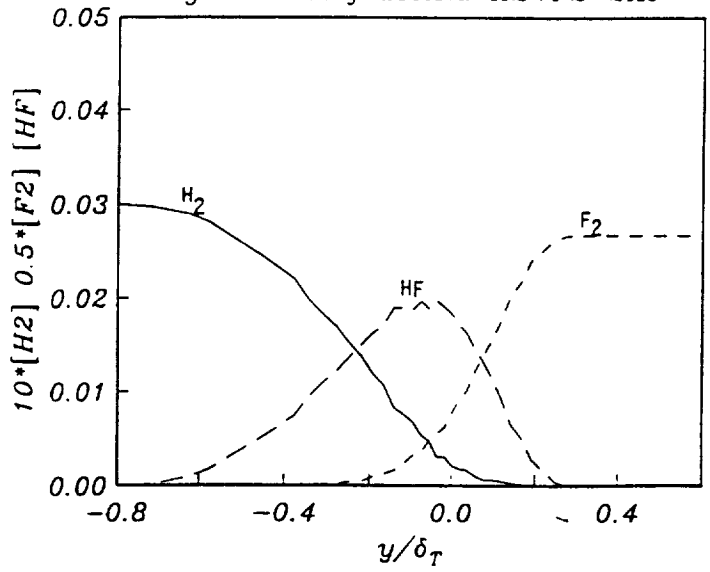

(U) Computed pdf of temperature distribution in the H2-F2 flame.

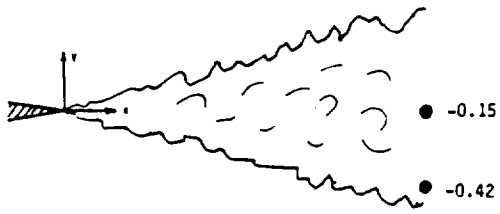

Fig.2 probability mass function

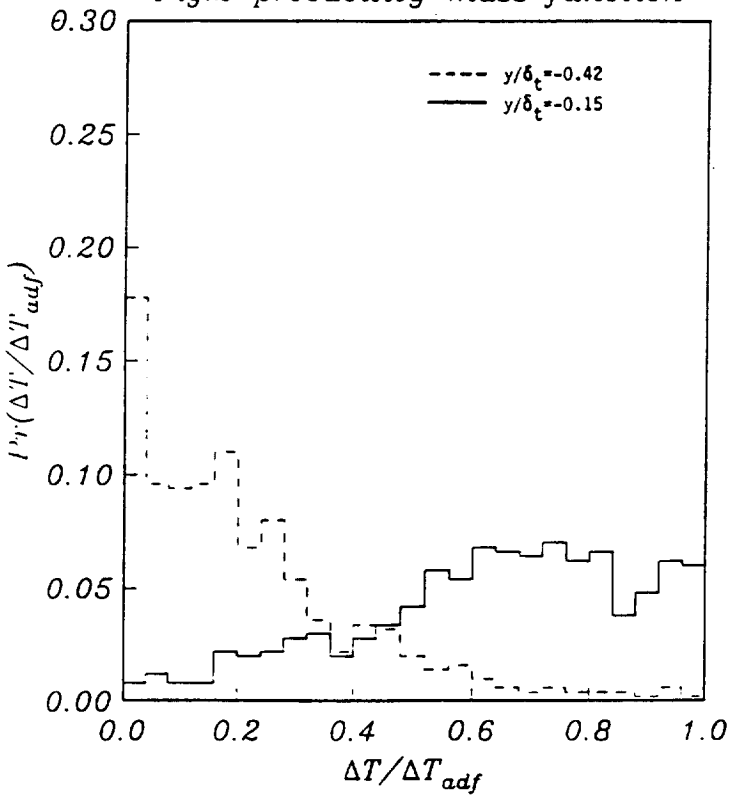

Acknowledgement

This work is supported by the NASA Lewis Research Center under Contract NAS3-25266.

References

1. Hsu, A.T. "A Numerical Study of Combusting Shear Layers Using PDF Turbulence Model," to be presented at the 8th Symposium on Turbulence Shear Flows, Munich, Germany, Sept. 9-11, 1991.

2. Hsu, A.T. "The Study of PDF Turbulence Models in Combustion," 9th NASP Symposium, Orlando, Florida, Nov. 1-2, 1990.

3. Schlichting, H., "Boundary Layer Theory." McGraw-Hill, 1989.

4. Brandbury, L.J.S., JFM, Vol. 23, 1965, pp. 31-64.

5. Gutmark, E. and Wygnanski, I., JFM, Vol. 73, 1976, pp. 465-495.

6. Browne, L.J.S., Antonia, R.A., and Chambers, , A.J., JFM, Vol. 149, 1984, pp. 355-373.

7. Uberoi, M.S. and Singh, P.I., Physics of Fluids, Vol. 18, No.17, 1975, pp 764-769.

8. Jenkins, P.E. ASME J. of Eng. for Power., Vol. 98, 1976, pp.501-505.

9. Antonia, R.A., et al., Int. J. of Heat Mass Transfer, Vol. 26, No. 1, 1983, pp. 41-48.

10. Hermanson, J.C. and Dimotadis, P.E., JFM. (1989), vol. 199. pp.333-375.

A STUDY OF HYDROGEN DIFFUSION FLAMES USING PDF TURBULENCE MODEL

Andrew T. Hsu*
Sverdrup Technology, Inc.
NASA Lewis Research Center, Cleveland, Ohio 44145

Abstract

The application of probability density function (pdf) turbulence models is addressed in this work. For the purpose of accurate prediction of turbulent combustion, an algorithm that combines a conventional CFD flow solver with the Monte Carlo simulation of the pdf evolution equation has been developed. The algorithm has been validated using experimental data for a heated turbulent plane jet. The study of H_2–F_2 diffusion flames has been carried out using this algorithm. Numerical results compared favorably with experimental data. The computations show that the flame center shifts as the equivalence ratio changes, and that for the same equivalence ratio, similarity solutions for flames exist.

Introduction

It is the consensus of the combustion profession that the prediction of chemical reaction rate (the source term in a species conservation equation) is poor if a conventional turbulence model is used. The main difficulty lies in the fact that the reaction rate is highly non-linear, and the use of averaged temperature, pressure and density produces excessively large errors. Moment closure models for the source terms have attained only limited success because the assumptions for such models to be valid often can not be satisfied. The probability density function (pdf) method seems to be the only alternative at the present time that uses local instantaneous values of the temperature, density, etc., in predicting the chemical reaction rate, and thus is the only viable approach for more accurate turbulent combustion calculations. Two main lines are being followed in pdf methods: one uses an assumed shape for the pdf, the second solves a pdf evolution equation; the present paper addresses only the latter. There has been significant progress in the study of pdf turbulence models in low speed flows in the past decades. These developments were summarized in Refs. [1], [2] and [3]. In spite of this progress, pdf turbulence modeling remains a nascent discipline with many unresolved issues.

The fact that the pdf equation has a very large dimensionality renders the use of finite difference schemes extremely demanding on computer memories and thus impractical, if not entirely impossible. A logical alternative is the Monte Carlo scheme, which has been used extensively in statistical physics. The evolution equations for the joint pdf of the velocity and species mass fraction have been successfully solved using Monte Carlo schemes, see, e.g., Pope[1]. However, since CFD has reached a certain degree of maturity as well as acceptance, it seems, at least from the standpoint of practical applications, that the use of a combined CFD and Monte Carlo scheme is more beneficial. Therefore, in the present study a scheme is chosen that uses a conventional CFD algorithm to solve the Navier-Stokes equations and provide flowfield properties such as velocity, pressure, etc., and the chemical reactions are calculated by using a Monte Carlo scheme to solve a pdf evolution equation.

The combined CFD-pdf solver has been developed recently and validated using non-reacting flow data for a heated turbulent plane jet. The algorithm has been further tested in the numerical study of an H_2–F_2 diffusion flame. This diffusion flame was studied experimentally by Mungal & Dimotakis[4] and Hermanson & Dimotakis[5]. The numerical results from the present study are compared with these experimental data.

Theory

Governing equations for reacting flows.

Flows with chemical reaction are governed by the continuity equation, momentum equations, energy equation, and species transport equations:

$$\begin{aligned}
&\partial_t \rho + \partial_i \rho u_i = 0 \\
&\rho \partial_t u_i + \rho u_j \partial_j u_i = -\partial_i p + \mu \partial_j \tau_{ij} \\
&\rho \partial_t h + \rho u_j \partial_j - \partial_t p - u_j \partial_j p \\
&\quad = -\partial_j q_j + Q \\
&\rho \partial_t Y_k + \rho u_j \partial_j Y_k = \rho \partial_j (D \partial_j Y_k) + w_k \\
&\quad k = 1, 2, \cdots, N.
\end{aligned} \tag{1}$$

where u_i is the velocity, Y_k is the mass fraction, and w_k is the chemical source term. (In addition to these equations, one also needs the equation of state.) For turbulent flows, we substitute

$$\begin{aligned}
u_i &= \tilde{u}_i + u_i', \\
Y_i &= \tilde{Y}_i + Y_i',
\end{aligned} \tag{2}$$

into the above equation and take an ensemble average. In the process of averaging, new unknown quantities in the form of correlations appear, e.g., $\overline{u_i' u_j'}$, $\overline{u_i' Y_k'}$, etc. These quantities can all be modeled using conventional turbulence models, such as two equation models or second order closure models. A problem unique to flows with chemical reaction is the average

of the chemical source term, $\overline{\rho w_k}$, The major difficulty lies in the fact that w_k is a highly nonlinear (usually exponential) function of the temperature. It is well know that the use of averaged temperature, $\tilde{T}$, in evaluating $\overline{\rho w_i}$ can cause egregious errors. One may consider the effect of the temperature fluctuation, T'', by applying a moment closure model to the term $\overline{\rho w_i}$; however, such a closure model results in an infinite series that converges only when $T_a \sim \tilde{T}$ and $T'' \ll \tilde{T}$. In many combustion problems, these two conditions are violated: in fact, we often have $T_a \gg \tilde{T}$ and $T'' \sim \tilde{T}$ instead. In view of the above, the prospect of an accurate prediction of turbulent combustion using conventional turbulence models seems dismal. The above fact motivated the use of pdf methods.

Pdf evolution equation

Given a set of m random variables, $\psi_1, \psi_2, \cdots, \psi_m$, and the joint probability density function, $P(\psi_1, \psi_2, \cdots, \psi_m; x, y, z, t)$, the mean of any random function, $f(\psi_1, \psi_2, \cdots, \psi_m; x, y, z, t)$, can be calculated as

$$\overline{f(x,y,z,t)} = \int \cdots \int f\, P\, d\psi_1\, d\psi_2 \cdots d\psi_m. \quad (3)$$

For simple flows, one could assume the shape of the pdf and compute the source term, $\overline{\rho w_k}$, based on the assumed pdf using the above integral. For more general problems, one needs to solve a pdf evolution equation for a more accurate pdf distribution. In the latter case, the evaluation of the source term, $\overline{\rho w_k}$, is no longer necessary because the mean values of the temperature, species mass fractions, which we previously would obtain by solving the transport equations (Eq. 1), can now be evaluated directly from the pdf using the above integral.

The pdf evolution equation can be derived from the transport equations (Eq. 1) in many different ways, using a Dirac delta function, a characteristic function. or a characteristic functional. [1-3] The evolution equation of a single point probability density function of scalar random variables $\psi_1, \cdots, \psi_m$ can be written as

$$\bar{\rho}\partial_t \tilde{P} + \bar{\rho}\tilde{v}_\alpha \partial_\alpha \tilde{P} + \bar{\rho}\sum_{i=1}^{m} \partial_{\psi_i}\{w_i(\psi_1, \cdots, \psi_m)\tilde{P}\}$$
$$= -\partial_\alpha(\bar{\rho} < v''_\alpha | \phi_k(x) = \psi_k > \tilde{P})$$
$$-\bar{\rho}\sum_{i=1}^{m}\sum_{j=1}^{m} \partial^2_{\psi_i,\psi_j}(< \epsilon_{ij} | \phi_k(x) = \psi_k > \tilde{P}) \quad (4)$$

where the terms represent the rate of time change, mean convection, chemical reaction, turbulent convection, and molecular mixing, respectively; $\tilde{P}$ is the density-weighted joint pdf:

$$\tilde{P} = \rho P/\bar{\rho},$$

ϵ_{ij} is the scalar dissipation:

$$\epsilon_{ij} = D\partial_\alpha \phi_i \partial_\alpha \phi_j,$$

(where D is the diffusion coefficient), and $< x|y >$ denotes the mathematical expectation of a random function x conditioned upon y.

The left hand side of eq. (4) can be evaluated exactly and requires no modeling; the right hand side terms contain the conditional expectation of the velocity fluctuation and the conditional expectation of the scalar dissipation, which are new unknowns and require modeling.

Closure models for pdf equation

The first term that needs modeling is the turbulent convection term, for which one can use the following gradient model:

$$- < v''_\alpha | \psi_k > \tilde{P} \cong D_t \partial_\alpha \tilde{P},$$

where D_t is the turbulent diffusion coefficient, which is set to be equal to the eddy viscosity, i.e., the turbulent Schmidt number is equal to one.

The next term needs modeling is the molecular mixing term. A coalescence/dispersion model is used for this term, which has the following general form[6]:

$$-\bar{\rho}\sum_{i=1}^{N}\sum_{j=1}^{N} \partial^2_{\psi_i,\psi_j}(< \epsilon_{ij} | \psi_k > \tilde{P})$$
$$\cong \frac{C_D}{\tau}\int\int \tilde{P}(\psi')\tilde{P}(\psi'')T(\psi|\phi', \psi'')d\psi' d\psi'' - \tilde{P}$$
$$\equiv M(\tilde{P})$$

where T is the transition probability. A new mixing model continuous in time is recently developed by Hsu and Chen[7]. For more detail description of the molecular mixing models, see Refs. 6 and 7.

The modeled pdf equation is then

$$\bar{\rho}\partial_t \tilde{P} + \bar{\rho}\tilde{v}_\alpha \partial_\alpha \tilde{P} + \bar{\rho}\sum_{i=1}^{m} \partial_{\psi_i}\{w_i(\psi_1, \cdots, \psi_m)\tilde{P}\}$$
$$= \partial_j(D_t \partial_\alpha \tilde{P}) + M(\tilde{P}), \quad (5)$$

which can be solved using a Monte Carlo simulation.

Numerical Methods

In the present study, a combined finite difference–Monte Carlo solver is developed. For the velocity field, the Navier-Stokes equations and a $k-\epsilon$ turbulence model are solved using a finite difference method; for scalar variables such as the temperature, mass fractions, etc., the pdf evolution equation is solved using a Monte Carlo scheme. The CFD flow solver provides the Monte Carlo solver with the mean velocity and a turbulence time scale τ, where $\tau = k/\epsilon$, and the Monte Carlo solver provides the mean flow solver with the density, $\bar{\rho}$.

The solution of the Navier-Stokes equations

Since the primary concern of the present work is pdf modeling, we choose the simplest possible solver for the N-S equations. The equation is transformed into a general coordinate system using the following general relation:

$$x = \xi$$
$$y = y(\xi, \eta)$$

and

$$\partial_x = \partial_\xi - \frac{y_\xi}{y_\eta}\partial_\eta$$
$$\partial_y = \frac{1}{y_\eta}\partial_\eta$$

The transformed momentum equation for steady flows is

$$\bar{u}\partial_\xi \bar{u} + (\bar{v} - \bar{u}y_\xi)\frac{1}{y_\eta}\partial_\eta \bar{u} = -\frac{1}{\bar{\rho}}\partial_\xi p + \frac{1}{y_\eta}\partial_\eta(\nu_\tau \partial_\eta \bar{u}),$$

where the viscous term involves gradient in the ξ-direction is neglected since we are only interested in shear flows in the present study.

First order upwind difference is used in the ξ-direction so that a marching scheme for steady parabolic flows can be used. To ensure stability, a flux splitting scheme is used in the η-direction.

The solution of the pdf equation

A fractional step Monte Carlo method, as will be described in the following, is used to solve the pdf equation. We first discretize the time derivative in eq. (5) using finite difference: $\partial_t \tilde{P} = (\tilde{P}^{n+1} - \tilde{P}^n)/\Delta t$, then the pdf evolution equation (eq. 5) can be written as

$$\tilde{P}^{n+1} = \{1 - \Delta t\, \tilde{v}_\alpha \partial_\alpha - \Delta t \sum_{i=1}^{m} \partial_{\psi_i} w_i(\psi_1, \cdots, \psi_m) + \Delta t\, \partial_\alpha D_t \partial_\alpha + \Delta t\, M\}\, \tilde{P}^n$$

Using approximate factorization, the above equation is recast as

$$\tilde{P}^{n+1} = (1 - \Delta t \sum_{i=1}^{m} \partial_{\psi_i} w_i(\psi_1, \cdots, \psi_m)) \times (1 + \Delta t M)(1 - \Delta t \bar{\rho}\bar{v}\partial_\alpha + \Delta t \partial_\alpha D_t \partial_\alpha)\, \tilde{P}^n + O(\Delta t)$$
$$\equiv (1 + \Delta t C)(1 + \Delta t M)(1 + \Delta t R)\tilde{P}^n + O(\Delta t),$$

where C denotes the convection operator, m the molecular mixing, and R chemical reactions. With the above expression, we can three processes consecutively:

(1) convection:

$$\tilde{P}^* = (1 + \Delta t C)\tilde{P}^n,$$

(2) molecular mixing:

$$\tilde{P}^{**} = (1 + \Delta t M)\tilde{P}^*,$$

(3) chemical reaction:

$$\tilde{P}^{n+1} = (1 + \Delta t R)\tilde{P}^{**}$$

In the present study, only steady flows are considered, so ∂_t is replaced by ∂_ξ and a marching scheme in the ξ-direction is employed.

In a Monte Carlo simulation, the continuous pdf is replaced by $N \times M$ delta functions,

$$P^*(\psi_1, \psi_2, \cdots, \psi_m; x, y, z, t) = \frac{1}{N}\sum_{n=1}^{N} \delta(\psi_1 - \phi_1^{(n)}(t)) \times \delta(\psi_2 - \phi_2^{(n)}(t)) \cdots \delta(\psi_m - \phi_m^{(n)}(t)),$$

where each product of the m delta functions represents one event of an ensemble of N sample events. An event can be thought of as a fluid particle, and the evolution of P^* entails the movement of the particles in the physical space as well as the phase space (ψ−space). The movement of the particles is, of course, governed by the pdf evolution equation, and is simulated in the following three steps.

Step 1: convection

Replace $\tilde{P}$ by P^* in the pdf evolution equation and transform it into the $\xi - \eta$ coordinate system, the convection process for a steady flow can be written as

$$\bar{\rho}\bar{u}\partial_\xi P^* = -\bar{\rho}(\bar{v} - \bar{u}y_\xi)\frac{1}{y_\eta}\partial_\eta P^* + \frac{1}{y_\eta}\partial_\eta(\bar{\rho} D_t \partial_\eta P^*),$$

Discretizing the above equation using a finite difference scheme, we can write

$$P^*_{i,j} = \alpha P^*_{i-1,j+1} + \beta P^*_{i-1,j} + \gamma P^*_{i-1,j-1}$$

(Here again we used a one sided difference so that a marching scheme could be used.) The above equation states that if we divide the flow field into cells, then the pdf at point (i, j) can be written as a linear combination of the pdf at neighboring points, To simulate this process with a Monte Carlo scheme, we move the sample particles between cells according to the above equation. For instance, the particles of cell (i, j) will be obtained by choosing randomly αN particles form cell $(i-1, j+1)$, βN particles from cell $(i-1, j)$, and γN particles from cell $(i-1, j-1)$. In order for the total number of particles not to change, we require that $\alpha + \beta + \gamma = 1$.

It is worth noting that this method can easily be extended to elliptic flows and applied to general curvilinear coordinate systems.

Step 2: molecular mixing.

The molecular mixing process is simulated by the following binary interaction model:

$$\bar{\rho}\tilde{u}\partial_\xi \tilde{P} = \frac{C_D}{\tau}\int\int \tilde{P}(\psi')\tilde{P}(\psi'')T(\psi|\phi',\psi'')d\psi' d\psi'' - \tilde{P}$$

where T is the transition probability. By assigning various functions to T, we would have different mixing models. In the present study, the modified Curl model by Janicka et al. [8] is used. In this model, the transition probability is given as

$$T(\psi|\phi',\psi'') = \begin{cases} \frac{1}{|\psi''-\psi'|} & \text{for } \psi' \le \psi \le \psi'', \\ & \text{or } \psi'' \le \psi \le \psi', \\ 0 & \text{otherwise.} \end{cases}$$

with $C_D = 6.0$.

In the Monte Carlo simulation, the above model is realized in the following manner: Divide the flow domain into small cells, each containing N sample particles. Given a small time interval Δt and a turbulent time scale τ, select randomly N_{mx} pairs of particles, where

$$N_{mx} = 0.5\frac{\Delta t}{C\tau}N,$$

and let a pair, say, m and n, mix as follows

$$\phi_n(t+\Delta t) = A\phi_m(t) + (1-A)\phi_n(t)$$
$$\phi_m(t+\Delta t) = A\phi_n(t) + (1-A)\phi_m(t)$$

where $A = 0.5\xi$, with ξ a random variable uniformly distributed on the interval [0.1]. The remaining $N - 2N_{mx}$ particles remain unchanged:

$$\phi_n(t+\Delta t) = o_n(t)$$

The turbulent time scale is supplied by the finite difference solution of a $k-\epsilon$ turbulence model: $\tau = k/\epsilon$.

This model admits the non-physical jump condition and does not produce the correct long time behavior for decay problems in homogeneous turbulence. A continuous model that predicts the correct long time behavior for turbulence decay problem has been introduced by Hsu and Chen [7]. But as shown in Ref. [7], for practical combustion problems where the long time statistical behavior is not crucial, the modified Curl model gives acceptable results. In the present study, both the modified Curl model and the continuous model have been used.

Step 3: chemical reaction

Chemical reaction is represented in the Monte Carlo simulation by the movement of sample particles in the phase space due to reaction. A sample point with a given composition $\{o_1, \phi_2, \cdots, \phi_m\}$ at time t will acquire new composition at the next moment, and the changing rate is

$$\frac{d\phi_i}{dt} = w_i(\phi_1, \phi_2, \cdots, \phi_m), \quad i = 1, 2, \cdots, M,$$

where w_i is the reaction rate for that specific sample point. If we regard w_i as the convection velocity of the particle in the phase space, the it is clear that the above ODE represent the movement of a sample particle in the phase space.

The various chemistry models considered in this study are presented in the following section.

Chemistry Models for $H_2 - F_2$ Reaction

Finite rate chemistry.

The reaction of $H_2 + F_2 = 2HF$ can be represented by the following two step chain reactions[4]:

$$H_2 + F \longrightarrow^{k_1} HF + H$$
$$H + F_2 \longrightarrow^{k_2} HF + F$$

with

$$k_1 = 2.6 \times 10^{12} T^{0.5} exp\left(\frac{-610}{RT}\right),$$
$$k_2 = 3 \times 10^{9} T^{1.5} exp\left(\frac{-1680}{RT}\right),$$

where T is in K, R in $cal\ mol^{-1}\ K^{-1}$, and k in $cm^3\ mol^{-1}\ sec^{-1}$.

The above expressions only provide the forward reaction rate; the backward reaction rate can be calculated using the equilibrium coefficient:

$$k_b = k_f/k_{eq},$$

and the equilibrium coefficient can be evaluated using Gibbs free energy. Polynomials for Gibbs free energy for various species can be found in Ref. [8]. A numerical experiment shows that the backward reaction rates are much smaller than that of the forward reaction for the two reaction steps described above and can be neglected.

Let C denote the mole concentration; for each sample particle, we need to solve the following set of ODEs:

$$\frac{dC_{H_2}}{dt} = -k_1 C_{H_2} C_F = \omega_1$$
$$\frac{dC_{F_2}}{dt} = -k_2 C_H C_{F_2} = \omega_2$$
$$\frac{dC_H}{dt} = -\omega_1 + \omega_2 = \omega_3$$
$$\frac{dC_F}{dt} = \omega_1 - \omega_2 = \omega_4$$
$$\frac{dC_{HF}}{dt} = -\omega_1 - \omega_2 = \omega_5$$
$$\frac{dh}{dt} = -\sum_{i=1}^{5} h_{f_i}^0 \omega_i$$

where h is the enthalpy and $h_{f_i}^0$ is the heat of formation.

Using n to denote the time level, we found that the following semi-implicit scheme seems to be most stable:

$$C_{H_2}^{n+1} = \frac{C_{H_2}^n}{1 + \Delta t\, k_1 C_F^n}$$

$$C_{F_2}^{n+1} = \frac{C_{F_2}^n}{1 + \Delta t\, k_2 C_H^n}$$

$$C_H^{n+1} = \frac{C_H^n + \Delta t\, k_1 C_{H_2}^n C_F^n}{1 + \Delta t\, k_2 C_H^n}$$

$$C_F^{n+1} = \frac{C_F^n + \Delta t\, k_2 C_{F_2}^n C_H^n}{1 + \Delta t\, k_1 C_{H_2}^n}$$

$$C_{HF}^{n+1} = C_{HF}^n + \Delta t\,(k_1 C_{H_2}^n C_F^n + k_2 C_H^n C_{F_2}^n)$$

The energy equation is solved explicitly. To start the chain reaction 0.00002 mole fraction of F was released into the flowfield initially.

Using the above equations to calculate the reaction in a laminar premixed flame, we found that the time required for this reaction is the order of one microsecond (Figs. 1 and 2). The turbulence time scale in the calculation, $\tau = k/\epsilon$, is the order of one second. Considering this large difference of time scales, it is impractical to use finite rate chemistry in this calculation.

Fast reaction

Since the chemical reaction is very fast compared to the flowfield development and the reverse reactions are negligible, we chose to use the following complete irreversible reaction mechanism. We assume that after molecular mixing, complete reaction is achieved within each particle during the time interval of one marching step in the calculation. The reaction is calculated using the following equations.

For $C_{H_2}^n \geq C_{F_2}^n$:

$$C_{H_2}^{n+1} = C_{H_2}^n - C_{F_2}^n$$
$$C_{F_2}^{n+1} = 0$$
$$C_{HF}^{n+1} = C_{HF}^n + 2C_{F_2}^n$$

For $C_{H_2}^n \leq C_{F_2}^n$:

$$C_{H_2}^{n+1} = 0$$
$$C_{F_2}^{n+1} = C_{F_2}^n - C_{H_2}^n$$
$$C_{HF}^{n+1} = C_{HF}^n + 2C_{H_2}^n$$

The energy equation can be written as

$$\Delta h = -h_{f_{HF}}^0\ \Delta C_{HF} \left(\frac{M_{HF}}{\bar{\rho}}\right),$$

where M_{HF} if the molecular weight of HF.

Since the concentrations of reactants are low, the heat release is low, and the temperature rise is within a few hundred degrees Kelvin. Under these circumstances, the variation of specific heat C_p is negligible, and the temperature can be calculated as

$$T^{n+1} = T^n + \frac{\Delta h}{C_p}$$

The error involved in this approximation is less than 5%.

Results and Discussions

Code validation.

Before applied to the hydrogen-fluorine diffusion flames, the computer algorithm is first validated using experimental data for a heated turbulent jet. The non-reacting flow data serves as a check for the convection and molecular mixing process in the pdf solver as well as the $k-\epsilon$ model in the N.-S. solver.

Extensive experimental results for turbulent plane jet have been reported by many authors. Measurements for mean velocity field in a turbulent jet were first reported in the 1930's[9]; turbulent shear stress measurements had been reported more recently[10,11]. To determine the effect of turbulence on mixing, the temperature field of a heated turbulent jet had been studied by several authors. The turbulent jet has a slightly higher temperature than the ambient. Measurements of both the the mean temperature and the rms of the temperature fluctuations were given[12-17].

In the present study of this non-reacting flow case, the temperature field is treated as a conserved scalar and is simulated by the pdf of the temperature; the velocity field and turbulent shear stress are obtained by solving the N.-S. equation and a $k-\epsilon$ turbulence model.

In the finite difference solution of the flowfield, 41 grid points are used across half of the jet width. A symmetry boundary condition is used at the jet centerline. Fig. 3 shows the comparison of the present solution of the mean velocity field with the experimental data, and Fig. 4 presents the numerical solution of the turbulent shear stress as compared to the experimental data. Good agreements between numerical results and experimental data are observed for both the mean velocity field and the turbulent shear stress. The turbulent shear stress is calculated from $- < u'v' > = \nu_\tau \partial u/\partial y$, where $\nu_\tau = C_\mu k_2/\epsilon$. A good prediction of the turbulent shear stress ensures that the turbulent time scale, $\tau = k/\epsilon$, supplied to the Monte Carlo simulation is correct.

For the Monte Carlo simulation of the temperature field, two sample sizes of 1000 and 1500 sample particles per cell are used. The predicted mean temperature and the root mean square (rms) of the temperature variation are presented in Figs. 5 and 6. The results show that both calculations produce fairly good comparisons with the experimental data, which means a sample size of 1000 particles per cell is large enough.

The above validation lends credibility to the N.S. solver as well as the Monte Carlo solver developed in the present study.

$H_2 - F_2$ diffusion flames

The flow conditions for the $H_2 - F_2$ diffusion flames are set according to an experiment performed by Hermanson and Dimotakis (1989). The flame consists two streams. The upper stream contains N_2 and F_2, the flow velocity is $U_1 = 22\,m/s$; the lower stream contains of N_2 and of H_2, with velocity $U_2 = 8.8\,m/s$. In the present study, 6 cases involving various percentage of H_2 and F_2 in the upper and lower stream are considered; the conditions are listed in Table 1, where ΔT_{adj} is the difference between the adiabatic flame temperature and the free stream temperature.

case No.	equivalence ratio	lower stream, mole fraction of H_2	upper stream, mole fraction of F_2	ΔT_{adj}
1	1	0.02	0.02	186
2	1	0.04	0.04	368
3	1	0.06	0.06	554
4	1/4	0.01	0.04	151
5	1/4	0.02	0.08	302
6	1/4	0.04	0.16	600

Table 1. Initial conditions of the flames calculated in the present study.

Fig. 7 shows the calculated temperature rises due to combustion for cases 2 and 5 of Table 1 and the corresponding experimental data. In the figure, δ_T is the shear layer thickness determined by 1% of the temperature rise, ΔT is the actual temperature rise due to combustion, (the two streams have the same temperatures initially,) and ΔT_{adj} is the adiabatic flame temperature assuming complete reaction. The solution for case 2 agrees fairly well with the experimental data for the same case, while the mean temperature is slightly over predicted for case 5. The computation shows the flame center shifts as a result of change in equivalence ratio, which is consistent with the experimental results.

The rms of the temperature variance for cases 2 and 5 are given in Fig. 8. The results show that in a diffusion flame, the temperature variance has two peaks, and the highest values do not coincide with the maximum values of the temperature distribution. The shifting of the flame due to the change of equivalence ratio can also be observed from this figure.

The mass fractions of H_2, F_2 and HF for cases 2 and 5 are presented in FIgs. 9 and 10, respectively. One can see that although a complete reaction chemistry model was used, with the pdf method, results simular to that of a finite rate computation are produced, which is one of the many advantages of the pdf method.

One experimentally established fact is that for the same equivalence ratio, with various mole concentrations of fuel and oxidizer in the flowfield, the normalized temperature stays the same [4,5]. The present calculation confirmed this. Figs. 11 and 12 are the mean temperatures and rms's of the temperature variance for an equivalence ratio of one; three mole concentrations of fuel were considered. One can see that the curves coincide with each other. The same agreements are found for equivalence ratio 1/4 (Figs. 13 and 14).

The pdf distributions for flame temperature at the center and at the outer edge of the flame (for case 2 of Table 1) are plotted in Fig. 15, where the x-axis denotes $(T - < T >)/\sigma$, with $< T >= \bar{T}$ being the mean temperature and σ the rms. The pdf distributions show that at the center of the flame, the temperature with the highest probability is not far from the adiabatic flame temperature, while at the outer edge of the flame, most of the time one would find a temperature close to that of the free stream temperature. Nonetheless, as a result of external and internal intermittency, low temperature fluid does exist at the center and high temperature fluid the outer edge. Pdf distributions for various species concentration can also be obtained from the solution, but will not be presented here.

Concluding Remarks

A Monte Carlo solution algorithm for the pdf evolution equation has been developed and successfully combined with a finite difference flow solver in the study of turbulent combustion. The algorithm was validated using turbulent mixing data from non-reacting flows. Turbulent diffusion flames of H_2-F_2 were computed using the pdf method, and good agreements between numerical solution and experimental data were observed. The computation identified the change of equivalence ratio as the cause of flame shift, and demonstrated that similarity solution exists for flames with the same equivalence ratio. The present work showed that a grid dependent Monte Carlo scheme can be readily applied to a general curvilinear coordinate system; therefore, it is suitable for realistic reacting flow computations.

Acknowledgement

The author would like to thank Prof. S.B. Pope, Drs. J.-Y. Chen and J.S. Shuen for their helpful discussions. This work is supported by by NASA Lewis Research Center under Contract NAS-25266 with Dr. L.A. Povinelli as program monitor.

References

1. Pope, S.B., " PDF Methods for Turbulent Reactive Flows." Prg. Energy Combust. Sci., 1985, 11, 119-192.

2. Kollmann, W., "The PDF Approach to Turbulent Flow." Theoret. Comput. Fluid Dynamics, 1990, 1, 249-285.

3. Kuznetsov, V.R., and Sabel'nikov, V.A., *Turbulence and Combustion*, Hemisphere Publishing Corp., 1990.

4. Mungal, M.G. and Dimotakis, P.E., "Mixing and Combustion with Low Heat Release in a Turbulent Shear Layer" J. Fluid Mech. 1984, 148, 349-382.
5. Hermanson, J.C. and Dimotakis, P.E., "Effects of Heat Release in a Turbulent, Reacting Shear Layer." J. Fluid Mech. 1989, 199, 333-375.
6. Janicka, J., Kolbe, W., and Kollmann, W., "Closure of the Transport Equation for the Probability Density Function Scalar Field." J Non-Equilib. Thermodyn. 1979, 4, 47.
7. Hsu, A.T. and Chen, J.Y., "A Continuous Mixing Model for PDF Simulations and its Applications to Combusting Shear Flows." 8th Symposium on Turbulent Shear Flows, Munich, Germany, Sept. 9-11, 1991.
8. Gordon, S. and McBride, B.J., "Computer Program for Calculation of Complex Chemical Equilibrium Compositions, Rocket Performance, Incident and Reflected Shocks, and Chapman-Jouguet Detonations." NASA SP-273, March, 1976.
9. Forthmann, E., *Uber Turbulente Strahlausbreitung*, Diss. Gottingen 1933; Schlischting, H., p 747.
10. Bradbury, L.S., "The Structure of Self-Preserving Turbulent Plane Jet," J. Fluid Mech., 1965, 23, 31-64.
11. Gutmark, E. and Wygnanski, I., "The Plane Jet." J. Fluid Mech., 1976, 73, 465-495.
12. Antonia, R.A., Browne, L.W.B., Chambers, A.J., and Rajagopalan, S., "Budget of the Temperature Variance in a Turbulent Plane Jet." Int. J. Heat Mass Transfer, 1983, 26-1, 41-48.
13. Ashir, J. and Uberoi, M.S., "Experiments on Turbulent Structure and Heat Transfer in a Two Dimensional Jet." Physics of FLuids, 1975, 18-4, 405-410.
14. Browne, L.W.B., Antonia, R.A., and Chembers, A.J., "The Interaction Region of a Turbulent Plane Jet." J. Fluid Mech., 1984, 149, 355-373.
15. Jenkins, P.E. and Goldschmidt, V.W., "Mean Temperature and Velocity in a Plane Turbulent Jet," ASME J. Fluids Eng., 1973, 95, 581-584.
16. Uberoi, M.S. and Singh, P.I., "Turbulent Mixing in a Two-Dimensional jet," Physics of Fluids, 1975, 18-7, 764-769.
17. Bashir, J. and Uberoi, M.S., "Experiments on Turbulent Structure and Heat Transfer in a Two Dimensional Jet." Physics of Fluids, 1975, 14.4, 405-410.

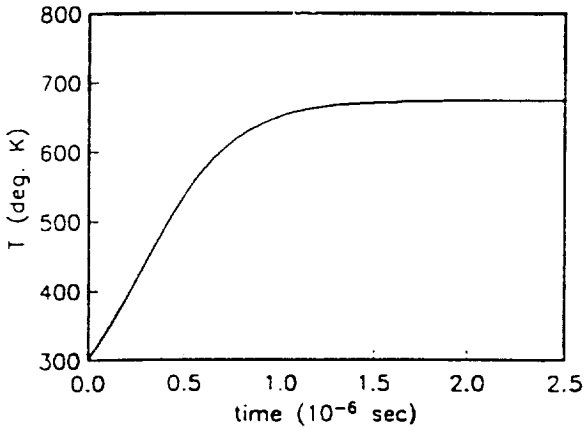

Figure 1. Temperature rise in a premixed laminar H_2–F_2 flame.

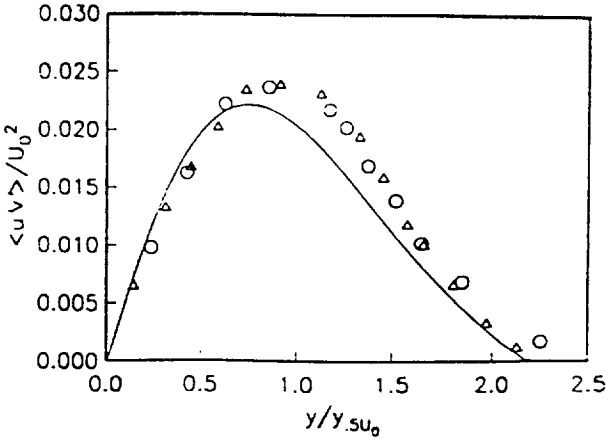

Figure 4. Turbulent shear stress in a 2D turbulent jet. ○ Ref [10], △ Ref [11], — Present calculation.

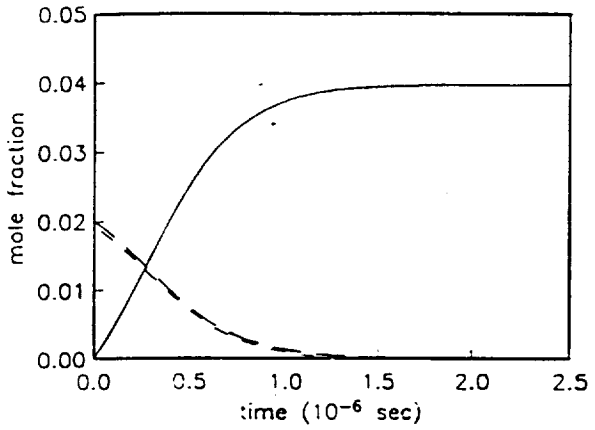

Figure 2. Changes of mass fractions in a premixed laminar H_2–F_2 flame. - - - H_2, – – – F_2, — HF.

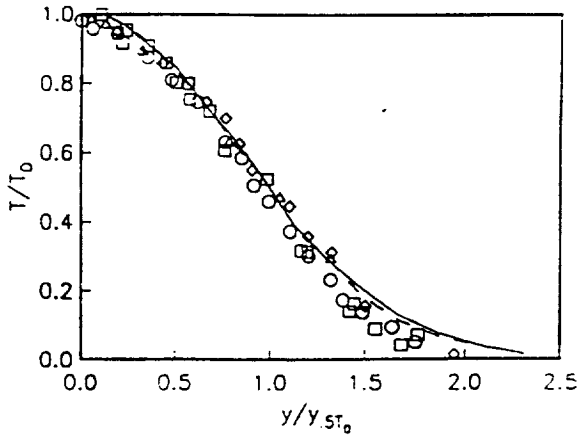

Figure 5. Mean temperature in heated plane jet. △ Ref [14], ⊓ Ref [17], ◇ Ref [16] ○ Ref [15]. — pdf solution. 1500 particles per cell; - - - pdf solution. 1000 particles per cell.

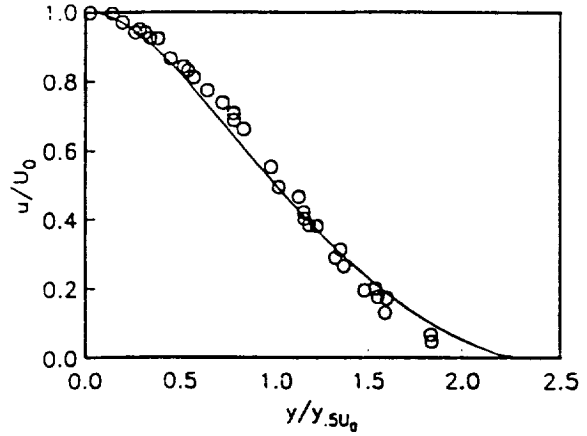

Figure 3. Mean velocity distribution in a 2D turbulent jet. ○ Ref [9], — Present calculation.

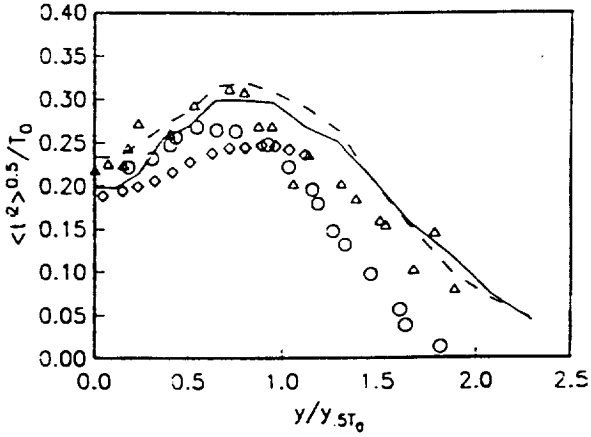

Figure 6. RMS of temperature variance in heated plane jet. ◇ Ref [12], ○ Ref [17], △ Ref [16], — pdf solution. 1500 particles per cell; - - - pdf solution. 1000 particles per cell.

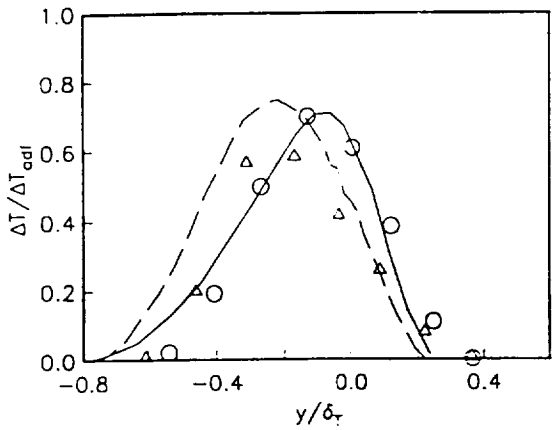

Figure 7. Mean temperature rises in H_2–F_2 diffusion flames. Case 2 (refer to Table 1): o Ref [5], — present; Case 5: Δ Ref [5], - - - present.

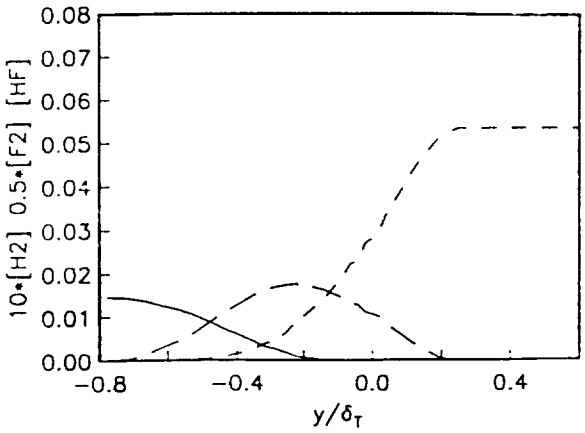

Figure 10. Mass fraction distributions in an H_2–F_2 flame, case 5, equivalence ratio 1/4. — H_2, - - - F_2, – – HF.

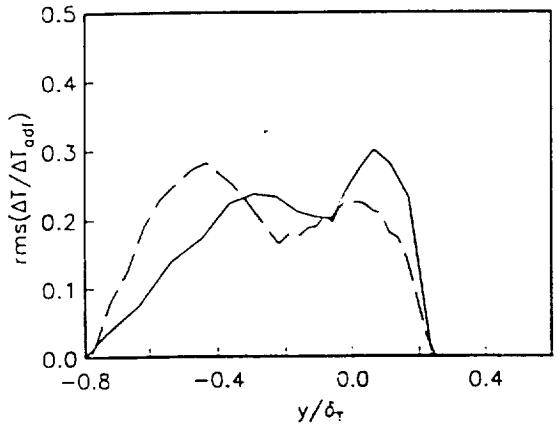

Figure 8. RMS of Temperature variance in H_2–F_2 diffusion flames. — equivalence ratio 1 (case 2, Table 1). - - - equivalence ratio 1/4 (case 5).

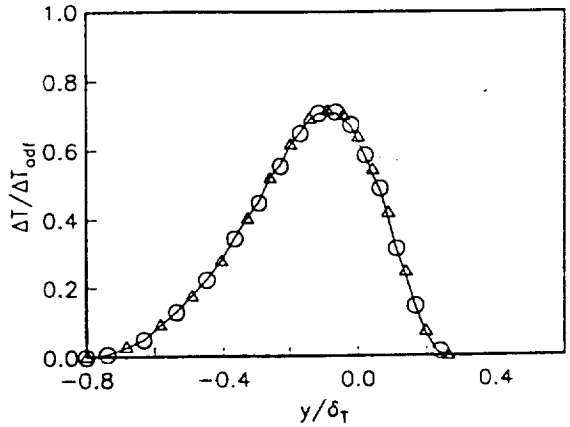

Figure 11. Mean temperature rises in H_2–F_2 flames, equivalence ratio 1. Referring to Table 1: — case 1, o case 2, Δ case 3.

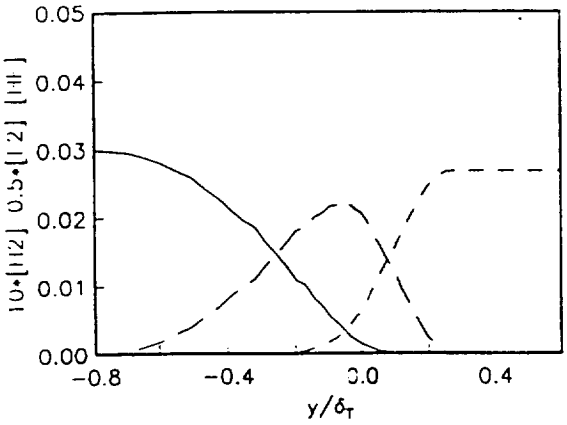

Figure 9. Mass fraction distributions in an H_2–F_2 flame, case 2, equivalence ratio 1. — H_2, - - - F_2, – – HF.

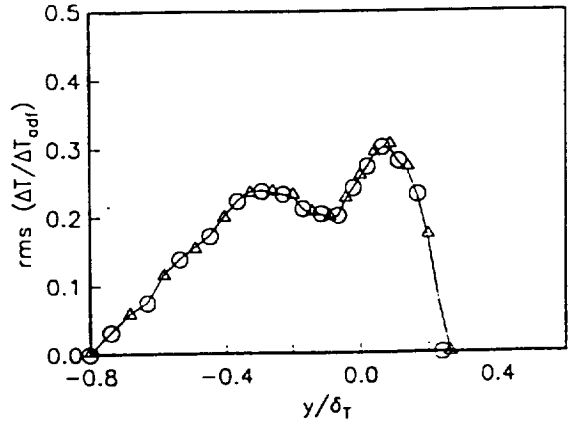

Figure 12. RMS of temperature variance in H_2–F_2 flames, equivalence ratio 1. Referring to Table 1: — case 1, o case 2, Δ case 3.

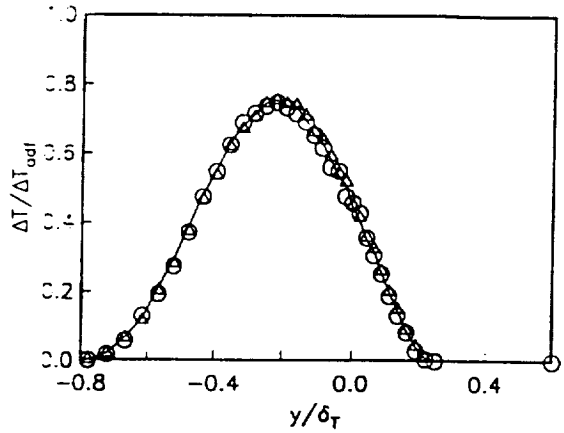

Figure 13. Mean temperature rises in H_2–F_2 flames, equivalence ratio 1/4. Referring to Table 1: — case 4, o case 5, Δ case 6.

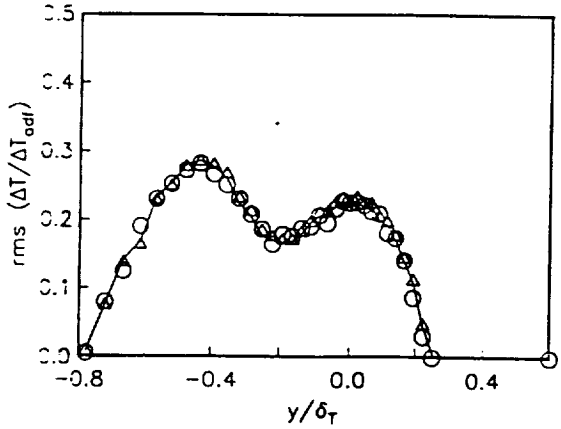

Figure 14. RMS of temperature variance in H_2–F_2 flames, equivalence ratio 1/4. Referring to Table 1: — case 4, o case 5, Δ case 6.

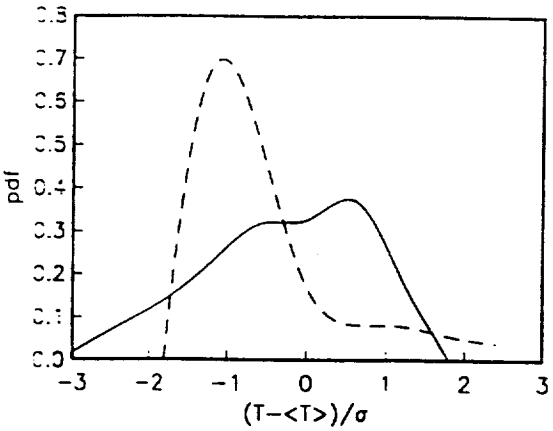

Figure 15. Probability density function distributions in an H_2–F_2 flame (case 2). — pdf at the center of the flame, - - - pdf at the out edge of the flame.

An Improved k-ϵ Model for Near Wall Turbulence

T.H. Shih* and A.T. Hsu**
Center for Modeling of Turbulence and Transition
NASA Lewis Research Center
Cleveland, Ohio 44135

Abstract

This paper presents an improved k-ϵ model for low Reynolds number turbulence near a wall. The work is twofold: In the first part, the near-wall asymptotic behavior of the eddy viscosity and the pressure transport term in the turbulent kinetic energy equation are analyzed. Based on these analyses, a modified eddy viscosity model with the correct near-wall behavior is suggested, and a model for the pressure transport term in the k-equation is proposed. In addition, a modeled dissipation rate equation is reformulated, and a boundary condition for the dissipation rate is suggested. In the second part of the work, one of the deficiencies of the existing $k-\epsilon$ models, namely, the wall distance (e.g., y^+) dependency of the equations and the damping functions, is examined. An improved model that does not depend on any wall distance is introduced. Fully developed turbulent channel flows and turbulent boundary layers over a flat plate are studied as validations for the proposed new models. Numerical results obtained from the present and other previous k-ϵ models are compared with data from direct numerical simulation. The results show that the present k-ϵ model, with added robustness, performs as well as or better than other existing models in predicting the behavior of near-wall turbulence.

1. Introduction

The k-ϵ model is one of the most widely used turbulence models in engineering applications. Patel et al.[1] recently reviewed existing two-equation models that can be integrated directly to the wall. One of their conclusions was that the damping functions used in turbulence models, especially the one for the eddy viscosity, need to be further modified in order to improve model performance. In fact, as we shall see later, many existing k-ϵ models do not provide the correct near-wall behavior of the eddy viscosity.

Shih[2] recently proposed a new near-wall $k-\epsilon$ model based on asymptotic analysis. The present paper is a direct extension of that work.

In the present paper, we will first analyze, in section 2, the near-wall asymptotic behavior of the eddy viscosity and the pressure transport term in the k-equation, and in sections 3 and 4, propose models according to their near-wall behaviors. The model equation for the dissipation rate is reformulated following an argument similar to that of Lumley,[5] and a boundary condition for ϵ is suggested.

An asymptotic analysis shows that, in the near wall region, while the pressure transport term in the turbulent kinetic energy equation is small compared to the dissipation and molecular diffusion terms, it is much larger than the turbulent transport term, and

* Institute for Computational Mechanics in Propulsion.
** Supervisor, Comput. Phys. Section, Sverdrup Technology, Inc., Member AIAA.

it plays an important role in the balance between the dissipation and molecular diffusion terms. This near-wall behavior is also observed in direct numerical simulation of fully developed channel flows (Mansour et al.[32], Kim et al.[4]). However, in existing k-ϵ models, this pressure transport term is either ignored or lumped into the turbulent transport model. The present work introduces a model for the pressure transport term explicitly.

Most of the existing k-ϵ models for near-wall turbulence use y^+ (defined as $u_\tau y/\nu$, where u_τ the friction velocity) as a parameter in constructing damping functions, with the Jones-Launder model being the only exception. While the use of y^+ is perfectly fine for simple attached boundary layer flows, it is inconvenient in more general applications such as separated flows and flows with corners, where y^+ is not well defined. The Jones-Launder model has the advantage of avoiding y^+; however, the model is known to perform poorly in predicting near wall turbulent quantities, especially the turbulence kinetic energy. In the present work, a new damping function is derived based on asymptotic analysis (Section 5). The new function is constructed upon a non-dimensional quantity that is independent of the coordinate system.

The new models proposed in this paper were validated using direct numerical simulation data for fully developed turbulent channel flows and turbulent boundary layers over a flat plate. These numerical results are reported in Section 6. Comparisons are also made with other popular $k-\epsilon$ models implemented in the same computer code. The numerical results show that the present model, in general, performs better than the existing models while providing added robustness.

2. Asymptotic Analysis

To analyze the near-wall asymptotic behavior of the eddy viscosity and other turbulent quantities, we expand the fluctuating velocities and pressure in Taylor series about the wall distance as follows:

$$\begin{aligned} u_1 &= b_1 y + c_1 y^2 + d_1 y^3 + \dots \\ u_2 &= c_2 y^2 + d_2 y^3 + \dots \\ u_3 &= b_3 y + c_3 y^2 + d_3 y^3 + \dots \\ p &= a_p + b_p y + c_p y^2 + d_p y^3 + \dots \end{aligned} \tag{1}$$

where the coefficients $a_p, b_1, c_2, \dots$ are functions of x, z and t. Using the continuity and momentum equations, Mansour et al.[3] derived the following relations between the coefficients,

$$\begin{aligned} 2c_2 &= -(b_{1,1} + b_{3,3}) \\ a_{p,1} &= 2\nu c_1 \\ a_{p,3} &= 2\nu c_3 \end{aligned} \tag{2}$$

The eddy viscosity is usually defined as

$$-\langle u_i u_j \rangle = \nu_T (U_{i,j} + U_{j,i}) - \frac{2}{3} k \delta_{ij} \tag{3}$$

where $\langle\ \rangle$ stands for ensemble average and $k \equiv \langle u_i u_i \rangle/2$ is the turbulent kinetic energy. For plane shear flows, we can write from Eq. (3)

$$\nu_T = \frac{-\langle uv \rangle}{\partial U/\partial y} \tag{4}$$

and using Eq. (1), we obtain the near-wall asymptotic behavior of the eddy viscosity:

$$\nu_T = \frac{-\langle b_1 c_2 \rangle}{\langle b_1 \rangle} y^3 + \frac{-\langle b_1 d_2 + c_1 c_2 \rangle + 2\langle b_1 c_2 \rangle \langle c_1 \rangle}{\langle b_1 \rangle} y^4 + O(y^5) \tag{5}$$

That is, near the wall ν_T is $O(y^3)$. A correct eddy viscosity model should have this near-wall behavior. We shall see later that many existing models do not have this near-wall behavior. For later use, let us examine also the near-wall asymptotic behavior of the turbulent kinetic energy k and its dissipation rate $\epsilon \equiv \nu \langle u_{i,j} u_{i,j} \rangle$. Using Eq. (1), we obtain the following relations for the k and ϵ:

$$k = \frac{\langle b_1^2 \rangle + \langle b_3^2 \rangle}{2} y^2 + (\langle b_1 c_1 \rangle + \langle b_3 c_3 \rangle) y^3 + O(y^4) \tag{6}$$

$$\frac{\epsilon}{\nu} = \langle b_1^2 \rangle + \langle b_3^2 \rangle + 4(\langle b_1 c_1 \rangle + \langle b_3 c_3 \rangle) y + O(y^2) \tag{7}$$

In addition, the pressure transport term in the k-equation, $\Pi \equiv -\frac{1}{\rho}\langle u_i p_{,i} \rangle$, becomes (using Eq.s (1) and (2))

$$\Pi = -2\nu(\langle b_1 c_1 \rangle + \langle b_3 c_3 \rangle) y + O(y^2) \tag{8}$$

The turbulent transport term in the k-equation, $-\langle k u_i \rangle_{,i}$, can be estimated as $O(y^3)$. Therefore, the pressure transport term is much larger than the turbulent transport term near the wall.

3. Eddy viscosity model

In this section, we will propose a model for the eddy viscosity using its near-wall behavior described in the previous section. In general, the eddy viscosity model can be written as

$$\nu_T = c\ u' \ell' \tag{9}$$

where u' and ℓ' are the turbulent characteristic velocity and length scale, respectively. Depending on how the velocity and length scales are specified, the eddy viscosity model can be a mixing length model, a one-equation (k) model or a two-equation (e.g. k-ϵ) model. For example, in plane shear flows, Prandtl's mixing length model specifies the characteristic velocity with $\ell' \partial U/\partial y$. For near wall turbulence, the Van Driest mixing length model further damps the length scale to $y[1 - \exp(-y^+/A)]$. For more advanced mixing length models, see Baldwin and Lomax[6], and King[7]. One-equation (k) models use $k^{1/2}$ as the characteristic velocity, which is determined by the turbulent kinetic energy

equation. In two-equation models, e.g. k-ϵ models, the length scale is usually specified by $k^{3/2}/\epsilon$, where ϵ is determined by a dissipation rate equation. In this paper we will concentrate on two-equation models, wherein the eddy viscosity is usually written as

$$\nu_T = C_\mu f_\mu \frac{k^2}{\epsilon} \tag{10}$$

where $C_\mu = 0.09$, and f_μ is a damping function. The form of the damping function is critical in such formulations, since the prediction of the mean velocity field depends primarily on the eddy viscosity model. Thus it is important for an eddy viscosity model to have the proper near-wall behavior. We have examined the near-wall behavior of eddy viscosity models based on various k-ϵ model equations. The results are listed in Table 1, which shows that some of the k-ϵ models do not have the correct near-wall behavior of the eddy viscosity, namely, $\nu_t = O(y^3)$.

The quantity $k^{3/2}/\epsilon$ is usually considered a characteristic length scale, ℓ', (or the size) of the energy containing eddies. One expects that near the wall the size of these eddies to be of the order of the distance from the wall, $O(y)$. However, Eq.s (6) and (7) show that $k^{3/2}/\epsilon$ is $O(y^3)$. Hence, $k^{3/2}/\epsilon$ is not an appropriate quantity to represent the length scale of the large eddies near the wall. We therefore introduce a new variable $\tilde{\epsilon}$:

$$\tilde{\epsilon} = \epsilon - \nu \frac{\partial k/\partial x_i \; \partial k/\partial x_i}{2k} \tag{11}$$

which has the following property: $\tilde{\epsilon}$ approaches ϵ away from the wall and is $O(y^2)$ near the wall. Therefore, $k^{3/2}/\tilde{\epsilon}$ is a proper quantity to characterize the length scale of the large eddies. With this length scale, the eddy viscosity should be written as

$$\nu_T = C_\mu f_\mu \frac{k^2}{\tilde{\epsilon}} \tag{12}$$

Now in order for ν_T to have the correct near-wall behavior, the damping function f_μ must be $O(y)$ near the wall and approaches 1 away from the wall. The damping functions used in various k-ϵ models are listed in Table 2. If we consider the presence of the wall as the main effect on the eddy viscosity, then we may assume f_μ is mainly a function of y^+. The form of f_μ can be determined quite accurately if we know ν_T, k and $\tilde{\epsilon}$ from, for example, the direct numerical simulation. One may optimize the following simple form by numerical experiments:

$$f_\mu = 1 - \exp(-a_1 y^+ - a_2 {y^+}^2 - a_3 {y^+}^3 - a_4 {y^+}^4) \tag{13}$$

The optimal values for channel flows are $a_1 = 6 \times 10^{-3}, a_2 = 4 \times 10^{-4}, a_3 = -2.5 \times 10^{-6}, a_4 = 4 \times 10^{-9}$. It can be shown that this form of damping function does provide the required near-wall behavior. As will be shown later, the above constants are valid for general boundary layer flows.

4. Modeled k-ϵ equation

To complete the eddy viscosity model, we need the modeled equations for the turbulent kinetic energy and its dissipation rate. In this section we will analyze the near-wall behavior of the k-equation and propose a model for the pressure transport term with a proper near-wall behavior. The equation for the dissipation rate is also reformulated with a formal invariant analysis.

4.1 k-equation

We start with the equation for the turbulent kinetic energy,

$$k_{,t} + U_j k_{,j} = D_\nu + T + \Pi + P - \epsilon \tag{14}$$

where D_ν, T and Π represent the transport of the turbulent kinetic energy due to the viscosity, turbulent velocity and pressure, respectively. P and ϵ are the rate of production and dissipation of the turbulent kinetic energy. The terms on the right hand side of Eq. (14) are defined as follows:

$$\begin{aligned} D_\nu &= \nu k_{,jj} \\ T &= -\langle k u_j \rangle_{,j} \\ \Pi &= -\frac{1}{\rho}\langle p u_j \rangle_{,j} \\ P &= -\langle u_i u_j \rangle U_{i,j} \\ \epsilon &\equiv \nu \langle u_{i,j} u_{i,j} \rangle \end{aligned} \tag{15}$$

Using Eq.s (1) and (2), we obtain the budget of the k-equation near the wall,

$$\begin{aligned} \frac{Dk}{Dt} &= O(y^3) \\ D_\nu &= \nu(\langle b_1^2 \rangle + \langle b_3^2 \rangle) + 6\nu(\langle b_1 c_1 \rangle + \langle b_3 c_3 \rangle)y + O(y^2) \\ T &= O(y^3) \\ \Pi &= -2\nu(\langle b_1 c_1 \rangle + \langle b_3 c_3 \rangle)y + O(y^2) \\ P &= O(y^3) \\ \epsilon &= \nu(\langle b_1^2 \rangle + \langle b_3^2 \rangle) + 4\nu(\langle b_1 c_1 \rangle + \langle b_3 c_3 \rangle)y + O(y^2) \end{aligned} \tag{16}$$

This budget shows that the term Π is much larger than the term T, and that Π cannot be neglected if we want the k-equation be balanced in the near-wall region. However, the existing models either do not consider this term or simply combine it with the term T and model them as

$$-\langle k u_j \rangle_{,j} = \left[\frac{\nu_T}{\sigma_k} k_{,j} \right]_{,j} \tag{17}$$

In this paper, we propose a model for Π which has a similar form to that of the standard turbulent transport model, but with a coefficient to ensure its correct near -wall behavior, Eq. (8). The proposed model form of Π is

$$\Pi = \left\{ \frac{C_0}{f_\mu [1 - \exp(-y^+)]} \frac{\nu_T}{\sigma_k} k_{,j} \right\}_{,j} \tag{18}$$

where $C_0 = 0.05$ is a model constant. In some existing k-ϵ models, it is assumed that $\epsilon = 0$ at the wall. In that case, in order to balance the term D_ν, a nonzero artificial term D must be added to the k-equation. The form of D for various k-ϵ models is listed in Table 3. Finally, the modeled k-equation becomes

$$\frac{\partial k}{\partial t} + U_j \frac{\partial k}{\partial x_j} = \frac{\partial}{\partial x_j}[(\nu + \frac{\nu_T}{\sigma_k})\frac{\partial k}{\partial x_j}] + \Pi + \nu_T(\frac{\partial U_i}{\partial x_j} + \frac{\partial U_j}{\partial x_i})\frac{\partial U_i}{\partial x_j} - \epsilon + D \tag{19}$$

In the present model, $D = 0$, since ϵ is nonzero at the wall. (The boundary condition for ϵ will be discussed later.)

4.2 ϵ-equation.

The exact dissipation rate equation is

$$\epsilon_{,t} + \bar{U}_j \epsilon_{,j} = D^\epsilon_\nu + T^\epsilon + \Pi^\epsilon + PD \tag{20}$$

where D^ϵ_ν, T^ϵ and Π^ϵ represent the diffusion rate of the dissipation rate due to the viscosity, turbulent velocity and pressure, respectively, and PD stands for the entire mechanism of the **production** and **destruction** of the dissipation rate ϵ. The terms on the right hand side of the above equation are as follows:

$$\begin{aligned} D^\epsilon_\nu &= \nu \epsilon_{,jj} \\ T^\epsilon &= -\nu \langle u_{i,k} u_{i,k} u_j \rangle_{,j} \\ \Pi^\epsilon &= -\frac{2\nu}{\rho} \langle p_{,k} u_{j,k} \rangle_{,j} \\ PD &= -2\nu(\langle u_{i,k} u_{j,k} \rangle + \langle u_{k,i} u_{k,j} \rangle) U_{i,j} - 2\nu \langle u_j u_{i,k} \rangle U_{i,kj} \\ &\quad - 2\nu \langle u_{i,k} u_{j,k} u_{i,j} \rangle - 2\nu^2 \langle u_{i,kj} u_{i,kj} \rangle \end{aligned} \tag{21}$$

The term Π^ϵ is usually neglected and the term T^ϵ is modeled as

$$T^\epsilon = \left[\frac{\nu_T}{\sigma_\epsilon} \epsilon_{,j}\right]_{,j} \tag{22}$$

To model PD, we define Ψ by

$$PD = -\frac{\epsilon \tilde{\epsilon}}{k} \Psi$$

At the level of the k-ϵ model, we assume Ψ is a function of ν, ν_T, k, ϵ, $\tilde{\epsilon}$, $U_{i,j}$ and $U_{i,jk}$. Since Ψ is an invariant, it must be a function of the invariants that can be constructed from these quantities. Therefore we can write

$$\Psi = \Psi(R_t, \frac{\nu_T U_{i,j} U_{i,j}}{\tilde{\epsilon}}, \nu \nu_T U_{i,jk} U_{i,jk} \frac{k}{\epsilon \tilde{\epsilon}})$$

where R_t is the turbulent Reynolds number $k^2/\nu\epsilon$. We expand Ψ in a Taylor series about $\nu_T U_{i,j} U_{i,j}/\tilde{\epsilon}$ and $\nu \nu_T U_{i,jk} U_{i,jk} k/\epsilon\tilde{\epsilon}$, and take only the linear terms. We obtain

$$\Psi = \psi_0 + \psi_1 \frac{\nu_T U_{i,j} U_{i,j}}{\tilde{\epsilon}} + \psi_2 \nu \nu_T U_{i,jk} U_{i,jk} \frac{k}{\epsilon \tilde{\epsilon}} \tag{23}$$

where the coefficients ψ_0, ψ_1 and ψ_2 are in general functions of R_t. Finally, the modeled dissipation rate equation becomes

$$\frac{\partial \epsilon}{\partial t} + U_j \frac{\partial \epsilon}{\partial x_j} = \frac{\partial}{\partial x_j}[(\nu + \frac{\nu_T}{\sigma_\epsilon})\frac{\partial \epsilon}{\partial x_j}] + C_1 f_1 \frac{\epsilon}{k} \nu_T U_{i,j} U_{i,j} - C_2 f_2 \frac{\epsilon\tilde{\epsilon}}{k} + E \tag{24}$$

where, C_1 and C_2 are the model constants, and f_1 and f_2 are functions of R_t. The term E in the present model comes from the last term in Eq. (23):

$$E = \nu\nu_T U_{i,jk} U_{i,jk} \tag{25}$$

where we have taken $\psi_2 = -1$. The form of E and C_1, C_2, f_1 and f_2 for various k-ϵ models are listed in Tables 3 and 4.

4.3 Boundary Condition for ϵ.

Many of the earlier $k - \epsilon$ models use $\epsilon = 0$ as the boundary condition for the dissipation rate. It is now generally agreed that this is not the physically correct boundary condition. However, controversy still exists in what boundary condition should be used for the dissipation rate. In some calculations, $\partial\epsilon/\partial y = 0$ is used. which clearly has no physical background. Most models use the second derivative of the turbulent kinetic energy at the boundary as the boundary condition for ϵ, as listed in Table 1. This condition comes directly from the k-equation and is physically correct; however, it makes the problem very stiff and thus put very stringent restrictions on the choice of initial profiles for k and ϵ. If the initial profile for k is not given correctly, the second derivative of k can become negative and cause the solution procedure to diverge.

We propose the following boundary condition based on the asymptotic analysis. At $y = 0$, it is obvious from eqs. (6) and (7) that

$$\epsilon = 2\nu \left(\frac{\partial \sqrt{k}}{\partial y} \right)^2 \tag{26}$$

This expression is exact at the wall, and it does not add stiffness to the solution procedure.

5. Deficiencies and Improvements of Existing Models

5.1 Damping functions

One of the deficiencies of the existing near wall models is that most of the wall damping coefficients are functions of a wall coordinate, such as the y^+. This types of damping function works well only in the cases of attached boundary layer flows with simple geometries where y^+ is well defined. For practical engineering problems with corner flows or separated flows, some ad hoc treatment to the damping function must be made. The same is also true for the length scale in an algebraic model. The only exception to the above is the Jones-Launder model in which the damping function is a function of $R_t = k^2/\nu\epsilon$.

Although the Jones-Launder model has the advantage of independent of y^+, it is known that this model does not predict correctly the near-all turbulence, especially,

the near-wall turbulent kinetic energy is underpredicted. One natural option could be to modify the J-L model such that it would predict the correct near-wall turbulent quantities. However, one basic difficulty met in such attempts is that the k-equation is very stiff. The fact that we are putting k^2 back into the equation by using the parameter R_t aggravates the situation.

To avoid the above difficulty and yet still achieve the same end, we introduce the following parameter:

$$R_u = \frac{U^4}{\nu\epsilon}, \tag{27}$$

where U is the total velocity. (Note: U is the total velocity in a coordinate frame fixed to the solid boundary.) From the results given in Section 3, since ϵ approaches a finite value at the wall, it is obvious from eq. (1) that $R_u = O(y^4)$ near the wall. Similar to eq. (13) of Section 3, we write the damping function for the eddy viscosity as:

$$f_\mu = 1 - exp(-a_1 R_u^{1/4} - a_2 R_u^{1/2} - a_3 R_u) \tag{28}$$

with $a_1 = 5 \times 10^{-3}$, $a_2 = 7 \times 10^{-5}$, and $a_3 = 8 \times 10^{-7}$. One can easily verify that with this damping function, the eddy viscosity has the correct near wall behavior, i.e., $\nu_T = O(y^3)$.

One point worth mentioning is the wide applicability of the above damping function. Though developed with Shih model (Section 3, 4) in mind, it can be used with any existing $k-\epsilon$ model that uses a non-zero boundary condition for the dissipation. This new parameter R_u, unlike R_t, by no means affect the stability of the solution procedure.

5.2 Pressure transport term.

In order to remove the coordinate dependency of the k-equation, we replace the pressure transport term given in eq. (18) by the following expression:

$$\Pi = \left[\frac{C_0}{f_\mu^2}\frac{\nu_T}{\sigma_k}k_{,j}\right]_{,j} \tag{29}$$

where the model constant is readjusted to $C_0 = 0.01$.

5.3 The formulation of $\tilde{\epsilon}$.

In order to obtain the correct wall behavior for the eddy viscosity, we have introduced $\tilde{\epsilon}$ in eq. (11), Section 3. Theoretical analysis shows that $\tilde{\epsilon}$ is always positive. However, in numerical calculations, the value of $\tilde{\epsilon}$ may become negative or even oscillatory due to round of errors. (Depending on the accuracy of the numerical procedure, this may or may not be the case.) Here, an alternative definition of $\tilde{\epsilon}$ is suggested:

$$\tilde{\epsilon} = (1 - exp(-R_t^{1/2}))\epsilon \tag{30}$$

This expression has the same near wall behavior as eq. (11) but is less likely to cause numerical instability.

With the modifications suggested above, the model constants need slight adjustment. The constants used in the present modified model are as shown in Table 4.

6. Numerical Testing

Flows with self-similar solutions are particularly useful for accurate model testing, because their solutions are independent of initial conditions, and one does not need to choose carefully the initial conditions for the k and ϵ. In this paper, we use a fully developed channel flow and a flat plate boundary layer for model testing. These flows are the simplest wall bounded turbulent shear flows with self-similar solutions. However, the complex features of the turbulence, for example, the effect of the wall on shear turbulence, are present. In the case of the channel flow, the k-ϵ equations form a one-dimensional problem, numerical calculations are easy and accurate. Recently, the measurements[8] confirmed the accuracy of the direct numerical simulation data.[4] These data are used for model validations.

In legends of the figures presented at the end of the paper, which will be discussed in detail in the following paragraphs, the word "present" refers to results obtained using the model suggested in Section 4 together with the new damping function and $\tilde{\epsilon}$ given in Section 5, while the label "Shih" refers to results obtained using strictly formulations given in Section 4.

6.1 Fully developed turbulent channel flow

Let h be the half width of the channel, u_τ the friction velocity and Re_τ the Reynolds number defined as $u_\tau h/\nu$. Let U, k, ϵ, ν_T and y be the non-dimensional quantities, normalized by u_τ, u_τ^2, $u_\tau^3/h, \nu$ and h, respectively. The modeled equations for the channel flow become

$$\frac{dU}{dy} = Re_\tau \frac{1-y}{1+\nu} \tag{31}$$

$$\frac{d}{dy}\{\frac{1}{Re_\tau}[1+(1+C)\frac{\nu_T}{\sigma_k}]\frac{dk}{dy}\} + \nu_T(\frac{dU}{dy})^2\frac{1}{Re_\tau} - \epsilon = 0 \tag{32}$$

$$\frac{d}{dy}\{\frac{1}{Re_\tau}(1+\frac{\nu_T}{\sigma_\epsilon})\frac{d\epsilon}{dy}\} + C_1\frac{\epsilon}{k}\nu_T(\frac{dU}{dy})^2\frac{1}{Re_\tau} - C_2 f_2\frac{\epsilon\tilde{\epsilon}}{k} + \nu_T(\frac{d^2U}{dy^2})^2\frac{1}{Re_\tau^2} = 0 \tag{33}$$

where

$$\begin{aligned}
\nu_T &= C_\mu f_\mu Re_\tau \frac{k^2}{\tilde{\epsilon}} \\
\tilde{\epsilon} &= \epsilon - \frac{(\frac{dk}{dy})^2}{2k\ Re_\tau} \\
f_\mu &= \text{equation(13)} \\
f_2 &= 1 - \frac{0.4}{1.8}\exp[-(\frac{Re_\tau k^2}{6\epsilon})^2] \\
C &= \frac{C_0}{f_\mu[1-\exp(-y^+)]}
\end{aligned} \tag{34}$$

The boundary conditions are simple. At the wall,

$$U = k = 0$$
$$\epsilon = \frac{(\frac{dk}{dy})^2}{2k\ Re_\tau} \tag{35}$$

and at the center of the channel,

$$\frac{dk}{dy} = \frac{d\epsilon}{dy} = 0 \tag{36}$$

The main results from different k-ϵ models for a channel flow with $Re_\tau = 180$ are plotted in figures 1 – 4. All the calculations are compared with the direct numerical simulation data. Figure 1 shows mean velocity profile, Figure 2 shows the turbulent kinetic energy, Figure 3 shows the turbulent shear stress distribution, and Figure 4 shows the Dissipation rate. From these numerical results we reach the following conclusions: The model of Jones and Launder[10] (JL) underpredicts the mean velocity as well as the peak value of the turbulent kinetic energy. Chien's model[11] performs better than the JL model, but it overpredicts the mean velocity near the center of the channel as well as the turbulent kinetic energy. In these two models, $\epsilon = 0$ at the wall is used as the boundary condition, so the dissipation rate near the wall cannot be correctly predicted. Lam and Bremhorst[12] use a nonzero boundary condition for ϵ and have made some improvement for the mean velocity and turbulent kinetic energy compared with the results of the JL model. However, the shear is much overpredicted, and the dissipation rate near the wall is not correct. The model of Nagano and Hishida[13] presents a very good prediction for the mean velocity and shear stress, while the peak value of k is underpredicted. Their main modification to the JL model is a change in the damping function f_μ and the form of E. A zero dissipation rate at the wall is used. The numerical results from the Shih model and the present modified Shih model show improvements in the prediction of all quantities, including the dissipation rate.

6.2 Boundary layer flows

The boundary layer equations and the corresponding $k-$ and $\epsilon-$equations are solved using a conventional semi-implicit finite difference scheme. In this scheme, the coefficients for the convection terms are lagged one step in the x-direction, and the source terms in the $k-$ and $\epsilon-$equation are linearized in such a way that stability is ensured.

In the present study, a grid of 100 points in the y-direction is used. The grid is stretched linearly with $\Delta y_{j+1}/\Delta y_j = 1.05$. The grids expands in the y-direction according the the boundary layer growth rate.

The results of this calculation are presented in Figure 5 through Figure 10.

Figure 5 and 6 show the comparison of the wall shear stress from various models to experimental data and some DNS data. As shown in Figure 5, at low Reynolds number (based on momentum thickness), J-L model overpredicts the shear stress while Chien model and NH model underpredict the shear stress. One common character of these three models is that they all used zero boundary condition for the dissipation, and thus unable

to predict the correct turbulence near wall behavior. At high Reynolds number (Figure 6) the JL model still overpredicts the wall shear stress, while the others seem to do a fare job.

Figure 7 and 8 are the results for $Re_\theta = 1410$, and Figure 9 and 10 are the results for $Re_\theta = 7700$. From these results one can reach similar conclusions as we did from the channel flow case: The JL model generally underpredicts the peak value of the turbulent kinetic energy while overpredicts it in the inertia layer; the model also underpredicts the mean velocity profiles. The LB model and the NH model also underpredict the peak value of the turbulent kinetic energy near the wall. The three models mentioned above either have zero boundary condition for ϵ or do not have the correct order of magnitude for eddy viscosity. The Figures show that, in general, the present model performs better than the existing models.

Conclusions

From the model testing, we conclude that the present k -ϵ model has made considerable improvement over previous k-ϵ models according to the comparison with the direct numerical simulation data. We find that the improvement is mainly due to the modified eddy viscosity model and the model of the pressure transport term in the k-equation. The proposed dissipation rate equation also shows a better near-wall behavior than the previous ones. The correct boundary condition for ϵ also seem to play an important role in the accurate prediction of the turbulence near wall behavior.

Acknowledgement

The first author is grateful to Drs. N.N. Mansour, D. Driver and Professor P. Moin for their many useful comments. The first author was supported in part by Center for Turbulence Research at Stanford; in part by Institute for Computational Mechanics in Propulsion, NASA Lewis Research Center. The second author is supported by NASA Lewis under Contract NAS3-25266.

References

1. Patel, V.C., Rodi, W. and Scheuerer, G., "Turbulence models for near–wall and low–Reynolds–number flows: A Review," *AIAA Journal*, 23, 1985, pp. 1308–1319.

2. Shih, T.H., "An Improved $k-\epsilon$ Model for Near Wall Turbulence and Comparison with Direct Numerical Simulation," NASA TM-103221, August, 1990.

3. Mansour, N.N., Kim,J. and Moin. P., "Reynolds–Stress and Dissipation Rate Budgets in a Turbulent Channel Flow," *J. Fluid Mech.*, Vol. 194, 1988, pp. 15–44.

4. Kim, J., Moin, P. and Moser, Robert., "Turbulent statistics in fully developed channel flow at low Reynolds number," *J. Fluid Mech.*, 177, 1987, pp. 133–166.

5. Lumley, J.L., "Computational modeling of turbulent flows," in *Advances in Applied Mechanics*, Vol. 18, 1978, Academic Press, New York, pp.123–176.

6. Baldwin, B.S. and Lomax H., "Thin Layer Approximation and Algebraic Model for Separated Turbulent Flows," *AIAA Paper* no. 78-257, Huntsville, Ala., 1978.

7. King, L.S., "A comparison of turbulence closure models for transonic flows about airfoils," *AIAA Paper* no. 87-0418, Reno, Nevada, 1987.

8. Nishino, K. and Kasagi, N., "Turbulent statistics measurement in a two dimensional channel flow using a three-dimensional particle tracking velocimeter," *Seventh Symposium on Turbulent Shear Flows*, Stanford University, 1989.

9. Spalding, D.B., GENMIX: "A General Computer Program for Two-dimensional Parabolic Phenomena," 1977, Pergamon Press.

10. Jones, W.P. and Launder, B.E., "The Calculation of Low -Reynolds Number Phenomena with a Two-Equation model of Turbulence," *International Journal of Heat and Mass Transfer*, Vol. 16, 1973, pp. 1119-1130.

11. Chien, K.-Y., "Predictions of Channel and Boundary -Layer Flow with a Low-Reynolds-Number Turbulence Model," *AIAA Journal*, Vol. 20, Jan. 1982, pp. 33-38.

12. Lam, C.K.G. and Bremhorst, K., "A Modified Form of the $K-\epsilon$ Model for Predicting Wall Turbulence,"*ASME Transactions, Journal of Fluids Engineering*, Vol. 103, Sept. 1981, pp.456-460.

13. Nagano, Y. and Hishida, M., "Improved Form of the $K-\epsilon$ Model for Wall Turbulent Shear Flows,"*ASME Transaction, Journal of Fluids Engineering*, Vol. 109, June 1987.

Table 1 Eddy viscosity and boundary condition for ϵ in various k-ϵ models

Model	ν_T	BC: ϵ_w
JL	$O(y^3)$	0
Reynolds	$O(y^5)$	$\nu\frac{\partial^2 k}{\partial y^2}$
LB	$O(y^4)$	$\nu\frac{\partial^2 k}{\partial y^2}$
Chien	$O(y^3)$	0
NH	$O(y^4)$	0
Shih	$O(y^3)$	$2\nu\left(\frac{\partial\sqrt{k}}{\partial y}\right)^2$
Present	$O(y^3)$	$2\nu\left(\frac{\partial\sqrt{k}}{\partial y}\right)^2$

Table 2 Damping functions used in various k-ϵ models

Model	f_μ	f_1	f_2
JL	$\exp(\frac{-2.5}{1+R_t/50})$	1.0	$1-.3\exp(-R_t^2)$
Reynolds	$1-\exp(-.0198R_k)$	1.0	$[1-.3\exp(-R_t^2/9)]f_\mu$
LB	$[1-\exp(-.0165R_k)]^2$ $\times(1+\frac{20.5}{R_t})$	$1+(\frac{.05}{f_\mu})^3$	$1-\exp(-R_t^2)$
Chien	$1-\exp(-.0115y^+)$	1.0	$1-.22\exp(-R_t^2/36)$
NH	$[1-\exp(-y^+/26.5)]^2$	1.0	$1-.3\exp(-R_t^2)$
Shih	Eq. (13)	1.0	$1-.22\exp(-R_t^2/36)$
Present	Eq. (28)	1.0	$1-.22\exp(-R_t^2/36)$

Table 3 Model terms in various k-ϵ models

Model	Π	D	E
JL	0	$-2\nu\left(\frac{\partial\sqrt{K}}{\partial y}\right)^2$	$2\nu\nu_T\left(\frac{\partial^2 U}{\partial y^2}\right)^2$
Reynolds	0	0	0
LB	0	0	0
Chien	0	$-\frac{2\nu K}{y^2}$	$-\frac{2\nu\epsilon}{y^2}\exp(-.5y^+)$
NH	0	$-2\nu\left(\frac{\partial\sqrt{K}}{\partial y}\right)^2$	$\nu\nu_T(1-f_\mu)\left(\frac{\partial^2 U}{\partial y^2}\right)^2$
Shih	Eq. (18)	0	$\nu\nu_T\left(\frac{\partial^2 U}{\partial y^2}\right)^2$
Present	Eq. (29)	0	$\nu\nu_T\left(\frac{\partial^2 U}{\partial y^2}\right)^2$

Table 4 Model constants in various k-ϵ models

Model	C_μ	C_1	C_2	σ_k	σ_ϵ
JL	.09	1.45	2.0	1.0	1.3
Reynolds	.084	1.0	1.83	1.69	1.3
LB	.09	1.44	1.92	1.0	1.3
Chien	.09	1.35	1.8	1.0	1.3
NH	.09	1.45	1.9	1.0	1.3
Shih	.09	1.45	2.0	1.3	1.3
Present	.09	1.5	2.0	1.3	1.3

$R_t = K^2/\nu\epsilon$, $R_k = \sqrt{K}y/\nu$, $y^+ = u_\tau y/\nu$.

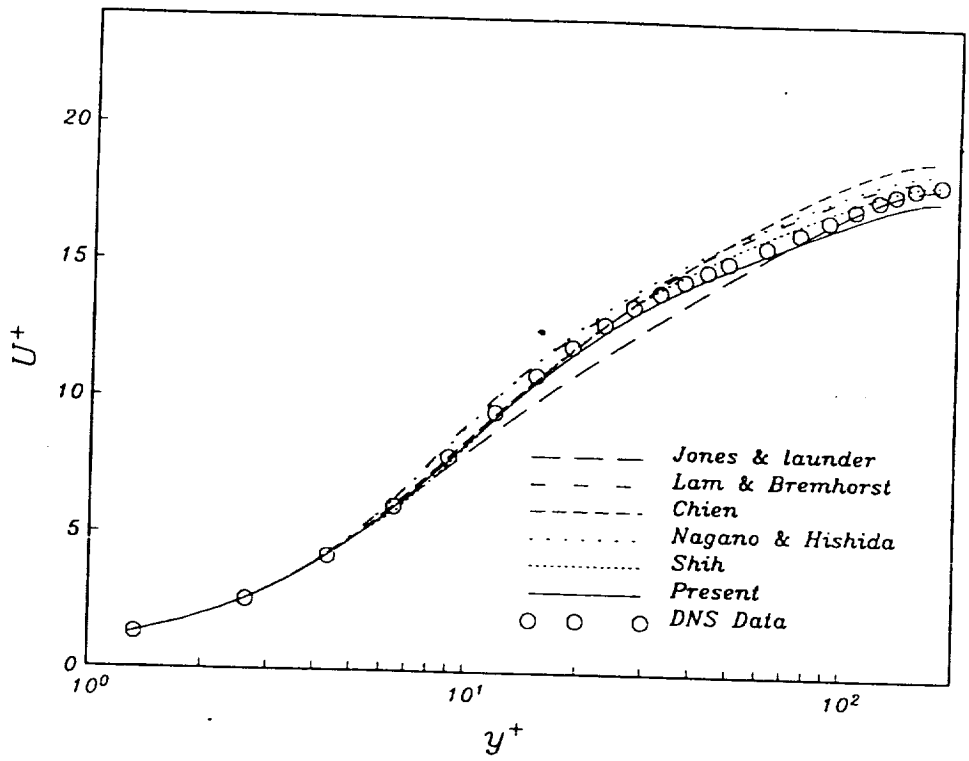

Figure 1. Mean velocity profile for channel flow, $Re_\tau = 180$.

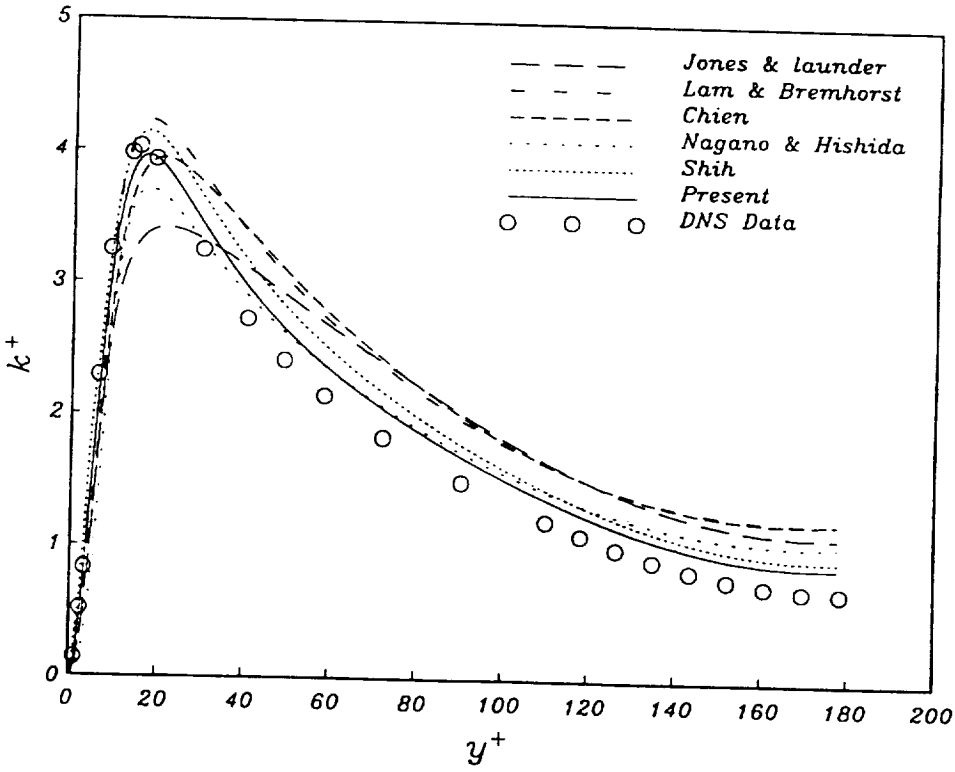

Figure 2. Turbulent kinetic energy for channel flow, $Re_\tau = 180$.

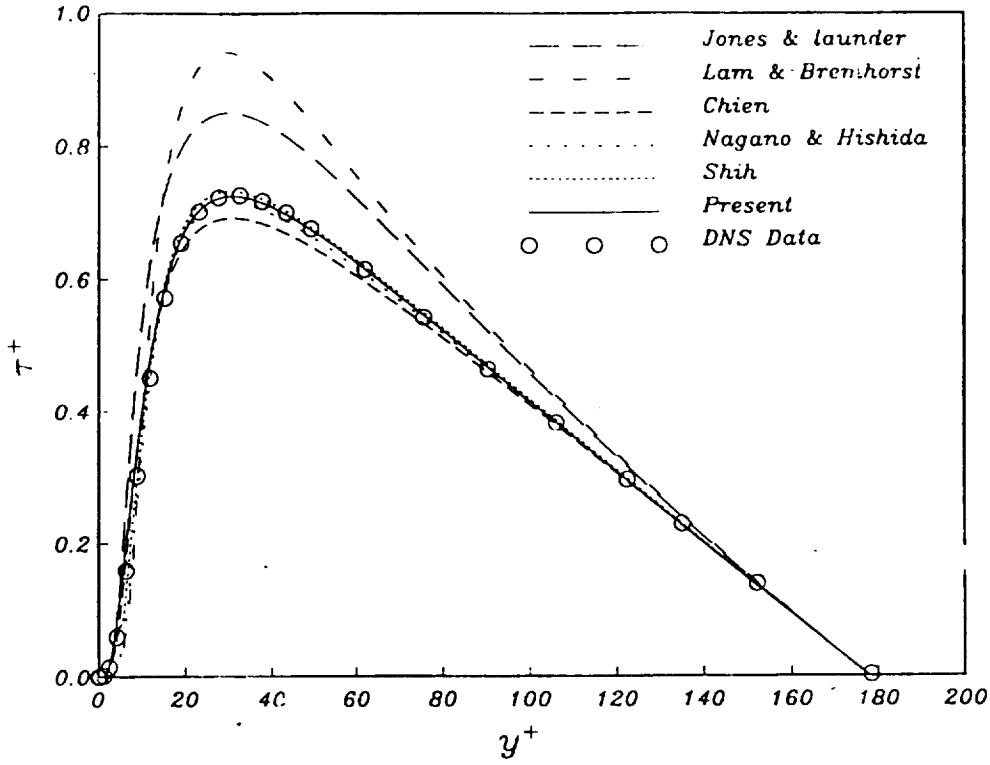

Figure 3. Turbulent shear stress for channel flow, $Re_\tau = 180$.

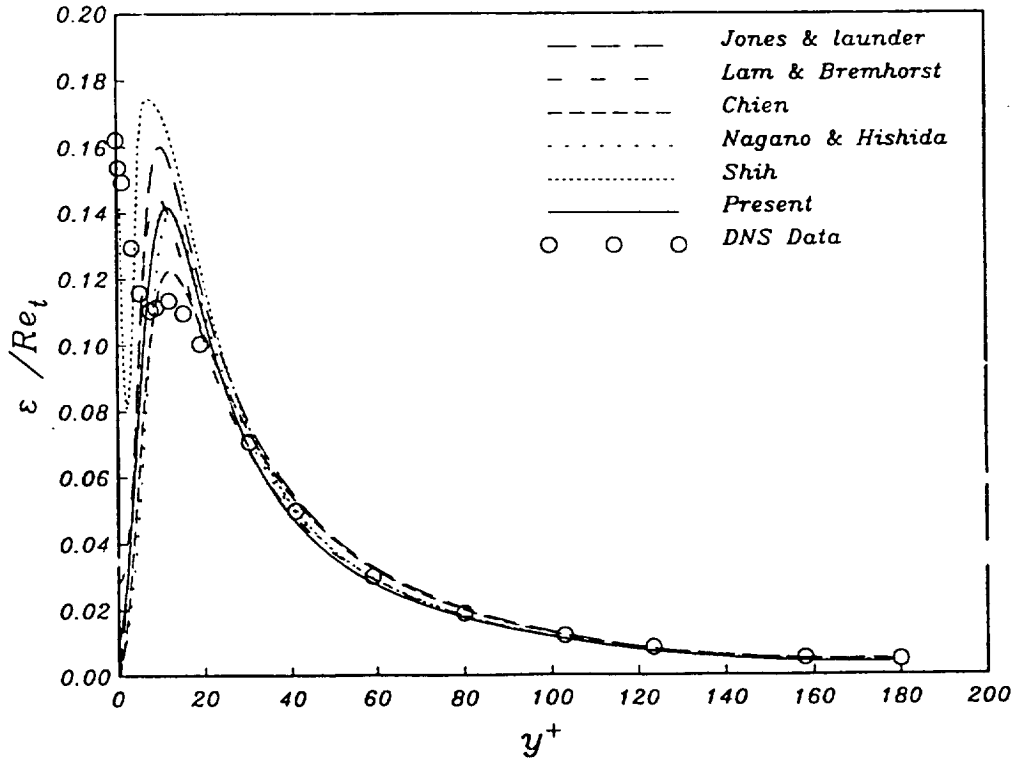

Figure 4. Dissipation rate for channel flow, $Re_\tau = 180$.

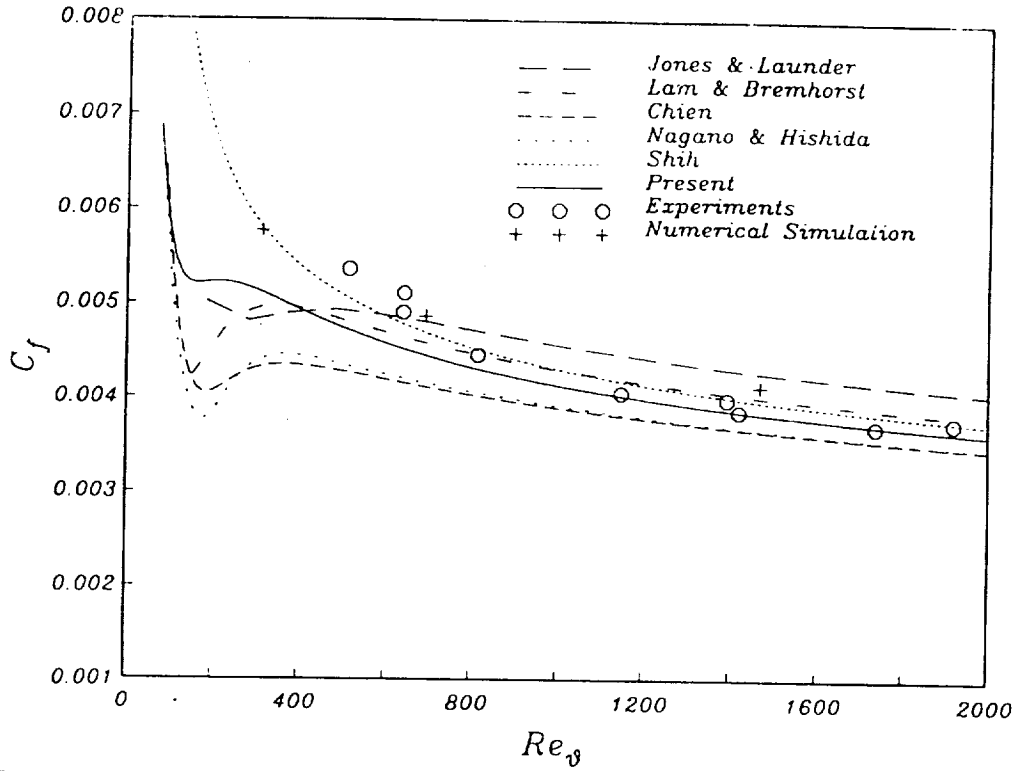

Figure 5. Wall shear stress coefficient, flat plate boundary layer flows, low Reynolds number data.

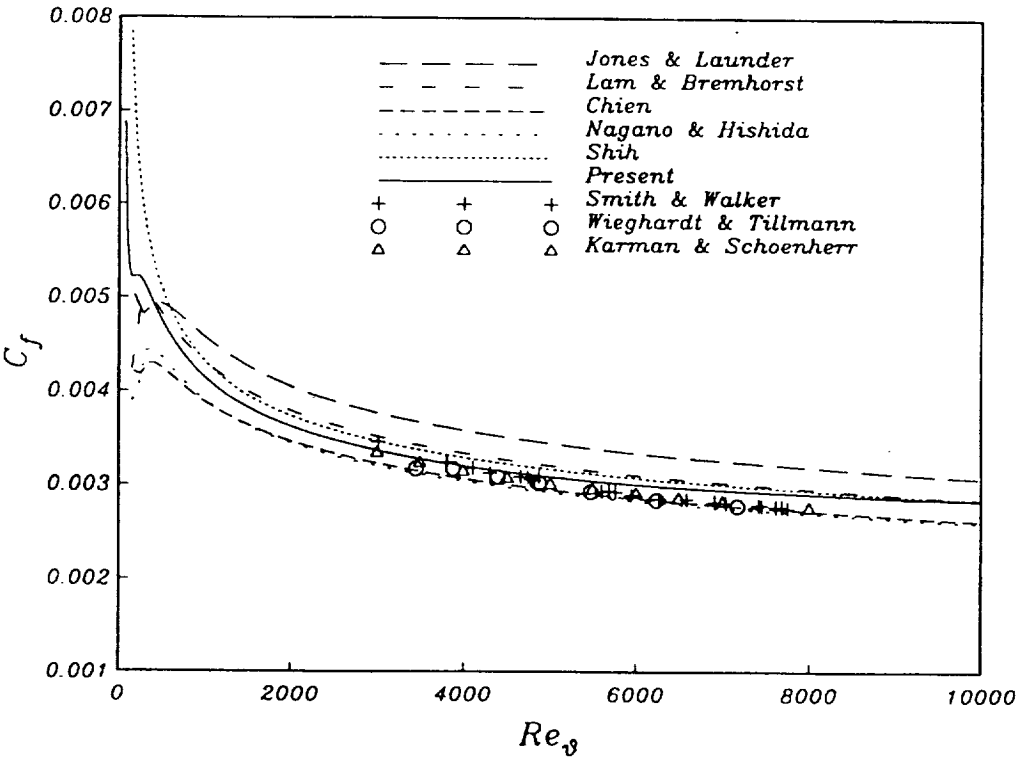

Figure 6. Wall shear stress coefficient, flat plate boundary layer flows, high Reynolds number data.

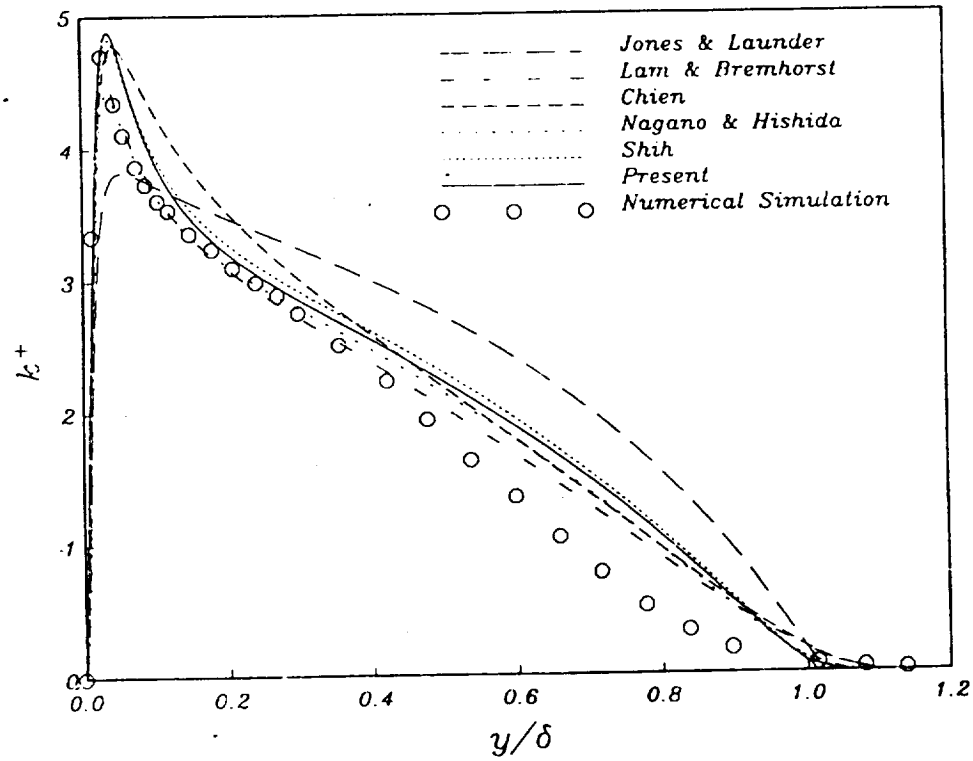

Figure 7. Turbulent kinetic energy for flat plate boundary layer, $Re_\theta = 1410$.

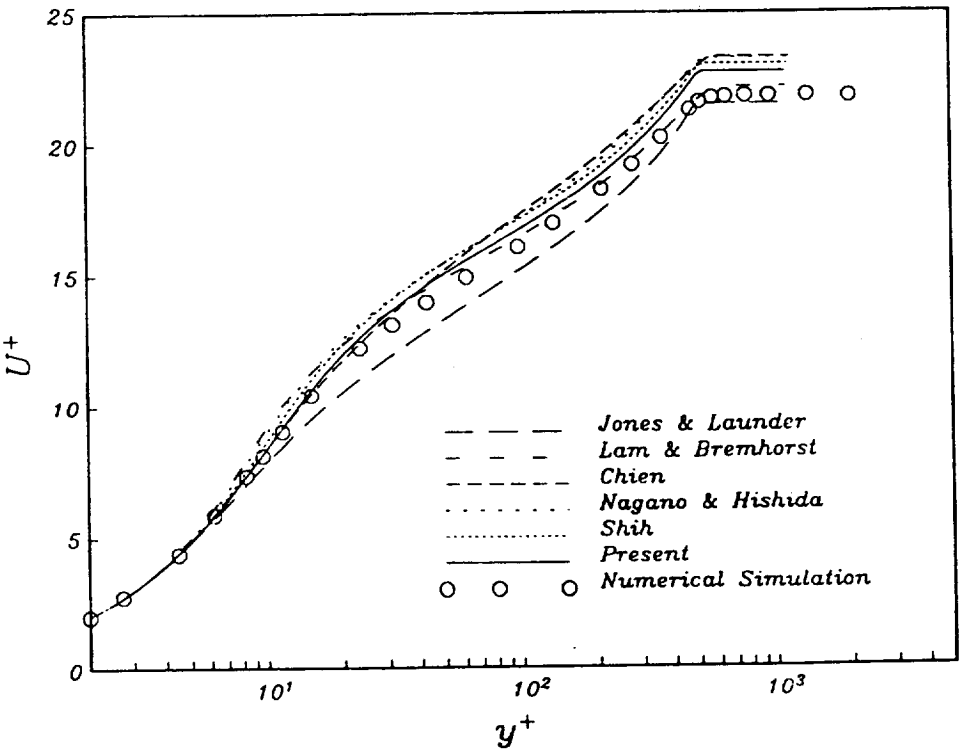

Figure 8. Mean velocity profile for flat plate boundary layer, $Re_\theta = 1410$.

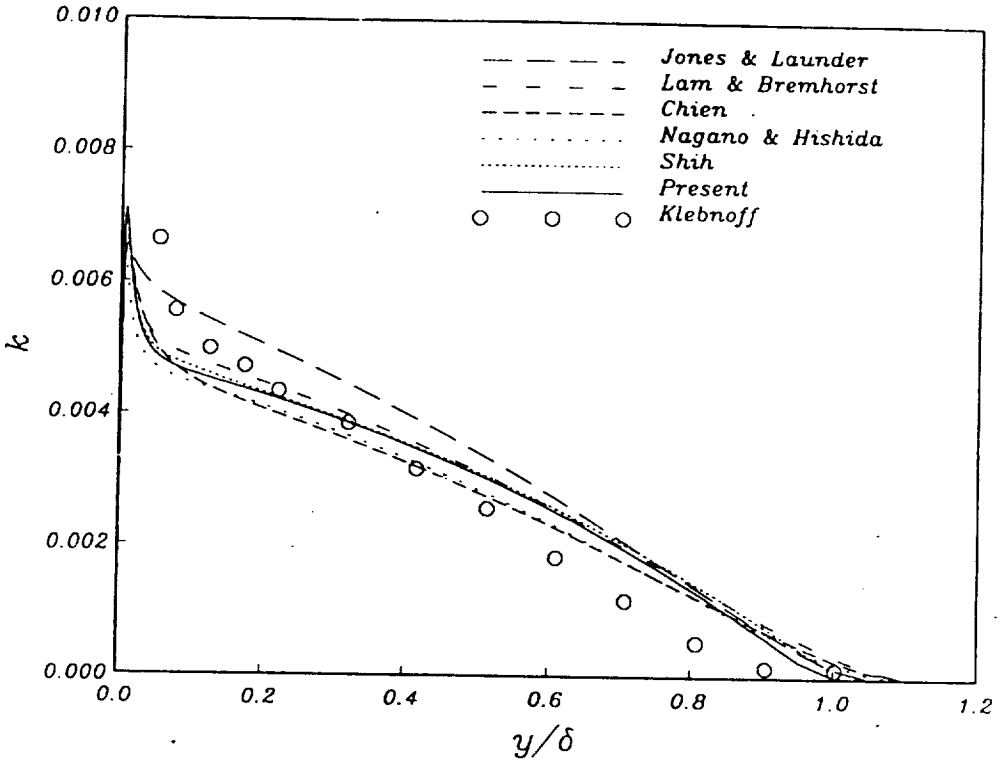

Figure 9. Turbulent kinetic energy for flat plate boundary layer, $Re_\theta = 7700$.

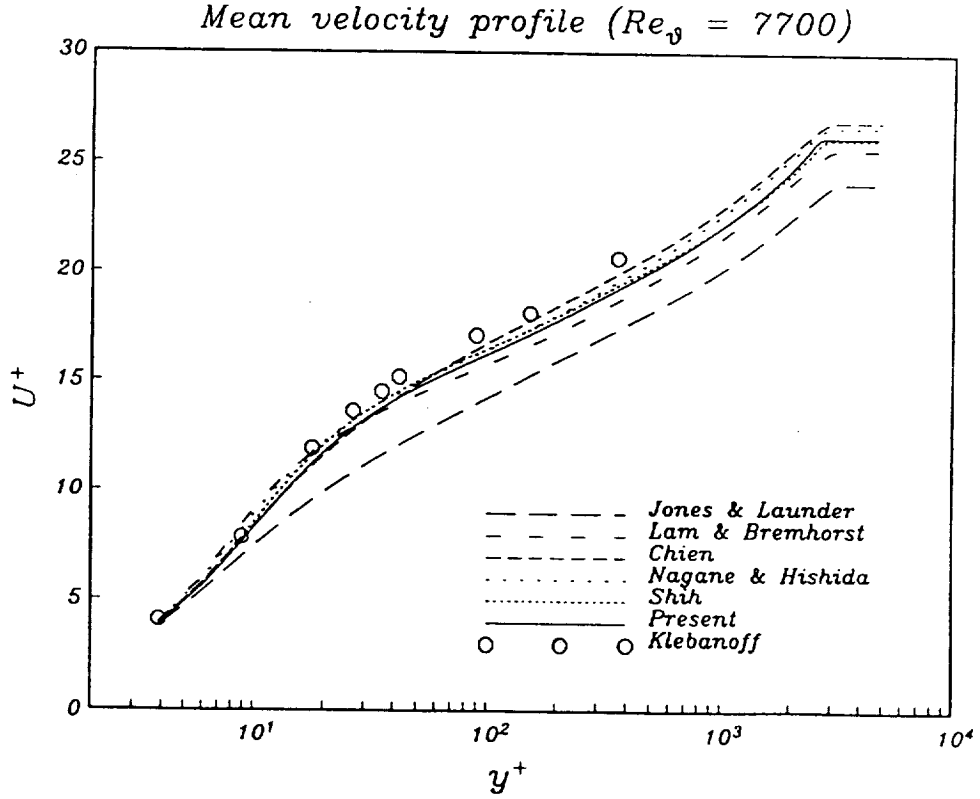

Figure 10. Mean velocity profile for flat plate boundary layer, $Re_\theta = 7700$.

SOURCE: NASA TM 104368, ICOMP-91-06, CMOTT-91-01

Low Reynolds Number Two-Equation Modeling of Turbulent Flows

V. Michelassi*, T.-H. Shih
Center for Modeling of Turbulence and Transition
NASA Lewis Research Center

March 28, 1991

Abstract

A new $k-\epsilon$ turbulence model that accounts for viscous and wall effects is presented. The proposed formulation does not contain the local wall distance thereby making very simple the application to complex geometries. The formulation is based on an existing $k-\epsilon$ model that proved to fit very well with the results of direct numerical simulation. The new form is compared with nine different two-equation models and with direct numerical simulation for a fully developed channel flow at $Re = 3300$. The simple flow configuration allows a comparison free from numerical inaccuracies. The computed results prove that few of the considered forms exhibit a satisfactory agreement with the channel flow data. The new model shows an improvement with respect to the existing formulations.

SOURCE: NASA TM 103222, ICOMP-90-0017

MODELING OF NEAR-WALL TURBULENCE

T.H. Shih*
Institute for Computational Mechanics in Propulsion
Lewis Research Center
Cleveland, Ohio 44135

N.N. Mansour
National Aeronautics and Space Administration
Ames Research Center
Moffett Field, California 94035

ABSTRACT

This paper presents an improved k-ϵ model and a second order closure model for low-Reynolds number turbulence near a wall. For the k-ϵ model, a modified form of the eddy viscosity having correct asymptotic near-wall behavior is suggested, and a model for the pressure diffusion term in the turbulent kinetic energy equation is proposed. For the second order closure model, we modify the existing models for the Reynolds-stress equations to have proper near-wall behavior. A dissipation rate equation for the turbulent kinetic energy is also reformulated. The proposed models satisfy realizability and will not produce unphysical behavior. Fully developed channel flows are used for model testing. The calculations are compared with direct numerical simulations. It is shown that the present models, both the k-ϵ model and the second order closure model, perform well in predicting the behavior of the near wall turbulence. Significant improvements over previous models are obtained.

SOURCE: NASA TM 104413, ICOMP-91-09, CMOTT-91-03

ADVANCES IN MODELING THE PRESSURE CORRELATION TERMS IN THE SECOND MOMENT EQUATIONS

Tsan-Hsing Shih and Aamir Shabbir
Institute for Computational Mechanics in Propulsion
and Center for Modeling of Turbulence and Transition
Lewis Research Center
Cleveland, Ohio 44135

and

John L. Lumley
Cornell University
Ithaca, New York 14853

ABSTRACT

In developing turbulence models, different authors have proposed various model constraints in an attempt to make the model equations more general (or universal). The most recent of these are the realizability principle (Lumley 1978, Schumann 1977), the linearity principle (Pope 1983), the rapid distortion theory (Reynolds 1987) and the material indifference principle (Speziale 1983). In this paper we will discuss several issues concerning these principles and will pay special attention to the realizability principle raised by Lumley (1978). Realizability (defined as the requirement of non-negative energy and Schwarz' inequality between any fluctuating quantities) is the basic physical and mathematical principle that any modeled equation should obey. Hence, it is the most universal, important and also the minimal requirement for a model equation to prevent it from producing unphysical results. In this paper we will describe in detail the principle of realizability, derive the realizability conditions for various turbulence models, and propose the model forms for the pressure correlation terms in the second moment equations. Detailed comparisons of various turbulence models (Launder et al. 1975, Craft et al. 1989, Zeman and Lumley 1976, Shih and Lumley 1985 and one proposed here) with experiments and direct numerical simulations will be presented. As a special case of turbulence, we will also discuss the two-dimensional two-component turbulence modeling.

Advancements in Engineering Turbulence Modeling

T.-H. Shih

Center for Modeling of Turbulence and Transition

ICOMP/NASA Lewis Research Center

9th National Aero-Space Plane

Technology Symposium

November 1-2, 1990

Paper Number 105

ABSTRACT

Some new developments in two-equation models and second order closure models will be presented. Two-equation models (e.g., k-ϵ model) have been widely used in CFD for engineering problems. Most of low-Reynolds number two-equation models contain some wall-distance damping functions to acount for the effect of wall on turbulence. However, this often causes the confusions and difficulties in computing flows with complex geometry and also needs an ad hoc treatment near the separation and reattachment points. In this paper, a set of modified two-equation models is proposed to remove abovementioned shortcomings. The calculations using various two-equation models are compared with direct numerical simulations of channel flows and flat boundary layers.

Development of second order closure model will be also discussed with emphasis on the modeling of pressure related correlation terms and dissipation rates in the second moment equations. All the existing models poorly predict the normal stresses near the wall and fail to predict the 3 dimensional effect of mean flow on the turbulence (e.g., decrease in the shear stress caused by the cross flow in the boundary layer). The newly developed second order near-wall turbulence model to be described in this paper is capable of capturing the near-wall behavior of turbulence as well as the effect of three dimension mean flow on the turbulence.

1. k-ϵ model

The two-equation model, especially k-ϵ model, is still the most widely used model for computing engineering flows. We first list some of the commonly used two-equation models,[1],[2],[3],[4],[5],[6] and their predictions on the fully developed channel flows and boundary layer flows compared with the corresponding direct numerical simulations. Then, we propose a modified k-ϵ model which does not contain any wall distance. The proposed k-ϵ model has been also tested using direct numerical simulation data.

The eddy viscosity ν_T is assumed in two-equation models as follows:

$$\nu_T = C_\mu f_\mu \frac{k^2}{\tilde{\epsilon}}$$

or

$$\nu_T = C_\mu f_\mu k\tau$$

where $\tau = k^2/\tilde{\epsilon}$

The general k-ϵ (or k-τ) model equations are of the following forms:

$$k_{,t} + U_j k_{,j} = \left[\left(\frac{\nu_T}{\sigma_k} + \nu\right) k_{,j}\right]_{,j} + \Pi + \nu_T \left(U_{i,j} + U_{j,i}\right) U_{i,j} - \epsilon + D$$

$$\epsilon_{,t} + U_j \epsilon_{,j} = \left[\left(\frac{\nu_T}{\sigma_\epsilon} + \nu\right) \epsilon_{,j}\right]_{,j} + C_1 \frac{\epsilon}{k} \nu_T \left(U_{i,j} + U_{j,i}\right) U_{i,j} - C_2 f_2 \frac{\epsilon\tilde{\epsilon}}{k} + E$$

$$\tau_{,t} + U_j \tau_{,j} = \left[\left(\frac{\nu_T}{\sigma_{\tau 2}} + \nu\right) \tau_{,j}\right]_{,j} + \frac{2}{k}\left(\frac{\nu_T}{\sigma_{\tau 1}} + \nu\right) k_{,i}\tau_{,i} - \frac{2}{\tau}\left(\frac{\nu_T}{\sigma_{\tau 1}} + \nu\right) \tau_{,i}\tau_{,i}$$
$$+ (1 - C_{\epsilon 1})\frac{\tau}{k}\nu_T (U_{i,j} + U_{j,i}) U_{i,j} + (C_{\epsilon 2} f_2 - 1)$$

This table lists the model terms, damping functions and model constants appeared in various two-equation models

$Model$	E	$\vec{\epsilon}$	C_1	C_2	f_1	f_2
JL	$2\nu\nu_t(\frac{\partial^2 u}{\partial y^2})^2$	ϵ	1.45	2.0	1.0	$1-.3e^{(-R_t^2)}$
LB	0	ϵ	1.44	2.0	$1+(\frac{.05}{f_\mu})^2$	$1-e^{(-R_t^2)}$
$Chien$	$\frac{-2\nu\epsilon}{y^2}$	ϵ	1.35	1.8	1.0	$1-.22e^{(-R_t^2/36)}$
NH	$\nu\nu_t(1-f_\mu)(\frac{\partial^2 u}{\partial y^2})^2$	ϵ	1.45	1.9	1.0	$1-.3e^{(-R_t^2)}$
$Shih$	$\nu\nu_t(\frac{\partial^2 u}{\partial y^2})^2$	$\epsilon-\frac{\nu}{2k}(\frac{\partial k}{\partial x_i})^2$	1.45	2.0	1.0	$1-.22e^{(-R_t^2/36)}$

$Model$	Π	D	f_μ	σ_k
JL	0	$-2\nu(\frac{\partial\sqrt{k}}{\partial y})^2$	$e^{(\frac{-2.5}{1+R_t/50})}$	1.0
LB	0	0	$[1-e^{(-.0165R_k)}]^2(1+\frac{20.5}{R_t})$	1.0
$Chien$	0	$-2\nu k/y^2$	$1-e^{(-.0155y^+)}$	1.0
NH	0	$-2\nu(\frac{\partial\sqrt{k}}{\partial y})^2$	$[1-e^{(-y^+/26.5)}]^2$	1.0
SAA	0	0	$(1+\frac{3.45}{\sqrt{Re_t}})tanh(\frac{y^+}{70})$	1.36
$Shih$	$\frac{.05\nu_t k_{,ii}}{\sigma_k f_\mu[1-exp(-y^+)]}$	0	$1-e^{(-6\times10^{-3}y^+-4\times10^{-4}y^{+2}+2.5\times10^{-6}y^{+3}-4\times10^{-9}y^{+4})}$	1.3

$$\nu_t = C_\mu f_\mu \frac{k^2}{\vec{\epsilon}} \qquad y^+ = \frac{u_\tau y}{\nu} \qquad R_t = \frac{k^2}{\nu\epsilon} \qquad R_k = \frac{\sqrt{k}y}{\nu}$$

The following figures show the predictions on fully develop channel flow using various two-equation models compared with the direct numerical simulation data.[7] Ploted quantities include the mean velocity U, turbulent shear stress $\langle uv \rangle$, turbulent kinetic energy k and dissipation rate EPS ϵ. The open circle represents direct numerical simulation, and the solid line represents the model prediction.

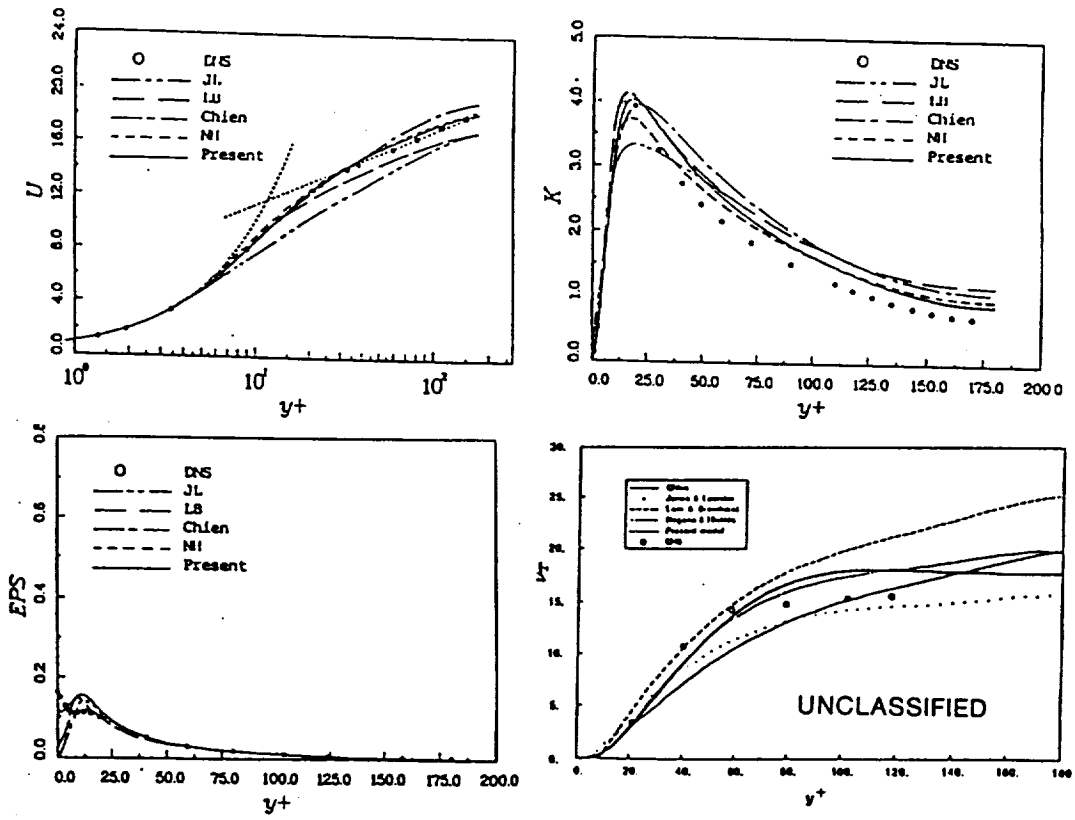

The figures below show the model predictions on flat plate boundary layer flow. A direct numerical simulation of boundary layer flow[8] is used for comparison. The skin friction coefficient C_f is also included in the comparisons.

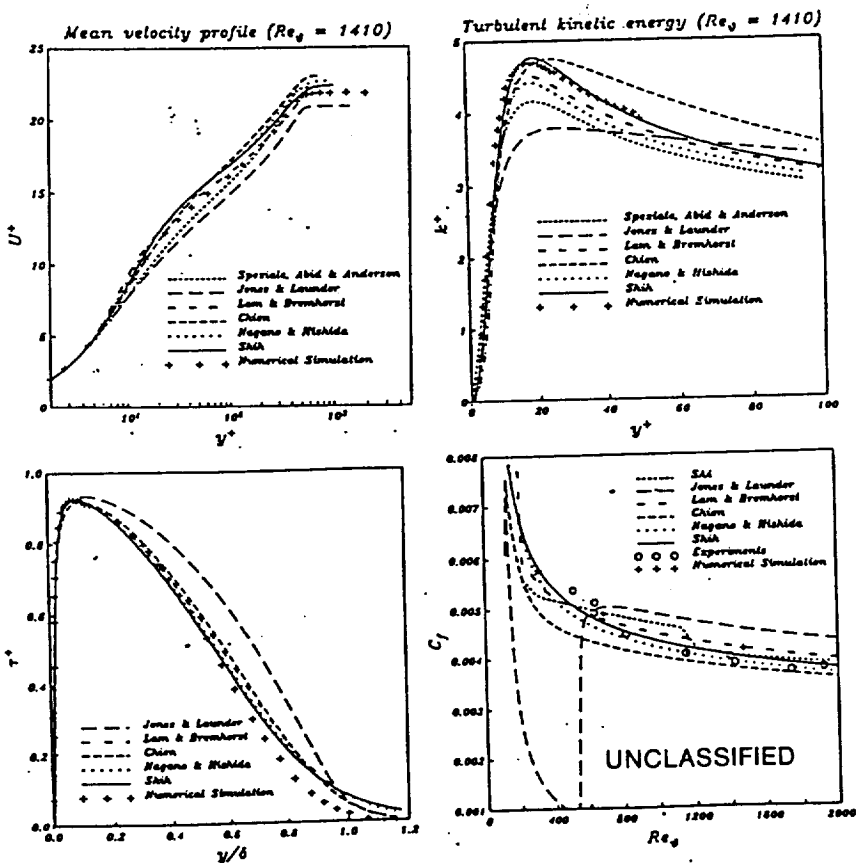

Overall, Shih's k-ϵ model gives better prediction in both fully developed channel flows and flat plate boundary layer flows according to the comparisons with corresponding direct numerical simulations. However, this model has the same problem as the others, that is it contains the wall distance parameter y^+, which is defined as

$$y^+ = \frac{u_\tau y}{\nu}$$

where u_τ is the friction velocity. The difficulty would occure in some situations. For example, near the seperation point u_τ aproaches zero and hence ν_t (through $f_\mu(y^+)$) will approach zero everywhere when this u_τ is used. Another example is the flow with complex geometry that the wall distance is not well defined. In the both cases, the ad hoc treatment is needed in the model implimentation. We notice that Jonse-Launder's model[1] does not contain y^+. However, its present form does not perform very well in the simple testing flows. Here, we based on the Shih's k-ϵ model modify the parts which is related the y^+ with another parameter $R = \frac{k^{3/2}}{\epsilon}\frac{|U|}{\nu}$. R is a ratio of turbulence length scale to viscous length scale. The modifications[9] made here are:

$$f_\mu = 1 - \exp\left\{C_3\left[1 - \exp(C_6 R^{1/4})\right]\right\}$$

$$\Pi = \left[\frac{C_0}{f_\mu^2}\frac{\nu_T}{\sigma_k}k_{,j}\right]_{,j}$$

$$\tilde{\epsilon} = \epsilon\left[1 - \exp(-R_t^{1/2})\right]$$

where $R_t = k^2/\nu\epsilon$, $C_0 = .004$, $C_3 = .0004$, $C_6 = 1.2$

The following figures show the predictions from the present model on fully developed channel flow compared with other models (including Jonse and Launder's model[1]) and direct numerical simulation data.[7] The open symbols represent direct numerical simulation, and the lines represent the model prediction.

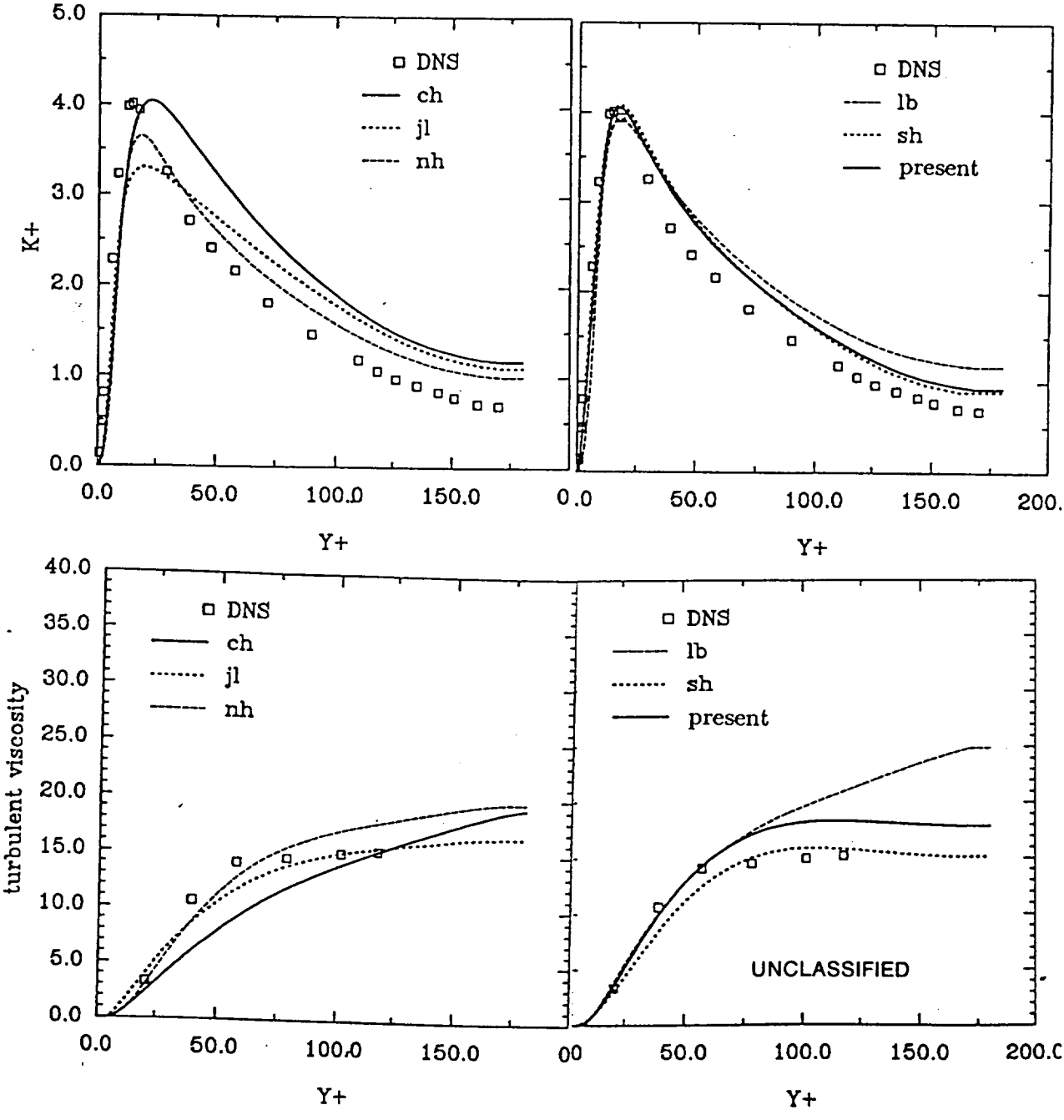

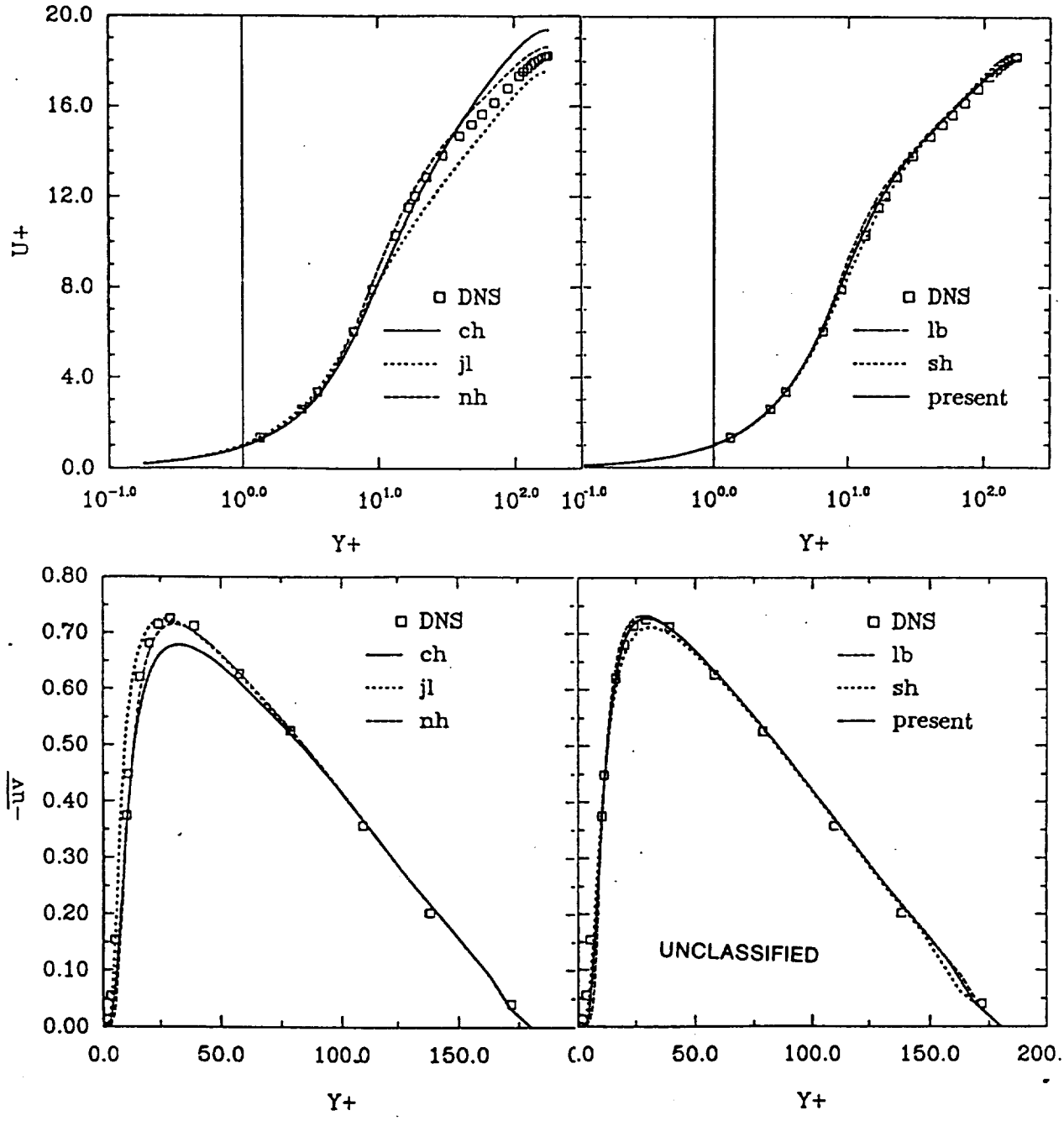
20.0
16.0
12.0
8.0
4.0
0.0
U+
DNS
ch
jl
nh
DNS
lb
sh
present
$10^{-1.0}$
$10^{0.0}$
$10^{1.0}$
$10^{2.0}$
Y+
0.80
0.70
0.60
0.50
0.40
0.30
0.20
0.10
0.00
$-\overline{uv}$
0.0
50.0
100.0
150.0
200.
UNCLASSIFIED

2. Second order modeling of near-wall turbulence

Using the near-wall asymptotic behavior of turbulence[10] as model constraints, we formed a set of modeled transport equations for the Reynolds-stress tensor and the dissipation rate of turbulent kinetic energy. The main emphasis was on developing a near-wall model for the pressure correlation and dissipation terms in the Reynolds-stress equation. A modeled dissipation rate equation is derived more rationally. Asymptotic analysis shows that near the wall, the viscous diffusion term in the Reynolds-stress equations becomes the leading term and is balanced by the pressure correlation and dissipation terms. We use this as a model constraint in the model development. The proposed models satisfy realizibility and ensure no unphysical behavior will occur. Here, we briefly describe and list the proposed models.

Reynolds stress equation

The exact equation for the Reynolds stress tensor is:

$$\frac{D}{Dt}\langle u_i u_j\rangle = P_{ij} + T_{ij} + D_{ij}^{(\nu)} + \Pi_{ij} - \varepsilon_{ij}$$

where $\langle\ \rangle$ stands for an ensemble average, $D/Dt = \partial/\partial t + U_k \partial/\partial x_k$. the terms P_{ij}, T_{ij}, $D_{ij}^{(\nu)}$, Π_{ij} and ε_{ij} represent the production, turbulent diffusion, viscous diffusion, velocity pressure-gradient correlation and dissipation tensor, and are identified as follows:

$$\begin{aligned}
P_{ij} &= -\langle u_i u_k\rangle U_{j,k} - \langle u_j u_k\rangle U_{i,k} \\
T_{ij} &= -\langle u_i u_j u_k\rangle_{,k} \\
D_{ij}^{(\nu)} &= \nu\langle u_i u_j\rangle_{,kk} \\
\Pi_{ij} &= -\frac{1}{\rho}\langle u_i p_{,j} + u_j p_{,i}\rangle \\
\varepsilon_{ij} &= 2\nu\langle u_{i,k} u_{j,k}\rangle
\end{aligned}$$

The proposed near-wall model for $\Pi_{ij} - \varepsilon_{ij}$ is:

$$\Pi_{ij} - \varepsilon_{ij} = -f_w \frac{\epsilon}{\langle q^2\rangle}[2\langle u_i u_j\rangle + 4(\langle u_i u_k\rangle n_j n_k + \langle u_j u_k\rangle n_i n_k) + 2\langle u_k u_l\rangle n_k n_l n_i n_j]$$

where n_i is a unit vector normal to the surface, and $f_w = \exp(-(R_t/C_1)^2)$, $R_t = \frac{\langle q^2\rangle^2}{9\nu\epsilon}$, $C_1 = 1.358 R_{e\tau}^{0.44}$, $R_{e\tau} = u_\tau \delta/\nu$. u_τ is the friction velocity, δ is the thickness of the boundary layer or the half width of the channel.

Away from the wall, the velocity pressure-gradient correlation Π_{ij} is split into the rapid part $\Pi_{ij}^{(1)}$ and the slow part $\Pi_{ij}^{(2)}$:

$$\Pi_{ij} = \Pi_{ij}^{(1)} + \Pi_{ij}^{(2)}$$

The proposed model for $\Pi_{ij}^{(2)} - \varepsilon_{ij}$ is:

$$\Pi_{ij}^{(2)} - \varepsilon_{ij} = -\epsilon(\beta b_{ij} + \frac{2}{3}\delta_{ij})(1 - f_w)$$

where

$$\beta = 2 + \frac{F}{9}\{\frac{72}{R_t^{1/2}} + 80.1\ln[1 + 62.4(-II + 2.3III)]\}\exp(-\frac{7.77}{R_t^{1/2}})$$

$$F = 1 + 27III + 9II$$

$$II = -\frac{1}{2}b_{ij}b_{ji}$$

$$III = \frac{1}{3}b_{ij}b_{jk}b_{ki}$$

$$b_{ij} = \langle u_i u_j\rangle/\langle q^2\rangle - \delta_{ij}/3$$

The rapid part of velocity pressure-gradient, $\Pi_{ij}^{(1)}$ is modeled as follows(Shih and Lumley[11,12]):

$$\begin{aligned}\Pi_{ij}^{(1)} &= (\frac{1}{5} + 2a_5)\langle q^2\rangle(U_{i,j} + U_{j,i}) - \frac{2}{3}(1 - a_5)(P_{ij} - \frac{2}{3}P\delta_{ij}) \\ &+ (\frac{2}{3} + \frac{16}{3}a_5)(D_{ij} - \frac{2}{3}P\delta_{ij}) + \frac{2}{15}(P_{ij} - D_{ij}) + \frac{6}{5}b_{ij}P \\ &+ \frac{2}{5\langle q^2\rangle}[(\langle u_i u_k\rangle U_{j,q} + \langle u_j u_k\rangle U_{i,q})\langle u_k u_q\rangle - \langle u_i u_p\rangle\langle u_j u_q\rangle(U_{p,q} + U_{q,p})]\end{aligned}$$

where,

$$P_{ij} = -\langle u_i u_k\rangle U_{j,k} - \langle u_j u_k\rangle U_{i,k}$$

$$D_{ij} = -\langle u_i u_k\rangle U_{k,j} - \langle u_j u_k\rangle U_{k,i}$$

$$P = \frac{1}{2}P_{ii}$$

$$a_5 = -\frac{1}{10}(1 + C_2 F^{1/2})$$

$$C_2 = 0.8[1 - \exp(-(R_t/40)^2)]$$

Finally the model for the third moments is modeled as:

$$\langle u_i u_j u_k\rangle = -.07\frac{\langle q^2\rangle}{2\epsilon}[\langle u_k u_p\rangle\langle u_i u_j\rangle_{,p} + \langle u_j u_p\rangle\langle u_i u_k\rangle_{,p} + \langle u_i u_p\rangle\langle u_j u_k\rangle_{,p}]$$

Dissipation rate equation

The modeled dissipation rate equation derived in this work is:

$$\begin{aligned}\epsilon_{,t} + U_i\epsilon_{,i} &= (\nu\epsilon_{,i} - \langle\epsilon u_i\rangle)_{,i} - \psi_0\frac{\epsilon\tilde{\epsilon}}{\langle q^2\rangle} \\ &- \psi_1\frac{\tilde{\epsilon}}{\langle q^2\rangle}\langle u_i u_j\rangle U_{i,j} - \psi_2\frac{\nu\langle q^2\rangle}{\epsilon}\langle u_k u_l\rangle(U_{i,jl} - U_{l,ij})U_{i,jk}\end{aligned}$$

where

$$\psi_0 = \frac{14}{5} + 0.98[1 - 0.33\ln(1 - 55II)]\exp(-2.83R_t^{-1/2})$$

$$\psi_1 \approx 2.1$$

$$\psi_2 = -.15(1 - F)$$

$$\tilde{\epsilon} = \epsilon - \frac{\nu\langle q^2\rangle_{,i}\langle q^2\rangle_{,i}}{4\langle q^2\rangle}$$

The turbulent flux term $\langle \epsilon u_k \rangle$ is modeled as:

$$\langle \epsilon u_k \rangle = -.07\frac{\langle q^2\rangle}{2\epsilon}\langle u_k u_p\rangle \epsilon_{,p}$$

These figures show some existing Reynolds stress models (for example, Launder and Shima[13], Lai and So[14]) and present model compared with the direct numerical simulations.[7]

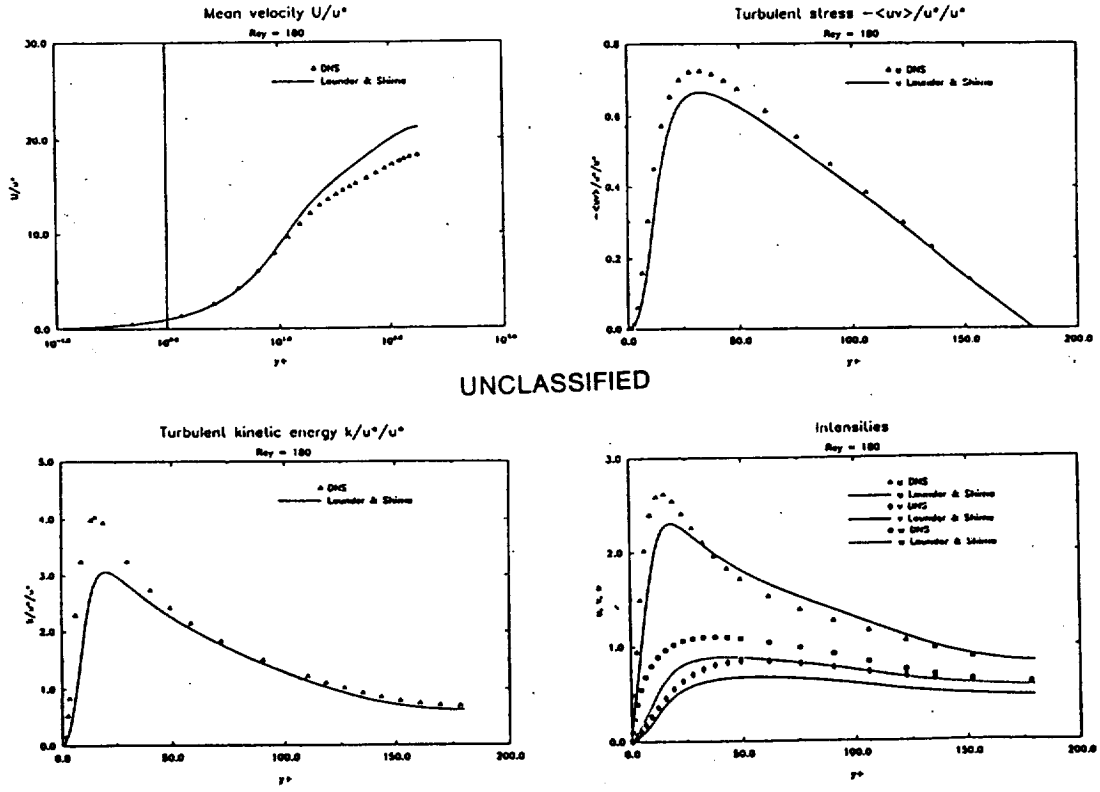

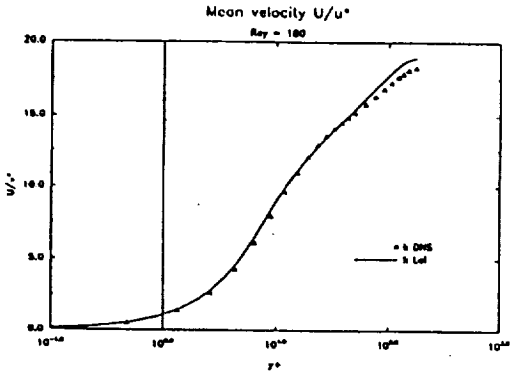

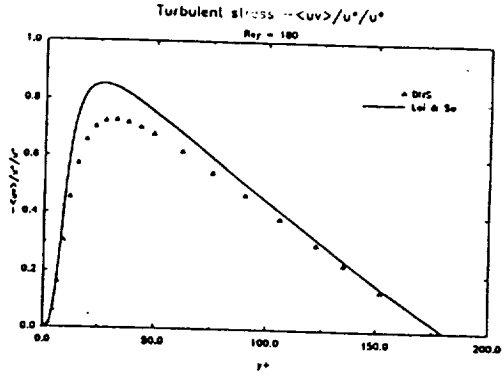

UNCLASSIFIED

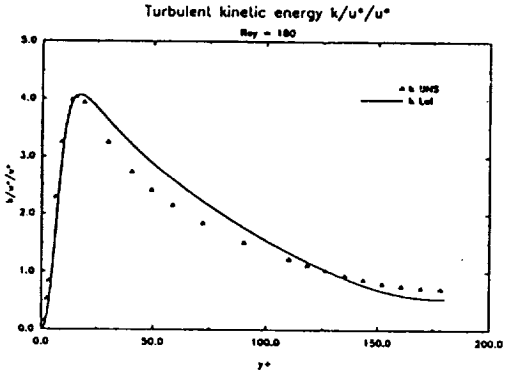

U – MEAN VELOCITY

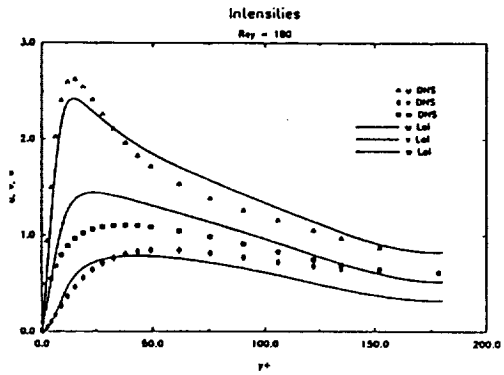

K – KINETIC ENERGY

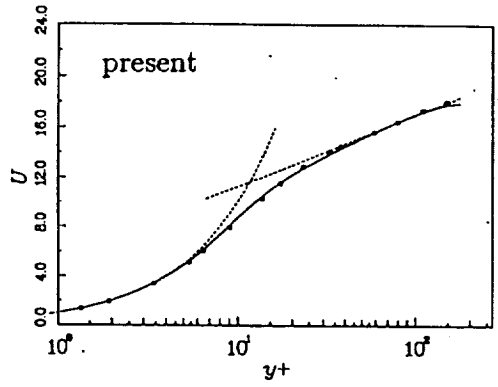

u, v, w -- RMS OF FLUCTUATING VELOCITY

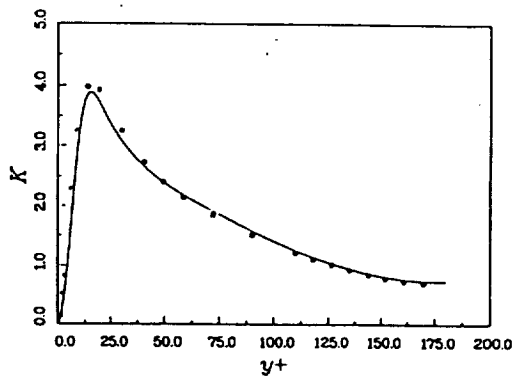

<UV> PROFILE

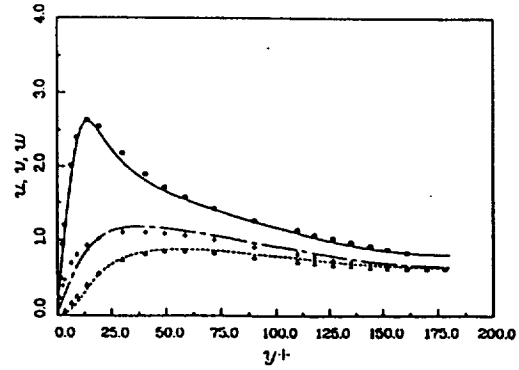

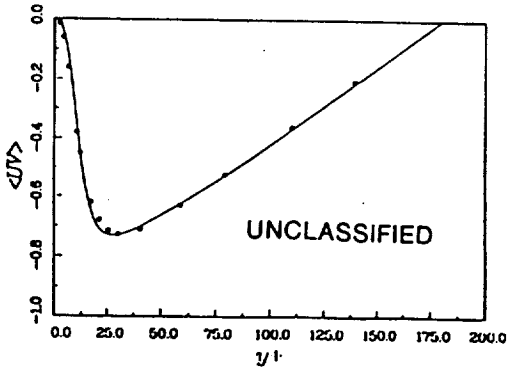

3. Second order modeling of a three-dimensional boundary layer

A study[15] of three-dimensional effects on turbulent boundary layer were achieved by direct numerical simulation of a fully developed turbulent channel flow subjected to transverse pressure gradient. The results show that, in agreement with experimental data[16], the Reynolds stresses are reduced with increasing three-dimensionality and that, near the wall, a lag develops between the stress and the strain rate. To model these three-dimensional effects on the turbulence, we have tried various two equation models and second order closure models. None of the current models can predict the reductions in the shear stress observed using direct numerical simulations. However, we found that the newly proposed second order closure model listed in the previous section do at least qualitatively capture these three-dimensional effects.

The following figures show the direct numerical simulation of the three dimensional boundary layer flow and the model predictions from Launder and Shima, Lai and So and the present models.

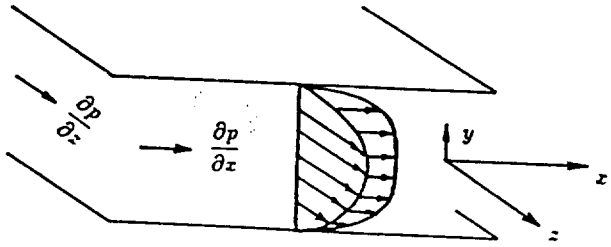

Schematic of three-dimensional channel flow.

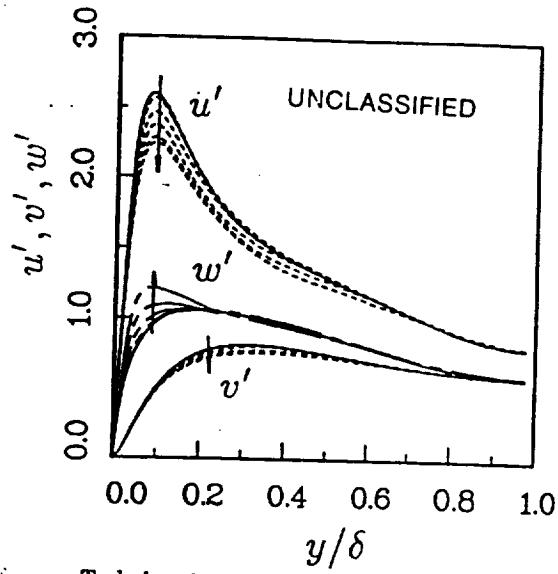

Turbulent intensities in fixed coordinates at Δt = 0.15 intervals.

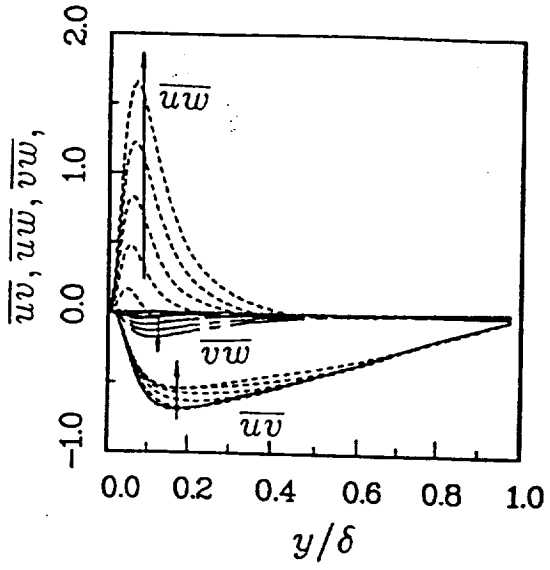

Reynolds stress component in fixed coordinate at Δt = 0.15 intervals.

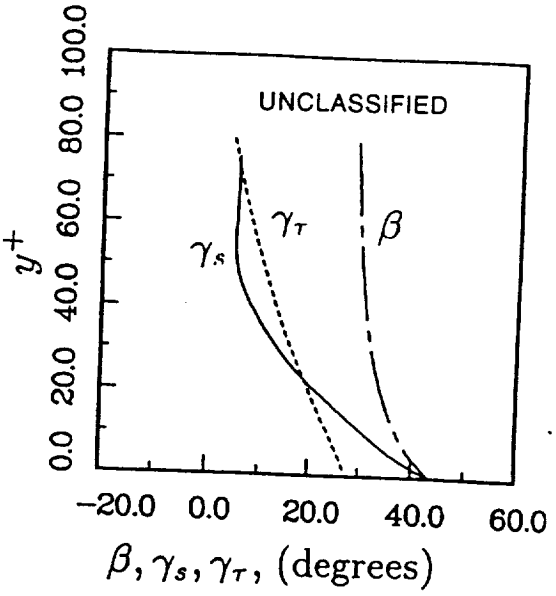

Distribution across the channel of the mean flow angle (——), the Reynolds shear stress angle (----), and the mean velocity gradient angle (——).

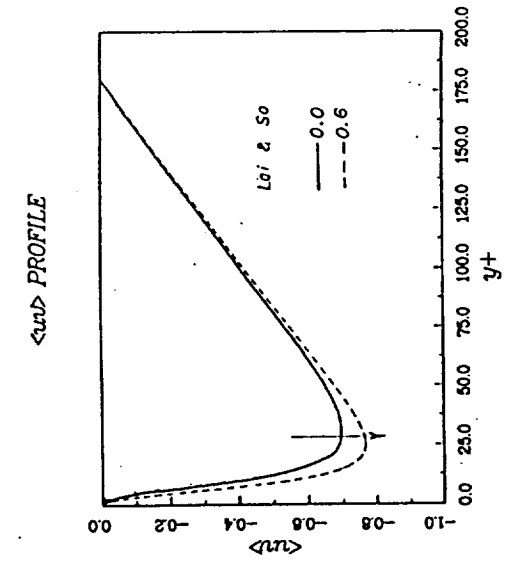
<uv> PROFILE
Loi & So
0.0
-0.6
<uv>
y+

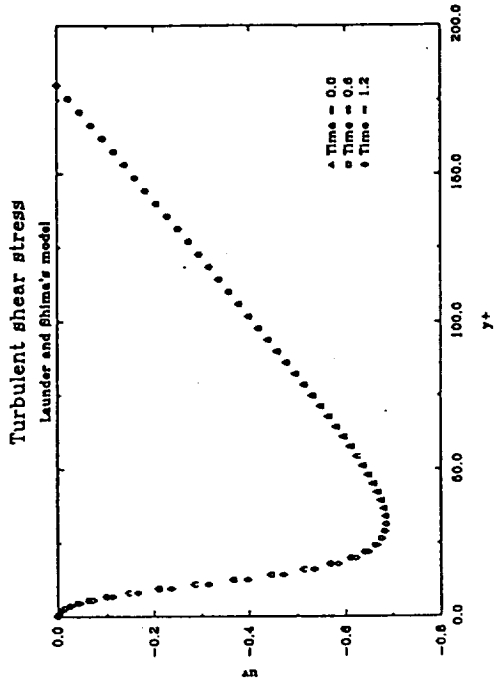
Turbulent shear stress
Launder and Shima's model
Time = 0.0
Time = 0.6
Time = 1.2
y+

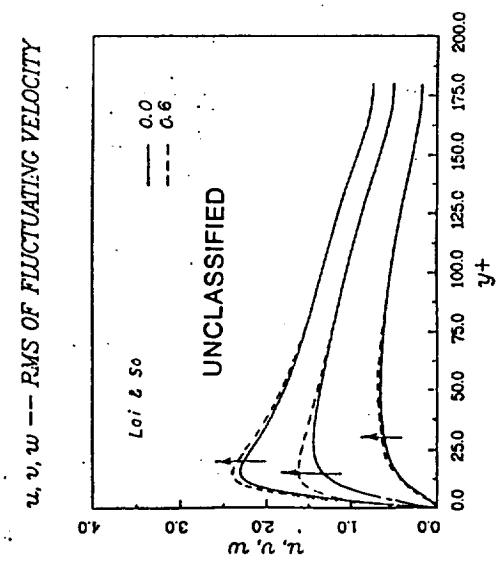
u, v, w -- RMS OF FLUCTUATING VELOCITY
Loi & So
0.0
0.6
UNCLASSIFIED
y+

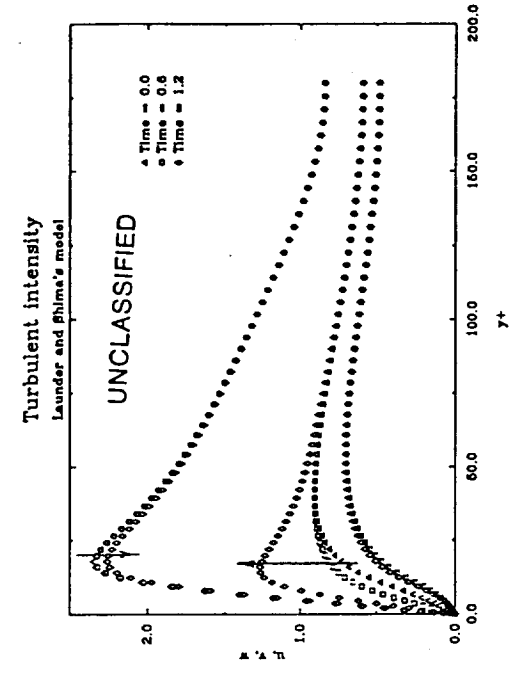
Turbulent intensity
Launder and Shima's model
UNCLASSIFIED
Time = 0.0
Time = 0.6
Time = 1.2
y+

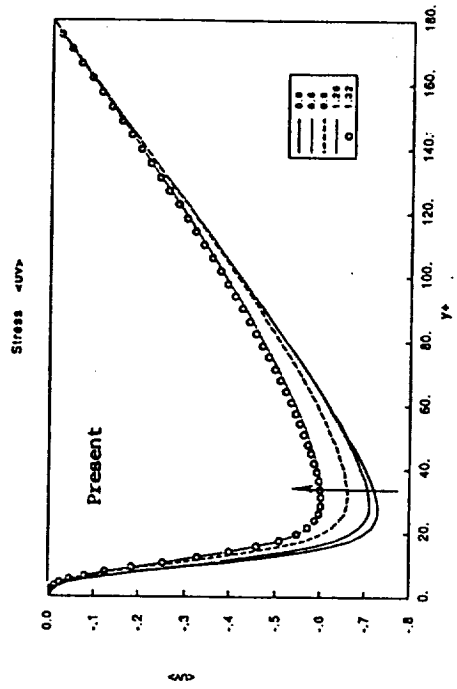
Present
Stress <uv>
<uv>
y+

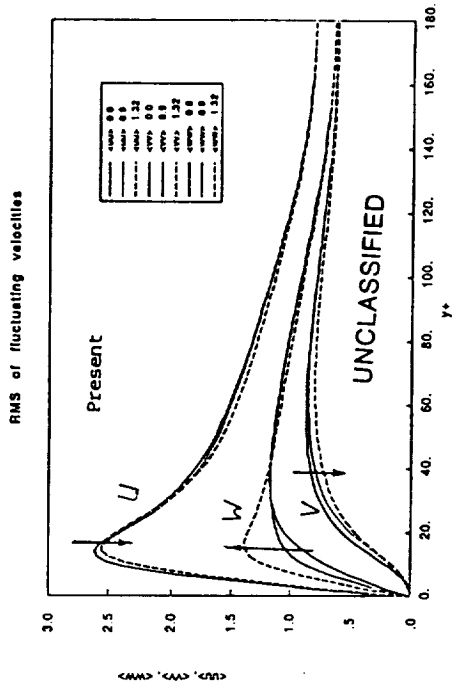
Present
RMS of fluctuating velocities
U
W
V
UNCLASSIFIED
y+

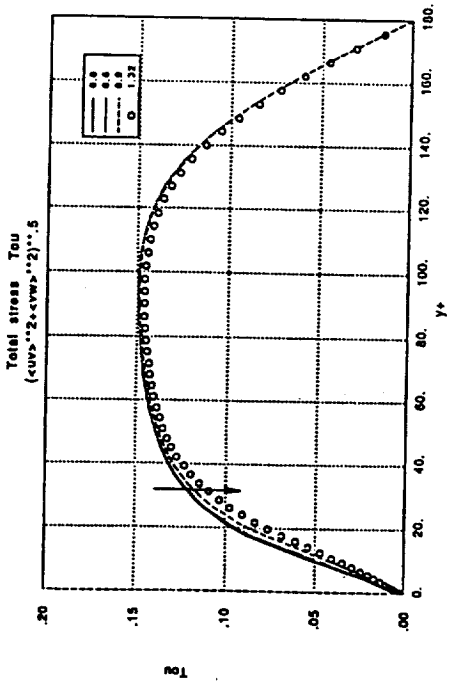
Total stress Tau
Tau
y+

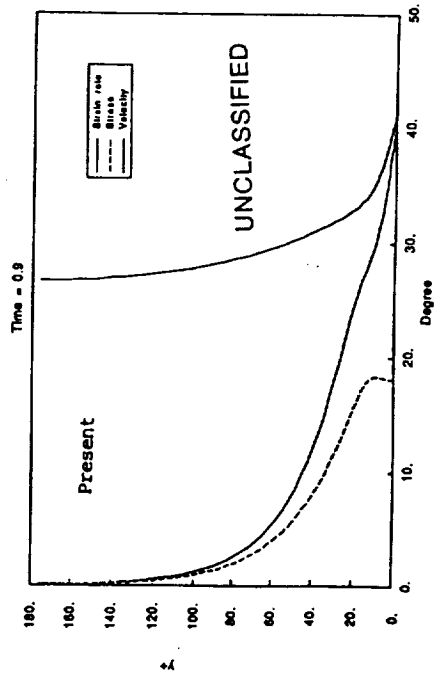
Present
UNCLASSIFIED
Time = 0.9
Degree
y+

References

1. Jones, W.P. and Launder, B.E., "The Calculation of Low-Reynolds Number Phenomena with a Two-Equation model of Turbulence," *International Journal of Heat and Mass Transfer*, Vol. 16, 1973, pp. 1119-1130.
2. Lam, C.K.G. and Bremhorst, K., "A Modified Form of the $K-\epsilon$ Model for Predicting Wall Turbulence,"*ASME Transactions, Journal of Fluids Engineering*, Vol. 103, Sept. 1981, pp.456-460.
3. Chien, K.-Y., "Predictions of Channel and Boundary-Layer Flow with a Low-Reynolds-Number Turbulence Model," *AIAA Journal*, Vol. 20, Jan. 1982, pp. 33-38.
4. Nagano, Y. and Hishida, M., "Improved Form of the $K-\epsilon$ Model for Wall Turbulent Shear Flows,"*ASME Transaction, Journal of Fluids Engineering*, Vol. 109, June 1987.
5. C.G. Speziale, R. Abid and E. Clay Anderson, "A Critical Evaluation of Two-Equation Models for Near Wall Turbulence," AIAA 21st Fluid Dynamics, Plasma Dynamics and Laser Conference, June 18-20, 1990/Seattle, WA.
6. T.-H. Shih, " An Improved k-ϵ Model for Near-Wall Turbulence and Comparison with Direct Numerical Simulation," NASA TM 103221, ICOMP-90-16.
7. Kim, J., Moin, P. and Moser, Robert., "Turbulent statistics in fully developed channel flow at low Reynolds number," *J. Fluid Mech.*, 177, 1987, pp. 133–166.
8. P.R. Spalart,"Direct simulation of a turbulent boundary layer up to $R_\theta = 1410$," bf J. Fluid Mech., vol. 187, 1988, pp. 61-98.
9. V. Michelassi, personal communication, 1990.
10. Mansour, N.N., Kim,J. and Moin. P., "Reynolds–Stress and Dissipation Rate Budgets in a Turbulent Channel Flow," *J. Fluid Mech.*, Vol. 194, 1988, pp. 15–44.
11. Shih, T.H. and Lumley, J.L., " Modeling of pressure correlation terms in Reynolds–stress and scalar flux equations," Rept. FDA-85-3, Sibley School of Mech. and Aerospace Eng., Cornell University.
12. Shih, T.H. and Lumley J.L., " Second-order modeling of near-wall turbulence," *Phys. Fluids*, 29, 1986, pp. 971–975.
13. Launder, B.E. and Shima, N., "Second-Moment Closure for the Near-Wall Sublayer: Development and Application,"*AIAA Journal*, Vol. 27, Oct. 1989, pp. 1319-1325.
14. Lai, Y.G. and So, R.M.C., *Int. J. Heat Mass Transfer*, to appear(1990).
15. Moin, P., Shih, T.H., Driver, D. and Mansour, N.N., "Numerical Simulation of a Three-Dimensional Turbulent Boundary Layer," AIAA 89-0373.
16. Bradshaw, P. and Pontikos, N., "Measurements in the Turbulent Boundary Layer on an Infinite Swept-Wing," **J. Fluid Mech**, 159, 1985, pp. 105-130.

SOURCE: NASA TM 104369, ICOMP-91-07, CMOTT-91-02

Second Order Modeling of Boundary-Free Turbulent Shear Flows

T.-H. Shih
Institute for Computational Mechanics in Propulsion
and Center for Modeling of Turbulence and Transition
Lewis Research Center
Cleveland, Ohio

J.-Y. Chen
Sandia National Laboratories
Livermore, California

J.L. Lumley
Cornell University
Ithaca, New York

Abstract

This paper presents a set of realizable second order models for boundary free turbulent flows. The constraints on second order models based on the realizability principle are re-examined. The rapid terms in the pressure correlations for both the Reynolds stress and the passive scalar flux equations are constructed to exactly satisfy the joint realizability. All other model terms (return-to-isotropy, third moments and terms in the dissipation equations) already satisfy realizability (Lumley 1978, Shih and Lumley 1986). To correct the spreading rate of the axisymmetric jet, an extra term is added to the dissipation equation which accounts for the effect of mean vortex stretching on dissipation. The test flows used in this study are the mixing shear layer, plane jet, axisymmetric jet and plane wake. The numerical solutions show that the new unified model equations (with unchanged model constants) predict all these flows reasonably as the results compare well with the measurements. We expect that these model equations would be suitable for more complex and critical flows.

A. Shabbir
Visiting Assistant Professor.

D. B. Taulbee
Professor.
Mem. ASME

Department of Mechanical and Aerospace Engineering,
University at Buffalo, SUNY
Amherst, NY 14260

Evaluation of Turbulence Models for Predicting Buoyant Flows

Experimental data for the buoyant axisymmetric plume are used to validate certain closure hypotheses employed in turbulence model equations for calculating buoyant flows. Closure formulations for the turbulent transport of momentum, thermal energy, kinetic energy, and squared temperature used in the k–ε and algebraic stress models are investigated. Experimental data for the mean velocity, mean temperature, and kinetic energy are used in the closure formulation to obtain Reynolds stresses, heat fluxes, etc., which are then compared with their measured values.

1 Introduction

Various turbulence models have been formulated for predicting buoyancy-driven flows. Some of the parameters in these models have been determined by keying the solution of the model equations to experimental data for certain basic flows such as decay of grid turbulence. Other parameters have been determined by calibrating closure formulations directly with experimental data. However, this approach may be somewhat inaccurate due to the lack of quality experimental data for certain correlations, especially dissipation. Finally, certain model parameters have been fine tuned or determined by requiring that the computed solution agree with experimental data for more complex flows, such as shear flows. In addition there have been instances where model parameters have been adjusted or empirical corrective terms added so that agreement with experimental data is accomplished for a particular flow. When model parameters are adjusted to get agreement, say for the mean velocity and temperature fields for a particular flow, little regard is given for the internal integrity of the model. In other words, are the various processes such as diffusional transport, pressure-strain interactions, etc., predicted correctly? Or are there compensating assumptions where one process is overpredicted at the expense of another and yet the end predicted result for the mean flow agrees with experiment? The lack of complete sets of data for higher moments, dissipation, and pressure-velocity correlations for various flows has prevented detailed verification of closure models for the various processes that have to be modeled.

The objective of this paper is to use the recently obtained and comprehensive experimental data of Shabbir and George (1987) and Shabbir (1987) on the axisymmetric buoyant plume to assess the various closure relations proposed for the kinetic-energy/dissipation and the algebraic stress models for buoyancy-dominated flows. The usual approach is to solve the modeled differential equations numerically, and then compare the computations with the experiment. However, this method does not help pinpoint the drawbacks in the various terms of the models. In this paper, instead of the usual approach, correlations obtained from measured velocity and temperature are used directly to verify the closure hypotheses for the turbulent transport of momentum, thermal energy, and turbulent kinetic energy.

2 Experimental Data

The data used were taken in an axisymmetric buoyant plume by Shabbir and George (1987) and Shabbir (1987), who measured velocity and temperature fields at several vertical levels above a heated source of air. Here we briefly summarize their experimental technique and results.

The three-wire probe used consisted of a cross-wire and a temperature wire. Thus the instantaneous values of the two velocity components (vertical and radial) and temperature were measured. The axisymmetry of the flow was established by using an array of 16 thermocouples and also by rotating the cross-wire by 90 deg. Profiles for the correlations between the velocity components and velocity components with temperature through the fourth order were determined from the instantaneous measurements.

Source conditions were continuously monitored in order to calculate the rate at which buoyancy was added at the source. The source Grashof number was 5.5. By integrating the mean energy equation, an integral constraint can be obtained for a buoyant plume. For a neutral environment this constraint implies that the rate at which buoyancy crosses each horizontal section is constant and must equal the rate at which buoyancy is added at the source, i.e., the ratio

$$\frac{F}{F_o} = \frac{1}{F_o}\left[2\pi \int_0^\infty g\beta(U\Delta T + \overline{ut})rdr\right] \qquad (1)$$

must be unity (F_o is the source buoyancy). This integral constraint was satisfied within 7 percent.

The correlation profiles at various heights were found to be similar in the coordinate $\eta = r/z$ (z accounted for the virtual origin) when the velocity is scaled by $U_z F_o^{1/3} z^{-1/3}$ and the temperature is scaled by $T_z = F_0^{2/3} z^{-5/3}/g\beta$. The measurements agreed well with the earlier study by George et al. (1977), who measured only the temperature and the vertical component of velocity. The scatter in the measurements of higher moments is typical for such flows and is also present in previous experiments, such as those of George et al. (1977). The primary reason for the scatter is that slow time scales of the flow require much longer averaging time for the higher moments in order to obtain the same statistical convergence as for the mean quantities. Other errors in the measurements arise from the flow reversal on the hot wire—a phenomenon most likely to occur toward the outer edges of the flow where local turbulent intensities are considerably higher. These are discussed in Shabbir and George (1987).

The various correlations in similarity variables were fitted with curves using a least-squares fitting procedure. This representation allows easy evaluation of the terms in the governing equations and closure formulations when they are cast in similarity variables. Using these profiles the balances for the mean momentum and energy differential equations were carried out to check whether the flow satisfied the equations of motion it is supposed to represent. Within the thin shear layer and the Boussinesq assumption the mean momentum and energy equa-

Contributed by the Heat Transfer Division and presented at the National Heat Transfer Conference, Pittsburgh, Pennsylvania, August 9–12, 1987. Manuscript received by the Heat Transfer Division March 3, 1988; revision received November 10, 1989. Keywords: Modeling and Scaling, Plumes, Turbulence.

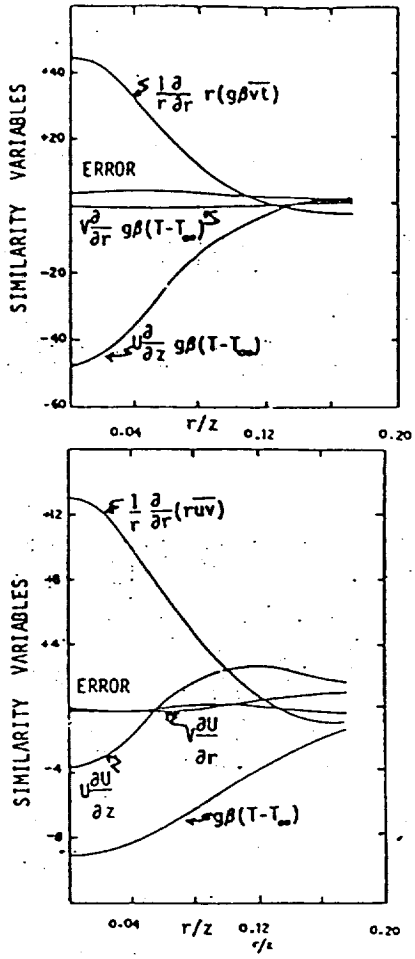

Fig. 1(*a*) Balances of mean energy and momentum equations (taken from Shabbir and George, 1987)

tions can be respectively written as

$$U\frac{\partial U}{\partial z} + V\frac{\partial U}{\partial r} = -\frac{1}{r}\frac{\partial}{\partial r}(r\overline{uv}) - g\beta\Delta T \tag{2}$$

$$U\frac{\partial \Delta T}{\partial z} + V\frac{\partial \Delta T}{\partial r} = -\frac{1}{r}\frac{\partial}{\partial r}(r\overline{vt}) \tag{3}$$

Since all the quantities appearing in these equations are measured, their profiles were substituted to see whether the measurements balance the equations. Figure 1(*a*), taken from Shabbir and George (1987), shows that the experiment satisfies this nontrivial test within 10 percent. An error of such magnitude is typical of turbulent shear flows.

The dissipation of mechanical energy was determined by balancing the turbulent energy equation

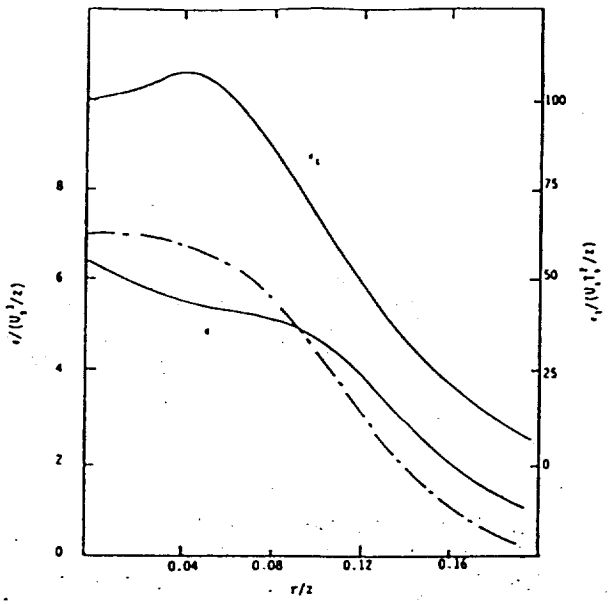

Fig. 1(*b*) Mechanical and thermal dissipation profiles! Full lines are experimental; the chained line is from model equation (10), which was solved for ϵ with all other quantities taken from experiment.

$$U_j\frac{\partial k}{\partial x_j} = -\frac{\partial}{\partial x_j}\left(\frac{1}{2}\overline{q^2u_j} + \frac{1}{\rho}\overline{pu_j}\right) + P + G - \epsilon \tag{4}$$

where $P = -\overline{u_iu_j}\,\partial U_i/\partial x_j$ is the mechanical production and $G = -\beta g\overline{u_jt}$ is the production due to buoyancy. Each term except for the dissipation ϵ and the pressure transport $\overline{pu_i}$ is determined from the experimentally determined correlations. The pressure transport was evaluated from $\overline{pu_j}/\rho = -\overline{q^2u_j}/5$, a formula given by Lumley (1978). Although this closure relation has not been verified experimentally, it was felt that since the pressure transport is significant, some correction should be included rather than simply neglecting it, as is often done. The dissipation determined from the balance of the turbulent kinetic energy equation is shown in Fig. 1(*a*) as a solid line.

By a similar procedure the dissipation of the mean-square temperature $\overline{t^2}$ is determined from

$$U_j\frac{\partial \overline{t^2}}{\partial x_j} = -\frac{\partial}{\partial x_j}\overline{u_jt^2} - 2\,\overline{u_jt}\frac{\partial T}{\partial x_j} - 2\epsilon_t \tag{5}$$

All terms are evaluated from experimental data and the resulting thermal dissipation is shown in Fig. 1(*b*).

The time scales $\overline{q^2}/\epsilon$ and $\overline{t^2}/\epsilon_t$ for the relaxation of the mechanical and thermal dissipation, respectively, are shown in Fig. 2, along with their ratio

$$R = (\overline{t^2}/\epsilon_t)/(\overline{q^2}/\epsilon) \tag{6}$$

Nomenclature

F_o = buoyancy flux, equation (1)
g = acceleration due to gravity
G = turbulence production from buoyancy
k = turbulent kinetic energy
p = fluctuating pressure
P = turbulence production by mean flow
Pr_T = turbulent Prandtl number
r = radial coordinate
R = time scale ratio, equation (4)
t = fluctuating temperature
T = mean temperature
u = fluctuating axial velocity component
U = mean axial velocity component
v = fluctuating radial velocity component
z = vertical coordinate
β = coefficient of thermal expansion
ϵ = dissipation of mechanical energy
ϵ_t = dissipation of mean-square temperature
ν_T = turbulent eddy viscosity
ρ = mean density

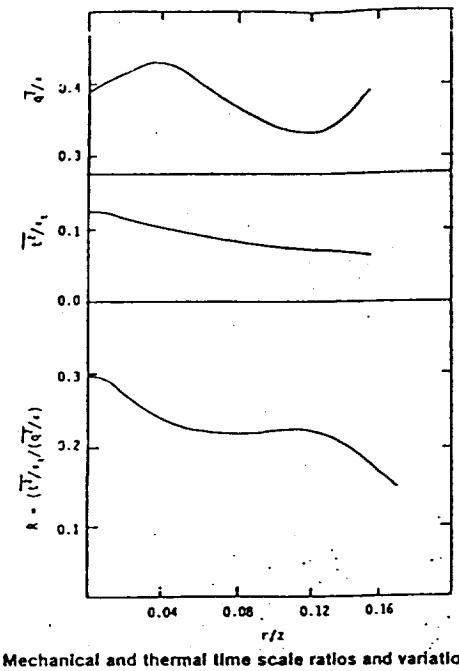

Fig. 2 Mechanical and thermal time scale ratios and variation of R as calculated from experimental data

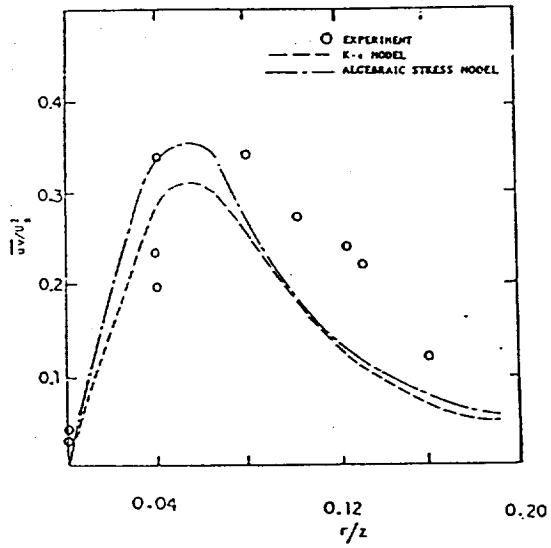

Fig. 3 Shear stress

These time scales appear extensively throughout the model formulations and will be further discussed in the next sections.

3 Assessment of Closure Hypotheses of k–ϵ Model

The form of the k–ϵ model, which is considered to be the standard one, is that used by Launder and Spalding (1974). In this model the Reynolds stress is given by

$$-\overline{u_i u_j} = \nu_T \left(\frac{\partial U_i}{\partial x_j} + \frac{\partial U_j}{\partial x_i} \right) - \frac{2}{3} k \delta_{ij} \tag{7}$$

and the heat flux by

$$-\overline{u_i t} = \frac{\nu_T}{\mathrm{Pr}_T} \frac{\partial T}{\partial x_i} \tag{8}$$

where $\nu_T = C_\mu k^2/\epsilon$ and $C_\mu = 0.09$ (see Launder and Spalding, 1974).

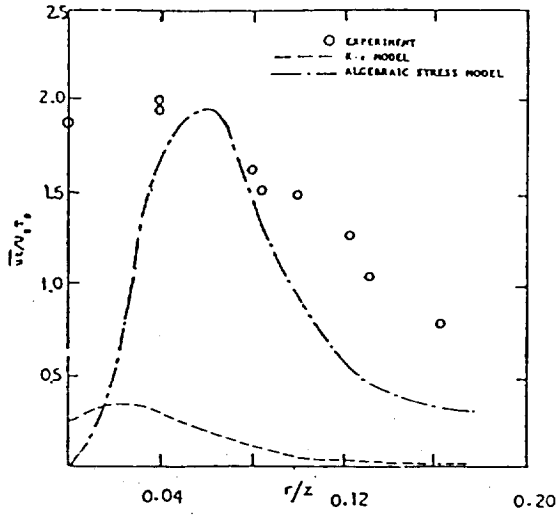

Fig. 4 Axial heat flux

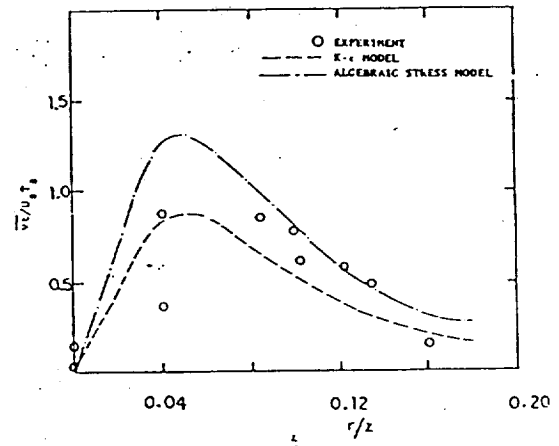

Fig. 5 Radial heat flux

By invoking the thin shear layer assumption for a buoyant plume, the above relations reduce to

$$\overline{uv} = -\nu_T \frac{\partial U}{\partial r}$$

$$\overline{ut} = -(\nu_T/\mathrm{Pr}_T) \frac{\partial T}{\partial z}$$

$$\overline{vt} = -(\nu_T/\mathrm{Pr}_T) \frac{\partial T}{\partial r}$$

Taking $\mathrm{Pr}_T = 1.0$, the right-hand sides of the above equations were evaluated experimentally. These are compared with measured values of $\overline{uv}$, $\overline{ut}$, and $\overline{vt}$ in Figs. 3–5. The points are experimental values and the chain lines are from the model.

The modeled values of $\overline{uv}$ and $\overline{vt}$ compare reasonably with the experimental profiles except in the outer portion of the curves. On the other hand the modeled profile of vertical heat flux $\overline{ut}$ is much smaller than the experimental one. It is well known that the simple gradient models given by equations (7) and (8) with an isotropic eddy viscosity are inadequate for determining streamwise turbulent momentum and heat fluxes. Usually these quantities do not influence the prediction for shear layers since only the radial fluxes are important in these flows. However, in the case of the buoyant plume the flux $\overline{ut}$ is a dominant production term in the turbulent kinetic energy

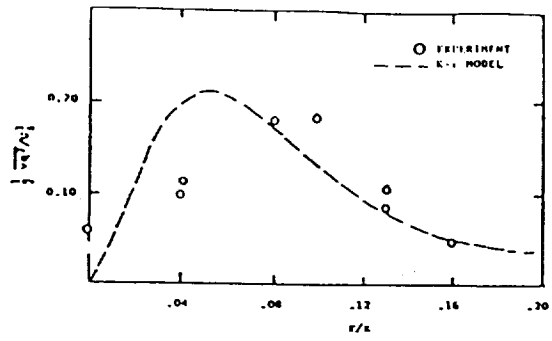

Fig. 6 Transport of kinetic energy

equation and its correct calculation is very important for accurate prediction of k.

The diffusional transport in the kinetic energy equation (4) for a thin shear layer is modeled as

$$\frac{1}{2}\overline{vq^2} + \frac{1}{\rho}\overline{pv} = -\nu_T \frac{\partial k}{\partial r} \tag{9}$$

Using $\overline{pv}/\rho = -\overline{vq^2}/5$ from Lumley (1978) gives $\overline{vq^2}/2 = -(5/3)\nu_T \partial k/\partial r$ from which the result, with the right side evaluated from experimental results, is shown in Fig. 6. It is seen that the predicted and experimental data peak at different radial locations; however, the predicted magnitude is more accurate, which indicates that the pressure diffusion needed to be taken into account.

In the k–ϵ model the dissipation is calculated from

$$U_j \frac{\partial \epsilon}{\partial x_j} = -\frac{\partial}{\partial x_j}\overline{\epsilon' u_j} + C_{\epsilon 1}\frac{\epsilon}{k}(P+G) - C_{\epsilon 2}\frac{\epsilon^2}{k} \tag{10}$$

where $\overline{\epsilon' u_j} = -(\nu_T/\sigma_\epsilon)\partial\epsilon/\partial x_j$ and $\sigma_\epsilon = 1.3$, $C_{\epsilon 1} = 1.44$, and $C_{\epsilon 3} = 1.92$ as given by Launder and Spalding (1974). In order to get an indication of the validity of equation (10), it was numerically solved for the dissipation ϵ with all other quantities needed to evaluate the coefficients determined from the experimental correlations. The result is shown in Fig. 1(b) and it is seen that it compares reasonably well with the curve obtained from balancing the turbulent kinetic energy equation with experimental data.

Launder et al. (1972) showed that the standard k–ϵ model yields a solution for the axisymmetric jet that overpredicts the spreading rate by about 30 percent. The standard k–ϵ model also does not correctly predict the axisymmetric buoyant plume (Hossain and Rodi, 1982). Proposals have been made (Pope, 1978; Hanjalic and Launder, 1980) for modifying the dissipation equation, based on arguments concerned with vortex or eddy structures characteristic of axisymmetric flows. The modified equation produces more dissipation, thus decreasing the turbulent eddy viscosity, which results in a smaller spreading rate of the flow. Here we use the empirical correction given by Rodi (1972) where $C_{\epsilon 2} = 1.92(1-0.035H)$ with $H = 1/(y_E/U_m)dU_m/dx|^{0.2}$ and where U_m is the maximum velocity and y_E is the distance from the centerline to the edge of the shear layer. This correction decreases the destruction term in the dissipation equation, hence producing an increased dissipation. However, when this correction is used in equation (10) there is very little change in the solution for ϵ when experimental data are used for the other quantities in the equation. This is probably due to the approach taken here, which does not allow for the nonlinear interactions between the various terms in the closure. If the kinetic energy and dissipation equations are solved simultaneously, then the axisymmetric correction will produce a significant change in the solution of the k–ϵ model.

4 Assessment of Closure Hypotheses for Algebraic Stress Model

Chen and Rodi (1975), Tamanini (1978), Chen and Chen (1979), and Hossain and Rodi (1982) have made predictions for the buoyant jet using algebraic stress models. Many of the ideas used in these models for calculating buoyant flows originated with Launder (1975, 1978). Algebraic stress models are obtained by simplifying the convective transport equations for Reynolds stresses and heat fluxes so they are no longer differential equations. The dynamic equation for the Reynolds stress tensor is

$$(C-D)_{\overline{u_iu_j}} = P_{ij} + G_{ij} - \frac{2}{3}\epsilon\delta_{ij} - C_1\epsilon\left(\frac{\overline{u_iu_j}}{k} - \frac{1}{3}\delta_{ij}\right) - C_2\left(P_{ij} - \frac{2}{3}P\delta_{ij}\right) - \frac{30C_2-22}{5}\left(D_{ij} - \frac{2}{3}P\delta_{ij}\right) - (8C_2-6)k\left(\frac{\partial U_i}{\partial x_j} + \frac{\partial U_j}{\partial x_i}\right) - C_3\left(G_{ij} - \frac{2}{3}G\delta_{ij}\right) \tag{11}$$

where $P_{ij} = -\overline{u_iu_k}\,\partial U_j/\partial x_k - \overline{u_ju_k}\,\partial U_i/\partial x_k$ is the mechanical production and $G_{ij} = -\beta g_i\,\overline{u_j t} - \beta g_j\,\overline{u_i t}$ is the buoyancy production. The left side represents convection minus diffusional transport, the dissipation is assumed isotropic, and the last three lines represent the closure formulation for $p(\partial u_i/\partial x_j + \partial u_j/\partial x_i)/\rho$ given by Launder et al. (1975) and Launder (1975, 1978). Launder assumes: (1) an equilibrium situation where convection is balanced by diffusion ($C - D = 0$) and production is balanced by dissipation ($P + G - \epsilon = 0$); (2) the second and third terms (third line) in the rapid part of the pressure-velocity correlation are negligible; the coefficient C_2 is adjusted so that the first term approximates the entire rapid part; (3) the parameter C_3 is taken equal to C_2. After applying all the assumptions

$$\overline{u_iu_j} = \frac{2}{3}\frac{C_1+C_2-1}{C_1}k\delta_{ij} - \frac{1-C_2}{C_1}\frac{k}{\epsilon}(P_{ij}+G_{ij}) \tag{12}$$

where $c_1 = 2.2$ and $C_2 = 0.6$. It should be pointed out that in free shear flows the equilibrium condition ($C - D = 0$ and $P + G - \epsilon = 0$) only applies in the outer portion of the flow. Also, Zeman and Lumley (1976) found $C_3 = 0.3$, after applying all the constraints applicable to determining the contribution of buoyancy to the pressure-strain correlation.

The dynamic equation for the heat flux is

$$(C-D)_{\overline{u_it}} = -\overline{u_iu_j}\frac{\partial T}{\partial x_j} - \overline{u_jt}\frac{\partial U_i}{\partial x_j} - \beta g_i\overline{t^2} - C_{1t}\frac{\epsilon}{k}\overline{u_it} + C_{2t}\,\overline{u_jt}\frac{\partial U_i}{\partial x_j} - \frac{1}{5}\overline{u_jt}\frac{\partial U_j}{\partial x_i} + C_{3t}\beta g_i\overline{t^2} \tag{13}$$

where the first line on the right side is the production and the second line is the closure for $p\partial t/\partial x_i/\rho$. Neglecting convection and diffusion ($C - D = 0$) and the third term in the second line, equation (13) becomes

$$\overline{u_it} = \frac{1}{C_{1t}}\frac{k}{\epsilon}\left[-\overline{u_iu_j}\frac{\partial T}{\partial x_j} - (1-C_{2t})\overline{u_jt}\frac{\partial U_i}{\partial x_j} - (1-C_{3t})\beta g_i\overline{t^2}\right] \tag{14}$$

where $C_{1t} = 3.0$, $C_{2t} = 0.5$, and $C_{3t} = 0.5$. Zeman and Lumley (1976) show that $C_{2t} = 0.8$ and $C_{3t} = 0.2$ from theoretical considerations.

Neglecting the convection and diffusional transport in equation (5) and eliminating ϵ_t with equation (6) gives

$$\overline{t^2} = -R\frac{k}{\epsilon}\overline{u_jt}\frac{\partial T}{\partial x_j} \tag{15}$$

which was given by Launder (1975, 1978) and used by Hossain and Rodi (1982).

Chen and Rodi (1975) and Chen and Chen (1979) used the differential equation (5), with ϵ_t eliminated by using equation (6) to determine $\overline{t^2}$ rather than using equation (15). In either case R is taken to be a constant equal to 0.8 (Hossain and Rodi, 1982; Chen and Rodi, 1975; Chen and Chen, 1979; Launder, 1975, 1978). It is seen in Fig. 2 that the experimentally determined value of R is much lower with an average value across the profile of roughly 0.25. Launder (1978) cites experimental evidence for R being in the range of 0.5 to 0.8. However, he found that the algebraic stress relations agreed best with an experiment for a stably stratified homogeneous shear flow with $R = 0.8$. Hence, that value has been adopted in the algebraic stress models. The experimental results of Shabbir and George (1987) indicate R is much lower for strongly buoyant flows. When the algebraic stress model is applied to this experiment with $R = 0.8$, the results are very poor for $\overline{t^2}$. Therefore, in the following evaluation of the algebraic stress model, the experimentally determined profile for R (Fig. 2) is used.

Equations (10), (12), and (13) represent a system of *algebraic equations* that can be solved for $\overline{u_i u_j}$, $\overline{u_i t}$, and $\overline{t^2}$. Employing the thin shear layer approximation, where only gradients in the radial direction are retained, Hossain and Rodi (1982) give

$$\overline{u^2} = \frac{2}{3}\frac{C_1 + C_2 - 1}{C_1}k + \frac{1 - C_2}{C_1}\frac{k}{\epsilon}\left(-2\overline{uv}\frac{\partial U}{\partial r} + 2\beta g\overline{vt}\right) \quad (16)$$

$$\overline{uv} = \frac{1 - C_2}{C_1}\frac{k}{\epsilon}\left(-\overline{v^2}\frac{\partial U}{\partial r} + g\beta\overline{vt}\right) \quad (17)$$

$$\overline{v^2} = \frac{2}{3}\frac{C_2 + C_2 - 1}{C_1}k \quad (18)$$

$$\overline{ut} = \frac{1}{C_{1t}}\frac{k}{\epsilon}\left[-\overline{uv}\frac{\partial T}{\partial r} - (1 - C_{2t})\overline{vt}\frac{\partial U}{\partial r} + (1 - C_{3t})\beta g\overline{t^2}\right] \quad (19)$$

$$\overline{vt} = \frac{-1}{C_{1t}}\frac{k}{\epsilon}\overline{v^2}\frac{\partial T}{\partial r} \quad (20)$$

$$\overline{t^2} = -2R\frac{k}{\epsilon}\overline{vt}\frac{\partial T}{\partial r} \quad (21)$$

from which $\nu_t = C_\mu k^2/\epsilon$ where

$$C_\mu = \frac{2}{3}\frac{(1 - C_2)(C_1 + C_2 - 1)}{C_1^2}\left(1 + \frac{1}{C_{1t}}\frac{k}{\epsilon}g\beta\frac{\partial T/\partial r}{\partial U/\partial r}\right) \quad (22)$$

The system of equations (16)–(21) was solved to determine the Reynolds stress and heat flux components with U, T, k, ϵ, and R given by the experiment. The following values for the constants were used:

$$C_1 = 2.2, \quad C_2 = 0.6, \quad C_3 = 0.6$$

$$C_{1t} = 3.0, \quad C_{2t} = 0.5, \quad C_{3t} = 0.5$$

The value of C_μ, which appears in the eddy viscosity relation $\nu_t = C_\mu k^2/\epsilon$ and is given by equation (22), is roughly 0.125 and is reasonably constant across the flow. This value is considerably larger than the value of $C_\mu = 0.09$ in the standard k–ϵ model. Rodi (1972), to correct for the discrepancies in the prediction for the axisymmetric jet, developed an empirical correction to C_μ. The parameter C_μ is replaced by $(1 - 0.465H)C_\mu$ where $H = |(y_E/U_m)dU_m/dx|^{0.2}$, U_m is the maximum velocity, and y_E is the distance from the centerline of the edge of the jet. Hossain and Rodi (1982), Chen and Rodi (1975), and Chen and Chen (1979) used this correction in their predictions for turbulent buoyant jets. When the correction is applied, we get approximately 0.09, which is the value of C_μ for the standard k–ϵ model.

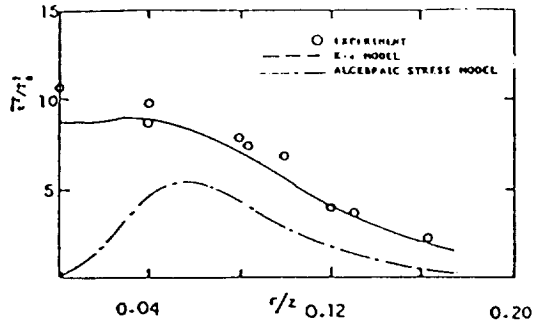

Fig. 7 Mean square temperature

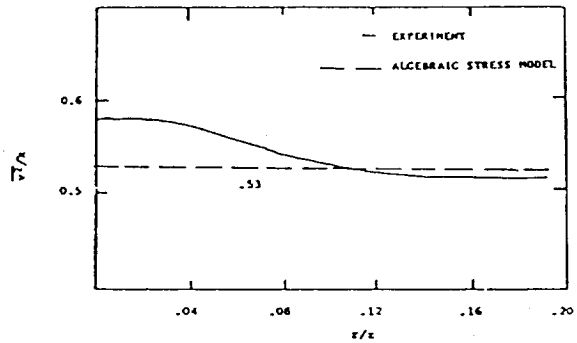

Fig. 8 Radial Reynolds stress $\overline{v^2}$

The question we are asking is, "given the turbulent energy, dissipation, velocity, and temperature, does the proposed algebraic stress expression correctly predict the Reynolds stress and heat flux components?" Figure 8 shows the radial Reynolds stress determined from equation (18). It is seen that the predicted value $\overline{v^2}/k = 0.53$ is a little smaller than the experimental curve in the center portion of the plume, but agrees quite well with experiment in the outer portion. The predicted shear stress $\overline{uv}$, the axial heat flux $\overline{ut}$, the radial heat flux $\overline{vt}$, and the mean squared temperature $\overline{t^2}$ are shown in Figs. 3, 4, 5, and 7, respectively. Again the points are experimental data and the broken lines are from the model. It is seen that the shear stress $\overline{uv}$ and radial heat flux $\overline{vt}$ are predicted reasonably. However, the vertical heat flux $\overline{ut}$ and temperature fluctuations $\overline{t^2}$ are predicted poorly and have incorrect shapes; unlike the experimental values they go to zero near the origin.

Equation (21) gives $\overline{t^2}$ proportional to the radial temperature gradient, which is zero at the centerline. Then since $\overline{t^2} = 0$ at $r = 0$, equation (19) gives $\overline{ut} = 0$ at $r = 0$. In order to obtain nonzero values for $\overline{ut}$ and $\overline{t^2}$ at the centerline from the model equations (12), (14), and (15), terms containing the axial gradient, i.e., $\partial U/\partial z$ and $\partial T/\partial z$, were retained. These terms were added to equations (19) and (21) and the system of equations was solved again. Although the centerline values of $\overline{ut}$ and $\overline{t^2}$ were found to be nonzero, the predictions still decreased to relatively small values near the centerline.

Another possibility for this behavior is the neglect of advection and diffusion terms in the model. Gibson and Launder (1976) have proposed the following model for these terms:

$$(C - D)_{\overline{u_i u_j}} = \frac{\overline{u_i u_j}}{k}(P + G - \epsilon) \quad (23)$$

$$(C - D)_{\overline{u_i t}} = \frac{\overline{u_i t}}{2\overline{t^2}}(P_t - \epsilon_t) + \frac{\overline{u_i t}}{2k}(P + G - \epsilon) \quad (24)$$

where P_t is the production term in the $\overline{t^2}$ equation. These were

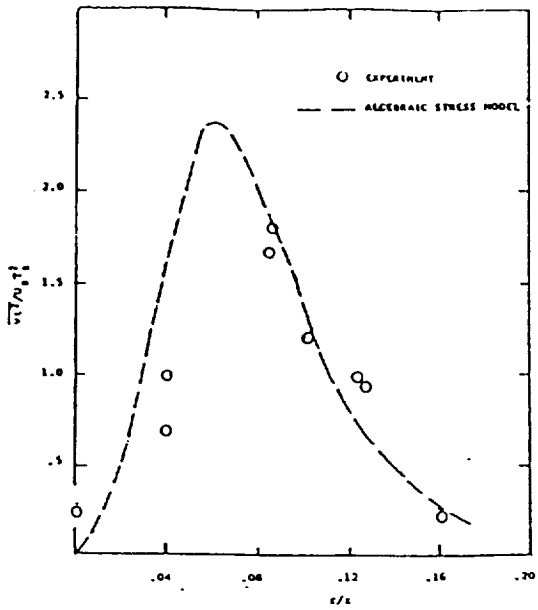

Fig. 9 Transport of temperature variance $\overline{t^2}$

incorporated in equations (16)–(21) and the resulting set of nonlinear coupled algebraic equations was solved simultaneously. The results did improve the prediction for the vertical heat flux $\overline{ut}$ and temperature variance $\overline{t^2}$ but the comparison for radial heat flux and shear stress became worse. As noted by Gibson and Launder (1976), the above model is not good near an axis of symmetry. This is why, by incorporating them in the original model, no overall improvement in the prediction is achieved.

Chen and Rodi (1975), Tamanini (1978), and Chen and Chen (1979) use the differential convective-transport equation (5) to determine $\overline{t^2}$ in their predictions of buoyant jets. Equation (6) was used to eliminate ϵ_t. Thus, the final form of the $\overline{t^2}$ equation becomes

$$U\frac{\partial \overline{t^2}}{\partial z} + V\frac{\partial \overline{t^2}}{\partial r} = \frac{1}{r}\frac{\partial}{\partial r}\left(C_t \frac{k^2}{\epsilon}\frac{\partial \overline{t^2}}{\partial r}\right) - 2\overline{vt}\frac{\partial T}{\partial r} - \frac{1}{R}\frac{\epsilon}{k}\overline{t^2} \quad (25)$$

This equation was numerically solved for the temperature variance $\overline{t^2}$ with all other quantities needed to evaluate the coefficients determined from experiments. The value of C_t was taken as 0.13. The best agreement, as shown in Fig. 7, was achieved with $R = 0.35$. When the average experimental value of $R = 0.25$ is used, the prediction peaks at about 6.0 ($\eta = 0.04$) as compared to the experimental value of $\overline{t^2}$ of about 8.0 ($\eta = 0.04$). When the standard value of $R = 0.8$ is used, $\overline{t^2}$ is overpredicted by a factor of four.

When $\overline{t^2}$ is calculated from the convective-transport equation (5), the diffusive transport is given by the simple gradient closure

$$\overline{vt^2} = -C_t \frac{k^2}{\epsilon}\frac{\partial \overline{t^2}}{\partial r} \quad (26)$$

with $C_t = 0.13$ as given by Chen and Rodi (1980). The prediction for $\overline{vt^2}$, using experimental information to evaluate the right-hand side of equation (26), is shown in Fig. 9. The predicted curve peaks somewhat above and toward the centerline as compared to the data.

Finally, we ask that if the models do not depict the axial heat flux $\overline{ut}$ and the temperature variance $\overline{t^2}$ correctly, then why do the predictions such as made by Hossain and Rodi (1982), Chen and Rodi (1975), Tamanini (1978), and Chen and Chen (1978) show reasonable agreement with the experiment for the mean velocity and buoyancy? The answer to this is that with $R = 0.8$ the temperature variance $\overline{t^2}$ from equation (21) or (25) is too large. This makes the vertical heat flux $\overline{ut}$ from equation (19) large enough so that the mean velocity and buoyancy are reasonably predicted.

5 Summary and Conclusions

The experimental data on buoyant plumes were used to evaluate various closure relations for turbulence transport. The objective was not to propose new models, but to evaluate the closure schemes proposed by other workers for buoyancy-dominated flows. The closures evaluated were those used in the k–ϵ and algebraic stress models. The results are summarized below.

1 The closure relations of the k–ϵ model compare reasonably with experimental data, except for the axial turbulent transport, which is drastically underpredicted. The axial heat flux governs the production due to buoyancy in the kinetic energy and dissipation equations and its correct prediction is very important. This is a probable reason why the results of Hossain and Rodi (1982) from the k–ϵ model underpredict the spreading rate for the plume by 10 percent even when axisymmetric jet corrections are included.

2 The ratio R of the time scales, which is used to determine the dissipation of the mean squared temperature in the algebraic stress model, was found to be considerably different from the accepted value of $R = 0.8$. Apparently R is not a universal constant, but can vary from flow to flow and is influenced by the strength of the buoyancy present. From the experimental data on a plume it appears that $R = 0.25$ for strongly buoyant flows.

3 The closure equations for the shear stress and radial heat flux of the algebraic stress models also compared well with experiment but are not better than the simple gradient closures used in the k–ϵ model. The axial heat flux and mean squared temperature are predicted poorly in the central core of the flow and had incorrect trends. This drawback could be attributed to the assumption of local equilibrium, which resulted in the neglect of convection and diffusion terms in the transport equations for Reynolds stress and heat flux. However, no substantial improvement was achieved by keeping the secondary derivatives or by incorporating the model for the convection and diffusion terms. Therefore, the full dynamic equations for Reynolds stress and heat flux with convection and diffusion are required to predict the axial heat flux and temperature variance properly.

Acknowledgments

This work was partially supported by the National Science Foundation under Grants ATM-8023699 and MSM 8316833.

References

Chen, C. J., and Chen, C. H., 1979, "On Prediction and Unified Correlation for Decay of Vertical Buoyant Jets," ASME JOURNAL OF HEAT TRANSFER, Vol. 101, pp. 532–437.

Chen, J. C., and Rodi, W., 1975, "A Mathematical Model for Stratified Turbulent Flows and Its Application to Buoyant Jets," *Proc. 16th Congress, IAHR*, Sao Paulo, Brazil, pp. 31–37.

George, W. K., Alpert, R. L., and Tamanini, F., 1977, "Turbulence Measurements in an Axisymmetric Buoyant Plume," *Int. J. Heat Mass Transfer*, Vol. 20, pp. 1145–1154.

Gibson, M. M., and Launder, B. E., 1976, "On the Calculation of Horizontal Non-equilibrium Turbulent Shear Flows Under Gravitational Influence," ASME JOURNAL OF HEAT TRANSFER, Vol. 98, pp. 81–87.

Hanjalic, K., and Launder, B. E., 1980, "Sensitizing the Dissipation Equations to Irrotational Strains," ASME *Journal of Fluids Engineering*, Vol. 102, pp. 34–40.

Hossain, M. S., and Rodi, W., 1982, "A Turbulence Model for Buoyant Flows and Its Application to Buoyant Jets," *Turbulent Buoyant Jets and Plumes*, W. Rodi, ed., Pergamon, NY, pp. 121–178.

Launder, B. E., 1975, "On the Effects of a Gravitational Field on the Turbulent Transport of Heat and Momentum," *J. Fluid Mech.*, Vol. 67, pp. 569-590.

Launder, B. E., 1978, "Heat and Mass Transport," *Topics in Physics, Vol. 12: Turbulence*, Springer-Verlag, New York, pp. 231-287.

Launder, B. E., Morse, A. P., Rodi, W., and Spalding, D. B., 1972, "The Prediction of Free-Shear Flows—A Comparison of the Performance of Six Turbulence Models," *Proc. Langley Free Shear Flows Conf.*, Vol. I, NASA SP 320.

Launder, B. E., Reese, G. J., and Rodi, W., 1975, "Progress in the Development of a Reynolds-Stress Turbulence Closure," *J. Fluid Mech.*, Vol. 68, pp. 537-566.

Launder, B. E., and Spalding, D. B., 1974, "The Numerical Computation of Turbulent Flow," *Comp. Meth. in Appl. Mech. and Engr.*, Vol. 3, p. 269.

Lumley, J. L., 1978, "Computational Modeling of Turbulent Flows," *Advances in Applied Mechanics*, Vol. 18, pp. 123-176.

Pope, S. B., 1978, "An Explanation of the Turbulent Round-Jet/Plane-Jet Anomaly," *AIAA J.*, Vol. 16, pp. 279-281.

Rodi, W., 1972, "The Prediction of Free Turbulent Boundary Layers by Use of a Two-Equation Model of Turbulence," Ph.D. Thesis, Univ. of London, United Kingdom.

Shabbir, A., 1987, "An Experimental Study of an Axisymmetric Turbulent Buoyant Plume and Evaluation of Closure Hypotheses," Ph.D. Dissertation, Univ. at Buffalo, SUNY.

Shabbir, A., and George, W. K., 1987, "Energy Balance Measurements in an Axisymmetric Buoyant Plume," *Sixth Symposium on Turbulent Shear Flows*, Toulouse, pp. 9-3-1 to 9-3-6 (also submitted to *J. Fluid Mech.*).

Tamanini, F., 1978, "The Effect of Buoyancy on the Turbulence Structure of Vertical Round Jets," ASME JOURNAL OF HEAT TRANSFER, Vol. 100, pp. 659-664.

Zeman, O., and Lumley, J. L., 1976, "Modeling Buoyancy Driven Mixed Layers," *J. Atm. Sci.*, Vol. 33, p. 1988.

SOURCE: CMOTT-91-06

On the Basic Equations for the Second-order Modeling of Compressible Turbulence

W. W. Liou and T.-H. Shih
Center for Modeling of Turbulence and Transition
ICOMP/NASA Lewis Research Center
Cleveland, OH 44135

Abstract

Equations for the mean and the turbulence quantities of compressible turbulent flows are derived in this report. Both the conventional Reynolds average and the mass-weighted Favre average were employed to decompose the flow variable into a mean and a turbulent quantities. These equations are to be used later in developing second-order Reynolds stress models for high-speed compressible flows. A few recent advances in modeling some of the terms in the equation due to compressibility effects are also summarized.

SCREEN IMAGE USER=*EBB SESSION=T20B*08 5/ 5/92 11:04:44 AM

DISPLAY 91A40793/2
91A40793*# ISSUE 17 PAGE 2932 CATEGORY 34 91/00/00 2 PAGES
UNCLASSIFIED DOCUMENT COPYRIGHT

UTTL: Development of a new flux splitting scheme
AUTH: A/LIOU, MENG-SING; B/STEFFEN, CHRISTOPHER J., JR. PAA: B/(NASA, Lewis Research Center, Cleveland, OH)
CORP: National Aeronautics and Space Administration. Lewis Research Center, Cleveland, OH.
CIO: UNITED STATES
IN: AIAA Computational Fluid Dynamics Conference, 10th, Honolulu, HI, June 24-27, 1991, Technical Papers (A91-40701 17-34). Washington, DC, American Institute of Aeronautics and Astronautics, 1991, p. 967, 968.
MAJS: /*AERODYNAMICS/*COMPUTATIONAL FLUID DYNAMICS/*FLUX VECTOR SPLITTING
MINS: / AIRFOILS/ HYPERSONIC FLOW/ SHOCK WAVE INTERACTION/ SUPERSONIC FLOW/ TURBULENCE MODELS/ TWO DIMENSIONAL FLOW
ABA: K.K.
ABS: The successful use of a novel splitting scheme, the advection upstream splitting method, for model aerodynamic problems where Van Leer and Roe schemes had failed previously is discussed. The present scheme is based on splitting in which the convective and pressure terms are separated and treated differently depending on the underlying physical conditions. The present method is found to be both simple and accurate.

ENTER:

AIAA-91-1801-CP

UNSTABLE VISCOUS WALL MODES IN ROTATING PIPE FLOW

Z. Yang*
Center for Modeling of Turbulence and Transition
ICOMP, NASA Lewis Research Center
Cleveland, OH 44135

S. Leibovich†
Sibley School of Mechanical and Aerospace Engineering
Cornell University
Ithaca, NY 14853

Abstract

Linear stability of flow in rotating pipe is studied. These flows depend on two parameters, which can be taken as the axial Reynolds number Re and the rotating rate, q. In the region of $Re \gg 1$ and $q = O(1)$, the most unstable modes are concentrated near the pipe wall, the so-called "wall" modes. These wall modes are found to satisfy a simpler set of equations containing two parameters rather than four parameters as in the full linear stability problem. The set of equations is solved numerically and asymptotically over a wide range of the parameters. In the limit of $Re \to \infty$, the eigenvalue goes to the inviscid limit. The eigenfunction shows a two layer structure. It reaches the inviscid limit over the main part of the domain, while near the wall of the pipe, the eigenfunction is represented by a viscous solution of boundary layer type.

1. Introduction

Swirling flow is common in nature and technology. Fully-developed flow in a rotating pipe is an exact solution of the Navier-Stokes equations, and is the simplest available model of swirling flows. Swirling flows are known to be subject to instability, and the question of stability of flow in rotating pipe has consequently attracted a reasonable amount of attention. Pedley[1] showed that these flows are unstable to inviscid non-axisymmetric perturbations when the rotation is fast (in a sense which will made definite). Stability to inviscid perturbations in the finite rotation rate region was studied numerically by Maslowe[2]. Later, Maslowe and Stewartson[3] extended this work in a significant way and established by asymptotic methods that the dominant unstable modes are wall modes (that is, modes of motion concentrated asymptotically close to the wall) in the limit of large azimuthal wave number.

For viscous perturbations, Pedley[4], and simultaneously Jesoph and Carmi[5] found that the critical Reynolds number at which the perturbation is neutral in the limit of fast rotation. Cotton and Salwen[6] carried out comprehensive computations in search of neutral stability curves and they discovered that the neutral modes are center modes when Reynolds number is large. Center modes in rotating pipe flow were later analyzed asymptotically by Stewartson, Ng and Brown[7], and these authors speculated that center modes dominate for large Reynolds number.

In this study, we investigate the effect of viscosity on the inviscid wall modes found by Maslowe and Stewartson[3] when the Reynolds number is large but finite. We find the proper scaling for Reynolds number in order for viscous wall mode to exist and derive simplified governing equations for them. These equations contain only two parameters instead of four parameters in the full linear stability problem. The wall mode equations are then solved both numerically and asymptotically.

The plan of this study is as follow: Linear stability analysis is formulated in section 2, where it is shown numerically that the most unstable modes are wall modes. The governing equations for viscous wall modes are derived in section 3. Numerical solutions of the viscous wall mode equations are presented in section 4. An asymptotic analysis for the viscous wall modes equations is carried out in section 5, and section 6 concludes the paper.

2. Linear Stability Formulation

If length is nondimensionalized by the radius of the pipe L and velocity by the the axial velocity at the axis U, the laminar base flow in a pipe rotating with

*Research Associate
†Professor

angular velocity Ω is then described in a cylindrical (x, θ, r) coordinate system by,

$$\mathbf{U} = (1 - r^2, q\, r, 0) \tag{1}$$

where the inverse Rossby number

$$q = \frac{\Omega L}{U} \tag{2}$$

measures the relative strength of rotation. This nondimensionalization also defines a Reynolds number

$$Re = \frac{UL}{\nu} \tag{3}$$

where ν is the kinematic viscosity of the fluid.

Linear stability analysis concerns the stability of the motion subject to infinitesimal perturbations. Since the linear stability problem with base flow given by (1) is then separable in the x and θ directions, the perturbation field may be written in the normal mode form. i.e.

$$A\,[u(r), v(r), w(r), p(r)]exp\,[i(kx + m\theta - \omega t)]$$

where A is an arbitrary constant, k is the axial wave number of the perturbation and m is the azimuthal wave number of the perturbation. ω is the complex frequency, with its real part being the frequency and the imaginary part being the growth rate. Without loss of generality, m is taken as positive, k is any real number, and ω is to be found. If $\mathrm{Im}(\omega)$ is positive, the flow is linearly unstable.

The Navier-Stokes equations linearized about the base flow, and the equation of continuity are of the following form in the cylindrical coordinate system used,

$$i\gamma u - 2rw + ikp = \frac{1}{Re}\left(\frac{\partial^2 u}{\partial r^2} + \frac{1}{r}\frac{\partial u}{\partial r} - \frac{m^2}{r^2}u - k^2 u\right)$$

$$i\gamma v + 2qw + \frac{imp}{r} = \frac{1}{Re}\left(\frac{\partial^2 v}{\partial r^2} + \frac{1}{r}\frac{\partial v}{\partial r} - \frac{m^2+1}{r^2}v + \frac{2imw}{r^2} - k^2 v\right)$$

$$i\gamma w - 2qv + \frac{\partial p}{\partial r} = \frac{1}{Re}\left(\frac{\partial^2 w}{\partial r^2} + \frac{1}{r}\frac{\partial w}{\partial r} - \frac{m^2+1}{r^2}w - \frac{2imv}{r^2} - k^2 w\right)$$

$$iku + \frac{im}{r}v + \frac{\partial w}{\partial r} + \frac{w}{r} = 0 \tag{4}$$

where

$$\gamma = k(1 - r^2) + m\,q - \omega$$

The above equations for the perturbations are supplemented by the following boundary conditions. On the wall of the pipe, the no slip boundary conditions require

$$u(1) = v(1) = w(1) = 0 \tag{5}$$

At the center of the pipe, the perturbation must satisfy the following conditions to ensure that to be single-valued[8]

for $m = 0$

$$u'(0) = v(0) = w(0) = p'(0) = 0,$$

for $|m| = 1$

$$u(0) = v(0) + im\,w(0) = p(0) = 0,$$

for m otherwise

$$u(0) = v(0) = w(0) = p(0) = 0. \tag{6}$$

The above ordinary differential equations (4) and the boundary conditions (5) and (6) form an eigenvalue problem with ω as the eigenvalue. Nontrivial solution exists only when ω takes some specific values given by

$$\omega = \omega(Re, q; m, k)$$

If $\mathrm{Im}(\omega)$ is less than zero, the flow is stable; if $\mathrm{Im}(\omega)$ is positive, the flow is said to be linearly unstable. We are interested in the regions where the instability occurs. Earlier studies show, and our results confirm, that instability occurs only for $mk < 0$. In the following, we will take m positive, and k negative.

The linear stability problem was studied extensively by numerical means by Cotton and Salwen[6] and by Yang[9]. Cotton and Salwen searched in the parameter space $(Re, q; m, k)$ for the neutral modes (modes with zero ω_i), and found that the neutral modes are center modes, with most of the nontrivial activities confined near the center of the pipe. Yang's study concentrated on the most unstable modes, and we shall briefly describe the most unstable modes that he found in the region $Re \gg 1$ and $q = O(1)$.

Table 1 gives the information for the most unstable modes at $Re = 10000$ and some different values of q's. As q is increased, the the most unstable mode has larger values of both the azimuthal and axial wave numbers. In addition, we find for $q = O(1)$, although the real part and the imaginary part of the eigenvalue have quite different size, the difference of the real part of the eigenvalue from mq is of the same order as that of the imaginary part. These findings

Table 1: The most unstable modes for different q's with $Re = 10000$.

m: the azimuthal wave number,
k: the axial wave number,
ω: the eigenvalue of the most unstable mode.

q	m	k	ω
0.5	3	-0.50	(1.25, 0.177)
1.0	5	-0.81	(4.67, 0.296)
1.5	7	-1.04	(10.13, 0.379)
2.0	9	-1.20	(17.61, 0.439)
3.0	11	-1.22	(32.63, 0.518)

suggest the viscous wall mode scalings studied in the next section. For $q = 3$, the most unstable mode has the wave numbers $m = 11, k = -1.22$. The eigenfunction corresponding to this most unstable mode is shown in Fig 1. The eigenfunction is normalized such that the maximum axial velocity is 1. The real part of the eigenfunction is drawn in solid lines, and the imaginary part is drawn in dotted lines. The nontrivial behavior of this eigenfunction takes place in a thin region near the wall of the pipe. This behavior justifies the "wall mode" terminology used, and will be the subject of further study in next section.

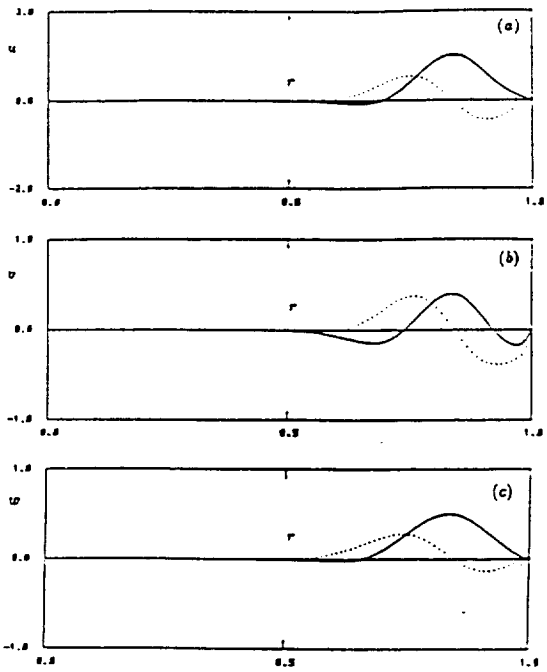

Figure 1: Eigenfunction for $Re = 10000, q = 3, m = 11, k = -1.22$. (a) axial velocity, (b) azimuthal velocity, (c) radial velocity.

3. The viscous wall mode equation

From the numerical computations in the last section, it is clear that in the region of $Re \gg 1$ and $q = O(1)$, the dominant modes are given by the asymptotic wall modes, a type of modes with large azimuthal wave number and with nontrivial behavior concentrated near the wall.

When azimuthal wave number m is large, there could be another type of mode for general swirling flows, the ring mode, as demonstrated by Leibovich and Stewartson[10]. In the case of rotating pipe flow, ring modes do not exist. Because of the existence of the pipe wall, wall modes characterize the behavior of perturbation with large azimuthal wave number.

Maslowe and Stewartson[3] studied the stability of inviscid pipe flow to perturbations of very large azimuthal wave number, and established that the prevailing modes are the wall modes in the limit of $m \to \infty$. Stewartson[11] analyzed the effect of the viscosity on ring modes and found that viscous effects come into play in higher order terms because the inviscid ring mode solution can satisfy the exact boundary conditions of the problem.

We study the wall mode when the viscosity is taken into account. Since the inviscid wall mode is close to the wall, where the no-slip condition is required but is not satisfied by the inviscid solution, it is expected that the viscous effect might be important in this case, at least in certain regions .

We are going to study the linear stability problem for large azimuthal wave number and large Reynolds number, i.e. both m and Re are large. In this case, the proper wall mode scalings are

$$\begin{aligned} r &= 1 - \frac{\eta}{(m^2+k^2)^{1/2}} \\ w &= i\bar{w} \\ p &= \frac{2\bar{p}}{m} \\ Re &= -\bar{R}e\frac{(m^2+k^2)^{3/2}}{2k} \\ \omega &= mq - \frac{2k\bar{\omega}}{(m^2+k^2)^{1/2}} \end{aligned} \tag{7}$$

The scaling for the radial variable means that the behavior of the wall mode is confined to a small distance to the wall comparable with the wave length of the perturbation. The scaling for the Reynolds number gives the balance between the viscous term and the inertia term. The form of the scaling for the complex

frequency is suggested by the numerical computations of the full linear stability problem. In above, a minus sign is introduced in places where k appears, for we know from the full linear stability problem that instability occurs only when $mk < 0$.

Upon substituting the above expressions into the linearized Navier-Stokes equations and the equation of continuity for the perturbation, and dropping the terms of order m^{-1} and smaller, we find that $\bar{w}$ should satisfy the following single equation, after $u, v, \bar{p}$ are eliminated.

$$LDLD\bar{w} - LL\bar{w} + LD\bar{w} - Q\bar{w} = 0 \qquad (8)$$

where

$$D = \frac{d}{d\eta}$$

$$L = \frac{i}{\bar{R}e}(D^2 - 1) - (\eta + \bar{\omega})$$

and

$$Q = -\frac{q(m + qk)}{k} \qquad (9)$$

which emerges as one of the independent parameters for the viscous wall mode.

The boundary conditions are

$$\bar{w} = D\bar{w} = D^2L\bar{w} - L\bar{w} = 0 \text{ at } \eta = 0 \qquad (10)$$

and

$$\bar{w} = D\bar{w} = D^2L\bar{w} - L\bar{w} = 0 \text{ as } \eta \to \infty \qquad (11)$$

Thus, we have established the formulation for the viscous wall modes. The governing equation takes a simpler form compared with the full problem, and the number of the independent parameters is reduced from *four* to *two*. Of these two parameters, $\bar{R}e$ and Q, Q measures the effect of rotation on the wall mode and $\bar{R}e$ measures the effect of viscosity on the wall mode. The solutions of above wall mode problem will give:

$$\bar{\omega} = \bar{\omega}(\bar{R}e, Q)$$

If $\mathrm{Im}(\bar{\omega})$ is less than zero, the flow is linearly stable; if $\mathrm{Im}(\bar{\omega})$ is positive, the flow is said to be linearly unstable.

4. Numerical Solution of Wall Mode Equations

In general, solutions of the wall mode equation have to be found numerically. Because the eigenvalue enters quadratically, this wall mode equation gives a nonlinear eigenvalue problem. This nonlinear eigenvalue problem is changed to a system of linear eigenvalue equations by letting

$$Y = L\bar{w} \qquad (12)$$

In Y, $\bar{w}$, the governing equations are

$$\begin{aligned} L(D^2 - 1)Y + 2DY - (Q - 2)\bar{w} &= 0 \\ Y - L\bar{w} &= 0 \end{aligned} \qquad (13)$$

and the boundary conditions are

$$\bar{w} = D\bar{w} = D^2Y - Y = 0 \quad \text{at } \eta = 0 \qquad (14)$$

$$\bar{w} = D\bar{w} = D^2Y - Y = 0 \quad \text{as } \eta \to \infty \qquad (15)$$

We employed a spectral method with Chebyshev polynomials as the basis functions to solve equations (13) - (15). Because the domain of definition extends to infinity, while Chebyshev polynomials are only defined over [-1, 1], the method of domain truncation was used to numerically truncate the domain of definition from $[0, \infty)$ to $[0, b]$ and the boundary conditions at infinity are replaced by

$$\bar{w} = D\bar{w} = D^2Y - Y = 0 \text{ at } \eta = b \qquad (16)$$

In the spectral method used, we write

$$\begin{aligned} \bar{w} &= \sum_{i=1}^{N} \bar{w}_i T_{i-1}(y) \\ Y &= \sum_{i=1}^{N} Y_i T_{i-1}(y) \end{aligned} \qquad (17)$$

where y is related to η by

$$y = 2\eta/b - 1.$$

Thus the domain of definition for y is [-1,1]. The reduction from the differential equations to a set of algebraic equations is made by a Galerkin-Tau projection — i.e. the Galerkin method is used to project the equations while the Tau method is used to enforce the boundary conditions on the spectral representations of the perturbation field. The Galerkin-Tau projection results in an set of algebraic equations, which are of the form of generalized eigenvalue problem with complex matrices.

Two methods are used in this study to find the eigenvalues and the eigenvectors of this complex generalized eigenvalue problem. One method uses the IMSL subroutine EIGZC which uses the QZ transformation to find all the eigenvalues and, optionally, all

the eigenvectors. The other method used is an inverse power iteration for the generalized eigenvalue problem developed by Kribus[12], which finds the eigenvalue closest to the initial guess and its corresponding eigenvector. The inverse power iteration is faster, so it is used whenever a good guess is available. The QZ is used to provide the starting values for the Inverse Power Iteration. It is also used when the phenomenon of mode jumping is suspected to occur.

Since the eigenfunctions decay exponentially as $\eta \to \infty$, $b = 10$ was found sufficient for most of the calculations. The number of terms in the Chebyshev representation, N, varies with $\bar{R}e$. For order one $\bar{R}e$, we must take $N = 60$, and $b = 10$ to achieve three digit accuracy in eigenvalue, and $O(10^{-4})$ accuracy for the eigenfunction. But when $\bar{R}e$ is large, the solution shows a behavior of boundary type for η near zero, i.e. near the wall of the pipe, and a large value of N is needed to resolved this region. The largest N needed for the parameter range covered here is 115.

There is a symmetry in the eigenvalue problem due to the replacement of the boundary conditions at infinity by the conditions at $\eta = b$. The solution is invariant under

$$\eta \quad \leftrightarrow \quad b - \eta$$

$$\bar{\omega} \quad \leftrightarrow \quad \bar{\omega}^* - b$$

$$\bar{w} \quad \leftrightarrow \quad \bar{w}^*$$

$$Y \quad \leftrightarrow \quad Y^*$$

where the star means the complex conjugate. This symmetry signifies that for a given solution, its image about $\eta = b/2$ is also a solution of this equation with the same growth rate. Apparently, this solution is a spurious mode in the sense that it is a solution of the differential equation after enforcing the boundary condition at finite b rather than the solution of the original differential equation defined over the infinite domain. This symmetry property can be used to check the resolution of the numerical solution of the algebraic problem, which should also exhibit this symmetry.

Extensive computations were carried out in the $(\bar{R}e, Q)$ plane. Fig 2 shows the imaginary part of the eigenvalue $\bar{\omega}$, which is proportional to the growth rate of the perturbation, vs. $\bar{R}e$ for some different values of Q. The eigenvalues shown are for $Q = 5$, 10, 20, 30, 40, 50 respectively, although numerical computations were carried out for a larger range of Q. The real part of the eigenvalue is shown in Fig 3. The growth rate increases as Q is increased, which means that rotation helps perturbations to extract energy from the

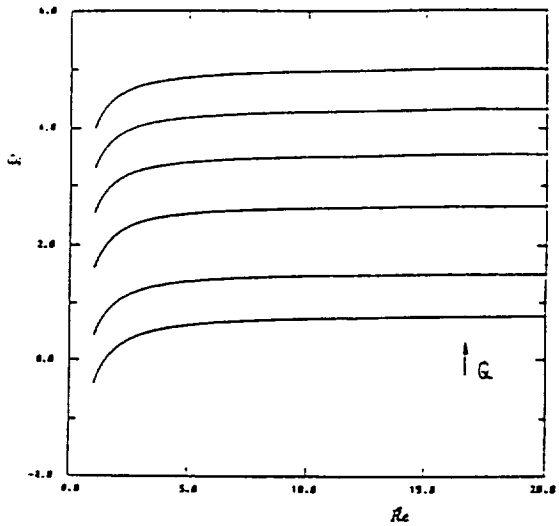

Figure 2: The imaginary part of the wall mode eigenvalues vs. $\bar{R}e$ for $Q = 5$, 10, 20, 30, 40, 50.

base flow. This result is in agreement with that of Pedley[1], who found that the maximum growth rate is 2.0 and is reached in the fast rotation limit. This is exactly the same as the upper bound for the growth rate for flow in the rotating pipe, as shown by Joseph and Carmi[5].

The growth rate increases with $\bar{R}e$. As $\bar{R}e$ gets large, the growth rate will increase. The eigenvalues seem to change smoothly as $\bar{R}e \to \infty$ and approach to the results found by Maslowe and Stewartson from their inviscid analysis. The limit of $\bar{R}e \to \infty$ will be analyzed asymptotically in the next section, and a comparison of the results with the inviscid case will be made.

Fig 4 shows the eigenfunction for $\bar{R}e = 2$, and $Q = 5$. The eigenfunction plotted is normalized such that its maximum modulus is 1 and its phase at the position of maximum modulus is 0. As in the eigenfunction plotted in Fig 1, the real part of the eigenfunction is drawn in solid line while the imaginary part of the eigenvalue is drawn in dotted line. To see the effect of increasing Q on the eigenfunction, we show in Fig 5 the eigenfunction for $\bar{R}e = 2$ and $Q = 20$. As Q increases, the eigenfunction is pushed outward, but this response is not very sensitive to Q. To see the effect of changing $\bar{R}e$, Fig 6 shows the eigenfunction for $\bar{R}e = 100$ and $Q = 5$. As $\bar{R}e$ increases, the eigenfunctions are pushed towards $\eta = 0$, i.e. toward the wall. The limit of $\bar{R}e \to \infty$ will be the further studied in the next section.

5. The Limit of $\bar{R}e \to \infty$

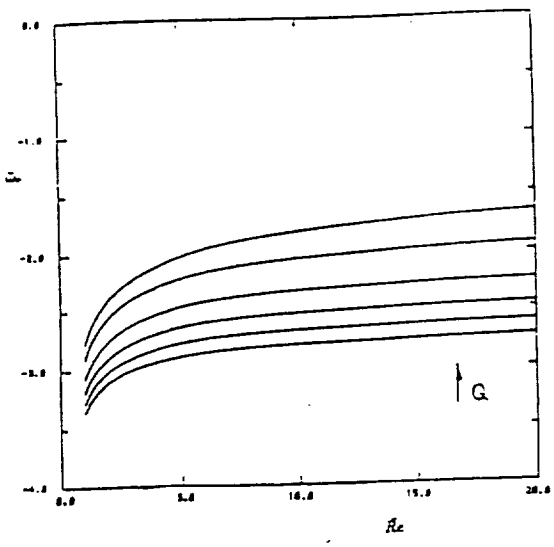

Figure 3: The real part of the wall mode eigenvalues vs. $\tilde{Re}$ for Q = 5, 10, 20, 30, 40, 50.

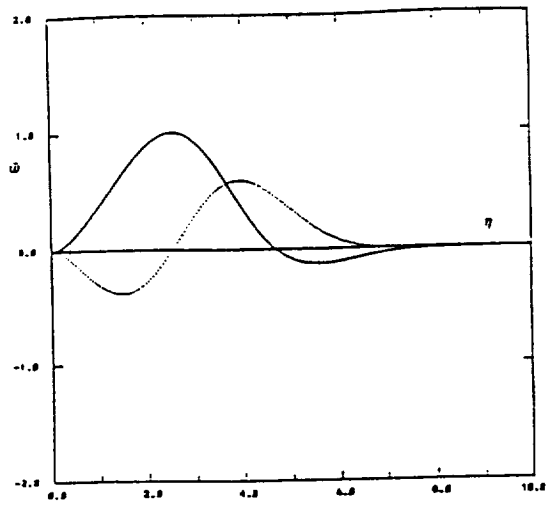

Figure 5: Wall mode eigenfunction, $\tilde{Re} = 2, Q = 20$

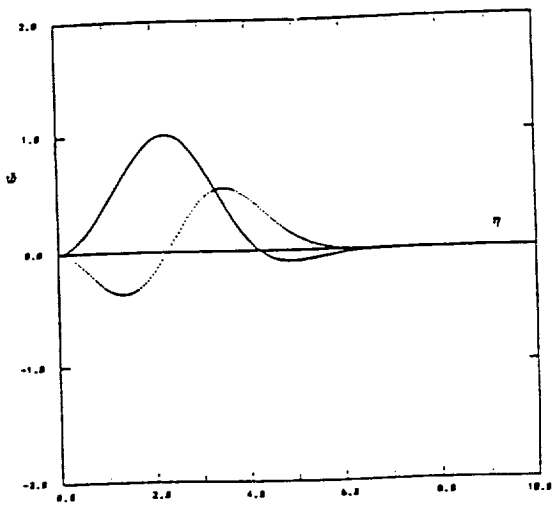

Figure 4: Wall mode eigenfunction, $\tilde{Re} = 2, Q = 5$

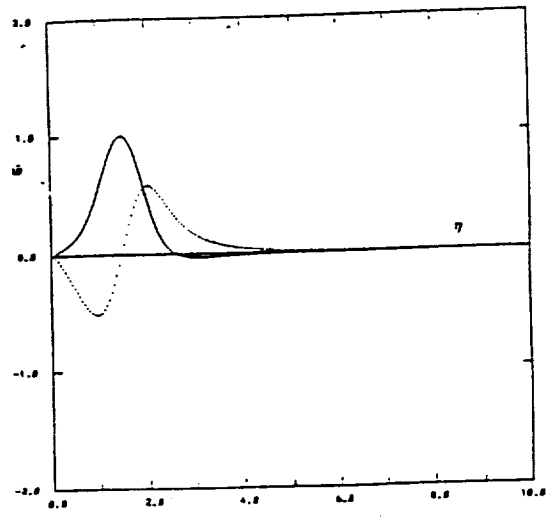

Figure 6: Wall mode eigenfunction, $\tilde{Re} = 100, Q = 5$.

Maslowe and Stewartson[3] carried out the wall mode analysis for $m \gg 1$ for the inviscid case. One of the purposes of our viscous wall mode analysis is to see if the results of their inviscid analysis is the limit of the viscous analysis for large Reynolds number. We use a perturbation technique to address this question in this section.

For $\bar{R}e \gg 1$, $\bar{w}$ can be expanded formally by taking $\bar{R}e^{-1}$ as the small parameter, we write:

$$\bar{w} = W_0^o(\eta) + \bar{R}e^{-1} W_1^o(\eta) + ...$$

To leading order, the equation for W_0^o is:

$$D^2 W_0^o - (1 + \frac{Q}{(\eta + \bar{\omega})^2}) W_0^o = 0 \qquad (18)$$

with the following boundary conditions:

$$W_0^o(0) = 0 \qquad (19)$$

$$W_0^o(\eta \to \infty) \to 0 \qquad (20)$$

This poses the same eigenvalue problem that was studied by Maslowe and Stewartson, thus their solutions (both the eigenvalue and the eigenfunction) may be viewed, as might have been expected, as the first term in a formal outer expansion in inverse powers of $\bar{R}e$.

The outer solution thus found can satisfy all the boundary conditions at infinity since the outer solution decays exponentially as $\eta \to \infty$. But not all the boundary conditions at $\eta = 0$ can be satisfied. For example, $DW_0^o(0) \neq 0$. Thus, another (inner) solution of boundary type near $\eta = 0$ is needed.

The inner variable is found to be:

$$\zeta = \eta \bar{R}e^{1/2}$$

The inner expansion is assumed to be:

$$\bar{w} = \bar{R}e^{d}(W_0^i(\zeta) + \bar{R}e^{-1/2} W_1^i(\zeta) + ...)$$

where d is to be determined.

After substituted into the governing equation, the equation to leading order is found to be:

$$(\bar{D}^2 + \bar{\omega})^2 \bar{D}^2 W_0^i = 0 \qquad (21)$$

where

$$\bar{D} = \frac{d}{d\zeta}$$

The boundary conditions for the inner solution are:

$$W_0^i(0) = 0$$

$$\bar{D} W_0^i(0) = 0$$

$$(\bar{D}^2 + \bar{\omega})^2 W_0^i(0) = 0 \qquad (22)$$

In addition, the solution is required to match the outer solution in the matched asymptotic sense.

The general solutions of the inner problem in the leading order can be found, and they are

$$W_0^i = \beta_1 \exp(\lambda_1 \zeta) + \beta_2 \zeta \exp(\lambda_1 \zeta) + \beta_3 \exp(\lambda_2 \zeta) + \beta_4 \zeta \exp(\lambda_2 \zeta) + \beta_5 + \beta_6 \zeta \qquad (23)$$

where

$$\lambda_{1,2} = \pm (i\bar{\omega})^{1/2}$$

and β_1, β_2, β_3, β_4, β_5, β_6 are constants to be determined by the boundary conditions and the matching conditions. $\bar{\omega}$ is given by the outer solution.

The boundary conditions at $\zeta = 0$ require that

$$\beta_1 + \beta_3 + \beta_5 = 0$$

$$\beta_1 \lambda_1 + \beta_2 + \beta_3 \lambda_2 + \beta_4 + \beta_6 = 0$$

$$2\lambda_1^3 \beta_2 + 2\lambda_2^3 \beta_4 = 0$$

As $\zeta \to \infty$, the inner solution must also match the outer solution. Near $\eta = 0$, the outer solution is, to leading order,

$$W_0^o = \alpha \eta$$

where $\alpha = DW_0^o(0) \neq 0$.

To carry out the matching, we need to know the behavior of W_0^i for large ζ. The behaviors of the exponential terms are determined by the sign of the real parts of λ_1, λ_2. Since λ_1, λ_2 are the square roots of $(i\bar{\omega})$, λ_1 is the negative of λ_2. In this study, we take

$$Re(\lambda_1) < 0$$

$$Re(\lambda_2) > 0$$

As $\zeta \to \infty$, the matching of the exponentially growing terms gives:

$$\beta_3 = 0$$

$$\beta_4 = 0$$

The exponentially small terms are immaterial, and the matching of the algebraic terms gives

$$\bar{R}e^{d} \beta_6 \zeta = \alpha \eta \qquad (24)$$

which gives

$$d = -\frac{1}{2}$$

and

$$\beta_6 = \alpha$$

All the other constants can be determined, yielding

$$\beta_1 = -\alpha/\lambda_1$$

$$\beta_2 = 0$$

$$\beta_5 = \alpha/\lambda_1$$

The inner solution, to the leading order, is

$$W_0^i(\zeta) = \alpha(\zeta + \frac{1}{\lambda_1}(1 - \exp(\lambda_1\zeta))) \qquad (25)$$

Thus, we have the following composite solution to the leading order:

$$W_0^c = W_0^o(\eta) + W_0^i(\zeta) - \alpha\eta \qquad (26)$$

Thus, one sees that indeed, the solutions for the most unstable modes found by Maslowe and Stewartson are the correct limit when $\bar{R}e \to \infty$, except in a thin layer near the wall of the pipe where the flow field is described by a viscous layer of the boundary layer type. The eigenvalues found are the same as for the inviscid case.

The above asymptotic analysis is confirmed by the numerical calculation. In Table 2, we present the eigenvalues for $\bar{R}e = 100$ and in Table 3, we present the eigenvalues from the inviscid calculation for a few values of Q. It is seen that differences of the eigenvalues in these two cases are small. In Fig 7, we show the eigenfunction for $Q = 5.0$ from the inviscid calculation. It is seen that the general shape agrees with the viscous calculation presented in Fig 6. To see the existence of a thin viscous layer near the wall, we present in Fig 8a a blow-up of Fig 6, and in Fig 8b a blow up of Fig 7 near the wall. It is seen that flow fields near the wall are different, the viscous solution has a zero slope while the solution from the inviscid equation has a non-zero slope.

6. Discussion

We have examined the linear stability of rotating pipe flow to perturbations of large azimuthal wave number. It is found that when the azimuthal wave number is large, the nontrivial behaviors are concentrated near the wall of the pipe, so the prevailing variations are manifested as wall modes. The equations governing wall modes are found to contain two parameters $\bar{R}e$ and Q, which measure the Reynolds number and swirl, respectively.

Table 2: Eigenvalue of viscous wall mode.

Q	eigenvalue ($\bar{R}e = 100$)
5.0	(-0.14917D+01, 0.72752D+00)
10.0	(-0.18163D+01, 0.15096D+01)
20.0	(-0.21617D+01, 0.26668D+01)
30.0	(-0.23766D+01, 0.35755D+01)
40.0	(-0.25358D+01, 0.43505D+01)
50.0	(-0.26633D+01, 0.50384D+01)

Table 3: Eigenvalue of inviscid wall mode.

Q	eigenvalue ($\bar{R}e = \infty$)
5.0	(-0.14142D+01, 0.68305D+00)
10.0	(-0.17476D+01, 0.14875D+01)
20.0	(-0.21038D+01, 0.26574D+01)
30.0	(-0.23247D+01, 0.35710D+01)
40.0	(-0.24877D+01, 0.43487D+01)
50.0	(-0.26181D+01, 0.50383D+01)

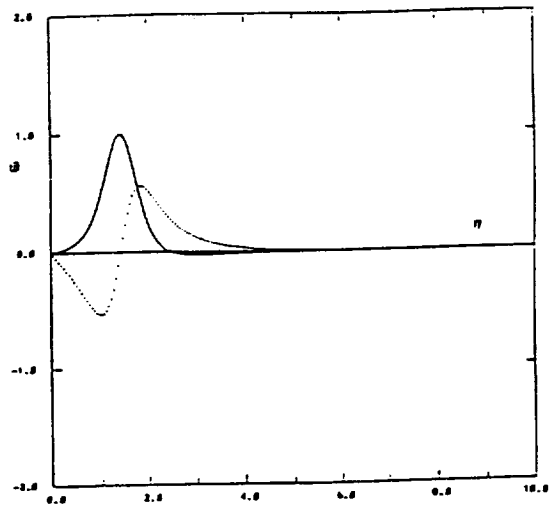

Figure 7: Wall mode eigenfunction for the inviscid case, $Q = 5$.

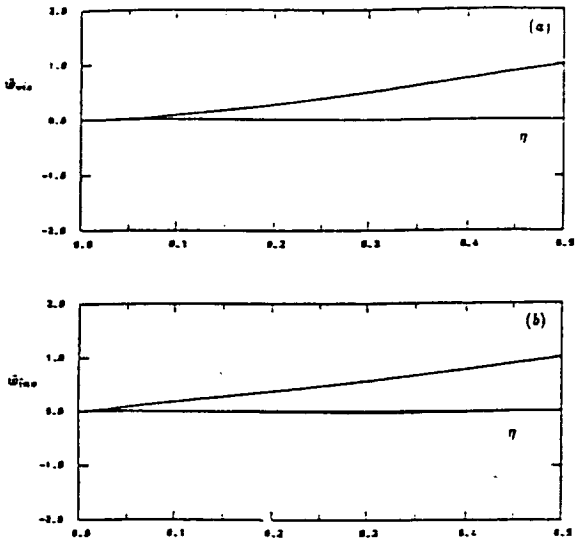

Figure 8: Comparison of the wall mode eigenfunctions near the wall. (a) the viscous solution at $\bar{R}e = 100$, (b) the inviscid solution.

For large azimuthal wave number, the wall mode is a distance $O(m^{-1})$ away from the wall. Viscous effects are confined to a layer with thickness of $O(Re^{-1/2})$ near the wall. The case treated here is when those two layers are of the same order, i.e. $Re = O(m^2)$. When $Re/m^2 \gg 1$, we would expect the solution to be mainly inviscid, as found by Maslowe and Stewartson, except in a thin viscous layer near the wall. This is indeed the case as shown both numerically and asymptotically.

The region for the rotation rate considered is $q = O(1)$. For large value of q, which corresponds to the fast rotation case, Pedley[4] shows that as Reynolds number is increased, the dominant mode is taken by perturbations of larger and larger values of m, the azimuthal wave number. In the limit of $Re \to \infty$, the azimuthal wave number for the dominant modes will also go to infinity, and these modes could be viewed as wall modes. Thus, our work here can be viewed as an extension of Pedley's work[1,4] to the region of $q = O(1)$.

Left unexamined is the case when the inviscid solution has a singularity, in which case the form of the expansion we assumed would break down. In the study of Maslowe and Stewartson, the leading mode is a neutral mode when $Q = 2$. For $Q > 2$, the leading mode is unstable, but there are still neutral modes. The neutral modes have a $1/(r - r_0)$ singularity, where r_0 is the location of the singularity. It is expected that a local viscous critical layer based on our viscous wall mode formulation would get rid of this singularity.

Acknowledgement

This work was supported by the Air Force Office of Scientific Research under contract AFOSR-89-0346 monitored by Dr. L. Sakell.

References

[1] T.J. Pedley. "On the instability of rapidly rotating shear flows to non-axisymmetric disturbances." *J. Fluid Mech.*, 31:603–607, 1968.

[2] S.A. Maslowe. "Instability of rigidly rotating flows to non-axisymmetric disturbances." *J. Fluid Mech.*, 74:303–317, 1974.

[3] S.A. Maslowe and K. Stewartson. "On the linear inviscid stability of rotating Poiseuille flow." *Phys. Fluids*, 25:1517–1523, 1982.

[4] T.J. Pedley. "On the instability of viscous flow in a rapidly rotating pipe." *J. Fluid Mech.*, 35:97–115, 1969.

[5] D.D. Joseph and S. Carmi. "Stability of Poiseuille flow in pipes, annuli, and channels." *Quart. Appl. Math.*, 26:575–599, 1969.

[6] F.W. Cotton and H. Salwen. "Linear stability of rotating Hagen-Poiseuille flow." *J. Fluid Mech.*, 108:101–125, 1981.

[7] K. Stewartson, T.W. Ng, and S.N. Brown. "Viscous center modes in the stability of swirling Poiseuille flow." *Phil. Trans. Roy.*, 324:473–512, 1988.

[8] G.K. Batchelor and A.E. Gill. "Analysis of the stability of axisymmetric jets." *J. Fluid Mech.*, 14:529–551, 1962.

[9] Z. Yang. *Two theoretical studies of stability of swirling flows*. PhD Thesis, Cornell University, 1990.

[10] S. Leibovich and K. Stewartson. "A sufficient condition for the instability of columnar vortices." *J. Fluid Mech.*, 126:335–356, 1983.

[11] K. Stewartson. "The stability of swirling flow at large Reynolds number when subject to disturbances of large azimuthal wavenumber." *Phys. Fluids*, 25:1953–1957, 1982.

[12] A. Kribus. "Computation of leading eigenspaces for generalized eigenvalue problems." *Trans. of the 7th Army Conf. on Appl. Math and Comp.*, 1990.

Development of A New Flux Splitting Scheme

Meng-Sing Liou* and Christopher J. Steffen, Jr.†
NASA Lewis Research Center
Cleveland, Ohio

Maximizing both accuracy and efficiency has been the primary objective in designing a numerical algorithm for computational fluid dynamics (CFD). This is especially important for solution of complex 3D problems which often involve Navier-Stokes equations with turbulence modeling and chemical species equations. Upwind schemes have been well received for both their capability of resolving discontinuities and their sound theoretical basis in characteristic theory for hyperbolic systems. Several flux splitting schemes, notably by Steger-Warming, Van Leer, Osher, and Roe, have been tested and discussed extensively in the past decade.

However, several inherent shortcomings exist in each of these schemes. For example, while the Van Leer scheme is simple, taking only $O(n)$ operations, n being the number of equations, and yields accurate solutions for inviscid problems, it suffers inaccuracy for predicting velocity and temperature fields in the viscous problems. The Roe scheme, commonly accepted as the most accurate scheme available currently, however is a great deal more complex and costly due to the matrix operation, requiring $O(n^2)$ operations. Moreover, the extension to the chemically reacting flows renders no unique way of defining the 'Roe-averaged' states. The Osher scheme has the smooth property and has recently been generalized by Suresh and Liou to deal with chemically reacting flows. But the determination of the intermediate states also requires $O(n^2)$ operations. Thus it is logical to ask whether there is room in the universe of upwind schemes for improvement to arrive at a simple ($O(n)$ operations) and accurate scheme for a wide range of problems.

In this paper, we summarize recent successes of a new splitting scheme for some model aerodynamic problems where Van Leer and Roe schemes failed. The new scheme is based on a rather different idea of splitting in which the convective and pressure terms are separated and treated differently in accordance with the underlying physical intuitions. We propose an appropriately defined cell-face advection Mach number using values from the two straddling cells via associated characteristic speeds. This interface Mach number is then used to determine the upwind extrapolation for the convective quantities. Next the pressure splitting is weighted using polynomial expansions of the characteristic speeds. Thus, the name of the present scheme is properly coined as Advection Upstream Splitting Method (AUSM). The scheme is remarkably simple and yet its accuracy in the present study rivals and in some cases surpasses the Roe scheme in the Euler and Navier-Stokes solutions at considerably reduced computational effort. The detailed formulation of the scheme is not shown here due to space limitation. However it will appear elsewhere.

The calculation of the hypersonic conical flow demonstrates the accuracy of the splittings in resolving the flow in the presence of strong gradients. The temperature and pressure profiles of the first order results are shown in Figs. 1 (a) and (b). The Van Leer splitting is seen to produce a thicker boundary layer which in turn further displaces the shock wave. Both AUSM and Roe solutions are in excellent agreement.

The second series of tests involve the 2D inviscid flow over a NACA 0012 airfoil. The results, not included here, demonstrate that the level of entropy generation at the stagnation point is about three times smaller than the Roe solution.

In the third case we calculate a series of supersonic flows over a circular cylinder. The Roe splitting in all conditions and grids tested yields anomalous solutions (sometimes referred to as the carbuncle phenomenon), which may appear as nonsymmetric, protuberant, or indented contours, see Fig. 2. The mode of these nonphysical solutions appears to be sensitive to changes in Mach number or grid. The AUSM, however, gives expected solutions in all calculations.

The fourth test deals with a 2D shock wave/laminar boundary-layer interaction. In Fig. 3, the AUSM is seen to give excellent agreement with the data especially in the reattachment region, which has been in defiance of many previous calculations in the literature. Also the oblique shock appears to be more tightly captured by the AUSM.

In summary, it appears that the new splitting scheme, AUSM, has delivered the promise by improving the accuracy as well as efficiency significantly. As usual, the final judgment will be decided via many more tests and further modifications of the scheme.

* Senior Scientist, Internal Fluid Mechanics Division. Member AIAA
† Aerospace Engineer, Computational Fluid Dynamics Branch. Member AIAA

fig. 1(a)

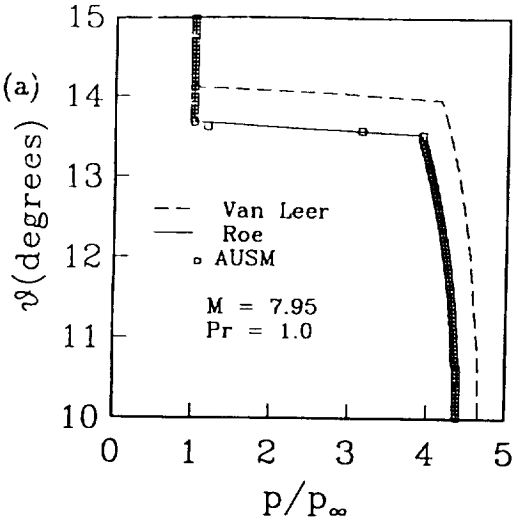

fig. 1(b)

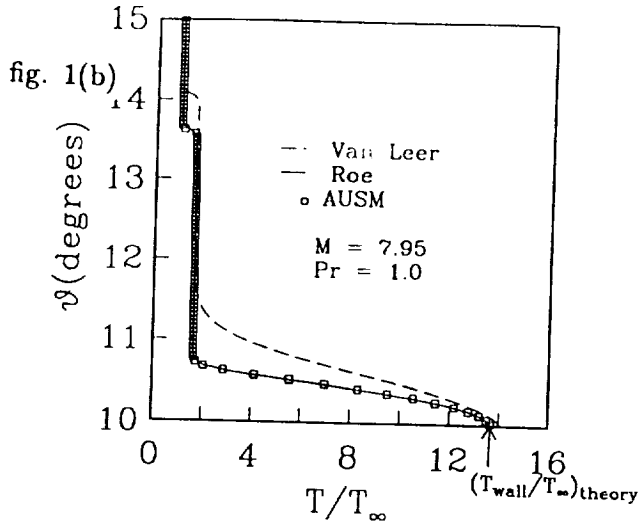

Fig. 1 Conic flow with $M_\infty = 7.95$, $Re = 4.2 \times 10^5$, and half cone angle = 10°: (a) pressure, and (b) temperature distributions.

fig. 2(a)

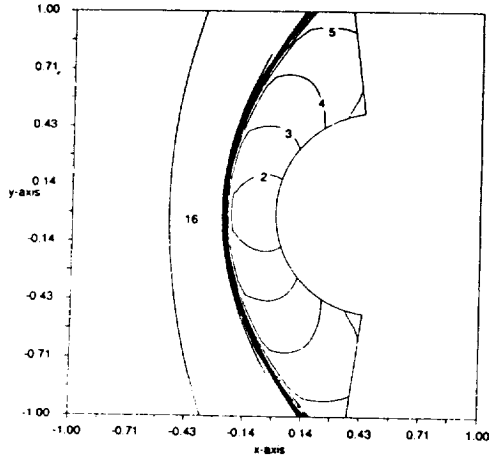

fig. 2(b)

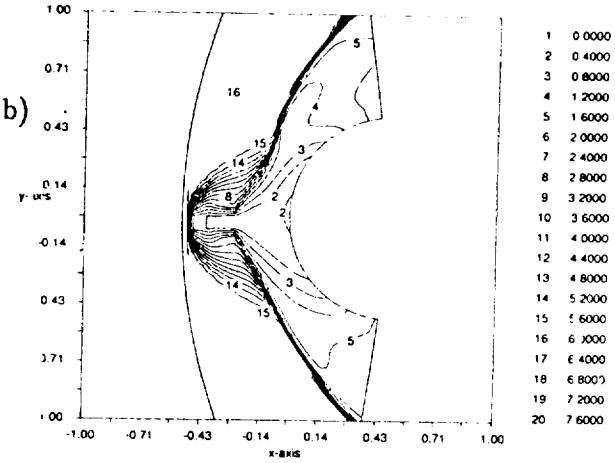

Fig. 2 Mach contours for a Mach 6 inviscid flow over a circular cylinder: (a) the AUSM solution, (b) the Roe solution displaying a protuberrant, two-shock contours.

fig. 3(a)

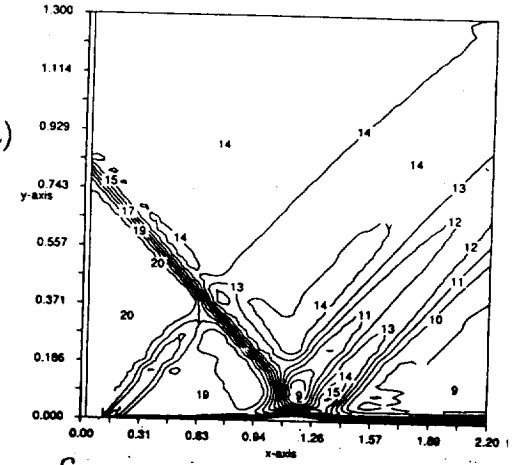

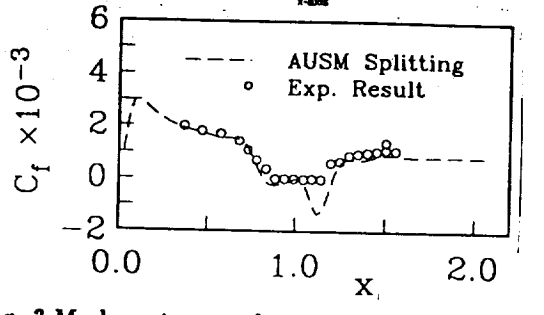

fig. 3(b)

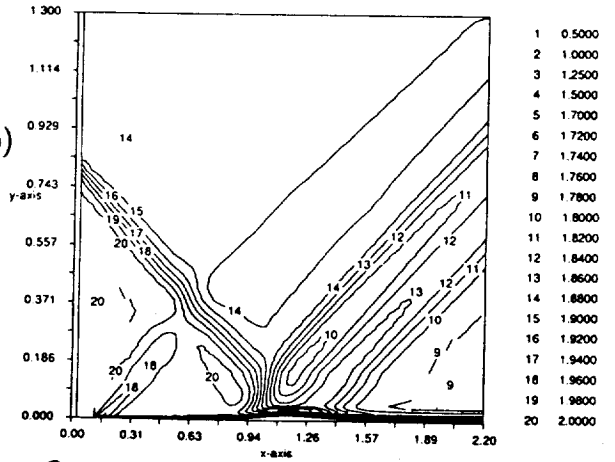

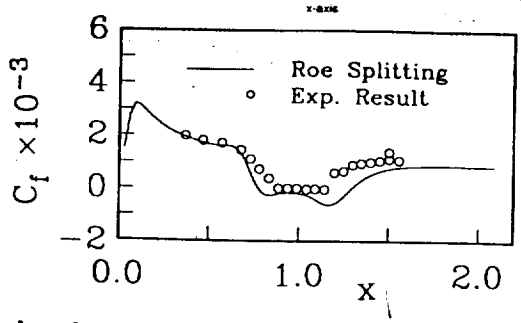

Fig. 3 Mach contours and comparison of skin friction with data for $M_\infty = 2.0$, $Re = 2.96 \times 10^5$ [Hakkinen et al]: (a) the AUSM solution, and (b) the Roe solution.

79807

N92-23353

High-Order Polynomial Expansions(HOPE) for Flux-Vector Splitting

Meng-Sing Liou† and Chris J. Steffen, Jr.*

NASA Lewis Research Center
Cleveland, OH 44135, U.S.A.

Summary

The Van Leer flux splitting is known to produce excessive numerical dissipation for Navier-Stokes calculations. One example is the incorrect prediction of boundary-layer profiles. We attempt in this paper to remedy this deficiency by introducing a higher-order polynomial expansion(HOPE for short) for the mass flux. In addition to Van Leer's splitting, a term is introduced so that the mass diffusion error vanishes at $M = 0$. Several splittings for pressure are proposed and examined. The effectiveness of the HOPE scheme is illustrated for 1-D hypersonic conical viscous flow and 2-D supersonic shock-wave/boundary-layer interactions. Also, we give the weakness and suggest areas for further investigation of the scheme.

Introduction

In the past decade, upwind differencing schemes have gained considerable attention for their accuracy and robustness in Euler flows with discontinuieties, shock waves in particular. Naturally, significant research effort in the CFD community has been focused on maxmizing the accuracy and efficiency, among other objectives. Four popular but conceptually different flux splitting ideas have been utilized for nearly 10 years: Steger and Warming, Van Leer, Roe, and Osher. However, each scheme has an associated weakness when numerical accuracy and efficiency are considered.

In this paper, we deal specifically with the improvement of Van Leer's flux vector splitting[1]. Besides its simplicity, Van Leer's splitting has the following properties: (1) it can be interpreted as a special member of a family of second-order polynomial expansions[2], and (2) the associated flux Jacobian and eigenvalues are continuous at the sonic points. Van Leer's choice allows one vanishing eigenvalue in the case of an ideal gas, thereby resulting in a crisp shock representation. Furthermore, the continuous differentiability is helpful for convergence acceleration, e.g., in multigrid schemes.

However, failing to recognize the contact discontinuity, the Van Leer splitting[1] produces excessive numerical diffusion and thus requires a huge number of cells to correctly resolve the boundary-layer flow. Some improvements have been demonstrated recently by Hänel et al[2] and Van Leer[3] for 1-D conical, hypersonic viscous flow, but a pressure glitch arises. A new scheme by the present authors[4] has been proposed that not only corrects this pressure difficulty, but also is remarkably simple to implement. Nevertheless, the above schemes[2-4] have already departed from the ideas of flux vector splitting

† Senior Scientist, Internal Fluid Mechanics Division
* Aerospace Engineer, Computational Fluid Dynamics Branch

and in fact become more like the flux difference splitting. Since the differentiability and simplicity are desirable properties, one would still wish to search for a better splitting scheme that is strictly based on the flux vector splitting.

In this paper, we propose a family of higher-order polynomial expansions for the mass flux that diminishes the diffusion error as $M \to 0$. We give a detailed study of the accuracy of the scheme for 1-D conical flow and 2-D shock wave/boundary-layer interactions. The weakness of the scheme is also pointed out and possibile improvements suggested.

Analysis

To exemplify the concept, let us consider the quasi two-dimensional system of equations for conical flows:

$$\frac{\partial \mathbf{U}}{\partial t} + \frac{\partial \mathbf{F}}{\partial \eta} = \mathbf{S}$$

where $\mathbf{U}^T = (\rho, \rho u, \rho v, \rho E)$, $\mathbf{F}^T = (\rho v, \rho v u, \rho v^2 + p, \rho v H)$, $E = e + 1/2(u^2 + v^2)$, and $H = E + p/\rho$. The flow considered consists of a very thin shear layer at the wall and a shock wave away from the wall. An algorithm must be capable of minimizing the numerical smearing(diffusion) at the locations where an eigenvalue changes sign or approaches zero. For example, Van Leer's splitting[1] can represent shock profile well, while greatly diffusing the boundary layer. The Van Leer split mass fluxes are:

$$F_1 = F_1^+ + F_1^-; \quad F_1^\pm = \pm \rho a/4(M \pm 1)^2.$$

The net difference from the curve it approximates is largest at $M = 0$; its value equals $\rho a/2$. This error, viz numerical diffusion, significantly broadens the boundary layer, leading to incorrect velocity and temperature profiles. A simple way to remove the diffusion at $M = 0$ is by adding an extra higher-order term that allows the split mass fluxes to pass through the origin(Fig. 1), i.e.,

$$F_1^\pm = \pm \rho a/4[(M \pm 1)^2 + m_1(M)(M^2 - 1)^2],$$

where the higher-order term has a coefficient m_1, in general function of M. It should have the following properties:

(1) $m_1 \to -1 \quad$ as $M \to 0$;

(2) $m_1(M) = m_1(-M)$;

(3) $m_1 \to 0 \quad$ as $M \to \pm 1$.

A formula satisfying those properties is chosen as:

$$m_1 = (M^2 - 1)/(M^2 + 1)^S,$$

where the exponent S is a free parameter; also shown in Fig. 1 is m_1 vs M with $S = 4$.

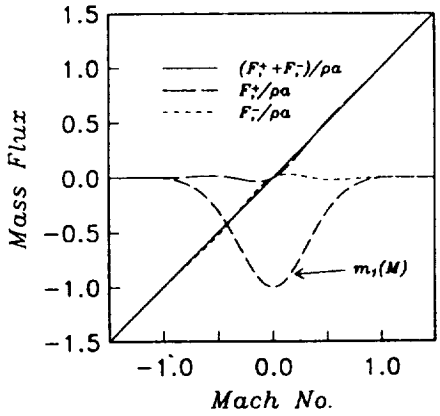

Fig. 1. Mass Flux Splitting in HOPE.

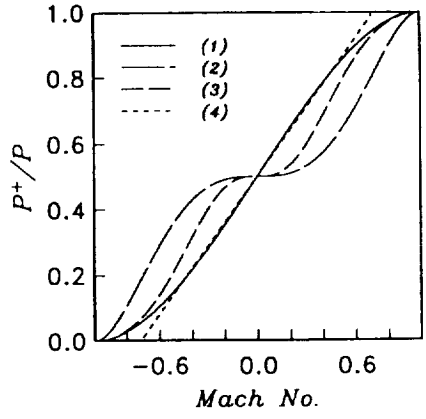

Fig. 2. Pressure Splitting.

In the conical flow calculations, the accuracy and convergence appear to be insensitive to the specified values of $S = 2, 4, 6$. Now, regarding the flux as a sum of convective and pressure terms, we can write the splitting formula for the flux vector:

$$\begin{pmatrix} F_1 \\ F_2 \\ F_3 \\ F_4 \end{pmatrix}^{\pm} = \begin{pmatrix} \rho v \\ \rho v u \\ \rho v v + p \\ \rho v H \end{pmatrix}^{\pm} = F_1^{\pm} \begin{pmatrix} 1 \\ u \\ v \\ H \end{pmatrix} + \begin{pmatrix} 0 \\ 0 \\ p^{\pm} \\ 0 \end{pmatrix}.$$

With the realization in [5] that the pressure splitting could be considered separately in the Van Leer formula[1], a whole host of freedoms for the pressure splitting becomes possible. Following is the list of formulas tested:

$$(p1): \quad p^{\pm} = \mp 1/4(M \pm 1)^2(M \mp 2)p,$$
$$(p2): \quad p^{\pm} = (p1) \mp 3/4M(M^2 - 1)^2 p,$$
$$(p3): \quad p^{\pm} = (p1) \pm 3/4m_1 M(M^2 - 1)^2 p,$$

and

$$(p4): \quad p^{\pm} = 1/2(1 \pm \gamma M)p.$$

Figure 2 displays the distribution of the split pressure vs M. The first formula is that used by Van Leer[1]. The second and third splits, $(p2)$ and $(p3)$, yield vanishing slope at $M = 0$, thus corresponding to central differencing. However, no instability was encountered in the conical flow problem with the $(p2)$ or $(p3)$ split used in an implicit code. The fourth split $(p4)$ is obtained from an approximate integration along characterics. As will be seen later, the four formulas give essentially the same results for the conical flow calculated.

Results And Discussion

In this paper, two cases were tested to check the accuracy and convergence of the HOPE scheme. The first case is the 1-D self-similar conical flow over a 10-degree half cone at hypersonic speed, for which a detailed comparison study was conducted.

The flow conditions are: $M_\infty = 7.95$, and $Re_\infty = 4.2 \times 10^5$. Since $P_r = 1.0$, exact solution gives adiabatic wall temperature, $13.64T_\infty$. The second case is the 2-D shock wave/laminar boundary-layer interactions, for which experimental measurements were available[6]. The conditions are: $M_\infty = 2.0, Re_\infty = 2.96 \times 10^5$, and oblique shock angle $\beta = 32.585$ degrees. In both cases, the results from the Roe splitting are also included for comparison. An implicit Newton iteration procedure was used to achieve steady-state solution with L_∞ residual dropped by five orders of magnitude.

Figures 3 and 4 show the pressure and temperature distributions from the first- and second-order solution on a 65-grid; little difference is seen. A monotone solution across the shock is obtained with the first-order scheme while oscillation appears in the second-order scheme, which can be eliminated by a TVD procedure. It is noted that the first-order pressure is smooth at the edge of the boundary layer, unlike the Roe solution which shows a slight discontinuity(not shown here). Although the boundary layer exhibits a steep temperature gradient, the HOPE scheme predicts the wall temperature correctly, indicating removal of the numerical diffusion associated with the original Van Leer splitting.

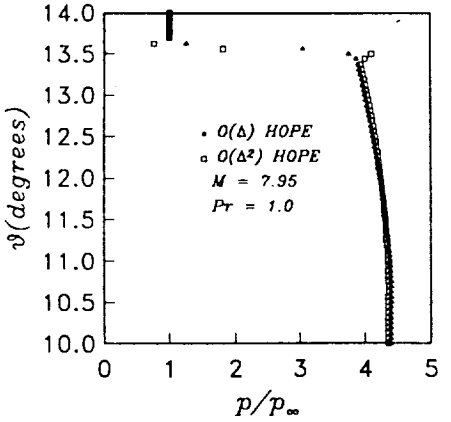

Fig. 3. Pressure Profile of Conic Flow.

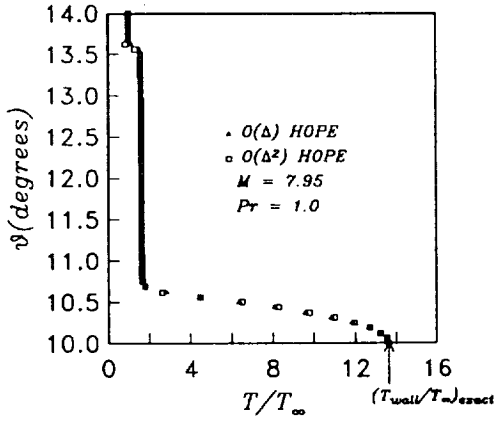

Fig. 4. Temperature Profile of Conic Flow.

Figure 5 displays the results using various pressure splittings; they are practically identical except the Van Leer pressure split ($p1$) shows some minor oscillation near the wall. However, the pressure splittings show significant effect on the convergence rate. The ($p3$) and ($p4$) splits are the best, comparable to the Roe splitting, while the other two are roughly two to three times slower. These may indicate possible instability in a more complex case.

Finally, for the 2-D case, the surface pressure and friction coefficient are plotted in Figs. 7 and 8. The first-order HOPE results compare fairly with Roe's splitting and experimental data. However, the second-order calculation experienced difficulty in convergence in which the residual was reduced by only two orders of magnitude and the result is not presented here.

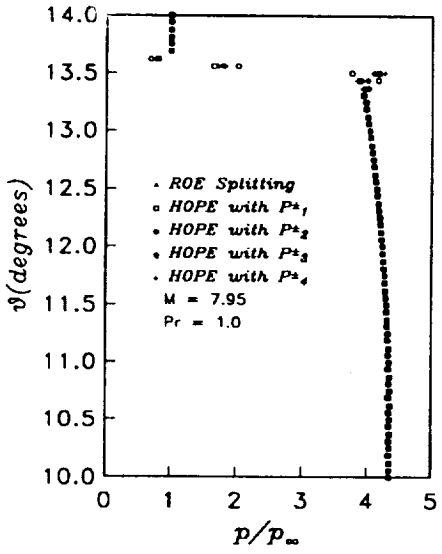

Fig. 5. Comparison of Pressure Splits.

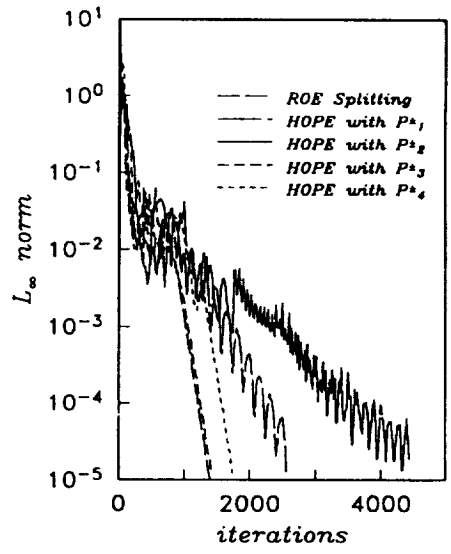

Fig. 6. Convergence History.

We suspect that a further investigation on other pressure splittings may lead to success in stability and convergence. Nevertheless, a systematic study of the eigenvalues of the split fluxes and the complete discretized system will prove to be a useful endeavor. Above all, the present research suggests that there are still possibilities in flux-vector splitting after Van Leer's appeared nearly 10 years ago. The possibilities may very well still lie in the mass-flux splitting.

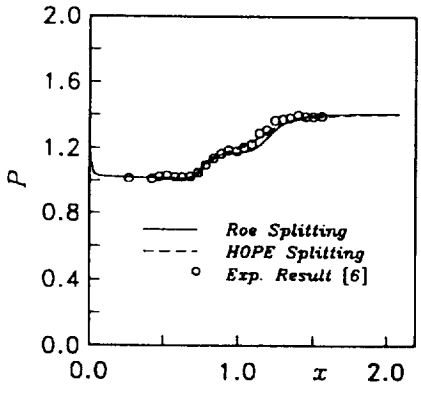

Fig. 7. Pressure at the Wall.

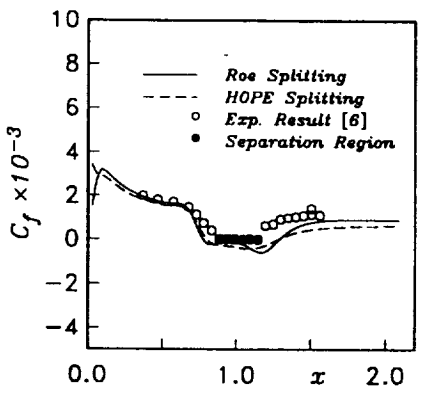

Fig. 8. Friction Coefficient at the Wall.

References

[1] B. van Leer, *Lecture Notes in Physics, Vol. 170*, 1982.

[2] D. Hänel and R. Schwane, AIAA Paper 89-0274, 1989.

[3] B. van Leer, CFD Symposium on Aeropropulsion, *NASA CP-10045*, 1990.

[4] M.-S. Liou and C. J. Steffen, Jr., (in preparation).

[5] M.-S. Liou, B. van Leer, and J. S. Shuen, *J. Comput. Physics, Vol. 87*, 1990.

[6] R. J. Hakkinen, I. Greber, L. Trilling, and S. S. Abarbanel, *NASA Memo 2-18-59W*, 1959.

Three-Dimensional Calculations of Supersonic Reacting Flows Using an LU Scheme

Sheng-Tao Yu, Y.-L. Peter Tsai, and Jian-Shun Shuen

Sverdrup Technology, Inc.,
NASA Lewis Research Center, Cleveland, Ohio

ABSTRACT

A new three-dimensional numerical program that incorporates comprehensive real gas property models has been developed to simulate supersonic reacting flows. The code employs an implicit, finite volume, Lower-Upper (LU), time-marching method to solve the complete Navier-Stokes and species equations in a fully-coupled and very efficient manner. A chemistry model with nine species and eighteen reaction steps is adopted in the program to represent the chemical reactions of H_2 and air. To demonstrate the capability of the program, flow fields of underexpanded hydrogen jets transversely injected into the supersonic airstream inside the combustors of scramjets are calculated. Results clearly depict the flow characteristics, including the shock structure, the separated flow regions around the injector, and the distribution of the combustion products.

N92-23355

Simulations of Free Shear Layers Using a Compressible $k-\epsilon$ Model

S.T. Yu*
Sverdrup Technology, Inc.,
NASA Lewis Research Group
Brook Park, OH 44142

C.T. Chang† and C.J. Marek‡
NASA Lewis Research Center
Cleveland, Ohio 44135

ABSTRACT

A two-dimensional, compressible Navier-Stokes equations with a $k-\epsilon$ turbulence model are solved numerically to simulate the flows of compressible free shear layers. The appropriate form of k and ϵ equations for compressible flows are discussed. Sarkar's modelling is adopted to simulate the compressibility effects in the k and ϵ equations. The numerical results show that the the spreading rate of the shear layers decreases with increasing convective Mach number. In addition, favorable comparison was found between the calculated results and Goebel and Dutton's experimental data.

INTRODUCTION

Recent national interest in trans-atmospheric vehicle has rekindled the hypersonic research. For this vehicle, a supersonic combustion ramjet (scramjet) engine was proposed to provide the power. Inside this scramjet engine, compressible mixing layers are important phenomena. The performance of the engine will depend on the supersonic mixing and the flame holding of shear layers.

The behavior of incompressible mixing layers has been studied extensively. However, additional study is required to understand the compressibility effects of free shear layers at high speeds. Figure 1 shows a sketch of a typical free shear layer. Two streams at different temperatures, densities, and Mach numbers merge together to form a free shear layer. Various combinations of flow conditions of high-speed streams and low-speed streams allow for the systematic study of compressible shear layers. In this paper, we report the incorporation of a $k-\epsilon$ model with compressibility effects to a two-dimensional flow equations solver for the simulation of compressible shear layers. First, we point out the derivation procedure of the compressible k and ϵ equations. Unlike the procedure in the incompressible equations, both Favre and Reynolds averaging procedures[1] are performed in deriving the flow and turbulence equations. Particularly, the additional terms in the Navier-Stokes equations due to the averaging procedure are illustrated. These terms are often omitted in CFD practices. The k and ϵ equations are presented in vector form for the convenience of illustrating the numerical method.

The lower-upper (LU) scheme developed by Yoon and Jameson[2] is adopted in this work. This method has proven very efficient for large systems of equations.[3] For completeness, a brief account of the numerical method is presented in this paper. The newly developed solver then is applied to simulate compressible free shear layers with five different convective Mach numbers from 0.05 to 1.48. One of five test conditions is a replica of that reported by Goebel and Dutton.[4] The most important feature of the compressible free shear layers one want to demonstrate in the calculations is the decrease of the shear layer thickness with increasing Mach number.[5] Favorable comparison were found between the experimental data and the calculated results.

THEORETICAL MODEL

In deriving the compressible flow equations of fully turbulent flows, all the flow properties are Favre averaged (mass weighted averaged) except the density, ρ, and pressure, p. The definition of the Favre average is

$$\tilde{\phi} = \overline{\phi\rho}/\overline{\rho}. \qquad (1)$$

* Research Engineer, Member AIAA.
† Aerospace Engineer, Member AIAA.
‡ Senior Research Scientist.

where ϕ is any flow property. Thus flow variables are decomposed in the following fashion,

$$\phi = \tilde{\phi} + \phi". \tag{2}$$

On the other hand, conventional Reynolds' average are used for the pressure and the density. According to the definition of Favre averaging, the following relations exist:

$$\begin{aligned} \overline{\phi"} &= -\frac{\overline{\rho'\phi'}}{\overline{\rho}}, \\ \overline{\rho\phi"} &= 0, \\ \overline{\phi'} &= 0. \end{aligned} \tag{3}$$

In doing so, all the terms associated with the density fluctuation, e.g., $\overline{\rho'u'}$, in the Reynolds' averaged equations were eliminated in the Favre's averaged equations. The resulting flow equations are much simpler compared to the equations derived by the Reynolds averaging procedures.

Written in a strong conservative form, the turbulent, compressible, flow equations can be expressed as follows:

$$\frac{\partial \mathbf{Q}}{\partial t} + \frac{\partial}{\partial x}(\mathbf{E} - \mathbf{E}_v) + \frac{\partial}{\partial y}(\mathbf{F} - \mathbf{F}_v) = \mathbf{H}. \tag{4}$$

Here x and y are Cartesian coordinates, $\mathbf{Q}$ is the dependent variable, $\mathbf{E}$ and $\mathbf{F}$ are the convective flux vectors and $\mathbf{E}_v$ and $\mathbf{F}_v$ are the viscous flux vectors. The equations are similar to the laminar equations. However, all variables in the equations are the averaged variables, and the transport properties are the effective, i.e., laminar plus turbulent, properties. Here, we want to point out that the viscosity multiplied by the dilatational terms in the normal stresses is still the laminar viscosity as illustrated in the following relations:

$$\begin{aligned} \tau_{xx} &= 2(\mu + \mu_t)\frac{\partial \tilde{u}}{\partial x} - \frac{2}{3}\mu\left(\frac{\partial \tilde{u}}{\partial x} + \frac{\partial \tilde{v}}{\partial y}\right), \\ \tau_{yy} &= 2(\mu + \mu_t)\frac{\partial \tilde{v}}{\partial y} - \frac{2}{3}\mu\left(\frac{\partial \tilde{u}}{\partial x} + \frac{\partial \tilde{v}}{\partial y}\right). \end{aligned} \tag{5}$$

The vector $\mathbf{H}$ on the right hand side of the flow equations, Eq. 4, represents the additional terms introduced by the averaging procedure. The vector $\mathbf{H}$ can be expressed as

$$\mathbf{H} = \begin{pmatrix} 0 \\ -\frac{2}{3}\frac{\partial \overline{\rho}k}{\partial x} \\ -\frac{2}{3}\frac{\partial \overline{\rho}k}{\partial y} \\ \frac{\partial}{\partial x}\left[(\mu + \frac{\mu_t}{\sigma_k})\frac{\partial k}{\partial x}\right] + \frac{\partial}{\partial y}\left[(\mu + \frac{\mu_t}{\sigma_k})\frac{\partial k}{\partial y}\right] \\ +2\tilde{u}\frac{\partial}{\partial x}(\overline{\rho}k) + 2\tilde{v}\frac{\partial}{\partial y}(\overline{\rho}k) + G \end{pmatrix}. \tag{6}$$

where k is the turbulent kinetic energy and is defined as

$$k = \frac{1}{2\overline{\rho}}\overline{\rho(u"u" + v"v")}, \tag{7}$$

G is the generation of the turbulent kinetic energy and is defined in the following section.

The equations of turbulent kinetic energy, k, and energy dissipation rate, ϵ, are derived by the manipulation of the flow equations and the averaging procedure. The derived equations of k and ϵ can not be solved directly due to the closure problem. Modelling of certain terms in the equations is necessary to make the governing equations well posed. The details of the modelling is beyond the scope of this work. Here, only the final form of the equations are presented. The k and ϵ equations in the Cartesian coordinate system can be cast into the vector form: .

$$\frac{\partial \mathbf{Q}_{ke}}{\partial t} + \frac{\partial \mathbf{E}_{ke}}{\partial x} + \frac{\partial \mathbf{F}_{ke}}{\partial y} = \frac{\partial \mathbf{E}_{vke}}{\partial x} + \frac{\partial \mathbf{F}_{vke}}{\partial y} + \mathbf{S}, \tag{8}$$

where

$$\begin{aligned} \mathbf{Q}_{ke} &= \begin{pmatrix} \overline{\rho}k \\ \overline{\rho}\epsilon \end{pmatrix}, \\ \mathbf{E}_{ke} &= \begin{pmatrix} \overline{\rho}\tilde{u}k \\ \overline{\rho}\tilde{u}\epsilon \end{pmatrix}, \\ \mathbf{F}_{ke} &= \begin{pmatrix} \overline{\rho}\tilde{v}k \\ \overline{\rho}\tilde{v}\epsilon \end{pmatrix}, \\ \mathbf{E}_{vke} &= \begin{pmatrix} (\mu + \frac{\mu_t}{\sigma_k})\frac{\partial k}{\partial x} \\ (\mu + \frac{\mu_t}{\sigma_\epsilon})\frac{\partial \epsilon}{\partial x} \end{pmatrix}, \\ \mathbf{F}_{vke} &= \begin{pmatrix} (\mu + \frac{\mu_t}{\sigma_k})\frac{\partial k}{\partial y} \\ (\mu + \frac{\mu_t}{\sigma_\epsilon})\frac{\partial \epsilon}{\partial y} \end{pmatrix}, \\ \mathbf{S} &= \begin{pmatrix} G - \overline{\rho}\epsilon(1 + \alpha M_t^2) \\ (C_1 G - C_2\overline{\rho}\epsilon)\frac{\epsilon}{k} \end{pmatrix}, \end{aligned} \tag{9}$$

where G is the generation term of the turbulent kinetic energy and can be expressed as:

$$G = \mu_t\left[\frac{1}{2}\left(\frac{\partial \tilde{u}_i}{\partial x_j} + \frac{\partial \tilde{u}_j}{\partial x_i}\right) - \frac{2}{3}\frac{\partial \tilde{u}_k}{\partial x_k}\right] - \frac{2}{3}\overline{\rho}k\frac{\partial \tilde{u}_k}{\partial x_k} \tag{10}$$

where the subscripts i, j, and k follows the convention of Cartesian tensor.

The eddy viscosity μ_t is derived in terms of appropriate length and velocity scales. For the $k - \epsilon$ turbulence model, the length scale and the velocity scale of turbulent fluctuations are taken as

$$\begin{aligned} \ell &\approx \frac{k^{3/2}}{\epsilon}, \\ u"_i &\approx k^{1/2}. \end{aligned} \tag{11}$$

These relations allow the eddy viscosity, μ_t, to be modelled as:

$$\mu_t = C_\mu \overline{\rho} \frac{k^2}{\epsilon}. \tag{12}$$

The constants used in the $k-\epsilon$ model are the standard Jones and Launder's values:[6] $C_\mu = 0.09$, $C_1 = 1.44$, $C_2 = 1.92$, $\sigma_k = 1.0$, and $\sigma_\epsilon = 1.3$. These constants were never altered during the course of this work.

In order to accommodate the compressibility effect, the dissipation term $\overline{\rho}\epsilon$ in the source term of the k equation is multiplied by a correction factor $(1+\alpha M_t^2)$. Here M_t is the local turbulence Mach number defined as $M_t = \sqrt{k}/a$ where a is the local speed of sound. The constant α in the term is taken as unity. This model is developed by Sarkar et al.[7] The physical meaning of the term is that for high turbulence Mach number (M_t) flows, the dissipation of the turbulence kinetic energy is enhanced by a factor of αM_t^2. For free shear layers at high convective Mach number, the turbulence intensity is greatly reduced due to compressibility.

In calculating the turbulent free shear layers, the inlet boundary conditions for mean velocities and temperature are specified based on the hyperbolic tangent profile with specified initial shear layer thickness. The hyperbolic tangent profile is an approximation of the self-similar solution for fully developed turbulent free shear layers. The inlet transverse velocities are set to be zero. The turbulent kinetic energy and dissipation are specified according to the local equilibrium assumption and a algebraic turbulence model:[8]

$$\mu_t = \overline{\rho} l_m^2 \frac{\partial \tilde{u}}{\partial y} \tag{13}$$

where $l_m = 0.125b$ and the shear layer thickness, b, is based on the distance between the two transverse locations where $\tilde{u} = \tilde{u}_1 - 0.1\Delta\tilde{u}$ and $\tilde{u} = \tilde{u}_2 + 0.1\Delta\tilde{u}$. The dissipation can be related to the local length scale which is specified based on the local shear layer thickness:

$$\epsilon = C_\epsilon \frac{k^{\frac{3}{2}}}{b} \tag{14}$$

where $C_\epsilon = 1.23$. Using Eqs. (13) and (14), and the equation for the eddy viscosity, i.e, Eq. (12), k and ϵ can be readily obtained for the upstream boundary conditions.

Numerical Method

The numerical solution of Eqs. (4) and (8) is performed in a general, body-fitted coordinate system, (ξ, η). For the purpose of discussion, we will concentrate on Eq. (4). However, the procedure is equally applicable to Eq. (8). Coordinate transformation of Eq. (4) results in:

$$\frac{\partial \hat{\mathbf{Q}}}{\partial \tau} + \frac{\partial}{\partial \xi}\left(\hat{\mathbf{E}} - \hat{\mathbf{E}}_v\right) + \frac{\partial}{\partial \eta}\left(\hat{\mathbf{F}} - \hat{\mathbf{F}}_v\right) = \hat{\mathbf{H}} \tag{15}$$

where

$$\begin{aligned} \hat{\mathbf{Q}} &= h\mathbf{Q} \\ \hat{\mathbf{E}} &= h(\xi_x \mathbf{E} + \xi_y \mathbf{F}) \\ \hat{\mathbf{F}} &= h(\eta_x \mathbf{E} + \eta_y \mathbf{F}) \\ \hat{\mathbf{E}}_v &= h(\xi_x \mathbf{E}_v + \xi_y \mathbf{F}_v) \\ \hat{\mathbf{F}}_v &= h(\eta_x \mathbf{E}_v + \eta_y \mathbf{F}_v) \\ \hat{\mathbf{H}} &= h\mathbf{H} \end{aligned} \tag{16}$$

in which h is the cell volume.

The transformed equation, Eq. (15), is solved using a time-marching, LU scheme. The LU scheme can be obtained by approximately factorizing the left-hand-side (LHS) of the equation. In time-marching form, the implicit upwind difference scheme of Eq. (15) can be written as

$$\begin{aligned} [\mathbf{I} + \Delta t(D_\xi^+ \hat{\mathbf{A}}^- + D_\eta^+ \hat{\mathbf{B}}^- - \hat{\mathbf{D}} + \\ D_\xi^- \hat{\mathbf{A}}^+ + D_\eta^- \hat{\mathbf{B}}^+)]\Delta\hat{\mathbf{Q}} = \Delta t RHS \end{aligned} \tag{17}$$

In Eq. (17), Δt is the time-step. Backward-difference operators are denoted by D_ξ^- and D_η^-, and forward-difference operators by D_ξ^+ and D_η^+. The flux Jacobians, $\hat{\mathbf{A}}^+$, $\hat{\mathbf{B}}^+$, $\hat{\mathbf{A}}^-$, and $\hat{\mathbf{B}}^-$ are constructed such that the eigenvalues of '+' matrices are nonnegative and those of '−' matrices are nonpositive. The matrix $\hat{\mathbf{D}}$ is the Jacobian matrix of the source term.

The LHS matrix of Eq. (21) is usually too large for direct inversion. An approximate-factorization procedure is implemented which results in the following LU scheme :

$$\begin{aligned} &\left[\mathbf{I} + \Delta t\left(D_\xi^- \hat{\mathbf{A}}^+ + D_\eta^- \hat{\mathbf{B}}^+ - \frac{\hat{\mathbf{A}}^-}{\Delta\xi} - \frac{\hat{\mathbf{B}}^-}{\Delta\eta} - \hat{\mathbf{D}}\right)\right] \\ &\left(\frac{\Delta t}{\Delta\xi}(\hat{\mathbf{A}}^+ - \hat{\mathbf{A}}^-) + \frac{\Delta t}{\Delta\eta}(\hat{\mathbf{B}}^+ - \hat{\mathbf{B}}^-) - \hat{\mathbf{D}}\right)^{-1} \\ &\left[\mathbf{I} + \Delta t\left(D_\xi^+ \hat{\mathbf{A}}^- + D_\eta^+ \hat{\mathbf{B}}^- + \frac{\hat{\mathbf{A}}^+}{\Delta\xi} + \frac{\hat{\mathbf{B}}^+}{\Delta\eta} - \hat{\mathbf{D}}\right)\right]\Delta\hat{\mathbf{Q}} \\ &= \Delta t \mathbf{R} \end{aligned} \tag{18}$$

where the grid spacing in the general coordinate, $\Delta\xi$ and $\Delta\eta$ are usually taken to be one. $\mathbf{R}$ represents the residual of each LU time marching step. In calculating the residual, $\mathbf{R}$, both the inviscid and viscous terms are discretized using the central-difference approach:

$$\mathbf{R} = D_\xi(\hat{\mathbf{E}}_v - \hat{\mathbf{E}}) + D_\eta(\hat{\mathbf{F}}_v - \hat{\mathbf{F}}) + \hat{\mathbf{H}} \tag{19}$$

where D_ξ and D_η are the central difference operators.

Equation (18) is the generic form for the LU scheme. Its derivation can be found in Ref. 3 and will not be repeated here. This LU scheme requires inversion of the matrix,

$$\left[\mathbf{I}+\Delta t\left(\hat{\mathbf{A}}^{+}-\hat{\mathbf{A}}^{-}+\hat{\mathbf{B}}^{+}-\hat{\mathbf{B}}^{-}-\hat{\mathbf{D}}\right)\right] \qquad (20)$$

for the L operator and

$$\left[\mathbf{I}+\Delta t\left(\hat{\mathbf{A}}^{+}-\hat{\mathbf{A}}^{-}+\hat{\mathbf{B}}^{+}-\hat{\mathbf{B}}^{-}-b\hat{f}D\right)\right] \qquad (21)$$

for the U operator.

Up to this point, no definition has been made to the exact form of the split flux Jacobians. Yoon and Jameson[2] proposed that the split flux Jacobians are defined as

$$\begin{aligned}\hat{\mathbf{A}}^{+}&=0.5(\hat{\mathbf{A}}+\gamma_{\hat{\mathbf{A}}}\mathbf{I})\\ \hat{\mathbf{A}}^{-}&=0.5(\hat{\mathbf{A}}-\gamma_{\hat{\mathbf{A}}}\mathbf{I})\\ \hat{\mathbf{B}}^{+}&=0.5(\hat{\mathbf{B}}+\gamma_{\hat{\mathbf{B}}}\mathbf{I})\\ \hat{\mathbf{B}}^{-}&=0.5(\hat{\mathbf{B}}-\gamma_{\hat{\mathbf{B}}}\mathbf{I})\end{aligned} \qquad (22)$$

where $\gamma_{\hat{\mathbf{A}}}$ and $\gamma_{\hat{\mathbf{B}}}$ are greater than the spectral radii of the associated flux Jacobians :

$$\begin{aligned}\gamma_{\hat{\mathbf{A}}}&\geq\max(|\lambda_{\hat{\mathbf{A}}}|)\\ \gamma_{\hat{\mathbf{B}}}&\geq\max(|\lambda_{\hat{\mathbf{B}}}|)\end{aligned} \qquad (23)$$

The purpose of constructing split flux-Jacobians by Eq. (22) is to make the matrices in Eqs. (20) and (21) diagonal for efficient inversion. Apparently, the eigenvalues of the split flux-Jacobians are not the characteristics speeds of the flow.

In solving the k and ϵ equations, the aforementioned numerical method, i.e., the LU scheme on the left hand side and central differencing on the right hand side, is used. The solution procedure of the whole equation set is decoupled into flow solver and turbulence solver. Thus, the turbulence solver stands alone and can be easily turned on or off. This arrangement does not affect the overall numerical stability due to the fact that the feedback from k and ϵ equations to the flow equations depends on the turbulent transport properties only. Thus, it is more efficient and convenient to separate the solution procedure into two parts.

The source terms of the k and ϵ equations demand special treatment. In linearizing the source terms for the numerical method, the Jacobian matrix is obtained through the derivative of the source terms with respect to the dependent variables, i.e., $\overline{\rho}k$ and $\overline{\rho}\epsilon$. Following the usual practice, the form of the source terms guarantee a 2×2 full matrix for the Jacobian matrix. However, special treatment in deriving the Jacobian matrix is applied in this work to enhance the numerical stability. In the k equation, ϵ has been replaced by $k(\epsilon/k)$ where ϵ/k is treated as a constant. A similar method is also applied to the source term of the ϵ equation. The Jacobian matrix obtained is:

$$\mathbf{D}=\begin{pmatrix}-\frac{\epsilon}{k}(1+\alpha M_t^2) & 0\\ 0 & -C_2\frac{\epsilon}{k}\end{pmatrix} \qquad (27)$$

Note that off-diagonal terms are eliminated and the diagonal terms are always negative. Thus, the implicit part of the source terms of k and ϵ equations behaves like a sink which always stabilize the numerical scheme.

Results and Discussions

Bogdanoff[5] introduced the convective Mach number as a parameter that collapses the growth rate date of plane shear layers. The convective Mach number is defined as

$$M_c=\frac{U_1-U_c}{c_1}=\frac{U_c-U_2}{c_2} \qquad (28)$$

where U_1 and U_2 are the freestream velocities, and c_1 and c_2 are the freestream sound speeds. U_c is the convective velocity of large structures and is defined as

$$U_c=\frac{U_1c_2+U_2c_1}{c_1+c_2} \qquad (29)$$

Table 1 shows the five test conditions of the simulated compressible free shear layers. The range of the convective Mach numbers, M_c, is from 0.05 to 1.48. The last two rows show the spreading rate and the ratio of the compressible spreading rate to incompressible spreading rate in which δ is the shear layer thickness and the superscript $'$ represents the derivative of δ with respect to the streamwise distance. As indicated in the last row of the table, the ratios of the spreading rate of the free shear layers decreases as the convective Mach number increases. The test conditions of Case 3 in the table are the same as in the experiments reported by Goebel and Dutton.[4] In the rest of the section, we will first show the direct comparison between the simulated results and the experimental data for Case 3. Then, detailed numerical solutions of Case 3 in terms of velocity, turbulent kinetic energy, turbulence dissipation rate, Reynolds stress, and eddy viscosity are presented in a coalesced fashion. Finally, the solutions of five cases are compared to each other in the figures of kinetic energy, Reynolds stress, and ratio of spreading rates.

The solutions of Case 3 are examined in detail. Figure 2 shows the development of the free shear layer.

Note that x and y axes are not on a 1:1 ratio for the convenience of illustration. The definition of the shear layer boundaries is the same that of the shear layer thickness. In Fig. 2, the boundaries of the shear layer corresponding to $10 - 90\%$ are drawn. Circles are the experimental data of Dutton et al. The calculated results agree well with the experimental data. After the developing region, the boundary of the shear layer is almost linear. Incidentally, Figs. 3a and 3b show the numerical convergence trends of the flow and $k - \epsilon$ equations. In about 2500 iterations, the residuals drop about 12 orders of magnitude and reach the machine accuracy.

Figure 4 shows the Mach number profile at various axial locations. The velocity gradient in the transverse direction decreases as the flow goes downstream. Figure 5 is the coalesced version of Fig. 4. The nondimensionalized y coordinate defined as $(y - y_c)/\delta$ is used, where y_c is the transverse location at the center of the shear layer, and δ is the shear layer thickness. Note that the upstream boundary condition of velocities is prescribed according to a hyperbolic tangent curve which is an approximation of self-similar solution of free shear layers. According to Fig. 5, this self similarity of velocity profiles never fail as the flow goes downstream.

Figure 6 shows coalesced turbulence kinetic energies at various locations. The turbulence kinetic energy is nondimensionalized by ΔU^2. This figure clearly shows that after the first three stations, i.e., about 150 mm, the turbulence kinetic energy retains self similarity. Thus, the developing region for the turbulence is about 150 mm. Figure 7 shows the turbulence dissipation profiles. As flow goes downstream, the peak values of turbulence dissipation at each stations decrease, and the turbulence dissipation never reach a fully developed condition. However, if the ϵ value is nondimensionalized by $\Delta U^3/\delta$ the coalesced profiles appear as shown in Fig. 7. A similar behavior is observed for the eddy viscosity profiles (Fig. 8). Figure 9 shows the nondimensionalized Reynolds stress profiles. Again, the turbulence Reynolds stress becomes the fully developed at about 150 mm downstream of the splitter plate.

Figure 10 shows the comparison between the predicted fully developed Reynolds stress and the experimental data reported by Dutton et al.[5] The predicted solution underestimated the peak value of the Reynolds stress profile by $6 \sim 8\%$; however, the overall trend of the predicted results is correct. Many factors contribute to the discrepancy between the predicted result and experimental data. Among them, the upstream boundary conditions are simplified in the solution procedure, i.e., no effort was made to simulate two boundary layers merging at the tip of the splitter plate. This could offset the solution in the developing region and shift the fully developed solutions.

Figure 11 shows the comparison of the turbulent kinetic energy between the five cases. Again, the turbulent kinetic energy is normalized by the square of the velocity difference of the two streams. It is clear that the normalized turbulence intensity decreases with increasing convective Mach number. A similar situation is observed in Fig. 12, the normalized Reynolds stress decreases with increasing convective Mach number. Figure 13 shows the distribution of the ratios of spreading rates for the five cases compared to experimental data. The ratio of the spreading rates decreases from about unity to 0.45 as the convective mach number increases from about 0. to 1.45. Both the experimental data and the simulated results show the spreading rate ratio reaches an asymptotic value after the convective mach number exceeds unity. Simular phenomenon can be seen in Figs. 11 and 12. Both figures show that the normalized turbulence kinetic energy and Reynolds stress reach asymptotic values as the convective Mach number increases.

CONCLUDING REMARKS

In this paper, we report the incorporation of a compressible $k - \epsilon$ model with a two-dimensional Navier Stokes solver to study compressible free shear layers. Sarkar's modelling is adopted to simulate the compressibility effects of the k and ϵ equations. The model enhances the turbulence dissipation rate of flows at high speeds. In deriving the governing equations, the Favre averaging procedure for the fully trubulent flow equations is elaborated. The equation sets are presented in the vector form for the convenience of the discussion of the numerical method. Yoon and Jameson's LU scheme is used to solve the equation sets. Details of boundary conditions and the treatment of the source terms of the k and ϵ equations are discussed. Then the program is applied to simulate compressible free shear layers with five different convective Mach numbers. The decrease of the spreading rate of the shear layers with increasing Mach number is observed in the calculated results. Results also show favorable comparison with Goebel and Dutton's experimental data.

REFERENCES

1. Kuo, K.K., 1986 "Principles of Combustion," John Wiely & Sons, p. 412.
2. Yoon, S. and Jameson, A., 1989 "Lower-Upper Implicit Schemes with Multiple Grids for the Euler Equations," *AIAA J.* Vol. 25, No. 7, p. 929.

3. Yu, S.T., Tsai, Y.P., and Shuen, J.S., 1989 "Three-Dimensional Calculation of Supersonic Reacting Flows Using an LU Scheme," AIAA paper 89-0391 (accepted for publications in J. of Compt. Phys.)

4. Goebel, S.G., and Dutton, J.C. 1991 "Experimental Study of Compressible Turbulent Mixing Layers," *AIAA J.* Vol. 29, No. 4, p.538.

5. Bogdanoff, D.W., 1983 "Compressibility Effects in Turbulent Shear Layers," *AIAA J.* Vol. 21, No. 6, p.926.

6. Jones, W.P., and Launder, B.E., 1972 "The Prediction of Laminarization with a Two-Equation Model of Turbulence," *Int. J. Heat Mass Transfer*, Vol. 15, p. 301.

7. Sarkar, S., Erlebacher, G., Hussaini, M.Y., and Kreiss, H.O., 1989 "The Analysis and Modeling of Dilatational Terms in Compressible Turbulence," ICASE Report No. 89-79, NASA Langley Research Center.

8. Burr, R.F. and Dutton, J.C., 1990 "Numerical Modeling of Compressible Reacting Turbulent Shear Layers," AIAA Paper 90-1463.

9. Papamoschou, D. and Roshko, A. 1988 "The Compressible Turbulent Mixing Layer: An Experimental Study," J. Fluid Mech., Vol. 197, p.453.

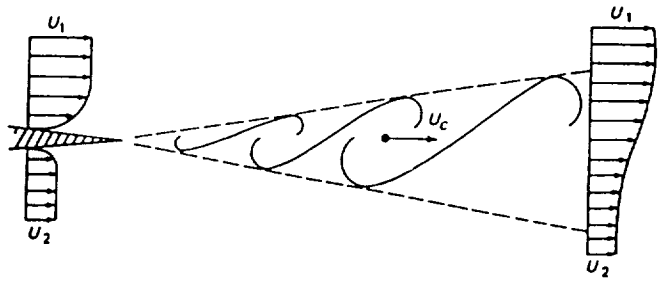

Fig. 1: Schematic of free shear layer.

Table 1: Test conditions of the calculated shear layer.

CASE	1	2	3	4	5
M_1,M_2	1.2, 1.1	2.0, 1.4	1.91, 1.37	2.5, 1.1	6.1, 3.15
M_c	0.05	0.31	0.45	0.70	1.48
U_1,U_2 [m]	419, 384	676, 465	702, 404	865, 380	3461, 1786
T_1,T_2 [K]	300, 300	275, 275	334, 215	295, 295	800, 800
ρ_1,ρ_2 [Kg/m^3]	0.64,0.64	0.7,0.7	0.57,0.89	0.64,0.64	0.24,0.24
P [atm]	0.55	0.55	0.55	0.55	0.55
δ'	0.007	0.021	0.027	0.035	0.024
δ'/δ'_i	1.01	0.7	0.54	0.47	0.40

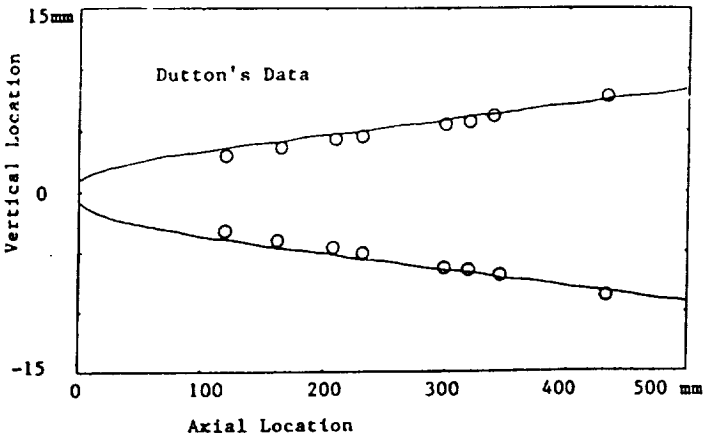

Fig. 2: The boundaries of the free shear layer (10−−90%).

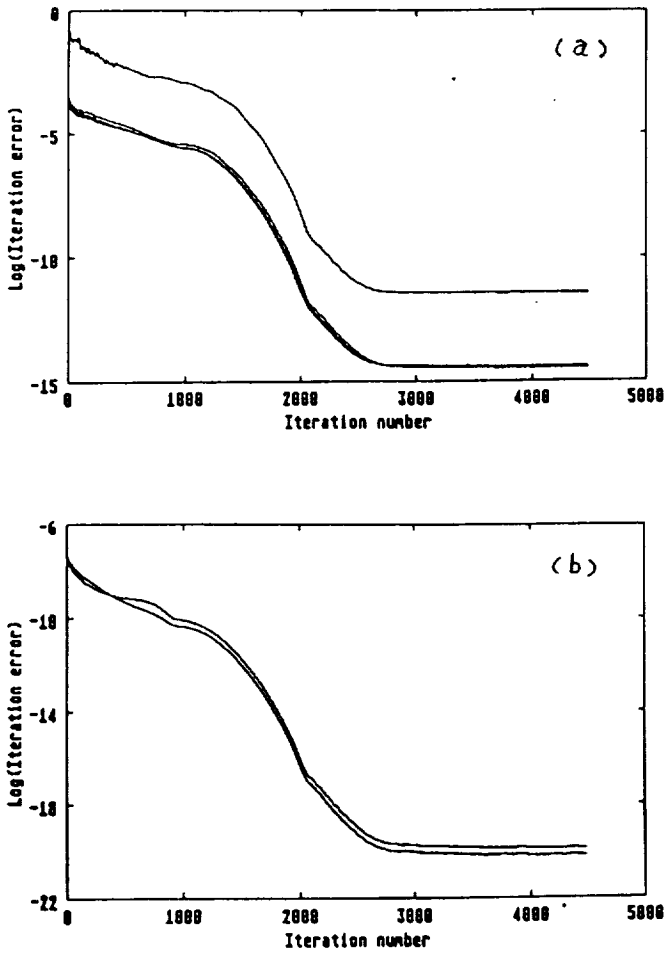

Fig. 3: Convergence trends of the flow and turbulence equations.

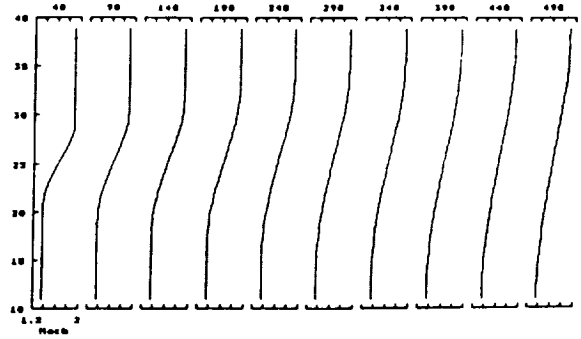

Fig. 4: The velocity profiles of the free shear layer at different axial locations.

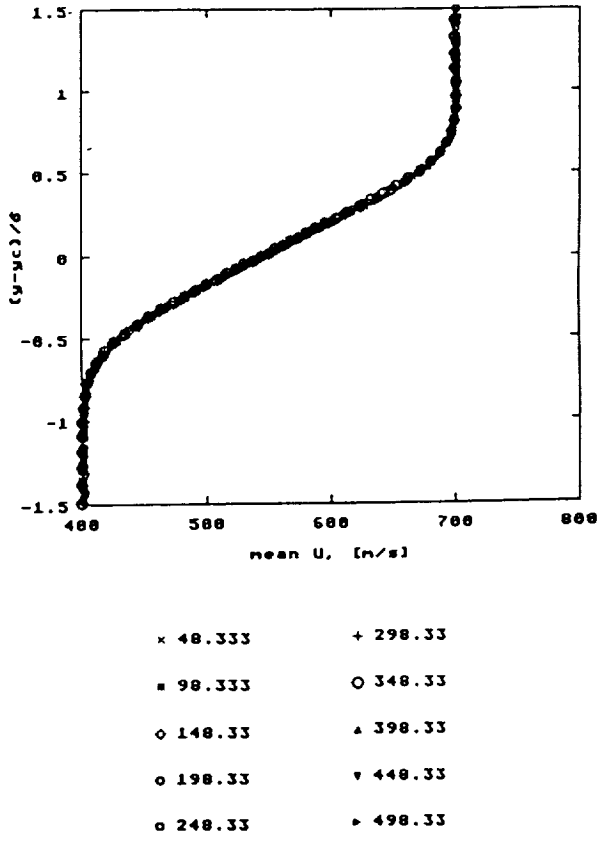

Fig. 5: Coalesced velocity profiles of different axial locations.

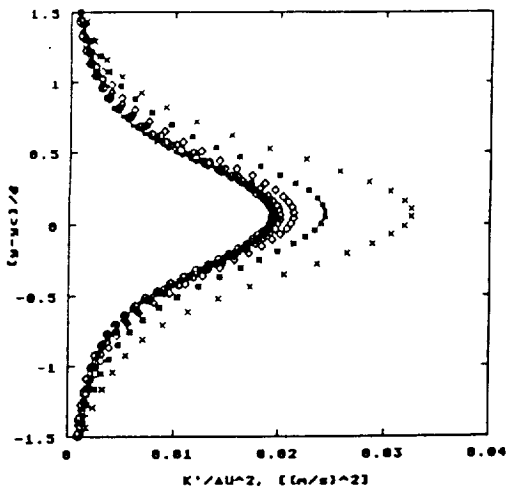

Fig. 6: Coalesced turbulent kinetic energy profiles of different axial locations.

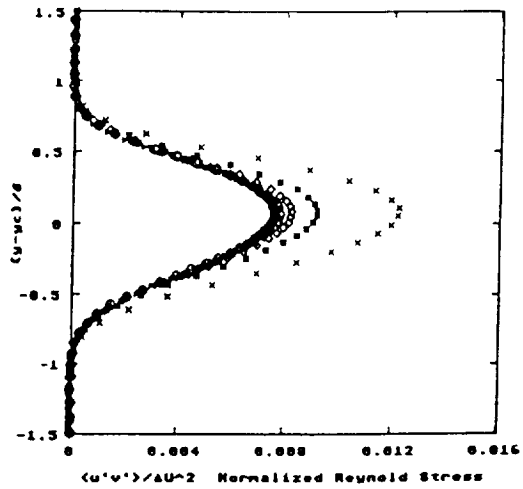

Fig. 9: Coalesced Reynolds stress profiles of different axial locations.

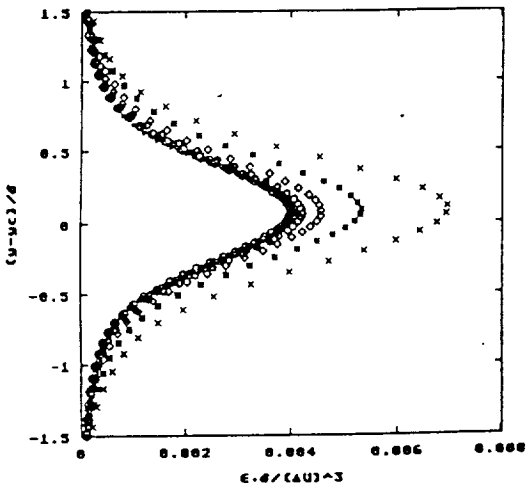

Fig. 7: Coalesced turbulence dissipation profiles of different axial locations.

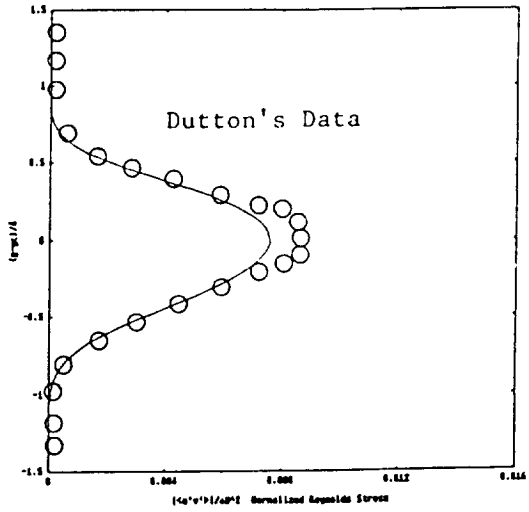

Fig. 10: Comparison of Reynolds stresses between experimental data and predicted results.

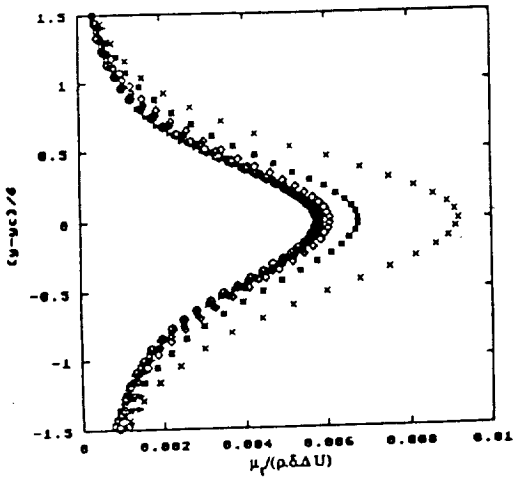

Fig. 8: Coalesced eddy viscosity profiles of different axial locations.

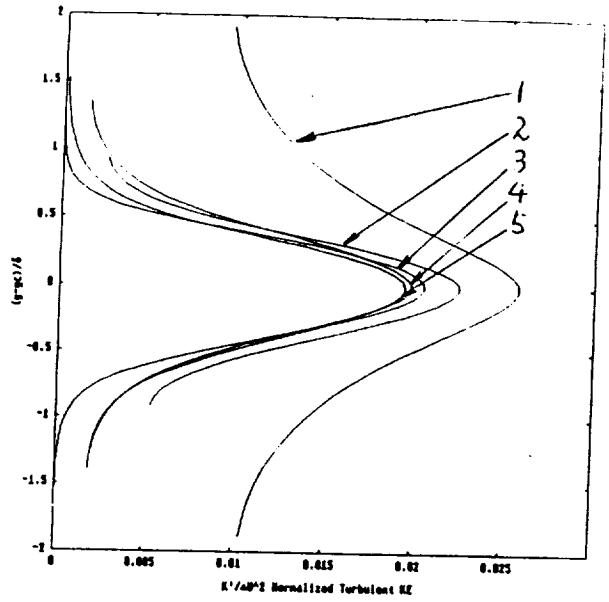

Fig. 11: Comparison of turbulent kinetic energy with five different convective Mach numbers.

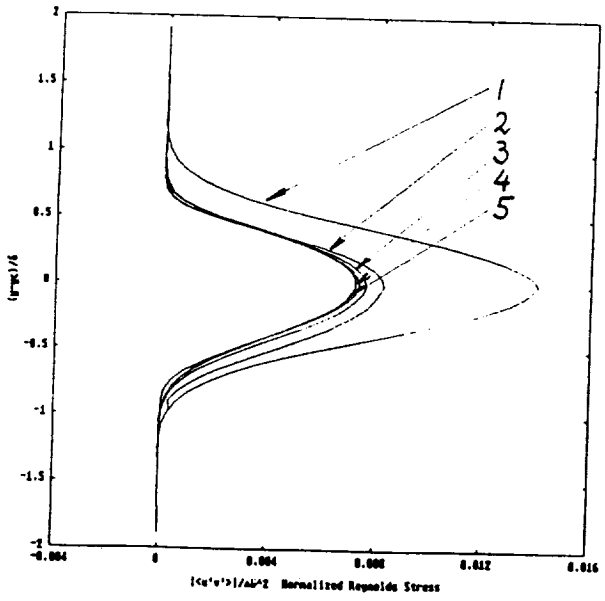

Fig. 12: Comparison of Reynolds stresses with five different convective Mach numbers.

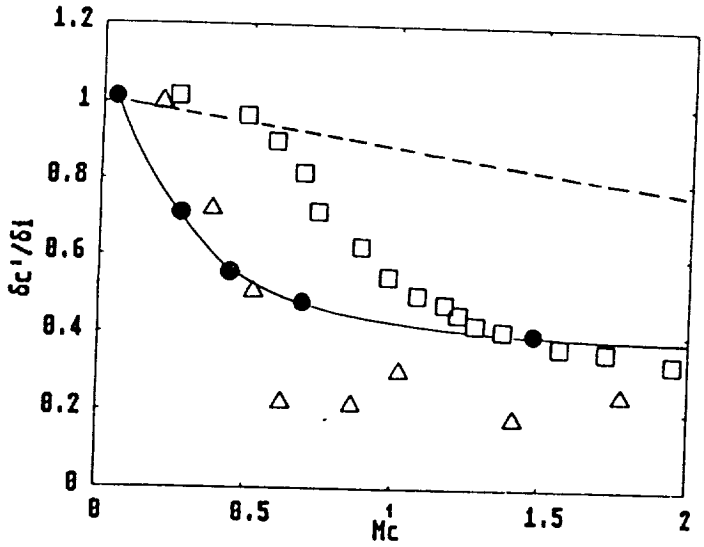

△ Papamoschou and Roshko [9]

□ Langley's data [7]

—●— With Compressibility Model

- - - Without Compressibility Model

Fig. 13: Comparison of ratios of spreading rate between experimental data and predicted results.